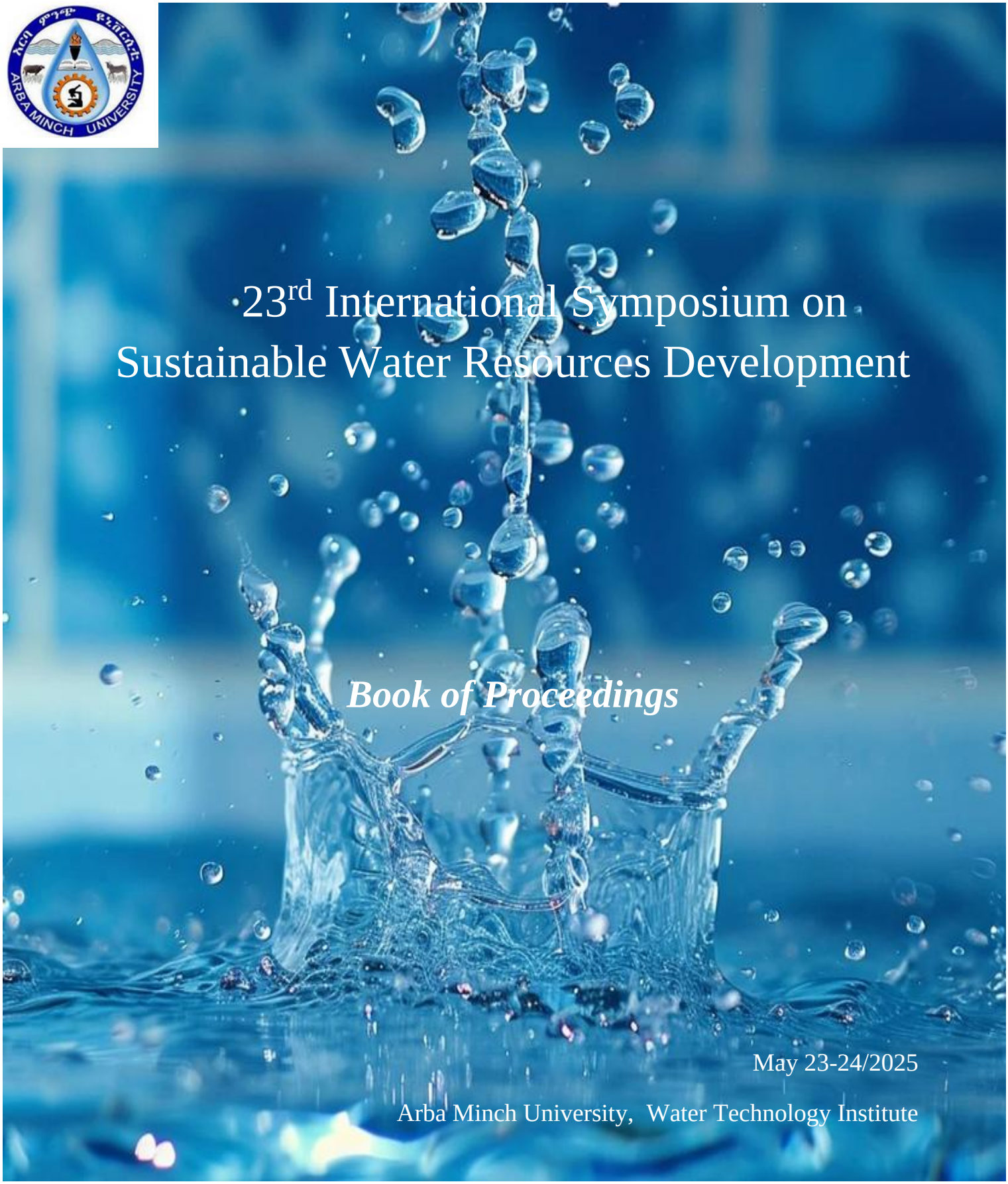

23rd International Symposium on Sustainable Water Resources Development

Book of Proceedings

May 23-24/2025

Arba Minch University, Water Technology Institute

Proceeding Editors

Dr. Elias Gebeyehu

Mr. Andarge Alaro

Mr. Endale Seyoum

Mr. Behailu Hussien

Mr. Dagmawi Matewos

Mr. Chirotaw Kentib

Table of Contents

Forward

Arba Minch University, Water Technology Institute, Water Resources Research Center, has been organizing an international symposium on “Sustainable Water Resources Development” for the past twenty-three years.

The symposium aims to provide a platform for professionals, researchers, practitioners, and decision-makers to present research findings, share best practices, and exchange innovative ideas on sustainable water resources development.

For the 23rd symposium, over 157 papers were submitted by authors from across the country and abroad. Following a rigorous selection process, 17 papers have been chosen for oral presentation and 4 papers for poster presentation. All selected papers will be presented in person.

The organizing committee extends its congratulations and warm welcome to the authors whose papers were selected. We appreciate their participation and look forward to their valuable contributions.

We would like to thank each of you for attending our symposium and bringing your expertise to our gathering.

Acknowledgement

We would like to express our sincere gratitude to all the organizationss and individuals whose contributions made this symposium possible. We are particularly grateful for the generous support from our sponsors: the Ministry of Water and Energy, Menschen für Menschen, Rift Valley Lakes Basin Development Office, Space Science and Geospatial Institute, Ethiopian Engineering Corporation, International Water Management Institute (IWMI), Ethiopian Meteorology Institute, Ethiopian Water Technology Institute, Ministry of Agriculture and Lowlands, Anwar Seid General Contractor and Haverim Construction General Contractor. Their partnership and commitment were vital to the success of this event. We also extend our deepest appreciation to our distinguished keynote speaker, Dr. Semu Moges, as well as Dr. Trusew Assefa and Eng. Gedion Asfaw, for sharing their valuable insights and expertise. Special thanks go to all the paper contributors, reviewers, and organizing committee members for their dedication and tireless efforts in ensuring the symposium's success. Without their collective contributions, this event would not have been possible.

Dr. Eng. Elias Gebeyehu Ayele (PhD)
Director, Water Resources Research Center

Welcome Address

His Dr. Michael Mehari, Special Advisor to the Federal Ministry of Water and Energy/ Delegate of the minister.

His Excellency Dr. Ing. Abdela Kemal; Arba Minch University President.

His Excellency Dr. Bogale GebreMariam; Vice President for Academic Affairs and Delagate for the Presendent, Arba Minch University.

His Excellency Dr. Teklu Wegayehu; Vice President for Research and Community Service.

Her Excellency Professor Paulos Taddesse; Vice President for Administration and Development.

His Excellency Dr. Muluneh Lemma, Scientific Director of Arba Minch Institute of Technology.

Invited Keynote Speakers

Invited Paper Presenters and Distinguished Guests.

Ladies and Gentlemen;

It is a great honor to me to welcome you all to the 23rd International Symposium on Sustainable Water Resources Development.

I would like to extend warm welcome to our distinguished guests, many of whom travelled from far to be with us. We are delighted to have everyone to join us here today.

I hope that you will take the time to learn, exchange and interact with speakers, paper presenters, stakeholders and participants from various disciplines across the globe that we have brought today to share their thoughts and insights on the issues related to sustainable water resources development.

The 22nd International Symposium demonstrates our commitment to strengthen our regional, national and global ties for mutual benefits through exchange of knowledge and practices. This symposium has lived up to 21 years legacy to get national accreditation for the Ethiopian Journal of Water Science of Technology after publication of the 7th volume recently. May I take this occasion to congratulate the Editorial Board of the journal and acknowledge all those who have contributed in every aspect for its success?

I would like to thank and recognize our first rank sponsors, Ministry of Water and Energy, and Ethiopian Metrological Institute, and our second rank sponsors, Rift Valley Lakes Basin

Administration Office, Safeguarding Sahelian Wetlands for Food Security (SaWeL), and Improving Water Security for the Poor (REACH) programs.

We thank all our sponsors for continuous support and commitment to the symposium over years.

I would also like to acknowledge the symposium organizers, Water Resources Research Center and organizing committee who all have worked hard to bring this symposium to you.

I wish you all two great days in Arba Minch.

Please join me to invite Dr. Ing. Abdella Kemal to the podium to give opening speech.

Thank you

Dr. Tamiru Teseme

Opening Speech

His Dr. Michael Mehari, Special Advisor to the Federal Ministry of Water and Energy/ Delegate of the minister.

His Excellency Dr. Bogale GebreMariam

Vice President for Academic Affairs

His Excellency Dr. Teklu Wegayehu

Vice President for Research and Community Service

Her Excellency Professor Paulos Taddesse

Vice President for Administration and Development

His Excellency Dr. Muluneh Lemma, Scientific Director of Arba Minch Institute of Technology

Invited Keynote Speaker Dr. Abdulkarim S. Director, IWMI.

Invited Paper Presenters and Distinguished Guests

Ladies and Gentlemen

It is with great pleasure and honor that I welcome you all to the 23rd International Symposium on Sustainable Water Resources Development. Today, we gather here to address one of the most pressing challenges of our time: the sustainable management of water resources.

Water, as we all recognize, is not merely a commodity; it is the essence of life itself. From quenching our thirst to nurturing crops and supporting industries, water plays an indispensable role in every facet of human existence. Yet, despite its fundamental importance, we find ourselves confronted with a looming crisis – the scarcity of water resources, coupled with concerns over its quality. In Ethiopia, a nation blessed with abundant water resources, the challenge lies not in the availability of water but in its equitable distribution and efficient utilization. With a growing population, the demand for water is increasing, particularly in vital sectors such as agriculture. To meet this demand sustainably, it is imperative that we adopt innovative approaches to water management, focusing on maximizing productivity while minimizing waste.

Moreover, as we strive to harness the potential of our water resources for economic development, we must not overlook the importance of ensuring access to clean water and sanitation for all.

The health and well-being of our citizens depend on it, and it is incumbent upon us to prioritize investments in water infrastructure and sanitation systems. The government of Ethiopia has long recognized the significance of water-based development projects and has committed itself to their implementation. However, the task ahead requires collective action and international cooperation. The challenges we face are complex and multifaceted, but together, through collaboration and innovation, we can overcome them.

As we embark on this symposium, let us seize this opportunity to exchange knowledge, share best practices, and forge partnerships that will pave the way for a sustainable future where water resources are managed wisely and equitably for the benefit of all.

Dear esteemed participants, Ladies and gentlemen,

As we gather here today to address the critical issue of sustainable water resources development, it is essential to recognize the interconnected nature of our challenges. Ethiopia, like many nations, faces a growing demand for energy driven by population growth, urbanization, and industrialization. To meet this demand while safeguarding our environment, we must prioritize the development of renewable energy sources such as hydropower.

The government's commitment to projects like the Grand Renaissance Dam underscores its dedication to providing reliable and sustainable energy for national development. However, despite these efforts, challenges such as power shortages and interruptions persist, highlighting the need for continuous research and innovation in the management of our hydroelectric infrastructure. Moreover, the long-term impacts of socio-economic activities on our environment cannot be ignored. Environmental degradation and climate change pose significant threats to our water resources and livelihoods, making sustainability a paramount concern. Therefore, it is imperative that we integrate principles of sustainability into all aspects of water resources development.

Arba Minch University stands ready to contribute to this endeavor through its focus on human resource capacity building and research. By nurturing skilled professionals, generating knowledge, and facilitating technology transfer, the university plays a vital role in driving sustainable development in our water sector. I extend my gratitude to the Water Technology Institute, the scientific and research directors, and the organizing committee for their tireless

efforts in sustaining this annual symposium. It is through forums like these that researchers and practitioners can come together to exchange ideas, share research findings, and promote best practices in water management.

With these words, I officially declare the 23rd International Symposium on Sustainable Water Resources Development open. May this gathering be a catalyst for fruitful scientific discourse and may your time in Arba Minch be both enriching and enjoyable.

Thank you,

Dr. Ing. Abdela Kemal; Arba Minch University President.

ORAL PRESENTATIONS

Theme 1

Hydrology and Integrated Water Resources Management

Golina River Discharge Monitoring Using Remote-Sensing and Hydrological Model Products

Mengesha Tesfaw*[1], Mekete Dessie[1], Thomas Hermans[2], Fenta Nigate[3], Mulatu Kassa[4], Kasye Shitu[5], and Kristine Walraevens[2]

[1]Faculty of Civil and Water Resources Engineering, Bahir Dar Institute of Technology, Bahir Dar University, Bahir Dar, P.O. Box 26, Ethiopia; mekete.dessie@bdu.edu.et (M.D.)
[2]Laboratory for Applied Geology and Hydrogeology, Department of Geology, Ghent University, 9000 Ghent, Belgium; kristine.walraevens@ugent.be (K.W.); thomas.hermans@ugent.be (T.H.)
[3]School of Earth Science, Bahir Dar University, Bahir Dar, P.O. Box 79, Ethiopia; fenta.nigate@bdu.edu.et (F.N.)
[4]Department of Water Resource Engineering and Management, Woldia University, Woldia, Ethiopia; mulugetakassa004@gmail.com (M.K.)
[5]Department of Natural Resource Management, Mekdela Amba University, Tulu-Awlia, Ethiopia; kasaye_shita@mkau.edu.et (K.S.),
*Correspondence: mengesha816@gmail.com

Abstract

River discharge gauging is scarce in many regions, especially in arid and semi-arid regions. It is therefore crucial to develop an indirect way to infer this important component of the water balance system. Recently, remote sensing and hydrological model results have become important means of estimating river discharge. However, given their indirect nature, it is important to develop methodologies to appropriately select the best suited approach in a given study area. In this study, the multiple pixel ratio (MPR) method is compared with hydrological model results in the Global Flood Awareness System (GloFAS) for the Golina River, Danakil basin, Ethiopia. In the MPR method, the river discharge was estimated based on the relationship between river discharge and the near-infrared reflectivity (NIR) of the Landsat 8 image. This study utilized 251 Landsat images (2013–2024) to monitor the Golina river discharge near the outlet region. The influence of the selected length and width of the river discharge estimation was also analyzed. In the river channel lengths of 300 m in the upper reach and 600 m in the lower reach of the temporal station (Addis-Alem) were calibrated. The measured data in the year between 2022–2024 was used to calibrate the discharge data. The correlation of the observed and the remote sensing products is 0.77 in the upper reach (length of 300 m) while in the lower reach (length of 600 m) the correlation is 0.75. The correlation results are lower in GloFAS (reanalysis) products. The multiple pixel ratio (MPR) approach applied with the lowest distance from the river channel can better monitor river discharges than the GloFAS products. More studies using the highest temporal resolution with different selected inundated river channel (SIRC) lengths will be important for further improving the methods and monitoring similar ungauged rivers.

Keywords: *Ungauged River; Remote Sensing; GloFAS; Golina River; Ethiopia*

1. Introduction

River discharge monitoring is important to understand the concepts of climate change impacts, water resource management, and flood management analysis [1] [2] [3] [4]. There are significant hydrological challenges to monitoring river discharges, especially in semi-arid regions because of data scarcity, limited research in the area, increasing water demands, and spatial and temporal variability of hydrological

processes [5][6][7]. Several approaches have been proposed for monitoring river discharge. Among them, remote sensing (RS) has been proven to be an effective method for discharge estimation in data-scarce regions. However, this is not a direct method. Remote sensing methods are widely applied worldwide to monitor river discharge [8][9][10][11][12]. They are often related to remotely sensing hydraulic variables, including surface velocity, water surface width, and river stage height. River discharge has been effectively monitored using remote sensing products of water surface depth and hydraulic properties [13] [14].

Satellite images such as multispectral and aerospace radar have been widely used to monitor rivers [15] [16]. These satellite images have different spatial and spectral resolutions, area coverage, and recycle periods depending on the natural features. The spectral appearance of water in near-infrared (NIR) images is different from other land cover features and offers a way to monitor discharge [13]. Developing a relationship between the observed discharge and NIR reflectivity ratio of the dry area and the river network has been broadly used to monitor discharge [8]. The Moderate Resolution Imaging Spectroradiometer (MODIS) has also been efficiently used to monitor discharge with NIR images [17][18]. Developing the relationship between the river width and discharge is also a recognized method for river discharge estimation. Multispectral images are commonly used to assess surface water width [19] [20].

Landsat MSS/TM/ETM/OLI [21] [22][23], and MODIS [18] [24] images are universally used to extract information on the water surface. Altimeter satellites are also used to monitor rivers because they can quantify the elevation changes of surface water [23]. The optical and radar datasets have also been used for river discharge monitoring [25][26]. Monitoring ungauged river discharge fully from RS data products is important for hydrological studies [27][28].

Considering the physical characteristics and spatial resolution, the NIR images have a significant potential for monitoring the small river discharge [29]. The calibration (C) and measurement (M) ratio methods are extensively used to monitor discharge in different parts of the world [30][31][32][18]. The multiple pixel ratio (MPR) approach is another important approach in discharge estimation that uses NIR band reflectivity. The MPR approach has been successfully used for monitoring the river discharge on the Tibetan Plateau [29].

The reanalysis product is also a global gridded dataset with a resolution of 0.1^0 at a daily time step extracted from the climate data store (CDS), available from 1 January 1979 till the present. The reanalysis products were assessed against a global daily discharge in several areas [33][34][35]. The results found on the GloFAS-ERA5 reanalysis product correlation coefficient was varied from 0.44 to 0.74 [36].

The Global Flood Awareness System (GloFAS) can be used to provide daily assessments of historical flood events for the globe, such a spatiotemporal reliable outline is required by several researchers [37]. During the evolution GloFAS data service, two hydrological modeling conformations were used to produce the hydrological reanalysis datasets: (1) until GloFAS v2 [38]; (2) from GloFAS v3, used as input to OS LISFLOOD with all rainfall-runoff processes associated with river discharge. The GloFAS products have been run in two spatial resolutions. The earlier product has 0.1° for versions up to GloFAS v3 and then 0.05° (around 5 km) for GloFAS v4 [39].

The GloFAS has an operational system for historical and forecast monitoring of floods at a global level [40]. The GloFAS-ERA5 dataset is a reanalysis product [41] that provides a spatiotemporally historical daily river discharge for the whole world. It is generated for every 0.1° river cell from 1979 to the present

time. The ERA5 product is modified operationally with an expectancy of 2 to 5 days behind real-time atmospheric reanalysis [42]. An assessment of GloFAS-ERA5 against a global system of 1801 observed river discharge stations was undertaken [36].

Monitoring stations are available along the large river basins, and few stations are accessible on the small perennial rivers in Ethiopia. The Golina River is located in northern Ethiopia, the Danakil Basin. The Golina River is an important source of water for the Kobo Valley, for domestic and irrigation purposes [43]. In Kobo Valley, several ungauged streams still lack sufficient hydrological data. The challenge of obtaining stream flow data is a limiting factor for many researchers analyzing flood and drought conditions. Accurate hydrological information from these areas is crucial for scientific study. Therefore, this study aims to monitor the ungauged Golina river using RS and GloFAS reanalysis products.

2. Material and Methods

2.1. Area description

The Golina river is located in the Danakil Basin, Ethiopia. Figure 1 shows the pilot site of the gauging stations in the Golina River near the watershed outlet. The gauging station is located at the Addis-Alem pilot site near the outlet of the Golina River.

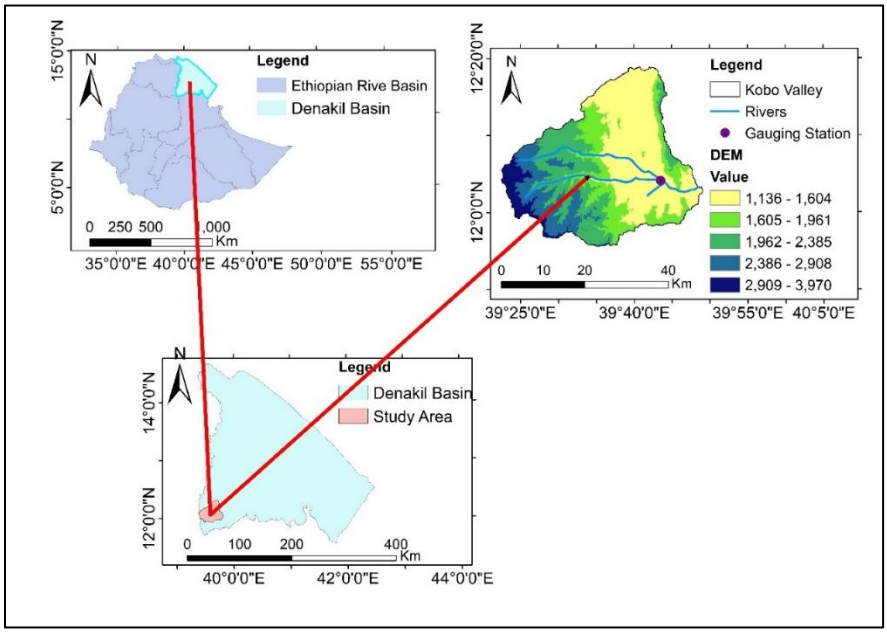

Figure 1: The location of the gauging station

2.2. NIR data processing

The seasonal coverage of the whole planet's landmass is provided by the two sensors (OLI and TIRS) at spatial resolutions of 30 meters (NIR) and 100 meters (thermal) in the Landsat 8 image. We used Landsat 8 images from the operational land image (OLI) sensors. Due to the sensor malfunction, some OLI images have poor quality. A total of 251 cloud-free OLI images were selected from 02 April 2013 to 08 July 2024. NIR images from Landsat 8 were used to monitor the Golina River discharge. They were atmospherically

corrected, and obtained from the following Google Earth Engine platform (https://earthengine.google.com/), Landsat Surface Reflectance.

Landsat surface reflectance (LaSRC) algorithms were used to analyze the images that were converted into pixel values. The pixel values vary between the permanent dry area and the inundated river width. The MPR approach calculates the difference in NIR band reflectance from a reference area (permanent dry pixel) and an inundated river channel (water pixel). The river discharge estimation used a multiple-pixel ratio (MPR) technique based on the correlation between the observed discharge and near-infrared reflectivity ratio. Figure 2 represents the reflectivity ratio of dry area and wet mean reflectivity.

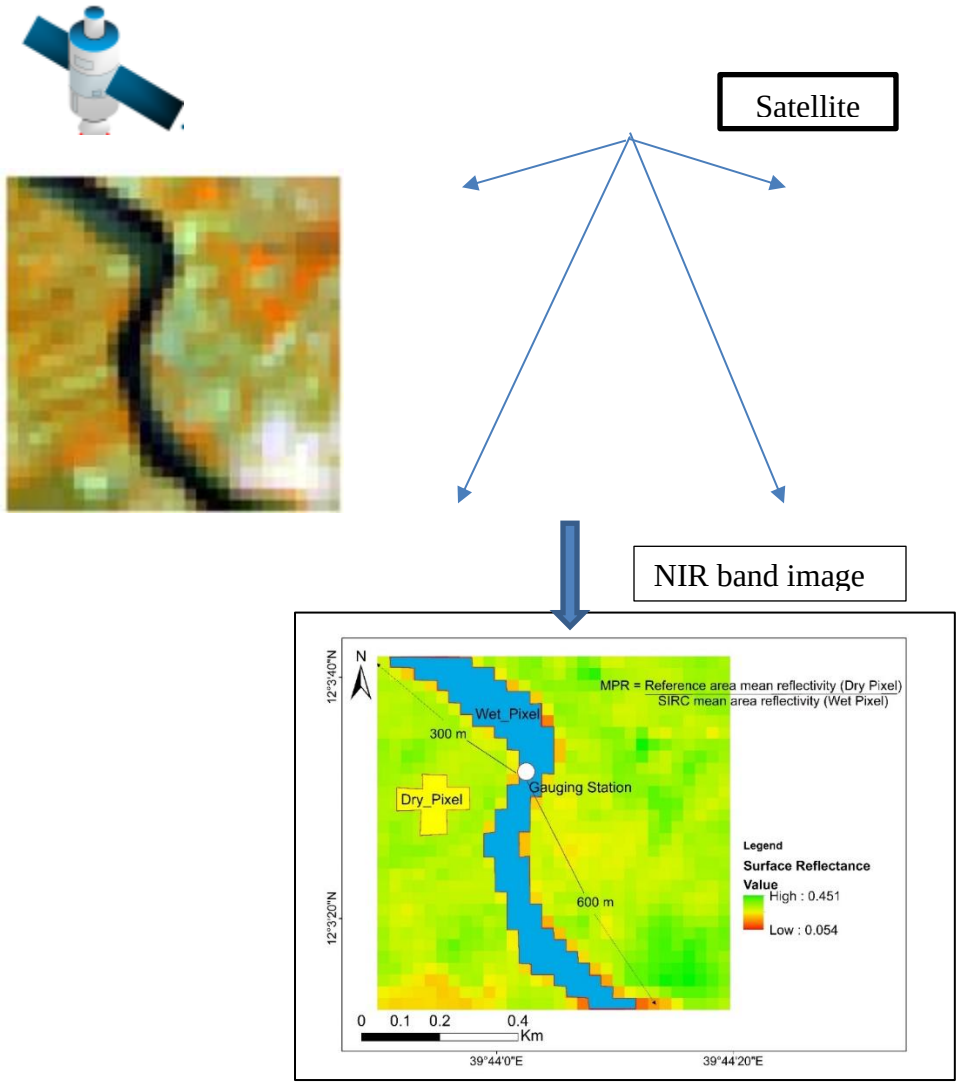

Figure 2: The reflectivity ratio of dry area and wet mean reflectivity.

The MPR technique significantly extends the river length that is to be monitored with RS techniques by continuously controlling the river width using NIR imagery [18]. In the MPR approaches, the NIR identifies the dry pixel (C) and the water pixel (M). Equation 1 shows the reflectivity ratio of dry and wet pixels.

$$P = \frac{\text{mean } C}{\text{mean } M} = \frac{\frac{1}{n}\sum_{i=1}^{n} Ci}{\frac{1}{W*L}\sum_{j=1}^{W*L} Mj} \quad 1$$

Where P is the pixel ratio, C is the permanent dry area average pixels, and M is the river channel average pixels. The terms i and j are pixel numbers in the dry land and the river respectively. The terms W and L are the river width and length respectively.

Generally, the most commonly used stage-discharge rating curves treat the discharge as a unique function of the stage which typically follows a power curve [44]. Equation 2 shows the relationship between remote sensing discharge and mean reflectivity ratio.

$$Qrs = a(P)^{b} \quad 2$$

Where, Qrs is remotely sensing discharge, and P is the mean reflectivity ratio. The terms a and b are fitting coefficients adjusted based on the observed discharges.

The remote sensing discharge was calibrated using in-situ measuring techniques. The relationship between the observed discharge and the NIR reflectivity ratio was evaluated using the model performance indexes.

2.2.1. Permanent area and sirc selection

The permanent dry area is selected near the gauging station (Addis-Alem station), which has high and stable reflectivity (Abuare small town). To ensure the stable reflectivity of the permanent dry area (Abuare town), multiple pixels were selected. We considered the optimal width, length, and location of the channel near the temporary gauging station.

Urban areas are assigned as the best sites for the permanent dry areas [22]. In this study, two SIRC lengths are considered, including a 300 m length at the upper river reach and a 600 m length at the downstream river reach. Considering the reflectivity stability of the SIRC, we used 600 m (the twenty Landsat pixels, 30 m × 20) as the longest SIRC length in this study.

The composite type SR_B(564) displayed as red, green, and blue (RGB) was used to evaluate land/water distributions using the visual interpretation method [45]. Figure 3 represents the Surface reflectance product from the Landsat image.

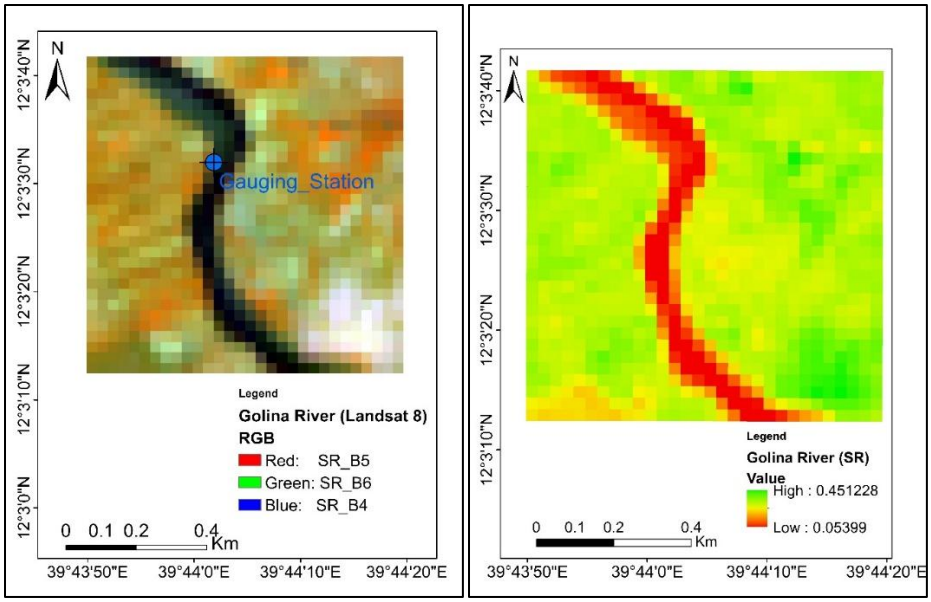

Figure **3**: Landsat 8 band combinations and their surface reflectance.

2.3. Hydrological analysis

In the hydrological analysis [46], the observed discharge of a gauged river basin can be applicable to monitor an ungauged river basin having comparable geographical characteristics and climate conditions. The selected reanalysis products were extracted from the Copernicus Climate Data Store (CDS) in the following platform (https://cds.climate.copernicus.eu/#!/home) accessed on: 27 July 2024). However, the reanalysis products are still coarser (around 5 Km), and a bias correction method was applied. A linear-regression-based bias correction was applied. We use a GloFAS reanalysis product to ensure the reliability of remote sensing discharge.

2.4. Observed data acquisition

In this study, a staff gauge was installed on the side of the railway bridge, close to the outlet of the Golina river. The gauge measures 2 meters long and is marked at every 0.1 meter. The surface flow velocity was determined using floating methods. The surface flow velocity varied vertically over time [47]. The vertical flow velocity profile was measured at 0.2, 0.6, and 0.8 of the cross-section's length. Surface velocities are typically higher than mean velocities [48]. The mean flow velocity was calculated using a correction factor of 0.85. The surface flow velocity and the mean velocity can be determined from the following equations (eq 3 and 4).

$$\text{Vsurface} = \frac{\text{travel distance}}{\text{travel time}} \quad (3)$$

$$\text{Vmean} = \text{kVsurface} \quad (4)$$

Where k is the coefficient.

The discharge data were collected at 16-day intervals from February 9, 2022, to July 8, 2024. The amount of water passing a specific point on the stream channel over a given time depends on both the velocity and the cross-sectional area of the flowing water, as described by the following equation (eq. 5).

$$Q = AVmean \quad 5$$

Where Q is stream discharge (m^3/s), A is cross-sectional area (m^2), and Vmean is the mean flow velocity (m/s). The stage-discharge relationships were developed using the rating curve equations [49]. This stage-discharge data was validated using the Area-Velocity method. Figure 4 illustrates the locations of the staff gauges and the determination of surface flow velocity at the Golina River.

A B

Figure 4: The location of staff gauging (A) and surface flow velocity determination (B).

We used the correlation coefficient (R), and root-mean-square error (RMSE) model performance indexes. The trend test was conducted using the Mann-Kendall trend test.

3. Results and Discussion

3.1. The MPR approach validation

Initially, the MPR approach was proposed by [18][1], which uses the NIR reflectivity ratio of permanent dry areas and river areas to monitor rivers. In this study, we found that the highest correlation between the observed discharge and the NIR reflectivity ratio in the river's upper reach is approximately 300 meters (or ten pixels) from the Addis-Alem station. Our findings indicate that discharge monitoring using the MPR approach is strongly correlated with river width. This study supports previous research that has primarily focused on monitoring large river discharges [50][14][51][29]. Figure 5 illustrates the surface reflectivity for the upper reach (300 m) and the lower reach (600 m), which is located farther from the gauging station.

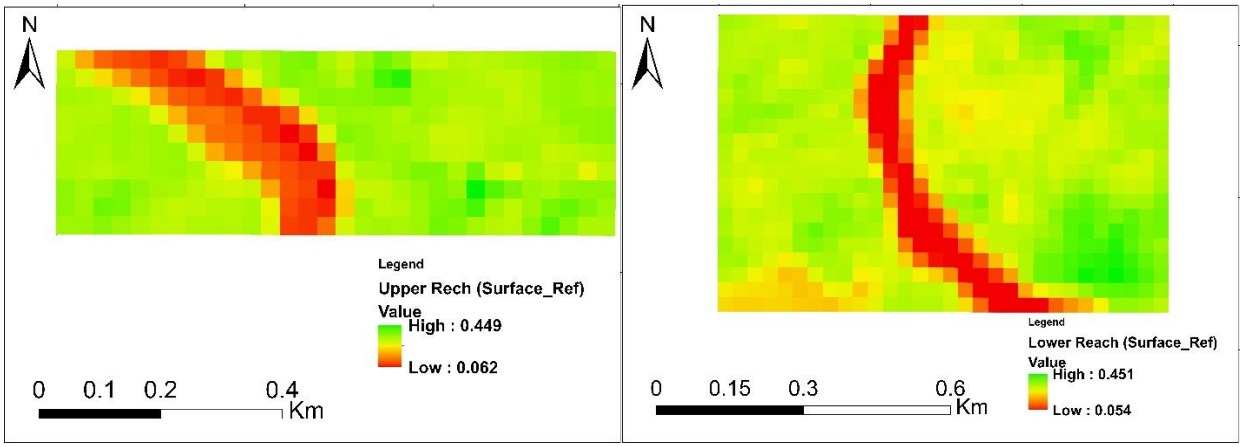

A B

Figure 5: Surface reflectivity for upper reach (A) and lower reach (B).

3.2. Golina River discharge rating curves

We developed a fitting equation that correlates the observed data from temporary gauging stations with satellite products for both the upper and lower reaches during the calibration period (2022-2024). The following equations (Eq 6 and 7) were derived using power law rating curve equations for the upper and lower reaches.

$$Qrs = 1.98 \times (P)^{3.01} \quad 6$$

$$Qrs = 1.86 \times (P)^{3.64} \quad 7$$

Figure 6 represents the statistical relationship of observed, GloFAS and remote sensing discharge.

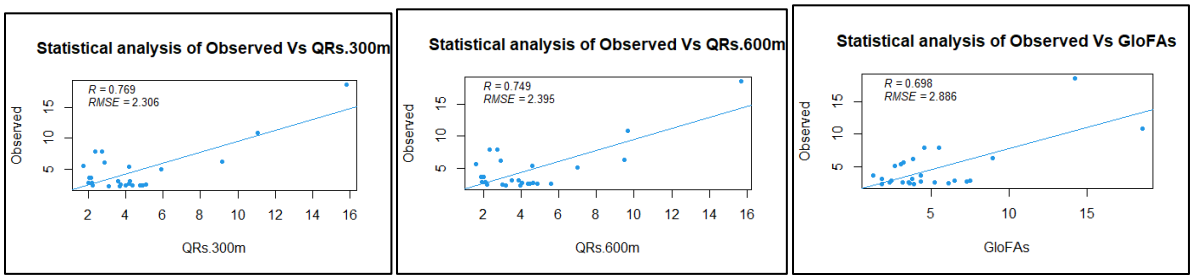

Figure 6: Statistical relationship of observed, GloFAS and remote sensing discharge (m^3/s).

The estimated equations were used to evaluate the discharge from remote sensing in the period 2013-2024. Figure 7 represents the calibration between observed, GloFAS and RS products.

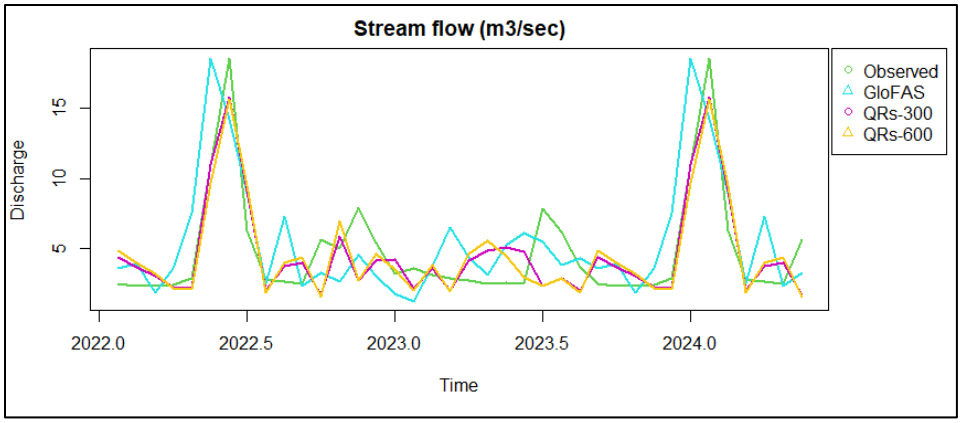

Figure 7: The calibration between observed, GloFAS and RS products.

Table 1 shows the fitting equation and its correlation of the observed and the remote sensing discharge at the different SIRC lengths.

Table 1: The fitting equation and correlation between the observed and the RS products.

	Length	Fitting equation	Correlation (R^2)	RMSE
Remote sensing discharge	Upper reach 300 m	$Qrs = 1.98 \times (P)^{3.01}$	0.77	2.306
Remote sensing discharge	Lower reach 600 m	$Qrs = 1.86 \times (P)^{3.64}$	0.75	2.395
GloFAs discharge	$0.05° \times 0.05°$	Bias corrected	0.70	2.886

The results of the trend test indicate that the amount of discharge product is decreasing over time. Figure 8 represents the remote sensing discharge and GloFAs (reanalysis) products in the multi-year.

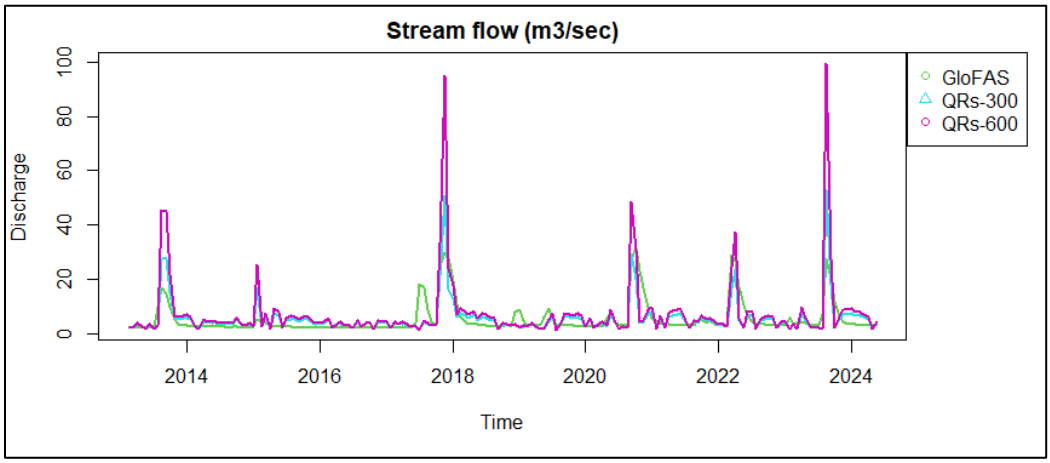

Figure 8: Remote sensing discharge and GloFAS (reanalysis) products.

3.3. MPR and GloFAS discharge comparison

The results obtained from the MPR are compared to the GloFAS data in the calibration year has a higher correlation. The MPR results are slightly higher in statistical measurement (Table 1) than the GloFAS. This study supports previous research that has primarily focused on monitoring river discharges using GloFAS [52][53][54][34]. A similar study by [35] stated that a 0.68 correlation coefficient was attained to determine the river discharge estimation methods from GloFAS products in the study valley.

3.4. Limitations of the study

The MPR approach cannot be applied to rectangular river channels with a fixed width because the differences in discharge are influenced by the observed river width. Additionally, the accuracy of gauging stations is often limited when measuring peak discharge during the flood season, leading to potential oversight of peak flood information. This oversight can affect the equations developed for observed discharge, potentially resulting in an underestimation of discharge from the MPR approach. The efficiency of monitoring is affected by sediment load. Additionally, the location, width, and length of the selected SRIC area have a substantial impact on our results. Furthermore, the reanalysis products have a coarser resolution of 5 kilometers.

4. Conclusions

Obtaining accurate hydrological data is essential for scientific studies. Satellite and reanalysis products are commonly used to monitor river systems. In the MPR (Multi-Pixel Ratio) approach, it is crucial to choose the appropriate permanent dry area and river width to accurately simulate river discharge. The river width, location, and SIRC (Satellite Imagery for River Channel) length are key limiting factors that affect the precision of river monitoring. The MPR method is particularly effective for monitoring rivers wider than 30 meters. It offers a viable alternative for river discharge monitoring in areas where gauging stations are no longer operational. Additionally, a 300-meter SIRC shows higher precision compared to a 600-meter SIRC at the riverbed below the gauging station. The results of the trend test indicate that the amount of discharge product is decreasing over time. The NIR reflectivity and GloFAS reanalysis products have been successfully implemented for effective monitoring of river discharge. However, low spatial resolution remains a significant limitation. We recommend that the MPR approach can be successfully applied to rivers wider than 30 meters. Enhancing the accuracy of river discharge monitoring during peak flood events will improve the fitting equations used in remote sensing discharge estimation.

References

A. W. Sichangi et al., “Estimating continental river basin discharges using multiple remote sensing data sets,” Remote Sens. Environ., vol. 179, pp. 36–53, 2016, doi: 10.1016/j.rse.2016.03.019.

H. Apel et al., “Statistical forecast of seasonal discharge in Central Asia using observational records: Development of a generic linear modelling tool for operational water resource management,” Hydrol. Earth Syst. Sci., vol. 22, no. 4, pp. 2225–2254, 2018, doi: 10.5194/hess-22-2225-2018.

B. Merz et al., “Floods and climate : emerging perspectives for flood risk assessment and management,” no. 2, pp. 1921–1942, 2014, doi: 10.5194/nhess-14-1921-2014.

D. Viviroli et al., “Climate change and mountain water resources: Overview and recommendations for research, management and policy,” Hydrol. Earth Syst. Sci., vol. 15, no. 2, pp. 471–504, 2011, doi: 10.5194/hess-15-471-2011.

S. Manfreda et al., “Advancing river monitoring using image-based techniques: challenges and opportunities,” Hydrol. Sci. J., vol. 69, no. 6, pp. 657–677, 2024, doi: 10.1080/02626667.2024.2333846.

S. Hishinuma, K. Takeuchi, and J. Magome, “Défis de l’analyse hydrologique pour le développement des ressources en eau dans les régions montagneuses semi-arides: Étude de cas en Iran,” Hydrol. Sci. J., vol. 59, no. 9, pp. 1718–1737, 2014, doi: 10.1080/02626667.2013.853879.

A. M. De Girolamo, A. Drouiche, G. F. Ricci, G. Parete, F. Gentile, and T. H. Debieche, “Characterising flow regimes in a semi-arid region with limited data availability: The Nil Wadi case study (Algeria),” J. Hydrol. Reg. Stud., vol. 41, no. November 2021, p. 101062, 2022, doi: 10.1016/j.ejrh.2022.101062.

D. M. Bjerklie, S. L. Dingman, C. J. Vorosmarty, C. H. Bolster, and R. G. Congalton, “Evaluating the potential for measuring river discharge from space,” J. Hydrol., vol. 278, no. 1–4, pp. 17–38, 2003, doi: 10.1016/S0022-1694(03)00129-X.

D. M. Bjerklie, “Estimating the bankfull velocity and discharge for rivers using remotely sensed river morphology information,” J. Hydrol., vol. 341, no. 3–4, pp. 144–155, 2007, doi: 10.1016/j.jhydrol.2007.04.011.

M. J. Tourian, C. Schwatke, and N. Sneeuw, “River discharge estimation at daily resolution from satellite altimetry over an entire river basin,” J. Hydrol., vol. 546, pp. 230–247, 2017, doi: 10.1016/j.jhydrol.2017.01.009.

H. McMillan, J. Freer, F. Pappenberger, T. Krueger, and M. Clark, “Impacts of uncertain river flow data on rainfall-runoff model calibration and discharge predictions,” Hydrol. Process., vol. 24, no. 10, pp. 1270–1284, 2010, doi: 10.1002/hyp.7587.

G. Robert Brakenridge et al., “Calibration of satellite measurements of river discharge using a global hydrology model,” J. Hydrol., vol. 475, pp. 123–136, 2012, doi: 10.1016/j.jhydrol.2012.09.035.

M. K. Mersel, L. C. Smith, K. M. Andreadis, and M. T. Durand, “Estimation of river depth from remotely sensed hydraulic relationships,” Water Resour. Res., vol. 49, no. 6, pp. 3165–3179, 2013, doi: 10.1002/wrcr.20176.

P. A. Garambois and J. Monnier, “Inference of effective river properties from remotely sensed observations of water surface,” Adv. Water Resour., vol. 79, pp. 103–120, 2015, doi: 10.1016/j.advwatres.2015.02.007.

H. Lou et al., “Combining and comparing an unmanned aerial vehicle and multiple remote sensing satellites to calculate long-term river discharge in an ungauged water source region on the Tibetan plateau,” Remote Sens., vol. 12, no. 13, 2020, doi: 10.3390/rs12132155.

Y. Xue, C. Qin, B. Wu, D. Li, and X. Fu, “Automatic Extraction of Mountain River Surface and Width Based on Multisource High-Resolution Satellite Images,” Remote Sens., vol. 14, no. 10, 2022, doi: 10.3390/rs14102370.

A. Tarpanelli, S. Barbetta, L. Brocca, and T. Moramarco, “River discharge estimation by using altimetry data and simplified flood routing modeling,” Remote Sens., vol. 5, no. 9, pp. 4145–4162, 2013, doi: 10.3390/rs5094145.

A. Tarpanelli et al., “Toward the estimation of river discharge variations using MODIS data in ungauged basins,” Remote Sens. Environ., vol. 136, pp. 47–55, 2013, doi: 10.1016/j.rse.2013.04.010.

L. C. Smith and T. M. Pavelsky, “Estimation of river discharge, propagation speed, and hydraulic geometry from space: Lena River, Siberia,” Water Resour. Res., vol. 44, no. 3, pp. 1–11, 2008, doi: 10.1029/2007WR006133.

D. Spada, P. Molinari, W. Bertoldi, A. Vitti, and G. Zolezzi, “Multi-temporal image analysis for fluvial morphological characterization with application to Albanian rivers,” ISPRS Int. J. Geo-Information, vol. 7, no. 8, 2018, doi: 10.3390/ijgi7080314.

Z. Du et al., “Estimating surface water area changes using time-series Landsat data in the Qingjiang River Basin, China,” J. Appl. Remote Sens., vol. 6, no. 1, p. 063609, 2012, doi: 10.1117/1.jrs.6.063609.

D. Feng, C. J. Gleason, X. Yang, and T. M. Pavelsky, “Comparing Discharge Estimates Made via the BAM Algorithm in High-Order Arctic Rivers Derived Solely From Optical CubeSat, Landsat, and Sentinel-2 Data,” Water Resour. Res., vol. 55, no. 9, pp. 7753–7771, 2019, doi: 10.1029/2019WR025599.

A. Asadzadeh Jarihani, J. N. Callow, K. Johansen, and B. Gouweleeuw, “Evaluation of multiple satellite altimetry data for studying inland water bodies and river floods,” J. Hydrol., vol. 505, pp. 78–90, 2013, doi: 10.1016/j.jhydrol.2013.09.010.

H. Lin et al., “Discharge Estimation With Improved Methods Using MODIS Data in Greenland: An Application in the Watson River,” IEEE J. Sel. Top. Appl. Earth Obs. Remote Sens., vol. 15, pp. 7576–7588, 2022, doi: 10.1109/JSTARS.2022.3204544.

A. Tarpanelli, E. Santi, M. J. Tourian, P. Filippucci, G. Amarnath, and L. Brocca, “Daily River Discharge Estimates by Merging Satellite Optical Sensors and Radar Altimetry Through Artificial Neural Network,” IEEE Trans. Geosci. Remote Sens., vol. 57, no. 1, pp. 329–341, 2019, doi: 10.1109/TGRS.2018.2854625.

H. Meresa, “Modelling of river flow in ungauged catchment using remote sensing data: application of the empirical (SCS-CN), Artificial Neural Network (ANN) and Hydrological Model (HEC-HMS),” Model. Earth Syst. Environ., vol. 5, no. 1, pp. 257–273, 2019, doi: 10.1007/s40808-018-0532-z.

Q. Huang, D. Long, M. Du, Z. Han, and P. Han, “Daily Continuous River Discharge Estimation for Ungauged Basins Using a Hydrologic Model Calibrated by Satellite Altimetry: Implications for the SWOT Mission,” Water Resour. Res., vol. 56, no. 7, pp. 0–1, 2020, doi: 10.1029/2020WR027309.

Y. Li, S. Grimaldi, V. R. N. Pauwels, and J. P. Walker, “Hydrologic model calibration using remotely sensed soil moisture and discharge measurements: The impact on predictions at gauged and ungauged locations,” J. Hydrol., vol. 557, pp. 897–909, 2018, doi: 10.1016/j.jhydrol.2018.01.013.

H. Li, H. Li, J. Wang, and X. Hao, “Extending the Ability of Near-Infrared Images to Monitor Small River Discharge on the Northeastern Tibetan Plateau,” Water Resour. Res., vol. 55, no. 11, pp. 8404–8421, 2019, doi: 10.1029/2018WR023808.

Z. Yu, J. Wu, H. Yao, X. Chen, and Y. Cai, “Calibrating a hydrological model in ungauged small river basins of the northeastern Tibetan Plateau based on near-infrared images,” J. Hydrol., vol. 618, no. August 2022, p. 129158, 2023, doi: 10.1016/j.jhydrol.2023.129158.

Z. Shi, Y. Chen, Q. Liu, and C. Huang, “Discharge estimation using harmonized landsat and sentinel-2 product: Case studies in the murray darling basin,” Remote Sens., vol. 12, no. 17, pp. 1–12, 2020, doi: 10.3390/rs12172810.

H. N. Yoon, L. Marshall, A. Sharma, and S. Kim, “Bayesian Model Calibration Using Surrogate Streamflow in Ungauged Catchments,” Water Resour. Res., vol. 58, no. 1, pp. 1–19, 2022, doi: 10.1029/2021WR031287.

L. Liu, L. Zhou, M. Gusyev, and Y. Ren, “Unravelling and improving the potential of global discharge reanalysis dataset in streamflow estimation in ungauged basins,” J. Clean. Prod., vol. 419, no. April, p. 138282, 2023, doi: 10.1016/j.jclepro.2023.138282.

S. Miguel, R. Basin, and E. Salvador, “Evaluating the Potential of GloFAS-ERA5 River Discharge Reanalysis Data for Calibrating the SWAT Model in the Grande,” Remote Sens., vol. 13, no. 3299, pp. 1–20, 2021.

B. Z. Abate, T. T. Assefa, T. B. Tigabu, W. B. Abebe, and L. He, “Hydrological Modeling of the Kobo-Golina River in the Data-Scarce Upper Danakil Basin, Ethiopia,” Sustain., vol. 15, no. 4, 2023, doi: 10.3390/su15043337.

S. Harrigan et al., “GloFAS-ERA5 operational global river discharge reanalysis 1979-present,” Earth Syst. Sci. Data, vol. 12, no. 3, pp. 2043–2060, 2020, doi: 10.5194/essd-12-2043-2020.

S. Harrigan, E. Zsoter, H. Cloke, P. Salamon, and C. Prudhomme, “Daily ensemble river discharge reforecasts and real-time forecasts from the operational Global Flood Awareness System,” Hydrol. Earth Syst. Sci., vol. 27, no. 1, pp. 1–19, 2023, doi: 10.5194/hess-27-1-2023.

L. Alfieri et al., “GloFAS-global ensemble streamflow forecasting and flood early warning,” Hydrol. Earth Syst. Sci., vol. 17, no. 3, pp. 1161–1175, 2013, doi: 10.5194/hess-17-1161-2013.

C. Prudhomme et al., “Global hydrological reanalyses: The value of river discharge information for world-wide downstream applications – The example of the Global Flood Awareness System GloFAS,” Meteorol. Appl., vol. 31, no. 2, pp. 1–23, 2024, doi: 10.1002/met.2192.

G. Nearing et al., “Global prediction of extreme floods in ungauged watersheds,” Nature, vol. 627, no. 8004, pp. 559–563, 2024, doi: 10.1038/s41586-024-07145-1.

R. L. Bain, M. J. Shaw, M. P. Geheran, A. A. Tavakoly, M. D. Wahl, and E. Zsoter, “Intercomparison of global ERA reanalysis products for streamflow simulations at the high-resolution continental scale,” J. Hydrol., vol. 616, no. December 2021, 2023, doi: 10.1016/j.jhydrol.2022.128624.

H. Hersbach et al., “The ERA5 global reanalysis,” Q. J. R. Meteorol. Soc., vol. 146, no. 730, pp. 1999–2049, 2020, doi: 10.1002/qj.3803.

M. Tesfaw, T. Assefa Nigussie, and S. Tekleab, “Analysis of Groundwater Flow Modelling: The Case of Hormat-golina Sub-basin, Golina Basin, Ethiopia,” Hydrology, vol. 9, no. 2, p. 48, 2021, doi: 10.11648/j.hyd.20210902.13.

M. I. Alfa, D. B. Adie, M. A. Ajibike, and O. J. Mudiare, “Development of rating curve for Ofu River at Oforachi Hydrometric Station,” Niger. J. Technol. Dev., vol. 15, no. 1, p. 14, 2018, doi: 10.4314/njtd.v15i1.3.

M. A. Dwiputra and A. Mustofa, “The Comparison of RGB 564 and RGB 573 Band Composite of Landsat 8 for Mangrove Vegetation Distribution Identification on Pahawang Island, Lampung,” IOP Conf. Ser. Earth Environ. Sci., vol. 830, no. 1, 2021, doi: 10.1088/1755-1315/830/1/012017.

A. Tarpanelli, G. Amarnath, L. Brocca, C. Massari, and T. Moramarco, “Discharge estimation and forecasting by MODIS and altimetry data in Niger-Benue River,” Remote Sens. Environ., vol. 195, pp. 96–106, 2017, doi: 10.1016/j.rse.2017.04.015.

T. Moramarco, S. Barbetta, and A. Tarpanelli, “From surface flow velocity measurements to discharge assessment by the entropy theory,” Water (Switzerland), vol. 9, no. 2, 2017, doi: 10.3390/w9020120.

Y. C. Chen, Y. C. Hsu, and E. O. Zai, “Streamflow Measurement Using Mean Surface Velocity,” Water (Switzerland), vol. 14, no. 15, 2022, doi: 10.3390/w14152370.

M. Rojas, F. Quintero, and N. Young, “Analysis of stage-discharge relationship stability based on historical ratings,” Hydrology, vol. 7, no. 2, 2020, doi: 10.3390/HYDROLOGY7020031.

A. Tarpanelli, S. Camici, K. Nielsen, L. Brocca, T. Moramarco, and J. Benveniste, "Potentials and limitations of Sentinel-3 for river discharge assessment," Adv. Sp. Res., vol. 68, no. 2, pp. 593–606, 2021, doi: 10.1016/j.asr.2019.08.005.

J. W. Fulton et al., "Near-Field Remote Sensing of Surface Velocity and River Discharge Using Radars and the Probability Concept at 10 U . S . Geological Survey Streamgages".

H. Hooker, S. L. Dance, D. C. Mason, J. Bevington, and K. Shelton, "A multi-system comparison of forecast flooding extent using a scale-selective approach," Hydrol. Res., vol. 54, no. 10, pp. 1115–1133, 2023, doi: 10.2166/nh.2023.025.

G. Passerotti, G. Massazza, A. Pezzoli, V. Bigi, E. Zsótér, and M. Rosso, "Hydrological model application in the Sirba river: Early warning system and GloFAS improvements," Water (Switzerland), vol. 12, no. 3, 2020, doi: 10.3390/w12030620.

F. A. Hirpa et al., "Calibration of the Global Flood Awareness System (GloFAS) using daily streamflow data," J. Hydrol., vol. 566, no. March, pp. 595–606, 2018, doi: 10.1016/j.jhydrol.2018.09.052.

Mountain Block Driven Groundwater Recharge in the Marginal Graben Area: the Case of Raya Valley, Northern Ethiopia

Asmelash Tilahun*[1, 2], Dessie Nedaw[3], Taye Alemayehu[1], Tenalem Ayenew[3], GebreRufael Hailu[4], Dawit Berhane[5], Merhawi GebreEgziabher[6]

[1]College of Technology and Built Environment, Addis Ababa University P.O. Box 1176, Ethiopia,

[2]School of Water Technology, Shire Campus, Aksum University, Ethiopia,

[3]School of Earth Science, Addis Ababa University, Addis Ababa P.O. Box 1176, Ethiopia,

[4]Institute of Geo-information and Earth Observation Sciences, Department of Geo-information and Earth Observation Sciences for Natural Resource Management, Mekelle University, Ethiopia

[5]New South Wales Office of Water, Gunnedah, New South Wales, Australia,

[6]Bren School of Environmental Science and Management, University of California, Santa Barbara, USA.

* Corresponding Author: ashueg@gmail.com

Abstract

Groundwater recharge is a vital component of the hydrological cycle and impacts the accessibility, allocation, and sustainable use of groundwater resources for water supply, irrigation, and industries. However, estimating groundwater recharge remains challenging due to climate variability and limited hydrological and hydrogeological data availability. Groundwater recharge investigations in mountain block and mountain front settings are critical as the recharge mechanism is highly determined by topography, precipitation characteristics, and heterogeneity of unsaturated and saturated zones. Here, we presented a comprehensive approach to understand the spatial distribution of recharge and the conceptualization of recharge mechanisms in the Raya Valley Aquifer System, in Ethiopia. The isotope hydrogeological, hydrogeochemical, well hydraulic, and hydrological data were compiled to understand the recharge mechanism and estimate recharge by considering the mountain blocks and linkage to the lowland graben alluvial deposits. The hydrochemistry data reveal the quaternary formation-dominated aquifer systems, and the mountain blocks depict a geochemical evolution signature dominated by Mg-HCO_3 ≥ mixed ≥ Na-HCO_3 ≥ NaCl waters along the groundwater flow. The evidence of the percentage of modern carbon isotope (carbon-14) and stable water isotopes (δ2H and δ18O) revealed the western and eastern mountain blocks receive recent recharge through direct rainfall infiltration both in the humid mountain blocks and arid lowlands. These methods highlight the alluvial valley recharges during intense rainfall event-based runoff on the western highlands, causing flooding and intermittent stream flow as mountain front recharge and seeping water of the mountain blocks through the basaltic volcanic via fractures and faults toward the valley alluvial floor. The estimated groundwater recharge using the water balance and chloride mass balance (CMB) methods showed that the western mountain blocks receive the highest annual rate, amounting to 73 mm and 106 mm, respectively. The groundwater flows from the western and eastern flanks towards the graben zone, then a cumulative flow in the southeastern direction heads to the Afar depression. This study highlights that the need for sustainable groundwater uses for irrigation and water supply requires adequate estimation of groundwater recharge and conceptualizing the recharge mechanisms.

Keywords: *Mountain block, Groundwater recharge, hydrogeochemical, Hydrogeological*

1. Introduction

Understanding the groundwater dynamics in mountainous landscape and associated valleys is important for planning sustainable water use[1], especially in areas where groundwater-dependent irrigation projects takes the prominent role in achieving food independency, the impact of unregulated and mismanaged exploitation is pronounced[2]. This may discourage legal agricultural investments, backing community based and private groundwater misuses, then policy makers will unable to manage and develop sustainably[3]. The varying topographic nature of Ethiopia and hydro-geological settings could make the groundwater resource to be influenced by climate variability, rainfall characteristics and land use/cover changes as a function of time and across space[4–9]. In mountain blocks and mountain fronts, understanding the source and mechanism of groundwater recharge has got the attentions of researchers in different regions of the globe[9,10]. Different approaches have been practiced for water budget components assessment, essentially the groundwater recharge, conversely depends on the hydrogeological setting, hydro-meteorological condition, data requirement and availability[11]. In Ethiopia, the state and non-state actors on groundwater-based irrigation practices, particularly in the Raya valley basin, made the area an irrigation corridor of the region[1,17]. Nevertheless, the groundwater inadequacy and usage along with the rising water demands is fundamental and could impact the groundwater sustainability[18], dulling the struggle for food independence amidst the national food insecurity concern, which is being reflected higher than the domestic water demand and supply gap.

Moreover, urbanization and agricultural development centered projects in the Raya valley has been expanding periodically[19], impacting the quality and quantity of the groundwater resources[20,21], where its availability for planned water development demands is becoming uncertain. Accordingly, it is imperative to comprehend precisely the linkage between the upland water sources, the mountain block, the valley potential zones, the mountain fronts, and the hydrogeochemical water types for sustainable and improved groundwater resources usages. Thus, the necessity of a comprehensive and coherent data driven study that optimizes the application of available field data for solving on-ground problems is considered in this work. The study details the hydrodynamics of the groundwater resource across mountain blocks, connected compartments, and mountain fronts. It further outlines the estimated recharge rates and mechanisms, along with the hydrogeochemical conditions and their evolution, and acknowledges the significant contributions of numerous researchers in establishing the foundational groundwater-related data for the area[1,7,19,20,22–25].

2. Material and Method

2.1. Study Area

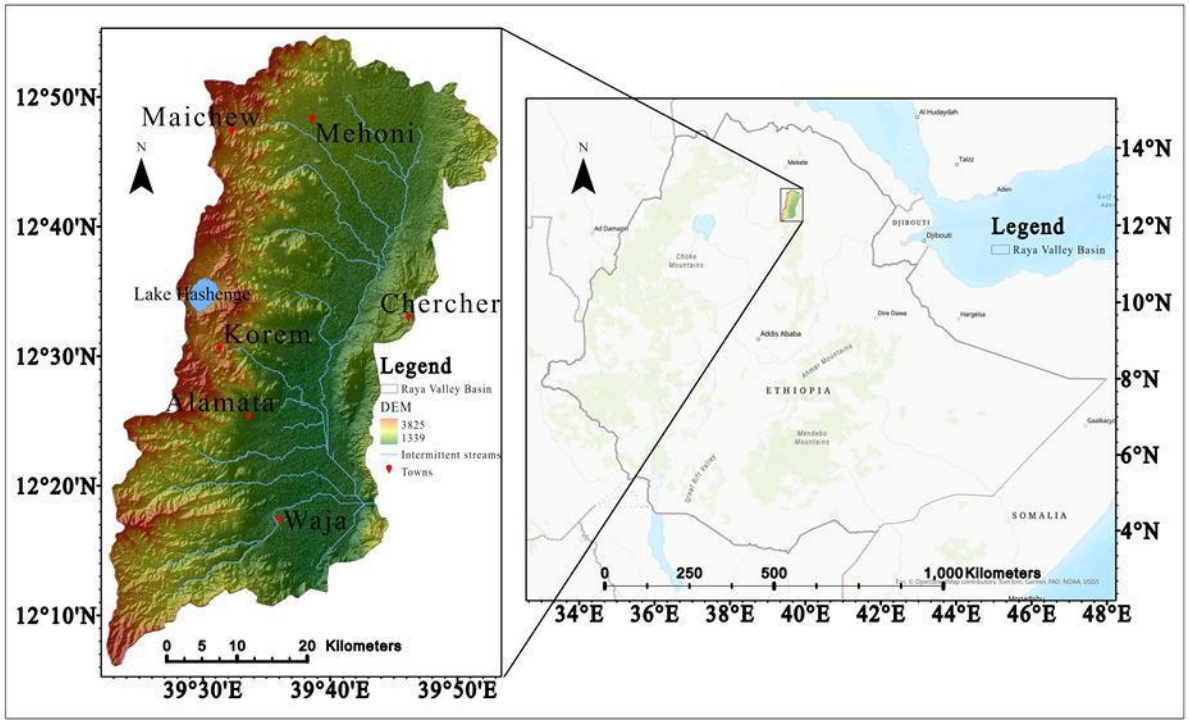

Figure 1: The Raya valley basin is located in the northern part of Ethiopia

This area bounded by Maichew mountains in the north, central Ethiopian highlands in the west, Chercher mountains in the east, and Waja village in the south, with a total area of 2653 km^2. Geomorphologically the western highland is predominantly volcanic rocks and valley floor is recent unconsolidated to semi-consolidated formation. The Eastern highland composed of various rock formations.

2.2. Hydrogeological Setting

The study area exhibits a diverse geological setting characterized by Precambrian meta-dunite and meta-pyroxenite having low-permeability basement rocks, jointed Mesozoic Antalo Limestone possessing fracture-controlled aquifer, and friable Amba Aradam sandstone characterized as porous aquifer[1,17,20]. Quaternary alluvial and fluvio-lacustrine deposits in the central valley form productive multilayered aquifers, with thickness and grain size ranging from gravel to clay decreasing westward, while floodplain sediments act as aquicludes. Tertiary-Quaternary basaltic volcanics, the Ashange formation, dominantly found in the western and eastern highlands, where fracturing and weathering create high-recharge zones, evidenced by springs. Colluvial deposits along the western escarpment and inter-fluvial sediments further contribute to groundwater storage, though productivity varies spatially, with the highest yields in coarse-grained alluvium and fractured volcanics. Lake Hashange's unconsolidated margins and the valley's structural compartments, the Western and Eastern highlands and central valley define distinct groundwater flow regimes[5,47].

2.3. Methods

2.3.1. Data compilation

A daily record of operating meteorological stations collected from the national meteorological agency of Ethiopia, consisting of one or more meteorological parameters was considered. The Ethiopian Ministry of Water Resources, the Ethiopian Institute of Geological Survey (EIGS), the Relief Society of Tigray (REST), and the Tigray Regional Water Resources Bureau (TRWRB) were sources of the water quality and lithological log data, in addition to the pre-existing technical reports on hydrogeological conditions of the study area. The stable and radioactive water isotope compositions were collected from the database of the Ethiopian Ministry of Water Resources and the Ethiopian Institute of Geological Survey technical report[26]; where manual extraction with visual inspection techniques was used to trace the sampling site locations. Generally, two hundred sixty data points of transmissivity and hydraulic conductivity and ninety-nine stable water isotope (δ^2H and $\delta^{18}O$) compositions, collected from different water types, were considered for this study. The water samples for the stable isotope composition were labeled based on the sampled water type and sampling site; and the samples were represented as fourteen rainfalls, sixty borehole waters, twelve hand-dug waters, seven spring waters, two lake waters, two samples from stream flow, one from swamp, and one from flood water. Moreover, thirteen groundwater samples for the percentage modern carbon (carbon-14), one hundred ninety-nine static water level data points, two hundred seventy-six hydrochemical data, one hundred fifty-five lithological logs, and twenty-three chloride concentration data were assembled for this work after being checked for data quality standards.

2.3.2. Water isotope composition and hydrochemistry analysis

The stable isotope of water (deuterium and oxygen-18) collected and analyzed following scientific analytical procedures and labeled as per the water types[26,27]. The stable isotope concentrations were measured as a ratio of the rare to the abundant isotope and expressed as the difference in this ratio between the sample and a known reference as per VSMOW. Moreover, data of IAEA/WMO stations found in different parts of Ethiopia were combined for a concise and particular understanding of the isotopic nature of Raya Valley waters relative to the national meteoric water line. Besides, the thirteen radioactive water isotopes (carbon-14) of groundwater were collected and integrated with complementary data[26,27].

The hydrochemical data collected was further screened based on the purpose and data quality requirement of this work. Water samples were collected from locations across the alluvial valley and the highland mountain blocks; the measured ion concentrations were checked. Considering 10% as the threshold, 274 samples are screened and used for this purpose.

2.3.3. Groundwater Indications

2.3.3.1. Groundwater Flow and Hydrogeochemical Status

The cation and anion concentrations of the groundwater samples were used to prepare piper diagram aiming to recognize the origin and hydrogeochemical evolutions of the Raya valley groundwater resources. The electrical conductivity parameter as water quality and salinity indicator was used along the piper plot and corresponding lithological formations. The temperature effect was neglected as the mean temperature of the Raya valley groundwater is same as the default value, 25^{o}c, but the measured PH value was considered[1].

A joint implications of static water level, electrical conductivity, percentage of modern carbon (carbon-14) in the groundwater resource, and composition of $\delta^{18}O$, and associated change in the waters of the mountain blocks and mountain fronts were used to describe groundwater flow and accumulations[16,28]. The groundwater residence time from the percentage of modern carbon content (carbon-14) indicates the possible flow paths across the hydrogeological setting and groundwater accumulations[26]. The spatial representativeness of the groundwater data samplings in central valley, the groundwater potential zone, and varying hydro-geologic settings were comprehended for the rationale of this work. Moreover; previous groundwater sampling campaigns for $\delta^{18}O$ water isotopes and hydrogeological investigation of the area[27], and other groundwater related data such as the static water level and electrical conductivity were amassed and incorporated. The integrated retrospective source and flow[27], interpreting the percentage of carbon-14 content mainly in the Raya graben[26], was implemented. Thus, cross-sectional profiling approach was adopted to produce a broader image of groundwater flow directions and accumulations.

2.3.3.2. Groundwater Recharge

The groundwater recharge sources and mechanism were explained based on water isotopic compositions collected and analyzed from different sources in the wet and dry months; such as surface water, lake water, and wells. The stable isotopic composition of deuterium ($\delta^{2}H$) and heavy oxygen ($\delta^{18}O$) in each sample as analyzed in a laboratory and expressed relative the international standard mean ocean water (SMOW). This approach has the advantage of exploring groundwater recharging sources and mechanism minimizing the uncertainty in zones demonstrating little recharges, and is recommended in arid and semi-arid areas[29]. The CMB and water balance approaches were applied to estimate the groundwater recharge in the plain area and interconnected highland. The samples were collected from the central alluvial valley, eastern and western compartments from rainfall, wells and lake Hashenge waters. The residence time of surface flowing from the head water, the mountain blocks, to plain areas was considered small[30]; implying chloride concentration of the recharging flood water could be equivalent to groundwater in the lowland.

3. Result and Discassion

3.1. Results

3.1.1. Isotope of WATERS

The spatiotemporal variability of stable water isotopes ($\delta^{18}O$ and $\delta\ ^{2}H$) signatures across Ethiopia doesn't depict a linear pattern, which could due to variations in climatological, seasonal, and topographical features [add citation]. The IAEA/WMO stations indicated that the seasonal weighted mean of $\delta^{18}O$ compositions was 2.02 (summer), -0.51 (fall), 0.08 (winter), and 0.07 (spring); while the $\delta^{2}H$ indicator similarly revealed -2.55 (summer), 9.77 (fall), 13.64 (winter), and 13.29 (spring) expressed in per mil (‰) and the $\delta^{18}O$ versus $\delta^{2}H$ relationship showed positive correlation with Pearson correlation, r = 0.95. Likewise, the rainwaters in the Raya valley has ranged (-7.61 to 0.88)‰ and (-45.19 to 14.12)‰ respectively for $\delta^{18}O$ and $\delta^{2}H$ compositions. And, the average isotopic compositions and median were found -2.68 ‰ and -2.64 ‰ for $\delta^{18}O$ and - 6.83 ‰ and -6.21 ‰ for $\delta^{2}H$, respectively. This indicates mostly the Raya valley basin is characterized by depletion in isotopic signatures of $\delta^{18}O$ and $\delta\ ^{2}H$, which means the rainwater wasn't broadly open to overriding direct evaporation regardless of the existing spatial variabilities. Although the $\delta^{18}O$ and $\delta^{2}H$ isotopic composition differences have been observed among rainfall samples, resembled to the national LMWL, Ethiopia, defined by: $\delta^{2}H = 7.4*\delta^{18}O + 11.4‰$, $R^2 = 0.95$ and r = 0.95. Furthermore, the d-excess parameter of the rainfall samples gathered in the study area ranges from 1.63‰ to 22.34‰. The water samples gathered from boreholes, hand-dug wells, and spring water resources were used to infer groundwater recharge condition; and the $\delta^{18}O$ and $\delta^{2}H$ compositions were positively correlated with r = 0.85 and resemble the LMWL. The $\delta^{18}O$ and $\delta^{2}H$ relationship shown proper fit with the regression line, given as: $^{2}H = 5.92\ ^{18}O + 5.83‰$, ($R^2 = 0.72$). The samples collected of all water types showed similar trend with the local meteoric water line (LMWL), which implies water of local meteoric origin.

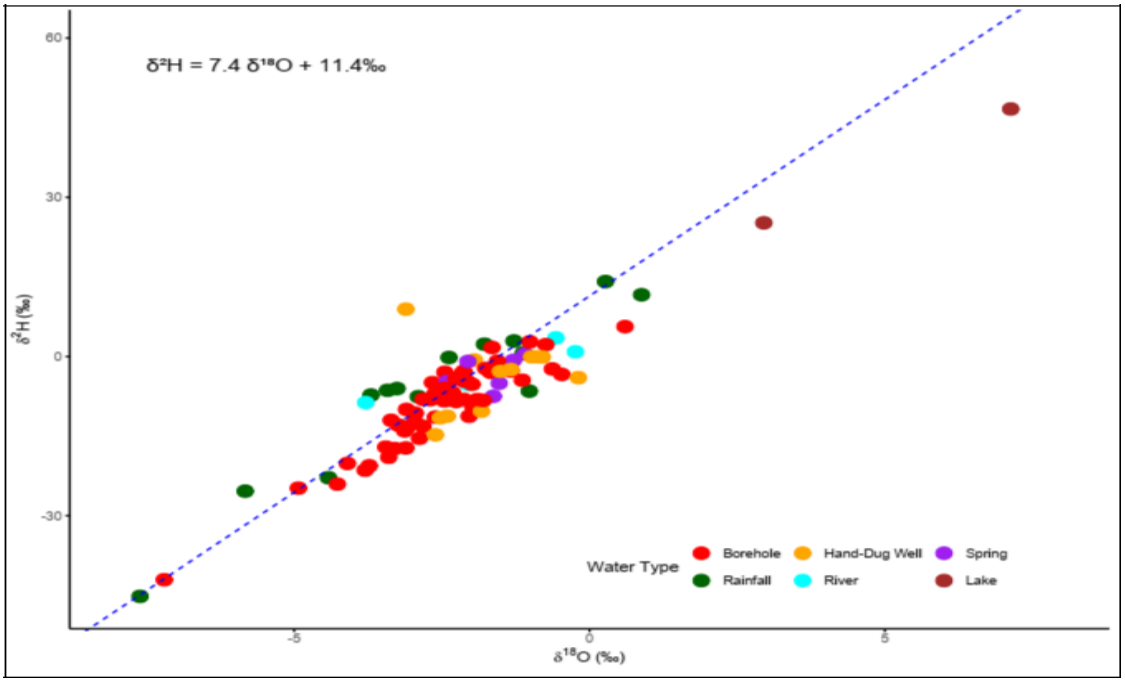

Figure 2: The isotopic composion ($\delta^{18}O$ and $\delta^{2}H$) of sampled water types) and LMWL

3.2.1. Hydrogeochemistry

The hydrochemical analysis of the groundwater samples are plotted on a Piper trilinear diagram (Figure 3). In essence, water samples from the quaternary sediment sources, more expressed in the central valley, have a bicarbonate source; however, some samples indicate a calcium type, and sodium, potassium and magnesium types. The samples collected from Hashenge formation marked all a bicarbonate source of water, but they have calcium dominant cations, and some with sodium and potassium sources. The samples obtained from the Fursa formation showed mostly sodium and potassium source types, and with no dominant anion. The quaternary lithological formations revealed magnesium bicarbonate waters, although exceptional samples identified mixed and sodium bicarbonate waters. However, the Fursa lithological formation has sodium chloride waters. Similarly, the Hashenge formation has mostly sodium bicarbonate water types next to magnesium bicarbonate. Generally, it reveals that though most of the water samples showed no dominant cations; Ca^{2+} is found expressively higher than Mg^{2+} and (Na^{+}, K^{+}). Likewise, the carbonates ($CO3^{2-}$, HCO3) were found more expressed then Cl^{-} and $SO4^{2+}$. Most of the samples collected from the quaternary geologic formation dominantly found in the central valley lied in the magnesium bicarbonate zone and some in sodium bicarbonate water types.

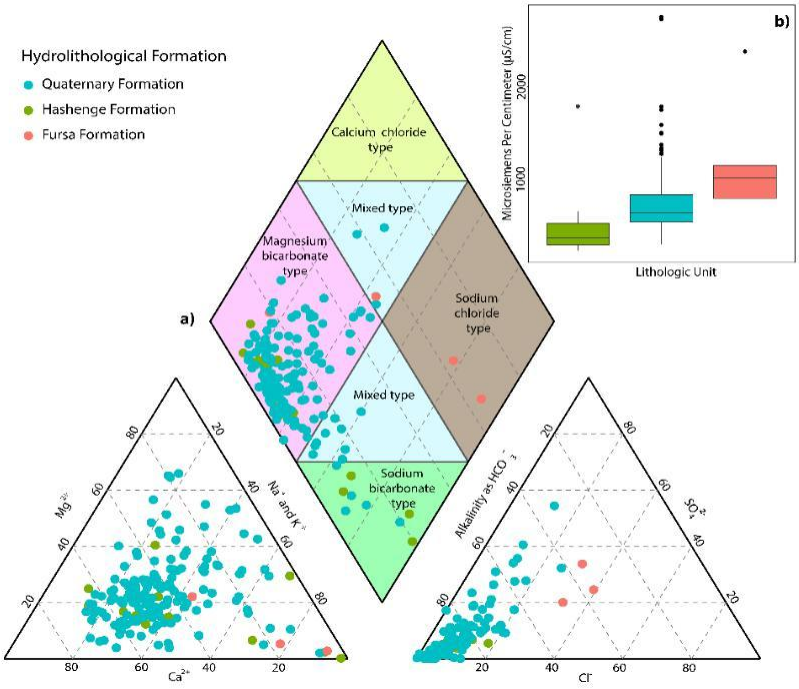

Figure 3: a) Piper diagram and b) box plot

In Figure 3: a) indicates the Piper diagram through which the hydrogeochemical composition and type of waters in the Raya valley basin was identified; where the anion composition is dominated by alkalinity as $HCO3^{-1}$ whereas percentage composition of most of the cations are below 50. While b) states box plot of the electrical conductivity of the waters as arranged based on their median value. The electrical conductivity of the quaternary, Hashenge, and Fursa formations ranges from 239 µS/cm to 2730 µS/cm, (1776 to 308) µS/cm, and (2360 to 446) µS/cm, respectively, while their corresponding analytical variables of mean and median were (744.8, 641) µS/cm, (501.4, 391.5) µS/cm, and (1031.7, 878) µS/cm.

3.2.3. Groundwater Recharge

The variability in $\delta^{18}O$ and $\delta^{2}H$ compositions in the volcanic highlands (western and eastern) and central alluvial valley compartments indicates the controlling hydroclimatological response through the hydrogeological settings. The subsurface seepage over the volcanic mountains tracing associated faults and fractures as mountain block-driven mountain front recharge, flash flooding, and rainfall through direct infiltration were identified as the dominant sources and mechanisms of groundwater recharge. The groundwater recharge occurs dominantly in the months of July and August following the rainy seasons. The chloride mass balance (CMB) approach revealed that the highest mountain front recharge (MFR) was in the wester highlands, estimated to be 106 mm/year; and the groundwater recharge in the eastern mountain blocks and central alluvial valley was similarly approximated to be 57 mm/year. The water balance approach indicated the mountain block recharge in the western highlands was estimated to be about 73 mm/year. And, the recharge in the eastern part and alluvial valley was 81mm/year and 66mm/year respectively; in addition to the flash flooding that could be generated from the western escarpments to the plain area.

3.2.4. Groundwater Flows and Accumulations

The groundwater flows through the western and eastern volcanic highlands towards the alluvial valley, and exits in south-eastern part of the study area; ensuing the course of routing and accumulations. The real-time rainfall characteristics, especially in the rugged topography and associated geologic settings, influences the groundwater depth. Generally, the peizometric surface exhibits a decreasing trend toward the quaternary alluvial valley compared to the western and eastern highlands, suggesting that groundwater flows to the central graben area, where groundwater-based irrigation development is commonly practiced. Moreover, the shallow groundwater depth in the swampy area around Gerjale, varying to one hundred (100) meters in the mountain fronts and central valley; then the groundwater interacts with various water source and geologic formation along the flow direction toward the outlet, Selen-Wuha, in the southeastern of the groundwater aquifer boundary. Similarly, the groundwater flow direction in the Alamata area is predominantly from West-East direction towards the Afar rift through Selen-Wuha.

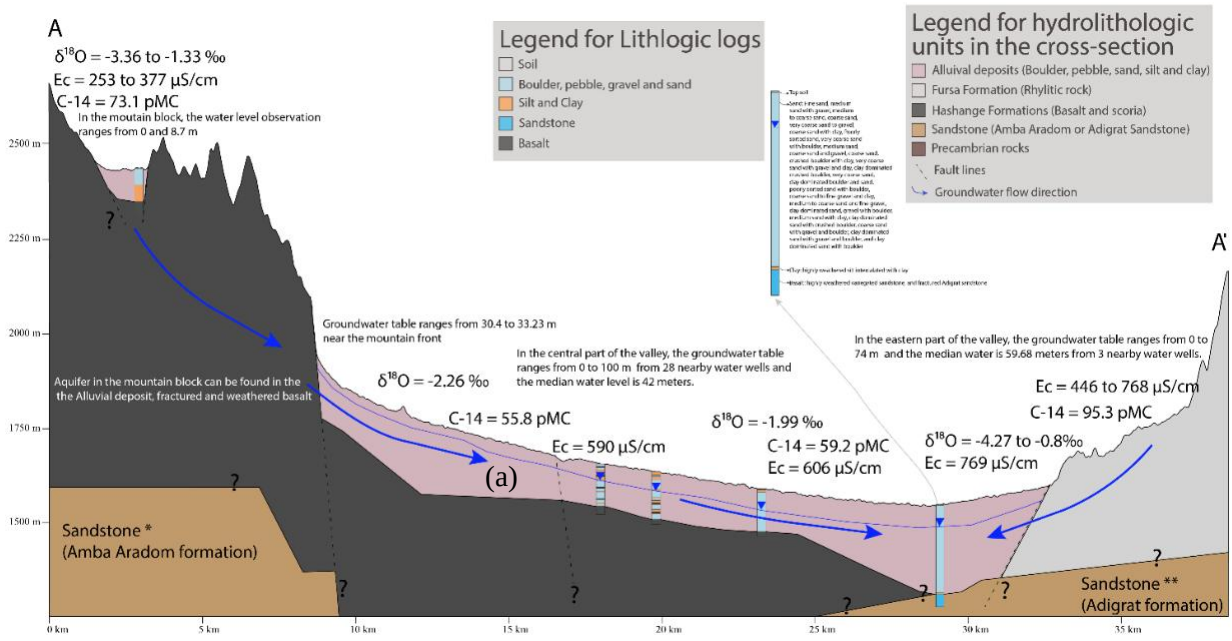

Figure 3: Groundwater flow direction in the Raya valley hydrogeological setting:

The profile line A-A' transects the western mountain blocks of northern area to the eastern counterpart and showed the groundwater flows from the western and eastern blocks draining into the plain valley following the alluvial graben.

3.2. Discussion

Hydrogeochemical and physiochemical data help explain groundwater flow direction, potential rock-water interactions, and the recharge rate and mechanisms. In the western highlands, low total dissolved solutes and a geochemical signature is dominated by Mg and Ca–HCO_3 indicate recent recharge with minimal rock-water interaction. However, along the flow path, increasing dissolved solutes and a shift toward Na–HCO_3 dominance reveal stronger rock-water interactions. Additionally, the groundwater system contains mixed and Na–Cl water types which were not yet addressed in previous works[23].

In line with studies conducted in the region, the stable isotope content of water samples collected from boreholes, hand-dug wells, springs, rivers, and lakes in the central valley and highlands suggested a local meteoric origin (LMWL); where groundwater recharge was largely from rainfall direct infiltration after some fractionation in the rainy seasons[33,34]. The groundwater samples collected in the western and eastern mountain blocks were found significantly depleted in $\delta^{18}O$ and $\delta^{2}H$ relative to the quaternary alluvial valley that were moderately enriched, implying recent groundwater recharge in the mountain blocks and has been the source of moisture through surface flooding and groundwater seepage, mainly the western mountains. Moreover, isotopic enrichment in $\delta^{18}O$ and $\delta\ ^{2}H$ was expressed in the central alluvial valley prior to joining into the groundwater reservoir due to atmospheric dehumidification and evapotranspiration, that indicated this was a governing hydrological process in the hydrogeological compartment.

The estimated groundwater recharge using water balance and CMB methods showed significant difference in the central alluvial valley and western mountain blocks. The CMB method underestimated in the valley, validating the main source of recharge in the graben zone was direct rainfall infiltration during the rainfall events, and overestimated in the western mountain chains which might due to the inherent weakness of the approach that failed to include the impact of the complex hydro-stratigraphic factors[35,36]. The spatial variability and partitioning of the water balance components based on the hydrogeological compartments and foot-hills showed disagreement with prior research works on groundwater assessment of the area[22]; but revealed hydrological conceptualization with the research

works[18,19]. The broader image of groundwater potential zonation, replenishment mechanism, and sources depicts similar implication to aforementioned works[1,24]. This is critical when it comes to groundwater resource management and sustainability.

Reference

Adomako, D. Geochemical and isotopic studies of groundwater conditions in the Densu River Basin of Ghana Geochemical and isotopic studies of groundwater conditions in the Densu River Basin of Ghana. (2019) doi:10.1007/s12665-010-0595-2.

Aishlin, P. & Mcnamara, J. P. Bedrock infiltration and mountain block recharge accounting using chloride mass balance. *Hydrol. Process.* **25**, 1934–1948 (2011).

Andualem, T. G., Demeke, G. G., Ahmed, I., Dar, M. A. & Yibeltal, M. Groundwater recharge estimation using empirical methods from rainfall and streamflow records. *J. Hydrol. Reg. Stud.* **37**, 100917 (2021).

Asfaha, T. G., Frankl, A., Haile, M., Zenebe, A. & Nyssen, J. Determinants of peak discharge in steep mountain catchments - Case of the Rift Valley escarpment of Northern Ethiopia. *J. Hydrol.* **529**, 1725–1739 (2015).

Ayenew, T., GebreEgziabher, M., Kebede, S. & Mamo, S. Integrated assessment of hydrogeology and water quality for groundwater-based irrigation development in the Raya Valley, northern Ethiopia. *Water Int.* **38**, 480–492 (2013).

Casillas-Trasvina, A. *et al.* Using helium-4, tritium, carbon-14 and other hydrogeochemical evidence to evaluate the groundwater age distribution: The case of the Neogene aquifer, Belgium. *J. Hydrol. X* **17**, (2022).

Clark, I. Water, Rocks, Solutes, and Isotopes. *Groundw. Geochemistry Isot.* 1–28 (2015) doi:10.1201/b18347-2.

Environmental Isotopes (δ18 O, δ2 H, and3 H) and Hydrogeochemical Studies. *Water (Switzerland)* **14**, (2022).

Fenta, A. A., Kifle, A., Gebreyohannes, T. & Hailu, G. Spatial analysis of groundwater potential using remote sensing and GIS-based multi-criteria evaluation in Raya Valley, northern Ethiopia. *Hydrogeol. J.* **23**, 195–206 (2015).

Funk, B., Amer, S. A. & Ward, F. A. Sustainable aquifer management for food security. *Agric. Water Manag.* **281**, 108073 (2023).

Gebremedhin, M. A., Kahsay, G. H. & Fanta, H. G. Assessment of spatial distribution of aridity indices in Raya valley, northern Ethiopia. *Appl. Water Sci.* **8**, (2018).

Groundwater Resource Core Assessment. Geological Survey of Ethiopia. 11645163 (2013).

Hulluka, T. A., Balcha, S. K., Yohannes, B., Bantider, A. & Negatu, A. Review: Groundwater research in the Ethiopian Rift Valley Lakes region. *Front. Water* **5**, (2023).

International Association of Hydrogeologists. Food Security & Groundwater. (2015).

International Atomic Energy Agency, V. (Austria). Isotope techniques in water resource investigations in arid and semi-arid regions. 104 (2001).

Kahsay, G. H. *et al.* Spatial groundwater recharge estimation in Raya basin, Northern Ethiopia: an approach using GIS based water balance model. *Sustain. Water Resour. Manag.* **5**, 961–975 (2019).

Kebede, S. & Travi, Y. Origin of the δ 18O and δ 2H composition of meteoric waters in Ethiopia.

Kebede, S., Travi, Y., Alemayehu, T. & Ayenew, T. Groundwater recharge, circulation and geochemical evolution in the source region of the Blue Nile River, Ethiopia. *Appl. Geochemistry* **20**, 1658–1676 (2005).

Kolokytha, E., Oishi, S. & Teegavarapu, R. S. V. *Sustainable Water Resources Planning and Management under Climate Change*. *Sustainable Water Resources Planning and Management Under Climate Change* (2016). doi:10.1007/978-981-10-2051-3.

Kumar, P. J. S., Schneider, M. & Elango, L. The state-of-the-art estimation of groundwater recharge and water balance with a special emphasis on India: A critical review. *Sustain.* **14**, (2022).

Lewis, A. C. & Cadol, D. Estimating Evapotranspiration Using Chloride Mass Balance in a New Mexico Paired Basin Study 2009-2019. *J. Water Resour. Prot.* **15**, 115–129 (2023).

Liang, P. Addis ababa university school of graduate studies. (2011).

Markovich, K. H., Manning, A. H., Condon, L. E. & McIntosh, J. C. Mountain-Block Recharge: A Review of Current Understanding. *Water Resources Research* vol. 55 8278–8304 at https://doi.org/10.1029/2019WR025676 (2019).

Meaza, H. *et al.* Water balance components of the potential agricultural grabens along the Rift Valley in northern Ethiopia. *J. Hydrol. Reg. Stud.* **24**, (2019).

Mekonen, S. S. *et al.* Recharge Estimation Approach in a Data-Scarce Semi-Arid Region, Northern Ethiopian Rift Valley. *Sustainability* **15**, 15887 (2023).

Murphy, B. L. & Katz, M. F. ISOTOPE METHODS FOR DATING OLD GROUNDWATER. *Environ. Claims J.* **10**, 135–150 (1998).

Nedaw, D. *et al.* Groundwater Based Irrigation and Food Security in Raya-Kobo Valley, Northern Ethiopia. *Asian Rev. Environ. Earth Sci.* **5**, 15–21 (2018).

Pradhan, R. M., Behera, A. K., Kumar, S., Kumar, P. & Biswal, T. K. Recharge and Geochemical Evolution of Groundwater in Fractured Basement Aquifers (NW India): Insights from *Quat. Int.* **257**, 4–12 (2012). Scanlon, B. R. Uncertainties in estimating water fluxes and residence times using environmental tracers in an arid unsaturated zon

Shishaye, H. A. *et al.* Development of an improved hydrogeological and hydro-geochemical conceptualization of a complex aquifer system in Ethiopia. (2020).

Tadesse, N., Nedaw, D., Woldearegay, K., Gebreyohannes, T. & Steenbergen, F. Van. Groundwater management for irrigation in the raya and kobo valleys, Northern Ethiopia. *Int. J. Earth Sci. Eng.* **8**, 1104–1114 (2015).

Teklehaimanot, A. G. WATER BALANCE MODELING WITH SWAT FOR INTEGRATED WATER RESOURCES ASSESSMENT IN WATER BALANCE MODELING WITH SWAT FOR INTEGRATED WATER RESOURCES ASSESSMENT IN Raya Valley (Tigray , Ethiopia). 1–89 (2010).Tracers, I., Kendall, C. & Eds, J. M. Book review. **23**, 441–442 (2000).

Wang, P., Yu, J., Zhang, Y. & Liu, C. Groundwater recharge and hydrogeochemical evolution in the Ejina Basin , northwest China. *J. Hydrol.* **476**, 72–86 (2013).

Wilson, J. L. & Guan, H. Mountain-Block Hydrology and Mountain-Front Recharge. *Groundw. Recharg. a Desert Environ. Southwest. United States* **9**, 113–137 (2013).

Yao, Y. *et al.* What controls the partitioning between baseflow and mountain block recharge in the Qinghai-Tibet Plateau? *Geophys. Res. Lett.* **44**, 8352–8358 (2017).

Yu, X. *et al.* Hydrochemical and Stable Isotope characteristics of surface water and groundwater in Xiliugou and Wulagai River basin, North China. *Ecohydrol. Hydrobiol.* 1–11 (2023) doi:10.1016/j.ecohyd.2023.11.001.

Satellite-Based Soil Moisture Estimation for Agricultural Drought Riak Monitoring in the Tana Sub-Basin, Upper Blue Nile River Basin, Ethiopia

Habtamu Abay Eshetiea*[2], Dejene Sahlu[3], Tena Alamirew[4], Abebech Abera[1], Ayenew Desalegn Ayalew[6], Wolfgang Korres[5] and Nicola Fohrer[6].

[1]Faculty of Civil and Water Resources Engineering, Bahir Dar Institute of Technology, Bahir Dar University, 79 Bahir Dar, Ethiopia
[2]Department of Water Resource and Irrigation Engineering, Kombolcha Institute of Technology, Wollo University, Kombolcha, Ethiopia.
[3]Institute of Disaster Risk Management & Food Security Studies, Bahir Dar University, 5501 Bahir Dar, Ethiopia
[4]Water and Land Resource Centre, P.O. Box, 3880 Addis Ababa, Ethiopia
[5]Federal Institute of Hydrology, Department M5: "Geodesy and Remote Sensing
[6]Department of Hydrology and Water Resources Management, Institute for Natural Resource Conservation, Kiel University, 24098 Kiel, Germany
* Corresponding Author: habtie229@gmail.com

Abstract

Soil moisture monitoring with multispectral satellite data is crucial for improving agricultural productivity and resilience to drought, particularly in data-scarce regions like Ethiopia. Existing studies overlook the distinction between antecedent and residual soil moisture, limiting its impact on drought evaluations during critical crop seasons. This study aimed to investigate the spatio-temporal patterns of antecedent and residual soil moisture and their influence on agricultural drought. The soil moisture data was obtained from six satellite sensors (SMAP, AMSR2, SMOS, ASCAT, GLDAS, Sentinel-2A) and in-situ measurements. Soil moisture level was estimated utilizing the OPTRAM (Optical Trapezoid Model) based on Sentinel-2A data, whereas agricultural drought was evaluated using the SMDI (Soil Moisture Deficit Index). The results show that both antecedent and residual soil moisture levels are rising, with residual moisture increasing at greater rates (0.03 cm/cm per year) than antecedent moisture (0.01 cm/cm per year). Moisture levels were higher in the northern and northeastern regions, while lower in the southern and southwestern districts. The most severe and extreme drought conditions happened between 2016 and 2024, with extreme drought mainly occurred in autumn and the severe drought in spring. The seasons with lower soil moisture levels suffered more extreme droughts, indicating the direct impact of soil moisture availability on drought severity. This study emphasizes the importance of in-situ soil moisture management in mitigating drought impacts, as well as the potential of global satellite information to guide local drought management and decision-making.

Keywords: Sentinel-2A, OPTRAM, Soil Moisture Estimation, SMDI, Agricultural Drought Monitoring, Tana Sub-Basin, Ethiopia.

1. Introduction

Soil moisture is crucial for agricultural production, water resource management, and ecosystem sustainability, particularly in rain-fed areas (An et al., 2024; Laker & Nortjé, 2024). Ethiopia, where more than 80% of the population relies on agriculture for a living, is extremely sensitive to the effects of irregular rainfall and drought (Molla et al., 2024; Tofu, 2024). The Tana Sub-Basin of Ethiopia's Upper Blue Nile River Basin, one of the country's most agriculturally productive areas, has experienced periodic droughts and variable rainfall patterns in recent decades (Wubaye et al., 2023; Sishah et al., 2024). These climatic changes imperil the region's food security and agricultural sustainability (Bouteska et al., 2024; Berhanu et al., 2024).

In-situ sensors and gravimetric method sampling are two popular ground-based techniques for determining soil moisture content, but their use is often limited by their high cost, labor requirements, and limited spatial coverage (Robinson et al., 2008; Schröter et al., 2015; Mukhlisin et al., 2021; Meshram et al., 2024). Satellite remote sensing, on the other hand, has become an essential instrument for tracking soil moisture across wide regions (Ahlmer et al., 2018; Zhuo, 2021; Abdulraheem et al., 2023; Veysi, 2024). Particularly in isolated and inaccessible locations, satellite-based soil moisture estimates provide provides an economical and effective way to monitor soil moisture variability (Entekhabi et al., 2010; Dorigo et al., 2015; Kerr et al., 2016; Peng & Loew, 2017; Balsamo et al., 2018).

Remote sensing technology has had a great advancement in the precision and spatial resolution of satellite-derived soil moisture estimates (Liu et al., 2021). Various satellite missions, including Soil Moisture Active Passive (SMAP), Soil Moisture and Ocean Salinity (SMOS), Advanced Microwave Scanning Radiometer (AMSR2), and Advanced Scatterometry (ASCAT), offer valuable datasets for soil moisture monitoring at various spatial scales (Entekhabi et al., 2010; Kerr et al., 2010; Chen et al., 2018). SMAP typically provides soil moisture data at a spatial resolution of 36 km using its L-band radar and radiometer, although higher-resolution data (~9 km) can be obtained with interpolation (Entekhabi et al., 2010). SMOS offers a resolution of 35 to 40 km (Kerr et al., 2010, 2016). AMSR2 has a resolution of 10 to 50 km, with a typical value of 25 km (Du et al., 2017), but ASCAT has a 25 km resolution (Wagner et al., 2013). These satellites use active and passive microwave sensors, with accuracy affected by factors such as vegetation cover and surface roughness (Wang & Qu, 2009; Panciera et al., 2014; Vereecken et al., 2014; Hajj et al., 2018).

Radar-based sensors, such as those on Sentinel-1, offer all-weather, day-and-night monitoring capabilities, making them ideal for continuous soil moisture measurements (Hateren et al., 2023; Gatagat et al., 2024). Sentinel-1 has a resolution of up to 250 kilometers (Torres et al., 2012; Petropoulos et al., 2015), and soil moisture assessment with Sentinel-1 can be difficult in areas with unique surface features, such as thin soil layers (Bazzi et al., 2024). Recent improvements in data fusion, such as the merging of the ASCAT and Sentinel-1 datasets, have addressed these limitations by producing higher-resolution outputs as fine as 1 km (Bauer-Marschallinger et al., 2017, 2019). The Global Land Data Assimilation System (GLDAS) integrates SMAP and Landsat data to offer a comprehensive assessment of soil moisture (Fang et al., 2008; Portal, 2022; Albano et al., 2023; Boutin et al., 2023), with a resolution of 25 km (Rodell et al., 2004).

High-resolution optical satellites, such as Sentinel-2 launched by the European Space Agency (ESA), have recently altered soil moisture monitoring (Sadeghi et al., 2017; Ambrosone et al., 2020; Burdun et al., 2020). The satellite excels at recording surface features with spatial resolutions ranging from 10 to 60 meters, allowing for extensive monitoring of vegetation, soil quality, and water distribution (Drusch et al., 2012). Sentinel-2 is an effective tool for estimating soil moisture for precision agriculture (Vreugdenhil et al., 2024; Shokati et al., 2024). The mission's dual satellites, Sentinel-2A and Sentinel-2B, launched in 2015 and 2017, respectively, deliver multispectral data critical for a wide range of environmental applications (Olivier et al., 2023). Nonetheless, their utility is occasionally limited by cloud cover and irregular sunlight, which affects data reliability (Tiede et al., 2021; Tarrio et al., 2020).

Sentinel-2 satellites provide multispectral images that can be utilized for estimating soil moisture using indices such the Normalized Difference Vegetation Index (NDVI) and Shortwave Infrared Transformed Reflectance (STR) (Sadeghi et al., 2017; Vreugdenhil et al., 2024; Shokati et al., 2024). These signals allow the monitoring of soil characteristics that have a direct or indirect relationship to soil moisture levels (Mehrez et al., 2023), surface water presence (Xue et al., 2024), and vegetation health (Kumar et al., 2023). High-resolution optical data from Sentinel-2A has been emphasized in recent research as being especially crucial for improving soil moisture estimation models (Vreugdenhil et al., 2024; Shokati et al., 2024; Shokati et al., 2024; Ya'nan et al., 2024; Xue et al., 2024).

Drought is a pervasive natural hazard that disrupts agricultural systems (Visessri & Heng, 2024), endangers food security (Roy et al., 2024), and undermines economic stability ((Song et al., 2024; Sharma et al., 2024). Ethiopia has experienced recurrent droughts, with serious consequences. The El Niño (2015–2016) drought caused rainfall shortages (OCHA, 2016; UNICEF, 2016), leading to crop failures and livestock losses, worsening food insecurity (Mulualem et al., 2024; Abdela, 2024). More recently, the Horn of Africa drought (2020–2023), the worst in decades, affected Ethiopia and neighboring countries (UNICEF., 2023; Mulualem et al., 2024; Abdela, 2024). Agricultural drought, characterized by insufficient soil moisture during critical crop growth stages, results in water stress, reduced yields, and in severe cases, complete crop failure (Boken et al., 2005; Fahad et al., 2017; Ajaz et al., 2018).

Agricultural drought risk monitoring can be effectively assessed by evaluating soil moisture deficits during critical cropping seasons (Zeri et al., 2022; Luan et al., 2024; Satapathy et al., 2024). Satellite-based soil moisture estimation has emerged as a vital tool for improving drought assessment and early warning systems (Ning et al., 2024; Blanka-Végi et al., 2025). Drought indices, such as the Standardized Precipitation Evapotranspiration Index (SPEI) and the Palmer Drought Severity Index (PDSI), are generally based on rainfall and temperature data (Tirivarombo et al., 2018; Tian et al., 2020). The Soil Moisture Deficit Index (SMDI) is particularly successful in monitoring agricultural drought risk (Martínez-Fernández et al., 2015, 2016; Zhu et al., 2019) and has excellent connections with vegetative health indices. This makes it a valuable tool for assessing the impact of drought on agricultural productivity (Ning et al., 2024; Wu et al., 2024; Hernández-López et al., 2024).

Several satellite-based soil moisture studies have been carried out in the Upper Blue Nile River Basin (Ayehu et al., 2020; Astuti et al., 2022; Daniel et al., 2023); however, research on antecedent (pre-existing) and residual (post-event) moisture soil moisture dynamics is limited and its implication for agricultural drought is not clearly understood. This study monitoring agricultural drought risk by using satellite-based antecedent and residual soil moisture estimates. Soil moisture dynamics estimation is critical for drought monitoring and optimizing water resource management in rain-fed agricultural systems (Ning et al., 2024; Wu et al., 2024). Satellite-derived soil moisture estimates effectively reflect antecedent and residual soil moisture levels, making them a reliable indicator of agricultural drought risk.

2. Materials and methods

2.1. Study area

The research was carried out in Ethiopia's Tana sub-basin, which is part of the Blue Nile River Basin and contains the country's largest freshwater body (Birara et al., 2018). The Sub-Basin is located between 10.9° N to 12.8° N and 36.5° E to 38.2° E (Fig. 1). The Tana Sub-Basin has an area of 15,321 km^2, including the Lake Tana area of 3041 km^2 and an altitude varying from 1784 m at Lake level to about 3400 meters above sea level (m.a.s.l.) in the Guna Mountain. Nevertheless, most of the basin is located at elevations ranging from 1780 to 2500 m.a.s.l.

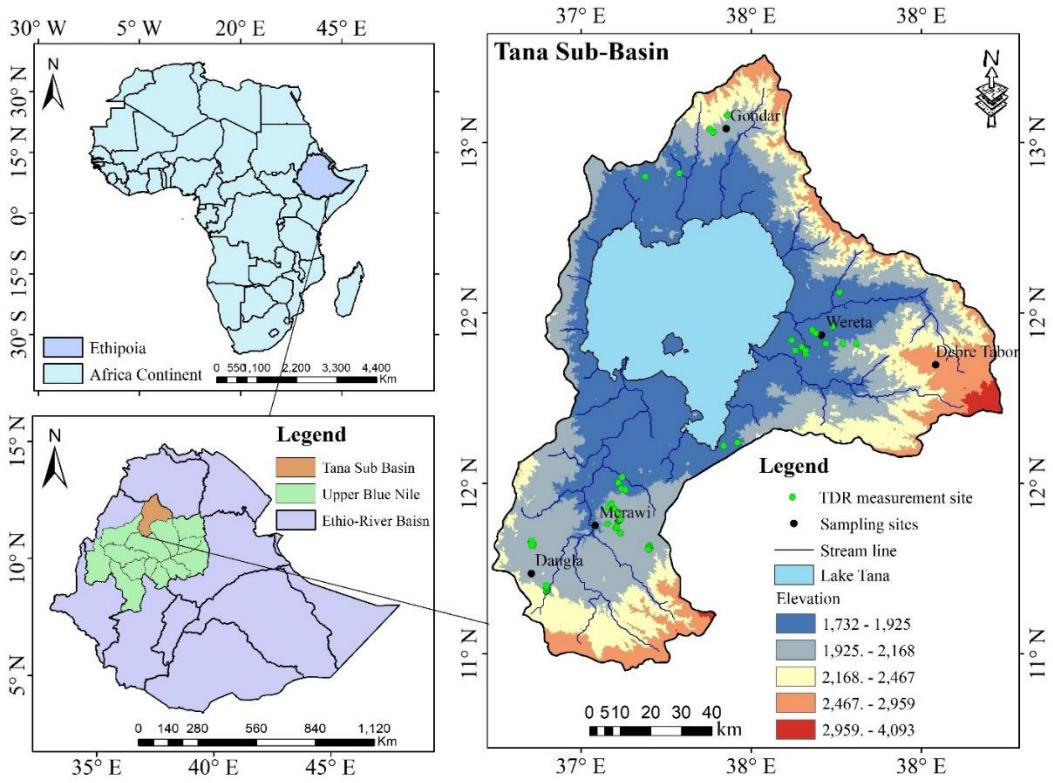

Figure 1. The study area map of the Tana Sub-Basin shows the location of the in-situ (gravimetric and TDR) measurements and a digital elevation model as a background.

2.2. Dataset

2.2.1. In-situ soil moisture data

In this study, the in-situ soil moisture measurements were collected from 114 locations in the basin: from 5 locations using gravimetric and 109 locations using TDR (Time Domain Reflectometry). A gravimetric method was also used to measure soil moisture at the sampling site. The sixty undisturbed soil samples were taken at a depth of 10 cm from five representative study sites in the basin (Fig. 1) in accordance with the dates of satellite acquisition. To capture seasonal fluctuations, sampling took place between April and May for antecedent soil moisture and between September and December 2023 for residual soil moisture.

2.2.2. Remote sensing data and image processing

This study utilizes soil moisture datasets from six satellite sensors (Table 2). These satellites were chosen based on the availability of data along with spatio-temporal resolution and revisit time. These involve direct download and extraction of data from ASCAT, AMSR2, SMOS, SMAP, and GLDAS from the access link (Table 2). Sentinel-2A images were retrieved from 2016 to 2024 for 114 sampling sites (378 images per site) between March and May, and September and December.

Table 2. Summary of satellite soil moisture products datasets.

Satellite	Sensor Type	Spatial Resolution	Temporal Coverage	Revisit Time	Retrieval Method	Data Source
SMAP	Passive microwave	~40 km	2015-present	2-3 days	L-band Radiometer (Level 2, 3)	NASA SMAP

AMSR2	Passive microwave	~10 km	2012-present	2 days	X- and K-band Radiometer	JAXA AMSR2
SMOS	Passive microwave	~25 km	2010-present	3 days	L-band Radiometer (Level 2, 3)	ESA SMOS
ASCAT	Active microwave (radar)	~ 12.5-25 km	2007-present	1-2 days	C-band Scatterometer	EUMETSAT ASCAT
GLDAS	Multiple Satellite	25 km (0.25°)	2000 - Present	3 hours	Land Surface Model (Noah)	GLDAS Data Access
Sentinel-2A	Optical multispectral	~ 10-60 m	2015-present	5 days (at equator)	Optical/Multispectral Retrieval	ESA Sentinel-2

2.3. Methods

2.3.1. OPTRAM parametrization

The OPTRAM (Optical Trapezoid Model) has been employed to estimate soil moisture from Sentinel-2A images. The model parameters for the dry (id, sd) and wet (iw, sw) edges were determined from the pixel distributions within the STR-NDVI space using Sentinel-2A imagery. This was conducted in a Python environment utilizing packages for data processing and parameter fitting ('pandas,' 'numpy,' 'scikit-learn'). A linear regression method was applied to the STR-NDVI point cloud to determine the dry and wet edge parameters. The dataset included atmospherically corrected imagery, filtered to the Tana Sub-Basin region (2022–2023), with less than 10% cloud coverage.

2.3.2. Calibration of the OPTRAM

The OPTRAM model was calibrated using in-situ soil moisture measurements and the Sentinel-2A dataset, and the dry and wet edge parameters were adjusted iteratively to meet the local conditions. These attributes were initially derived from the NDVI-STR pixel distributions. These initial parameters were then improved in Python using least-squares regression with the "scipy" package to reduce the sum of squared disparities between measured and estimated soil moisture values. The analysis focused on the antecedent and residual soil moisture levels. The residual soil moisture occurs in autumn, which is from September to December, and antecedent soil moisture is in spring, which spans April to May.

2.3.3. Accuracy assessment and validation

The accuracy of six satellite-derived soil moisture products (Table 2) was evaluated against with in situ measurements using six statistical criteria. These include Coefficient of Determination (R^2), Root Mean Square Error (RMSE), unbiased Root Mean Square Error (ubRMSE), Mean Absolute Error (MAE), Percentage of Bias (PBIAS), and Kling-Gupta Efficiency (KGE).

2.3.4. Agricultural drought indices

2.3.4.1. Soil Moisture Deficit Index (SMDI)

The SMDI has been recently proposed (Narasimhan & Srinivasan, 2005) and has shown good results to characterize the agricultural drought based on soil moisture series and basic soil water parameters (Martínez-Fernández et al., 2015, 2016; Zhu et al., 2019). The SMDI is calculated as follows:

$$SMDI = \left(\frac{(\theta - \theta_{FC})}{\theta_{AWC}}\right) \times 10$$

Where θ, θ_{AWC}, θ_{FC} represent volumetric soil moisture (m^3/m^3) at available water capacity (AWC) and field capacity (FC), respectively. Drought has occurred when the SMDI value is negative (Allen et al., 1998; Martínez-Fernández et al., 2015, 2016). According to Narasimhan & Srinivasan (2005), SMDI ≥ 0 is No Drought, -2 to 0 is Mild Drought, -2 to -5 is Moderate Drought, -5 to -10 is Severe Drought, and ≤ -10 is Extreme Drought.

3. Results and Discussion

3.3. Evaluating satellite soil moisture products

The effectiveness of six satellite-based soil moisture products was shown to differ greatly when compared to ground-based observations (Table 5).

Table 5: The performance evaluation of six satellite-based soil moisture products using in-situ measurements (collected using gravimetric and TDR) collected from January to December 2023.

Satellite products	Statistical metrics					
	R2	RMSE	MAE	PBIAS	KGE	ubRMSE
SMAP	0.691	0.048	0.044	-1.682	0.82	0.047
AMSR2	0.484	0.062	0.044	12.463	0.72	0.043
SMOS	0.798	0.039	0.033	1.719	0.85	0.038
ASCAT	0.642	0.051	0.034	-5.89	0.84	0.047
GLDAS	0.314	0.098	0.083	23.21	0.62	0.055
Sentinel-2A	0.890	0.030	0.026	-0.012	0.94	0.029

3.4. Spatiotemporal patterns of antecedent and residual soil moisture

The analysis of antecedent and residual soil moisture from 2016 to 2024 reveals a rising trend over time (Fig. 4). The antecedent soil moisture level (Fig 4a) was increased by 0.0024 per year, while residual soil moisture (Fig. 4b) exhibited a slightly higher annual increase of 0.0031 per year.

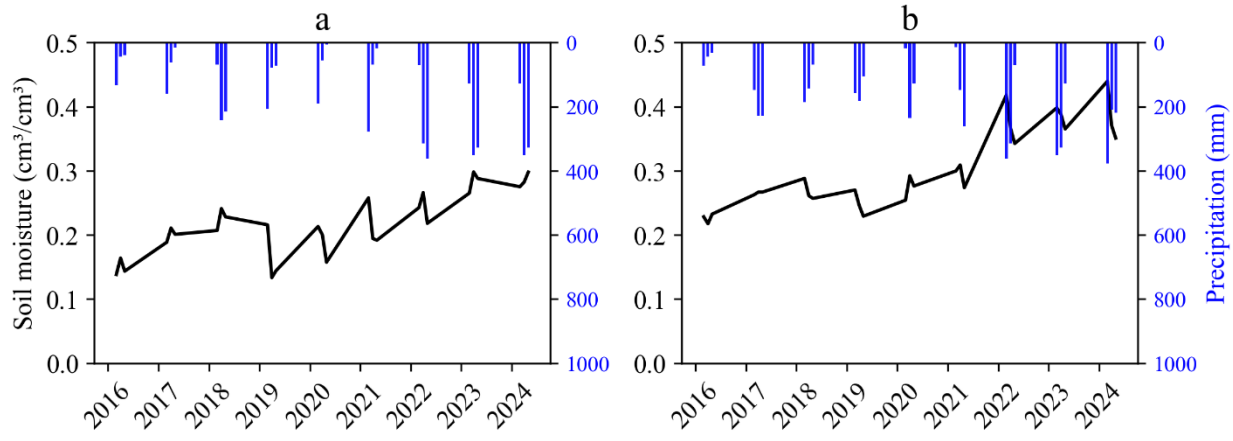

Figure 4. Trends in Antecedent (a) and Residual (b) Soil Moisture from 2016 to 2024 estimated using Sentinel-2 images.

The spatial distribution of antecedent and residual soil moisture across the basin exhibits significant variability. The result shows central and southwestern regions have greater antecedent soil moisture

levels (Fig. 5a), particularly around Lake Tana. The southern and southeastern regions of the basin, on the other hand, have the lowest antecedent moisture values. The highest levels of residual soil moisture (Fig. 5b) have been found in the basin's eastern and northeastern regions, where moisture retention appears to be more prevalent. The western and northwestern regions, on the other hand, have significantly lower residual moisture content.

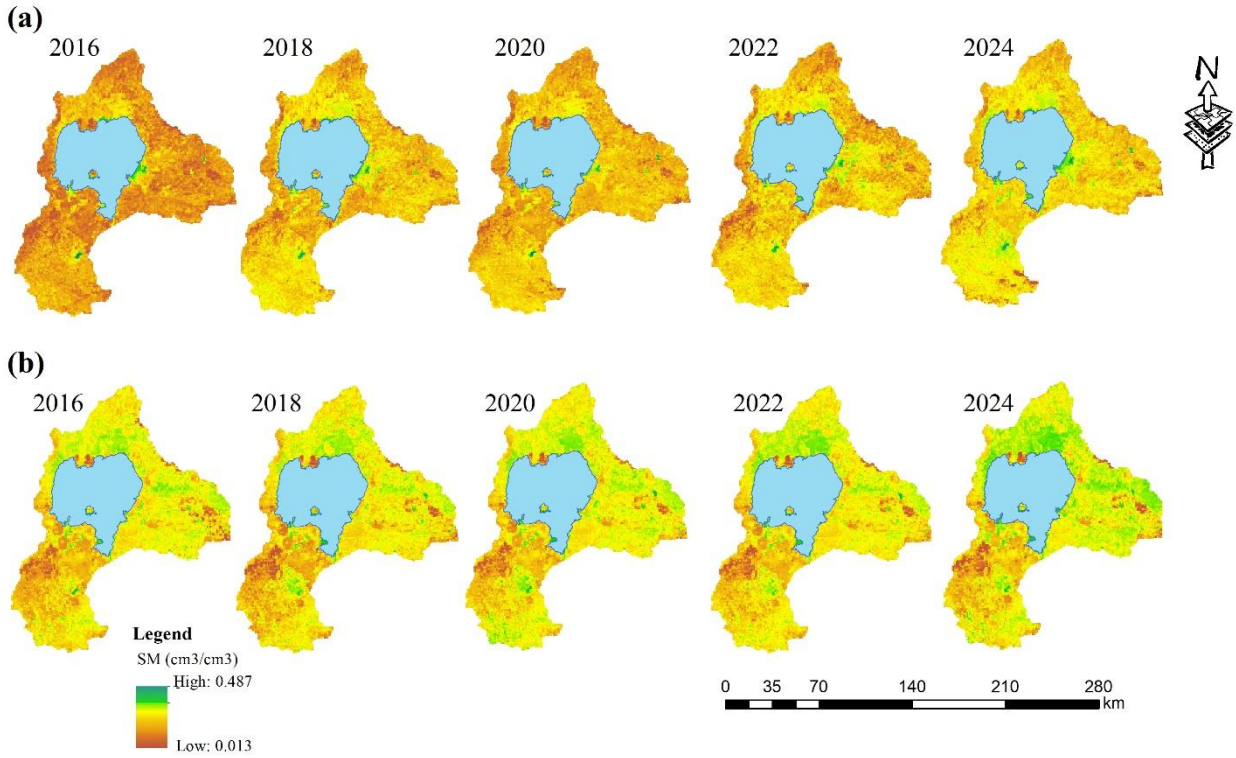

Figure 5. Spatial distribution of antecedent (a) and residual (b) soil moisture levels over the basin (excluding Lake Tana), produced using OPTRAM from Sentinel-2A images (2016-2024).

3.5. Agricultural drought evaluation

Drought conditions occurred in the region in spring (between 2016 and 2024 of March to May) was with varied severity (Fig. 6a). In 2016 and 2017, extreme drought prevailed across March, April, and May, with smaller SMDI values (below -11). In 2018, we identified a severe drought (SMDI value of -9.14) in April, but it remained extreme in March and May. In 2021, March saw severe drought (SMDI rating of -7.86), while April and May worsened to extreme drought. In 2023, there was a notable shift, with April marking the first instance of moderate drought (SMDI score of -4.75), but March and May remained in severe drought. The most severe drought remains in March and April of 2024, but moderate drought returns in May (SMDI score of -4.77).

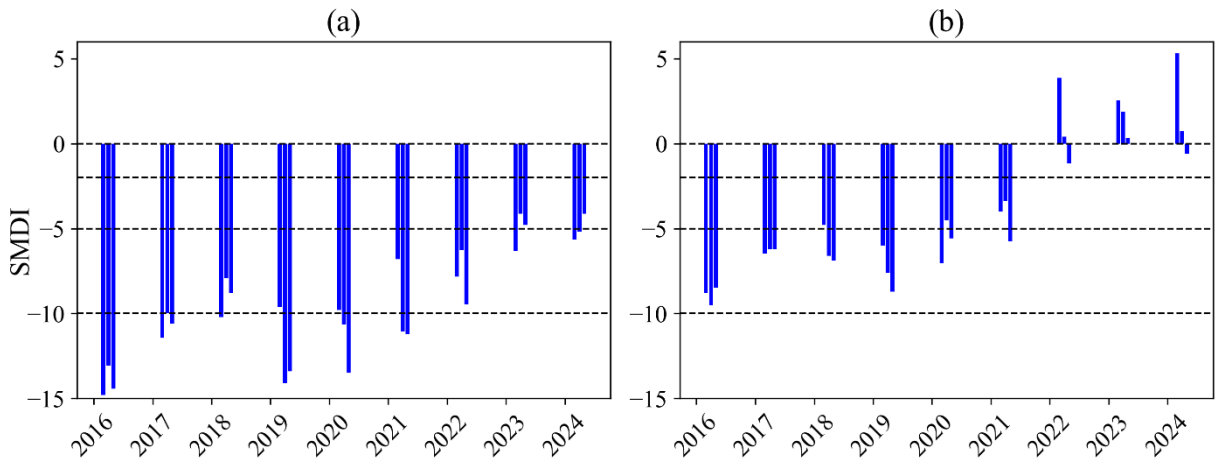

Figure 6. Agricultural drought evolution from 2016 to 2024 During March-May (a), and September to November (b).

The drought pattern in the region changed dramatically in autumn (between September and November), from high and severe drought to moderately wet and no drought scenarios (Fig. 6b). Drought conditions were severe in 2016, with extreme drought in September and October, but severe drought improved slightly in November. In 2017 and 2018, drought intensity gradually decreased, with all months categorized as severe drought and SMDI values slowly rising. This pattern continued into 2019 and 2020, with severe drought reigning supreme, with the exception of November 2019, when extreme drought briefly returned.

Drought conditions continued to improve by 2021, with mild drought in September and October, followed by severe drought in November. In 2022, a substantial shift occurred, marking the first transition to positive SMDI values, with September being classed as moderately rainy, October as somewhat wet, and November seeing only mild drought. This pattern continued in 2023, with September and October remaining fairly wet, and November rated as slightly wet. Drought conditions improved significantly in 2024, with no drought in September, slightly moist October, and a mild drought in November.

The soil moisture estimates derived from six satellite datasets identifies comparable biases. The results show AMSR2, GLDAS, and SMOS underestimate soil moisture, while ASCAT and SMAP overestimate it due to differences in spatial resolution, retrieval method, and sensor sensitivity. Passive microwave sensors, such as AMSR2 and SMOS, struggle in areas with dense vegetation and varying soil qualities (Owe et al., 2008; Wang, 2018), whereas active sensors, such as ASCAT, are prone to overestimation due to their sensitivity to surface roughness and vegetation water content. This is consistent with previous studies by Albergel et al. (2012) and Wang (2018), which demonstrated SMOS underestimation in humid regions and semi-arid zones. The Sentinel-2A emerges as the most reliable dataset for estimating soil moisture due to its high spatial resolution (10 m) and capacity to capture critical vegetation indices (Vreugdenhil et al., 2024; Shokati et al., 2024). These findings provide new insights into satellite-based soil moisture retrieval, stressing the importance of sensor-specific corrections in drought monitoring and agricultural water management.

The long-term trend of soil moisture is strongly influenced by rainfall variability. The findings suggest that both antecedent and residual soil moisture levels have increased over time, closely aligning with the observed rise in precipitation. This aligns with the work of Van Hateren et al. (2023), who observed that increasing rainfall contributes to higher soil moisture levels, as well as Ayehu et al. (2020) and Astuti et al. (2022), who reported seasonal soil moisture enhancements linked to shifting rainfall patterns. The results also reveal that residual soil moisture is invariably larger than antecedent

moisture, due to the accumulation of prior summer (kiremt) rainfall, which persists in the soil and extends into the autumn season. Besides, offset rainfall (late-season precipitation) surpasses onset rainfall (early-season precipitation), which enhances soil moisture retention. These findings offer understanding of the seasonal soil moisture balance and highlight the significance of rainfall distribution in preserving soil moisture availability.

The occurrence and severity of agricultural droughts are strongly influenced by the soil's ability to retain moisture. The results indicate that extreme drought conditions were most severe in 2016, 2020, and 2022, primarily due to the 2016 El Niño and the prolonged Horn of Africa drought (2020–2023). The 2015-2016 El Niño resulting in serious drought and rainfall shortages in Ethiopia (OCHA, 2016; UNICEF, 2016). Similarly, the Horn of Africa drought (2020–2023), considered the worst in decades, resulted in severe drought conditions across Ethiopia and neighboring countries (UNICEF., 2023; Mulualem et al., 2024; Abdela, 2024). It disrupted rainfall patterns and led to a reduction in soil moisture, which in turn intensified drought severity (Ning et al., 2024; Deng et al., 2024). The declining soil moisture levels contribute to extreme droughts, severely affecting agricultural productivity and water availability.

The seasonal variations in soil moisture significantly influence drought severity. The extreme drought conditions were highly dominant in spring, while severe droughts were noticed in autumn. These patterns are primarily driven by inadequate onset rainfall and insufficient antecedent moisture in spring, as well as insufficient offset rainfall and reduced residual moisture in autumn. It is consistent with the findings of other studies, such as Ogunrinde et al. (2025), who observed that lower antecedent soil moisture levels and onset rainfall deficits worsen droughts, and Shukla et al. (2021), who discovered that droughts are prolonged by late-season precipitation deficits. Soares & Lima (2022) stressed the importance of residual moisture. This highlights the crucial role of seasonal rainfall and soil moisture dynamics in influencing drought severity.

4. Conclusions

Sentinel-2A imagery is an effective product for monitoring soil moisture levels and evaluating drought risk. The rainfall and soil moisture are key factors in drought identification; the use of Sentinel-2A provides a scalable and accessible alternative, particularly in regions like Ethiopia where ground-based monitoring is challenging. The findings strengthen the applications of satellite sensors in soil moisture estimation and drought assessment. Nevertheless, further study is needed on Sentinel-2A's effectiveness across multiple agroecological zones to improve its usefulness. Such efforts will ensure that the sensor is resilient, flexible, and effective in a variety of environmental circumstances.

Reference

Abdela, U. (2024). Assessment of community-driven drought risk management strategies in pastoral and agro-pastoral district of Bale zones south east Ethiopia. Frontiers in Environmental Science. https://api.semanticscholar.org/CorpusID:271304800

Abdulraheem, M. I., Zhang, W., Li, S., Moshayedi, A. J., Farooque, A. A., & Hu, J. (2023). Advancement of Remote Sensing for Soil Measurements and Applications: A Comprehensive Review. Sustainability, 15(21). https://doi.org/10.3390/su152115444

Ahlmer, A. K., Cavalli, M., Hansson, K., Koutsouris, A. J., Crema, S., & Kalantari, Z. (2018). Soil moisture remote-sensing applications for identification of flood-prone areas along transport infrastructure. Environmental Earth Sciences, 77(14). https://doi.org/10.1007/s12665-018-7704-z

Ajaz, A., Taghvaeian, S., Khand, K., & Sutherland, A. (2018). Tracking Drought Using Soil Moisture Information. Oklahoma State University, October, 1–4.

Albano, R., Mazzariello, A., Lacava, T., Manfreda, S., & Sole, A. (2023). Intercomparison of recent Microwave satellite Soil Moisture Products on European Ecoregions. Journal of Hydrology, 626. https://doi.org/10.1016/j.jhydrol.2023.130311

Albergel, C., De Rosnay, P., Gruhier, C., Muñoz-Sabater, J., Hasenauer, S., Isaksen, L., Kerr, Y., & Wagner, W. (2012). Evaluation of remotely sensed and modelled soil moisture products using global ground-based in situ observations. Remote Sensing of Environment, 118, 215–226.

Allen, R. G., Pereira, L. S., Raes, D., & Smith, M. (1998). Crop evapotranspiration-Guidelines for computing crop water requirements-FAO Irrigation and drainage paper 56.

Ambrosone, M., Matese, A., Di Gennaro, S. F., Gioli, B., Tudoroiu, M., Genesio, L., Miglietta, F., Baronti, S., Maienza, A., Ungaro, F., & Toscano, P. (2020). Retrieving soil moisture in rainfed and irrigated fields using Sentinel-2 observations and a modified OPTRAM approach. International Journal of Applied Earth Observation and Geoinformation, 89. https://doi.org/10.1016/j.jag.2020.102113

An, S., Chen, X., Li, F., Wang, X., Shen, M., Luo, X., Ren, S., Zhao, H., Li, Y., & Xu, L. (2024). Long-term species-level observations indicate the critical role of soil moisture in regulating China's grassland productivity relative to phenological and climatic factors. The Science of the Total Environment, 929. https://doi.org/10.1016/j.scitotenv.2024.172553

Astuti, A. J. D., Annys, S., Dessie, M., Nyssen, J., & Dondeyne, S. (2022). To What Extent Is Hydrologic Connectivity Taken into Account in Catchment Studies in the Lake Tana Basin, Ethiopia? A Review. Land, 11(12). https://doi.org/10.3390/land11122165

Ayehu, G., Tadesse, T., & Gessesse, B. (2020). Monitoring residual soil moisture and its association to the long-term variability of rainfall over the upper blue nile basin in Ethiopia. Remote Sensing, 12(13). https://doi.org/10.3390/rs12132138

Balsamo, G., Agusti-Panareda, A., Albergel, C., Arduini, G., Beljaars, A., Bidlot, J., Blyth, E., Bousserez, N., Boussetta, S., Brown, A., Buizza, R., Buontempo, C., Chevallier, F., Choulga, M., Cloke, H., Cronin, M. F., Dahoui, M., De Rosnay, P., Dirmeyer, P. A., … Zeng, X. (2018). Satellite and In Situ Observations for Advancing Global Earth Surface Modelling: A Review. Remote Sensing, 10(12). https://doi.org/10.3390/rs10122038

Bauer-Marschallinger, B., Freeman, V., Cao, S., Paulik, C., Schaufler, S., Stachl, T., Modanesi, S., Massari, C., Ciabatta, L., Brocca, L., & Wagner, W. (2019). Toward Global Soil Moisture Monitoring with Sentinel-1: Harnessing Assets and Overcoming Obstacles. IEEE Transactions on Geoscience and Remote Sensing, 57(1), 520–539. https://doi.org/10.1109/TGRS.2018.2858004

Bauer-Marschallinger, B., Paulik, C., Schaufler, S., Jann, A., Giannakos, A., Jacobs, T., Smets, B., Lacaze, R., & Wagner, W. (2017). 1 Km Soil Moisture from Sentinel-1 and ASCAT: Evolutions Activities Within the Copernicus Global Land Service.

Bazzi, H., Baghdadi, N., Nino, P., Napoli, R., Najem, S., Zribi, M., & Vaudour, E. (2024). Retrieving Soil Moisture from Sentinel-1: Limitations over Certain Crops and Sensitivity to the First Soil Thin Layer. Water, 16(1). https://doi.org/10.3390/w16010040

Berhanu, A., Ayele, B., Dagnew, D., Melese, T., Fenta, A., & Kassie, K. (2024). Smallholder farmers' vulnerability to climate change and variability: Evidence from three agroecologies upper Blue Nile, Ethiopia. Heliyon, 10, e28277. https://doi.org/10.1016/j.heliyon.2024.e28277

Birara, H., Pandey, R. P., & Mishra, S. K. (2018). Trend and variability analysis of rainfall and temperature in the tana basin region, Ethiopia. Journal of Water and Climate Change, 9(3), 555–569. https://doi.org/10.2166/wcc.2018.080

Blanka-Végi, V., Tobak, Z., Sipos, G., Barta, K., Szabó, B., & van Leeuwen, B. (2025). Estimation of the Spatiotemporal Variability of Surface soil Moisture Using Machine Learning Methods Integrating Satellite and Ground-based Soil Moisture and Environmental Data. Water Resources Management. https://doi.org/10.1007/s11269-024-04069-3

Boken, V., CRACKNELL, A., & HEATHCOTE, R. (2005). Monitoring and Predicting Agricultural Drought: A Global.

Bouteska, A., Sharif, T., Bhuiyan, F., & Abedin, M. (2024). Impacts of the changing climate on agricultural productivity and food security: Evidence from Ethiopia. Journal of Cleaner Production. https://doi.org/10.1016/j.jclepro.2024.141793

Boutin, J., Yueh, S., Bindlish, R., Chan, S., Entekhabi, D., Kerr, Y., Kolodziejczyk, N., Lee, T., Reul, N., & Zribi, M. (2023). Soil Moisture and Sea Surface Salinity Derived from Satellite-Borne Sensors. Surveys in Geophysics, 44. https://doi.org/10.1007/s10712-023-09798-5

Burdun, I., Bechtold, M., Sagris, V., Lohila, A., Humphreys, E., Desai, A. R., Nilsson, M. B., De Lannoy, G., & Mander, Ü. (2020). Satellite Determination of Peatland Water Table Temporal Dynamics by Localizing Representative Pixels of A SWIR-Based Moisture Index. Remote Sensing, 12(18). https://doi.org/10.3390/rs12182936

Chen, F., Crow, W. T., Bindlish, R., Colliander, A., Burgin, M. S., Asanuma, J., & Aida, K. (2018). Global-scale Evaluation of SMAP, SMOS and ASCAT Soil Moisture Products using Triple Collocation. Remote Sensing of Environment, 214, 1–13. https://api.semanticscholar.org/CorpusID:134357552

Daniel, B., Agumassie, G., Daniel, M., & Derseh Andargachew. (2023). Remote Sensing Based Soil Moisture Estimation for Agricultural Productivity: A note from Lake Tana Sub Basin, NW Ethiopia. Intech, 11(tourism), 13. https://doi.org/doi: 10.5772/intechopen.109420

Deng, S., Tan, X., Tan, X., Wu, X., Huang, Z., Liu, Y., & Liu, B. (2024). On the development and recovery of soil moisture deficit drought events. Journal of Hydrology, 632, 130920. https://doi.org/https://doi.org/10.1016/j.jhydrol.2024.130920

Dorigo, W. A., Gruber, A., De Jeu, R. A. M., Wagner, W., Stacke, T., Loew, A., Albergel, C., Brocca, L., Chung, D., Parinussa, R. M., & others. (2015). Evaluation of the ESA CCI soil moisture product using ground-based observations. Remote Sensing of Environment, 162, 380–395.

Drusch, M., Del Bello, U., Carlier, S., Colin, O., Fernandez, V., Gascon, F., Hoersch, B., Isola, C., Laberinti, P., Martimort, P., Meygret, A., Spoto, F., Sy, O., Marchese, F., & Bargellini, P. (2012). Sentinel-2: ESA's Optical High-Resolution Mission for GMES Operational Services. Remote Sensing of Environment, 120, 25–36. https://doi.org/10.1016/j.rse.2011.11.026

Du, J., Kimball, J. S., Jones, L. A., Kim, Y., Glassy, J., & Jennifer, D. (2017). A global satellite environmental data record derived from AMSR-E and AMSR2 microwave earth observations. April, 1–30. https://doi.org/10.5194/essd-2017-27

Entekhabi, D., Njoku, E. G., O'Neill, P. E., Kellogg, K. H., Crow, W. T., Edelstein, W. N., Entin, J. K., Goodman, S. D., Jackson, T. J., Johnson, J., others, Kimball, J., Piepmeier, J. R., Koster, R. D., Martin, N., McDonald, K. C., Moghaddam, M., Moran, S., Reichle, R., … Van Zyl, J. (2010). The soil moisture active passive (SMAP) mission. Proceedings of the IEEE, 98(5), 704–716. https://doi.org/10.1109/JPROC.2010.2043918

Fahad, S., Bajwa, A. A., Nazir, U., Anjum, S. A., Farooq, A., Zohaib, A., Sadia, S., Nasim, W., Adkins, S., Saud, S., Ihsan, M. Z., Alharby, H., Wu, C., Wang, D., & Huang, J. (2017). Crop production under drought and heat stress: Plant responses and management options. Frontiers in Plant Science, 8(June), 1–16. https://doi.org/10.3389/fpls.2017.01147

Fang, H., Hrubiak, P. L., Kato, H., Rodell, M., Teng, W. L., & Vollmer, B. E. (2008). Global land data assimilation system (GLDAS) products from nasa hydrology data and information services center (HDISC). American Society for Photogrammetry and Remote Sensing - ASPRS Annual Conference 2008 - Bridging the Horizons: New Frontiers in Geospatial Collaboration, 1, 183–190.

Gatagat, P. A., Bharat, T. V., & Dey, A. (2024). Evaluation of Satellite-Based Models for Surface Soil Moisture Estimation Using Sentinel-1 Data: A Case Study. 5183–5186. https://doi.org/10.1109/igarss53475.2024.10642438

Hajj, M., Baghdadi, N., Zribi, M., Rodríguez-Fernández, N., Wigneron, J. P., Al-Yaari, A., Al Bitar, A., Albergel, C., & Calvet, J.-C. (2018). Evaluation of SMOS, SMAP, ASCAT and Sentinel-1 Soil Moisture Products at Sites in Southwestern France. In Remote Sensing (Vol. 10, Issue 4). https://doi.org/10.3390/rs10040569

Hernández-López, J. A., Andrade, H. J., & Barrios, M. (2024). Agricultural drought assessment in dry zones of Tolima, Colombia, using an approach based on water balance and vegetation water stress. Science of The Total Environment, 921, 171144. https://doi.org/https://doi.org/10.1016/j.scitotenv.2024.171144

Kerr, Y. H., Al-Yaari, A., Rodriguez-Fernandez, N., Parrens, M., Molero, B., Leroux, D., Bircher, S., Mahmoodi, A., Mialon, A., Richaume, P., Delwart, S., Al Bitar, A., Pellarin, T., Bindlish, R., Jackson, T. J., Rüdiger, C., Waldteufel, P., Mecklenburg, S., & Wigneron, J. P. (2016). Overview of SMOS performance in terms of global soil moisture monitoring after six years in operation. Remote Sensing of Environment, 180, 40–63. https://doi.org/10.1016/j.rse.2016.02.042

Kerr, Y. H., Waldteufel, P., Wigneron, J., Delwart, S., Cabot, F., Boutin jacqueline, Escorihuela, M. J., Jordi, F., Reul Nicolas, Gruhier Claire, Juglea Silvia Enache, Mark R.Drinkwater, Achim Hahne, Martin-Neira, M., & Mecklenburg Susanne. (2010). The SMOS Mission:New Tool for Monitoring Key Elements of the Global Water Cycle. Proceedings of the IEEE, 98(5)(5), 666–685.

Kumar, S., Ghosh, S., Mandal, D., Porwal, A., & Bhattacharya, A. (2023). A Sentinel-2 Vegetation Health Index. https://doi.org/10.1109/InGARSS59135.2023.10490434

Laker, M. C., & Nortjé, G. P. (2024). Chapter Two - The importance of understanding soil-water relationships in marginal rainfed cropping areas. In D. L. B. T.-A. in A. Sparks (Ed.), Advances in Agronomy (Vol. 185, pp. 75–117). Academic Press. https://doi.org/10.1016/bs.agron.2024.02.005

Liu, J., Xu, Y., Li, H., & Guo, J. (2021). Soil Moisture Retrieval in Farmland Areas with Sentinel Multi-Source Data Based on Regression Convolutional Neural Networks. Sensors, 21, 877. https://doi.org/10.3390/s21030877

Luan, Q., Gu, P., Sun, Q., Lai, B., Zhou, Y., & Weng, B. (2024). Agricultural drought evaluation based on a soil moisture index coupled hydrological model in North China Plain. Ecological Indicators, 166, 112473. https://doi.org/https://doi.org/10.1016/j.ecolind.2024.112473

Martínez-Fernández, J., González-Zamora, A., Sánchez, N., & Gumuzzio, A. (2015). A soil water based index as a suitable agricultural drought indicator. Journal of Hydrology, 522, 265–273. https://doi.org/10.1016/j.jhydrol.2014.12.051

Martínez-Fernández, J., González-Zamora, A., Sánchez, N., Gumuzzio, A., & Herrero-Jiménez, C. M. (2016). Satellite soil moisture for agricultural drought monitoring: Assessment of the SMOS derived Soil Water Deficit Index. Remote Sensing of Environment, 177, 277–286. https://doi.org/10.1016/j.rse.2016.02.064

Mehrez, Z., Simon, N., Emna, A., Simon, G., & Clement, Albergel Nicolas, Baghdadi Rémi, Madelon Nemesio, R.-F. (2023). A Hybrid Approach for Soil Moisture Estimation with Sentinel Data. 3186-3189. International Soil Moisture Network. https://doi.org/10.1109/igarss52108.2023.10281450

Meshram, S., Adla, S., Jourdin, L., & Pande, S. (2024). Review of low-cost, off-grid, biodegradable in situ autonomous soil moisture sensing systems: Is there a perfect solution? Computers and Electronics in Agriculture, 225, 109289. https://doi.org/10.1016/j.compag.2024.109289

Molla, S., Zeleke, M., & Tamiru, S. (2024). Rural Household Perception of Drought Occurrence and Its Influence on Livelihood Strategy in Northeast Ethiopia. Advances in Agriculture, 2024, 1–17. https://doi.org/10.1155/2024/8860956

Mukhlisin, M., Astuti, H. W., Wardihani, E. D., & Matlan, S. J. (2021). Techniques for ground-based soil moisture measurement: a detailed overview. Arabian Journal of Geosciences, 14(19), 2032. https://doi.org/10.1007/s12517-021-08263-0

Mulualem, G. M., Raju, U. J. P., Stojanovic, M., & Sorí, R. (2024). The phenomenon of drought in Ethiopia: Historical evolution and climatic forcing. Hydrology Research, 55(6), 595–612. https://doi.org/10.2166/nh.2024.192

Narasimhan, B., & Srinivasan, R. (2005). Development and evaluation of Soil Moisture Deficit Index (SMDI) and Evapotranspiration Deficit Index (ETDI) for agricultural drought monitoring. Agricultural and Forest Meteorology, 133(1–4), 69–88. https://doi.org/10.1016/j.agrformet.2005.07.012

Ning, J., Yao, Y., Fisher, J. B., Li, Y., Zhang, X., Jiang, B., Xu, J., Yu, R., Liu, L., Zhang, X., Xie, Z., Fan, J., & Zhang, L. (2024). Soil Moisture-Derived SWDI at 30 m Based on Multiple Satellite Datasets for Agricultural Drought Monitoring. Remote Sensing, 16(18). https://doi.org/10.3390/rs16183372

OCHA. (2016). United Nations Office for the Coordination of Humanitarian Affairs (OCHA). (2016). Ethiopia: El Niño-induced drought. 04(04), 1–8.

Ogunrinde, A., Adigun, P., Xue, X., Koji, D., & Jing, Q. (2025). Spatiotemporal analysis of drought patterns and trends across Africa: a multi-scale SPEI approach (1960–2018). International Journal of Digital Earth, 18, 2447342. https://doi.org/10.1080/17538947.2024.2447342

Olivier, M., Bellouard, R., Belhadj, T., Deslous, S., & Thomas, S. (2023). Copernicus Sentinel-2C/D Multi Spectral Instrument straylight characterization due to the Earth albedo. In K. Minoglou, N. Karafolas, & B. Cugny (Eds.), Society of Photo-Optical Instrumentation Engineers (SPIE) Conference Series (Vol. 12777, p. 1277748). https://doi.org/10.1117/12.2690678

Owe, M., de Jeu, R., & Holmes, T. (2008). Multisensor historical climatology of satellite-derived global land surface moisture. Journal of Geophysical Research: Earth Surface, 113(F1).

Panciera, R., Walker, J. P., Jackson, T. J., Gray, D. A., Tanase, M. A., Ryu, D., Monerris, A., Yardley, H., Rüdiger, C., Wu, X., Gao, Y., & Hacker, J. M. (2014). The Soil Moisture Active Passive Experiments (SMAPEx): Toward Soil Moisture Retrieval From the SMAP Mission. IEEE Transactions on Geoscience and Remote Sensing, 52(1), 490–507. https://doi.org/10.1109/TGRS.2013.2241774

Peng, J., & Loew, A. (2017). Recent Advances in Soil Moisture Estimation from Remote Sensing. Water, 9(7). https://doi.org/10.3390/w9070530

Petropoulos, G. P., Ireland, G., & Barrett, B. (2015). Surface soil moisture retrievals from remote sensing: Current status, products & future trends. Physics and Chemistry of the Earth, Parts A/B/C, 83-84, pp. 36-56. doi:10.1016/j.pce.2015.02.009.

Portal, G. (2022). Synergistic optical and microwave remote sensing approaches for soil moisture mapping at high resolution. https://api.semanticscholar.org/CorpusID:259986354

Robinson, D., Campbell, C., Hopmans, J., Hornbuckle, B. K., Jones, S., Knight, R. O., Ogden, F., Selker, J., & Wendroth, O. (2008). Soil Moisture Measurement for Ecological and Hydrological Watershed Scale Observatories: A Review. Vadose Zone Journal - VADOSE ZONE J, 7. https://doi.org/10.2136/vzj2007.0143

Rodell, M., Houser, P. ~R., Jambor, U., Gottschalck, J., Mitchell, K., Meng, C.-J., Arsenault, K., Cosgrove, B., Radakovich, J., Bosilovich, M., Entin*, J. ~K., Walker, J. ~P., Lohmann, D., & Toll, D. (2004). The Global Land Data Assimilation System. Bulletin of the American Meteorological Society, 85(3), 381–394. https://doi.org/10.1175/BAMS-85-3-381

Roy, D., Gillespie, S. A., & Hossain, M. S. (2024). Social-ecological systems modeling for drought-food security nexus. Sustainable Development, August 2024, 1333–1353. https://doi.org/10.1002/sd.3178

Sadeghi, M., Babaeian, E., Tuller, M., & Jones, S. B. (2017). The optical trapezoid model: A novel approach to remote sensing of soil moisture applied to Sentinel-2 and Landsat-8 observations. Remote Sensing of Environment, 198, 52–68. https://doi.org/10.1016/j.rse.2017.05.041

Satapathy, T., Dietrich, J., & Ramadas, M. (2024). Agricultural drought monitoring and early warning at the regional scale using a remote sensing-based combined index. Environmental Monitoring and Assessment, 196(11), 1132. https://doi.org/10.1007/s10661-024-13265-y

Schröter, I., Paasche, H., Dietrich, P., & Wollschläger, U. (2015). Estimation of Catchment-Scale Soil Moisture Patterns Based on Terrain Data and Sparse TDR Measurements Using a Fuzzy C-

Means Clustering Approach. Vadose Zone Journal, 14(11), 1–16. https://doi.org/10.2136/vzj2015.01.0008

Sharma, T., Amarnath, G., Amarasinghe, U., & Seid, A. (2024). Footprints of drought risk on Africa's agricultural, water and nutritional security. Environmental Research Letters, 19(10), 104046. https://doi.org/10.1088/1748-9326/ad7478

Shokati, H., Mashal, M., Noroozi, A., Abkar, A. A., Mirzaei, S., Mohammadi-Doqozloo, Z., Taghizadeh-Mehrjardi, R., Khosravani, P., Nabiollahi, K., & Scholten, T. (2024). Random Forest-Based Soil Moisture Estimation Using Sentinel-2, Landsat-8/9, and UAV-Based Hyperspectral Data. Remote Sensing, 16(11). https://doi.org/10.3390/rs16111962

Shukla, S., Husak, G., Turner, W., Davenport, F., Funk, C., Harrison, L., & Krell, N. (2021). A slow rainy season onset is a reliable harbinger of drought in most food insecure regions in Sub-Saharan Africa. PLoS ONE, 16(1 January), 1–21. https://doi.org/10.1371/journal.pone.0242883

Sishah, S., Roba, Z., Badasa, M., Deribew, K., Gemeda, D., & Hirpha, H. (2024). Rainfall prediction for data scares areas using metrological satellites in the case of the Lake Tana sub-basin, Ethiopia. Journal of Water and Climate Change, 15. https://doi.org/10.2166/wcc.2024.636

Soares, P. M. M., & Lima, D. (2022). Water scarcity down to earth surface in a Mediterranean climate: The extreme future of soil moisture in Portugal. Journal of Hydrology, 615, 128731. https://doi.org/10.1016/j.jhydrol.2022.128731

Song, Y., Joo, J., Kim, H., & Park, M. (2024). Development and Applicability Evaluation of Damage Scale Analysis Techniques for Agricultural Drought. Water, 16(10). https://doi.org/10.3390/w16101342

Tarrio, K., Tang, X., Masek, J. G., Claverie, M., Ju, J., Qiu, S., Zhu, Z., & Woodcock, C. E. (2020). Comparison of cloud detection algorithms for Sentinel-2 imagery. Science of Remote Sensing, 2, 100010. https://doi.org/https://doi.org/10.1016/j.srs.2020.100010

Tian, L., Leasor, Z. T., & Quiring, S. M. (2020). Developing a hybrid drought index: Precipitation Evapotranspiration Difference Condition Index. Climate Risk Management, 29, 100238. https://doi.org/https://doi.org/10.1016/j.crm.2020.100238

Tiede, D., Sudmanns, M., Augustin, H., & Baraldi, A. (2021). Investigating ESA Sentinel-2 products' systematic cloud cover overestimation in very high altitude areas. Remote Sensing of Environment, 252, 112163. https://doi.org/https://doi.org/10.1016/j.rse.2020.112163

Tirivarombo, S., Osupile, D., & Eliasson, P. (2018). Drought monitoring and analysis: Standardised Precipitation Evapotranspiration Index (SPEI) and Standardised Precipitation Index (SPI). Physics and Chemistry of the Earth, Parts A/B/C, 106, 1–10. https://doi.org/https://doi.org/10.1016/j.pce.2018.07.001

Tofu, D. (2024). Evaluating the impacts of climate-induced east Africa's recent disastrous drought on the pastoral livelihoods. Scientific African, 24, 11. https://doi.org/10.1016/j.sciaf.2024.e02219

Torres, R., Snoeij, P., Geudtner, D., Bibby, D., Davidson, M., Attema, E., Potin, P., Rommen, B., Floury, N., Brown, M., Traver, I. N., Deghaye, P., Duesmann, B., Rosich, B., Miranda, N., Bruno, C., L'Abbate, M., Croci, R., Pietropaolo, A., … Rostan, F. (2012). GMES Sentinel-1 mission. Remote Sensing of Environment, 120, 9–24. https://doi.org/https://doi.org/10.1016/j.rse.2011.05.028

UNICEF. (2023). Ethiopia's humanitarian crisis amid prolonged drought. UNICEF. https://www.unicef.org/press-releases/ethiopias-humanitarian-crisis-amid-prolonged-drought

UNICEF. (2016). Ethiopia El Nino Emergency. Fast Facts, JUNE.

Van Hateren, T., Chini, M., Matgen, P., Pulvirenti, L., Pierdicca, N., & Teuling, A. (2023). On the potential of Sentinel-1 for sub-field scale soil moisture monitoring. International Journal of Applied Earth Observation and Geoinformation, 120, 103342. https://doi.org/10.1016/j.jag.2023.103342

Vereecken, H., Huisman, J. A., Pachepsky, Y., Montzka, C., van der Kruk, J., Bogena, H., Weihermüller, L., Herbst, M., Martinez, G., & Vanderborght, J. (2014). On the spatio-temporal

dynamics of soil moisture at the field scale. Journal of Hydrology, 516, 76–96. https://doi.org/10.1016/j.jhydrol.2013.11.061

Veysi, S. (2024). Conceptual of soil moisture based on remote sensing and reanalysis dataset. In Remote Sensing of Soil and Land Surface Processes (pp. 77–98). https://doi.org/10.1016/B978-0-443-15341-9.00020-4

Visessri, S., & Heng, S. (2024). Drought-Induced Agricultural and Food Security Challenges in the Baribo Basin, Cambodia. Water, 16(20). https://doi.org/10.3390/w16203005

Vreugdenhil, M., Massart, S., Muguda Sanjeevamurthy, P., Villegas-Lituma, C., Enenkel, M., & Wagner, W. (2024). Drought monitoring and early warning with satellite soil moisture data. EGU General Assembly Conference Abstracts, 19536. https://doi.org/10.5194/egusphere-egu24-19536

Wagner, W., Hahn, S., Kidd, R., Melzer, T., Bartalis, Z., Hasenauer, S., Figa-saldaña, J., Rosnay, P., Jann, A., Schneider, S., Komma, J., Kubu, G., Brugger, K., Aubrecht, C., Züger, J., Gangkofner, U., Kienberger, S., Brocca, L., Wang, Y., & Rubel, F. (2013). The ASCAT Soil Moisture Product: A Review of its Specifications, Validation Results, and Emerging Applications. Meteorologische Zeitschrift, 22, 5–33. https://doi.org/10.1127/0941-2948/2013/0399

Wang, H. (2018). Soil Moisture Retrieval from Microwave Remote Sensing Observations. In G. Civeira (Ed.), Soil Moisture. IntechOpen. https://doi.org/10.5772/intechopen.81476

Wang, L., & Qu, J. J. (2009). Satellite remote sensing applications for surface soil moisture monitoring: A review. In Frontiers of Earth Science in China (Vol. 3, Issue 2, pp. 237–247). Higher Education Press. https://doi.org/10.1007/s11707-009-0023-7

Wu, X., Xu, H., He, H., Wu, Z., Lu, G., & Liao, T. (2024). Agricultural Drought Monitoring Using an Enhanced Soil Water Deficit Index Derived from Remote Sensing and Model Data Merging. Remote Sensing, 16(12). https://doi.org/10.3390/rs16122156

Wubaye, G. B., Gashaw, T., Worqlul, A. W., Dile, Y. T., Taye, M. T., Haileslassie, A., Zaitchik, B., Birhan, D. A., Adgo, E., Mohammed, J. A., Lebeza, T. M., Bantider, A., Seid, A., & Srinivasan, R. (2023). Trends in Rainfall and Temperature Extremes in Ethiopia: Station and Agro-Ecological Zone Levels of Analysis. In Atmosphere (Vol. 14, Issue 3). https://doi.org/10.3390/atmos14030483

Xue, J., Zhang, X., Chen, S., Su, Y., & Shi, Z. (2024). A new framework for retrieving bare soil information using multi-temporal Sentinel-2 images across China. EGU General Assembly Conference Abstracts, 4622. https://doi.org/10.5194/egusphere-egu24-4622

Ya'nan, Z., Binyao, W., Weiwei, Z. H. U., Li, F., Qisheng, H. E., Xin, Z., Tianjun, W. U., & Na'na, Y. A. N. (2024). Spatial-temporal constraints for surface soil moisture mapping using Sentinel-1 and Sentinel-2 data over agricultural regions. Computers and Electronics in Agriculture, 219, 108835. https://doi.org/10.1016/j.compag.2024.108835

Zeri, M., Williams, K., Cunha, A. P. M. A., Cunha-Zeri, G., Vianna, M. S., Blyth, E. M., Marthews, T. R., Hayman, G. D., Costa, J. M., Marengo, J. A., Alvalá, R. C. S., Moraes, O. L. L., & Galdos, M. V. (2022). Importance of including soil moisture in drought monitoring over the Brazilian semiarid region: An evaluation using the JULES model, in situ observations, and remote sensing. Climate Resilience and Sustainability, 1(1), 1–18. https://doi.org/10.1002/cli2.7

Zhu, Q., Luo, Y., Xu, Y.-P., Tian, Y., & Yang, T. (2019). Satellite Soil Moisture for Agricultural Drought Monitoring: Assessment of SMAP-Derived Soil Water Deficit Index in Xiang River Basin, China. Remote Sensing, 11(3). https://doi.org/10.3390/rs11030362

Zhuo, L. (2021). Satellite Remote Sensing of Soil Moisture for Hydrological Applications: A Review of Issues to Be Solved. In A. Scozzari, S. Mounce, D. Han, F. Soldovieri, & D. Solomatine (Eds.), ICT for Smart Water Systems: Measurements and Data Science (pp. 259–281). Springer International Publishing. https://doi.org/10.1007/698_2019_394

Enhanced flood Simulation Using a Novel CNN-ED-DLSTM Hybrid Deep Learning Model in Kulfo Watershed, Ethiopia

Nahom Bekele Mena[1]

[1]Nahom Bekele Mena, Water Resources & Hydraulic Engineering, College of Engineering, Bule Hora University, Bule Hora, Ethiopia, P. Box 144.

Corresponding Author Email: nahom.bekele@bhu.edu.et

Abstract

Accurate hydrological modeling supports sustainable water management, while reliable flood simulation ensures public safety and risk mitigation. However, traditional models often struggle to capture the dynamic and heterogeneous nature of hydrological processes, leading to inaccuracies in flood simulation. This research evaluates the performance of an advanced deep learning (DL) model that integrates Encoder-Decoder Double-Layer Long Short-Term Memory (ED-DLSTM) networks with one-dimensional Convolutional Neural Networks (CNNs) for flood simulation in the Kulfo Watershed, Ethiopia. This hybrid approach aims to enhance flood simulation accuracy by combining sequence modeling and spatial feature extraction. To evaluate its performance, two alternative models are considered: ED-DLSTM, which utilizes a stacked LSTM with an encoder-decoder architecture, and MLP, a fully connected neural network that serves as a baseline for comparison. The dataset underwent rigorous quality assurance to ensure integrity and reliability before being split into training (80%) and evaluation (20%) sets. Model performance was assessed using various graphical and statistical metrics. Results demonstrate that DL models hold significant promise for flood simulation, with the CNN-ED-DLSTM model outperforming others. It achieved a Nash-Sutcliffe Efficiency (NSE) of 0.96, Root Mean Square Error (RMSE) of 1.41, Mean Absolute Error (MAE) of 2.85, and a Coefficient of Determination (R^2) of 0.97. The study highlights the importance of input data selection and lag times, with precipitation as the most influential predictor. Scenario 4, prioritizing precipitation, achieved the best performance, underscoring the need for carefully selected input variables for accurate flood simulation.

Keywords: *Deep Learning, CNN-ED-DLSTM, MLP, Flood Simulation*

1. Introduction

Accurate flood simulation is critical for mitigating risks to public safety and infrastructure, particularly in flood-prone regions like the Kulfo Watershed, Ethiopia. Extreme hydrological events, such as floods, pose severe socio-economic and environmental consequences, necessitating robust predictive models that can aid in early warning systems, water resource management, and policy formulation [1]. Traditional hydrological models, including physically based and conceptual approaches, have been widely employed to simulate flood dynamics. While these models are foundational for understanding water distribution and flow processes, they often fail to capture the nonlinear and temporally dynamic nature of flood generation mechanisms, leading to unreliable predictions under complex climatic and hydrological conditions[2]. One of the primary challenges with conventional hydrological models lies in their dependence on predefined equations and assumptions regarding watershed behavior. These models, such as the Soil and Water Assessment Tool (SWAT) and Hydrologic Engineering Center's Hydrologic Modeling System (HEC-HMS), rely on parameter calibration, which is often constrained by data availability and spatial heterogeneity [3][4]. Moreover, traditional models struggle to generalize effectively in response to climate change-induced shifts in precipitation patterns, land use modifications, and increasing urbanization, all of which significantly impact flood generation [5]. These limitations underscore the need for advanced computational frameworks capable of capturing the intricate interactions between meteorological inputs, land surface properties, and hydrological responses in flood-prone watersheds.

In recent years, deep learning (DL) has emerged as a transformative approach for hydrological modeling, offering superior performance in handling nonlinear relationships and sequential patterns compared to conventional methods [6]. Among DL architectures, Long Short-Term Memory (LSTM) networks have gained prominence in hydrology due to their ability to model long-term dependencies in time-series data. LSTM models have demonstrated remarkable effectiveness in flood event simulations. They outperform traditional machine learning and empirical statistical methods by leveraging their gated memory structure to retain crucial hydrological information over extended periods [7]. However, standalone LSTMs may overlook localized temporal features, which are essential for resolving rapid hydrological responses during extreme rainfall events.

To address this gap, hybrid models integrating 1D Convolutional Neural Networks (1D CNNs) with LSTM variants have shown promise in enhancing flood prediction accuracy [8]. The 1D CNN excels at extracting high-resolution temporal features and local patterns from raw time-series data, such as rainfall, streamflow, and soil moisture, through its kernel operations [4]. By identifying spatially localized dependencies within time-series sequences, CNNs can enhance the feature representation of hydrological inputs, leading to improved flood forecasting performance. When coupled with LSTM-based architectures, these hybrid models effectively synergize the strengths of feature extraction and sequence modeling, thus refining the predictive capabilities of hydrological simulations. For instance, [9] highlighted the efficacy of CNN-LSTM hybrids in capturing multi-scale temporal dependencies and improving flood prediction accuracy in diverse climatic conditions.

Building on these advancements, this study introduces a novel CNN-Encoder-Decoder Double-Layer LSTM (CNN-ED-DLSTM) model, designed to enhance flood simulation accuracy in the Kulfo Watershed. The 1D CNN component processes input data to distill localized temporal features, while the ED-DLSTM framework, a stacked LSTM structure with an encoder-decoder architecture, captures long-term dependencies and maps input sequences to output predictions, such as water levels and peak flows. This dual mechanism enables the model to resolve both short-term fluctuations and prolonged hydrological dynamics, which are critical for simulating flood hydrographs [5]. Furthermore, the CNN-ED-DLSTM model will be rigorously compared with the ED-DLSTM and Multi-Layer Perceptron (MLP) models to evaluate its performance in capturing hydrological complexities and improving flood forecasting accuracy. This research leverages advanced deep learning techniques to enhance data-driven hydrological modeling and flood risk management. The findings offer insights into the use of hybrid DL models in complex watersheds, guiding future real-time flood forecasting developments for regions prone to extreme hydrological events.

2. Materials and Methods

2.1. Study area description

The study was carried out within the Kulfo River Watershed, situated in the Abaya-Chamo sub-basin of the Southern Ethiopian Rift Valley. This watershed drains into Lake Chamo and spans latitudes 5°55'N to 6°15'N and longitudes 37°18'E to 37°36'E (Figure 1). The region's elevation varies from 1,208 meters above sea level (masl) to 3,547 masl, encompassing a total area of roughly 384.56 km². Annual precipitation in the catchment ranges between 620 mm and 1,250 mm, with mean yearly temperatures fluctuating from 14°C to 23°C.

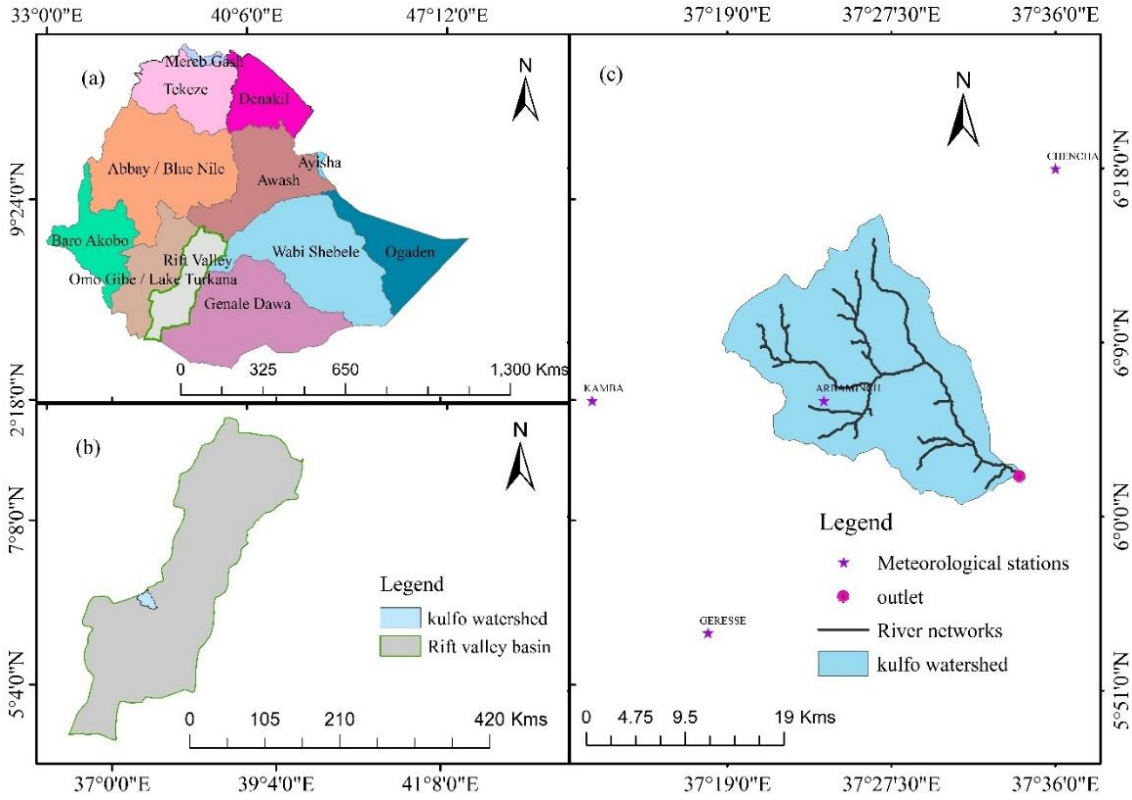

Figure 1 | Description of the study area: (a) Basins of Ethiopia, (b) Rift valley basin, and (c) Kulfo watershed.

2.2. Data collection and preprocessing

DEM data (30-meter resolution) for the Kulfo watershed was sourced from the USGS, while daily precipitation and temperature records were obtained from Ethiopia's EMI. Data quality and completeness are critical for ensuring reliable analysis outcomes [10]. This study comparatively applied machine learning (ML) and multiple imputation methods to address missing data, leveraging their capacity to model intricate patterns. Rainfall consistency was assessed via double mass curve analysis, while homogeneity was verified using non-dimensional parametrization. Long-term daily flow data (1991-2013) for Kulfo station was acquired from Ethiopia's Ministry of Water and Energy (MoWE). Rain gauges, limited by point-based sampling, struggle to represent spatial rainfall distribution. Hydrological analyses thus require estimating sub-watershed average rainfall depths to better assess patterns and impacts [11]. This study used ArcGIS 10.3 and the Thiessen polygon method to map rainfall distribution. Selecting input variables (e.g., rainfall, evaporation, temperature) for streamflow models remains challenging due to data availability and research scope (Apaydin et al., 2020). Van et al. (2020) noted that including temperature and evapotranspiration risks model overfitting. Optimal input combinations for DL models were tested using daily/monthly rainfall and discharge data with varied lag times. Pearson's correlation [6] revealed strong rainfall-discharge links (Figure 4), while autocorrelation highlighted lag-time variations (Figure 3). DL models were thus comparatively designed with diverse input scenarios to balance complexity and accuracy. Data normalization is critical to reduce discrepancies from differing scales/units [14]. This involves scaling variables to a common range (e.g., 0–1) using methods like min-max scaling. This study applied min-max scaling (Equation 1) for normalization.

$$x' = \frac{x - \min(x)}{\max(x) - \min(x)} \quad (1)$$

Where; x' is the scaled value, and x is the original value.

The datasets underwent quality control, including pre-processing (standardization) and post-processing (evaluation metrics and visualizations) using Python. Models were developed and executed in Python [14]. The data was split into 80% training and 20% testing sets, with the training set used for model training and hyperparameter tuning, while the testing set evaluated final performance (Figure 2). Figures 4 and 5 show ACF and PACF plots, revealing a gradual decline in autocorrelation with increasing lag. DL model integration requires selecting optimal input variables and hidden nodes, but no universal rule exists. A trial-and-error approach is used to address this. This study selects inputs based on correlation and lag analysis, using four and three scenarios to train models and assess input sensitivity (Table 2).

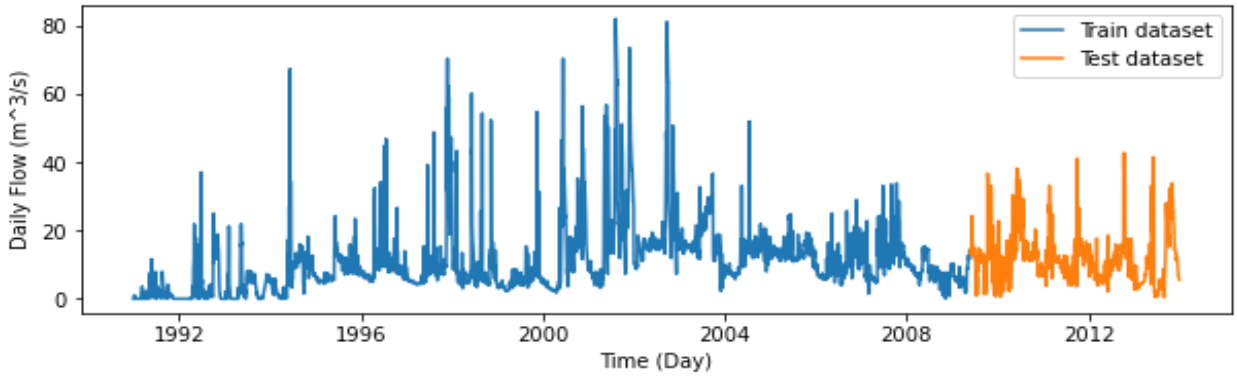

Figure 2 | Split dataset for training and testing purposes for the daily and Monthly simulation

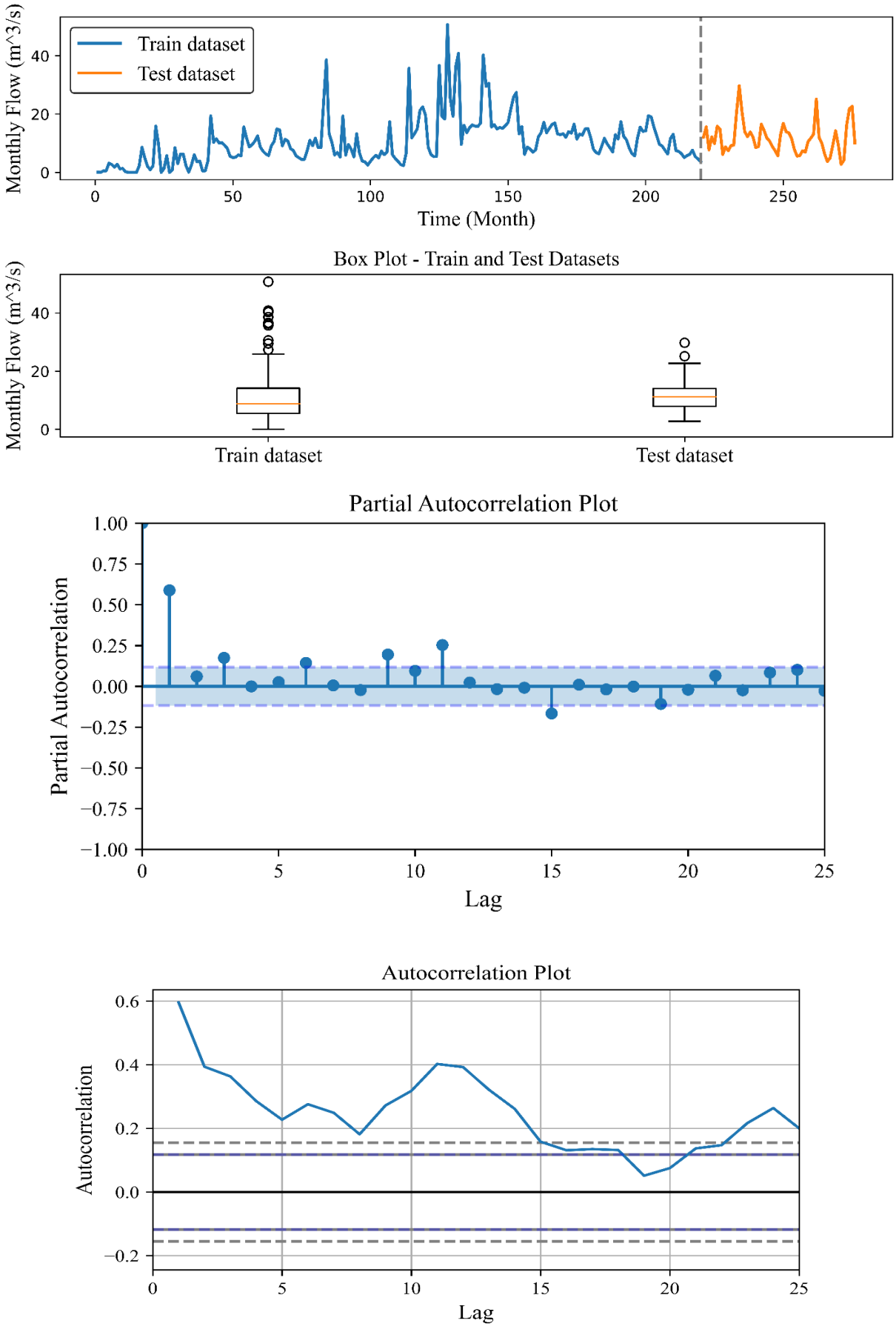

Figure 3| Pearson correlation plot for input variables for the Kulfo watershed.

Table 1| Descriptive statistics of time series data

Data type	Pearson correlation with streamflow	skewness	Mean	Min	Max	SD*	CV*
Streamflow	1.00	1.69	10.75	0.00	50.73	5.43	0.61
RF	0.68	1.90	11.25	0.00	56.87	6.34	0.67
PET	-0.14	-0.34	4.3	1.84	11.14	0.76	0.18

***** CV stands for co-efficient of variation; * SD stands for standard deviation

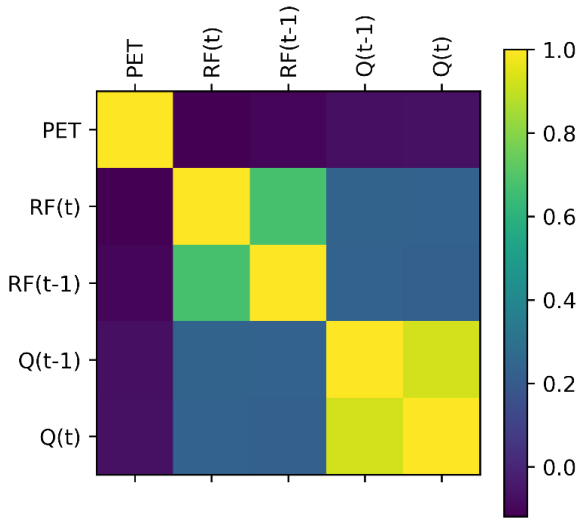

Figure 4| Pearson correlation plot for dependent and independent variables.

Table 2| Model input combinations for the Kulfo watershed

Input combination	*Output*	*Scenario*	*Model name*
Q_{t-1}, Q_{t-3}, Q_{t-6}	Q_t	*1*	*CNN-ED-DLSTM$_1$, ED-DLSTM$_1$ MPL$_1$*
Q_{t-1}, Q_{t-3}, Q_{t-6}, Q_{t-9}, Q_{t-11}, Q_{t-15}	Q_t	*2*	*CNN-ED-DLSTM$_2$, ED-DLSTM$_2$ MPL$_2$*
R_{t-1}, R_t, Q_{t-1}	Q_t	*3*	*CNN-ED-DLSTM$_3$, ED-DLSTM$_2$ MPL$_3$*
R_t, R_{t-1}, R_{t-2}, Q_{t-1}, Q_{t-2}	Q_t	*4*	*CNN-ED-DLSTM$_4$, ED-DLSTM$_4$ MPL$_4$*

2.3. Methods

2.3.1. Model Development

Two benchmark models are considered to evaluate the Novel CNN-ED-DLSTM model's performance: Encoder-Decoder Double-Layer LSTM (ED-DLSTM), a stacked LSTM model with an encoder-decoder architecture for capturing long-term dependencies in hydrological time series, and Multi-Layer Perceptron (MLP), a fully connected neural network used for baseline comparison.

2.3.1.1. Fully Connected Multi-Layer Perceptron (MLP)

A Fully Connected Multi-Layer Perceptron (MLP) is an artificial neural network with multiple layers of neurons, each fully connected to the next. It includes an input layer, one or more hidden layers, and an output layer [15]. The input layer receives data, hidden layers apply weighted sums and activation functions (e.g., ReLU, Sigmoid) for non-linear transformations, and the output layer produces predictions (e.g., Softmax for classification, linear for regression). MLPs are trained via backpropagation using optimization algorithms like SGD or Adam. For time series prediction, MLPs use a sliding window to transform sequential data into input-output pairs, treating time steps as independent features [16]. While MLPs lack inherent temporal modeling (unlike RNNs or LSTMs),

they can capture patterns with feature engineering (e.g., time-based features) and are efficient for short-term forecasting when long-term dependencies are not critical [17].

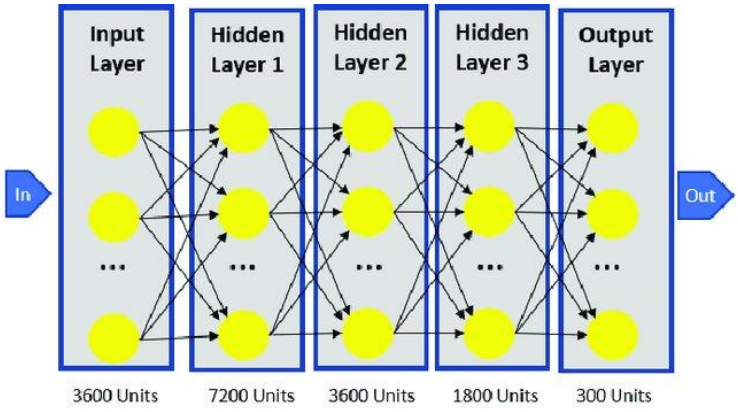

Figure 5| Architecture of a Fully Connected Multi-Layer Perceptron

2.3.2. Encoder-Decoder Double-Layer LSTM (ED-DLSTM)

The Encoder-Decoder Double-Layer LSTM (ED-DLSTM) is a deep learning model for sequential data, ideal for time series forecasting and sequence-to-sequence tasks. It features an encoder and a decoder, each with two stacked LSTM layers, enabling it to capture long-term dependencies and complex temporal patterns [18]. The encoder processes input data into a context vector, summarizing sequence dynamics, which the decoder uses to generate predictions step by step. A fully connected layer produces the final output, often for multi-step forecasting. ED-DLSTM excels in long-range forecasting for domains like hydrology, energy, and finance, thanks to its hierarchical feature extraction and ability to handle variable-length or irregular data [19]. However, it is computationally intensive, prone to overfitting, and requires careful tuning of input sequence length and hyperparameters [20]. Despite these challenges, ED-DLSTM is a powerful tool for non-stationary and complex time series, offering robust predictions when properly configured.

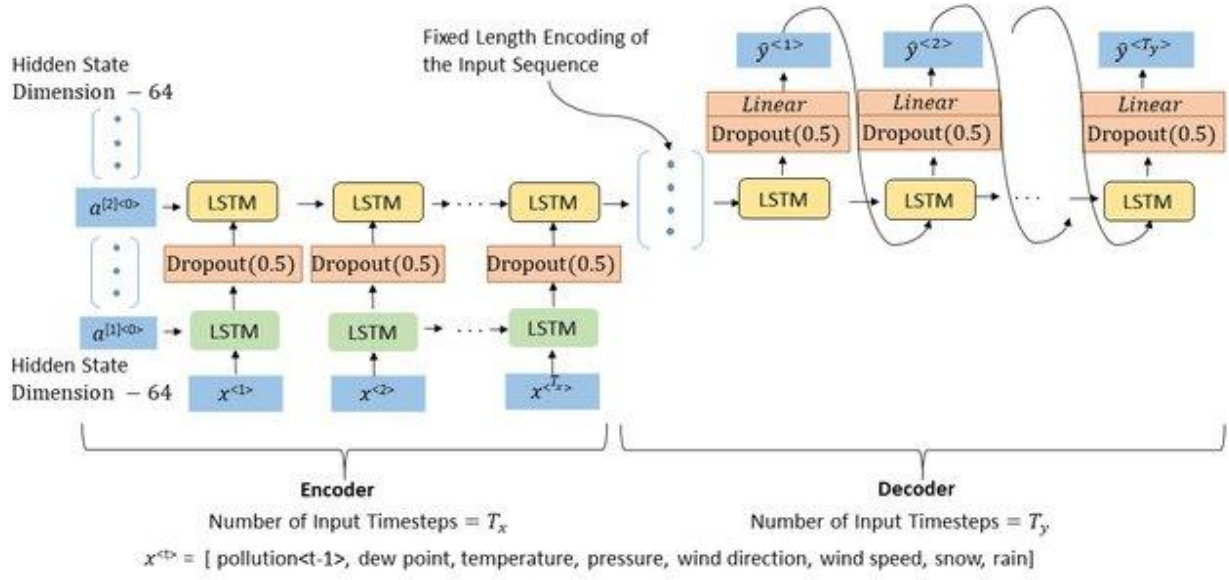

Figure 5| Architecture of the Encoder-Decoder LSTM Layer

2.3.3. The CNN-ED-DLSTM Novel Model Description and Architecture Design

The CNN-ED-DLSTM model is a hybrid deep learning architecture designed for flood forecasting, combining the strengths of 1D Convolutional Neural Networks (1D CNNs) and an Encoder-Decoder

Double-Layer LSTM (ED-DLSTM). This model is tailored to address the complexities of hydrological time-series data, leveraging localized feature extraction and long-term temporal dependency modeling to improve prediction accuracy. The 1D CNN processes raw hydrological inputs such as rainfall, streamflow, and soil moisture, applying convolutional filters to detect localized patterns and short-term fluctuations. By condensing raw time-series data into a more informative feature representation, the CNN reduces noise and enhances the quality of input features, improving the overall predictive capability of the model. The extracted features are then passed to the Encoder-Decoder Double-Layer LSTM, where the encoder, consisting of two stacked LSTM layers, processes the features into a fixed-length context vector that encapsulates the hydrological state of the watershed. The decoder, also a double-layer LSTM, reconstructs the sequence from this context vector and generates predictions for target variables such as peak discharge and water levels. This structure enables the model to capture both short-term flood dynamics and long-term hydrological trends effectively. Fully connected layers refine the outputs, with hidden layers using ReLU activation for non-linearity and the final output layer employing a linear activation function for continuous-valued flood predictions. The model is trained using backpropagation with the Adam optimizer, minimizing the Mean Squared Error (MSE) loss function to enhance prediction accuracy. Techniques like early stopping and hyperparameters tuning are employed to prevent overfitting and optimize parameters such as the number of LSTM units, CNN kernel sizes, and learning rates. Key hyperparameters include the number of hidden units, which determines the model's capacity to capture intricate patterns; activation functions like Sigmoid, Tanh, and Softmax for specific tasks (Equation 2,3,4,); and the learning rate, which balances fast convergence and stable training. The number of epochs, dropout rate, batch size, and optimization algorithm also play critical roles in model performance. Proper selection of input sequence length and feature engineering is essential to capture meaningful patterns without introducing noise.

$$f(x) = \frac{1}{1+e^{-x}} \quad (2)$$

$$f(x) = tanh(x) = f(x) = \frac{2}{1+e^{-2x}} - 1 \quad (3)$$

$$Softmax\ (\mathrm{Z})_i = \frac{e^{zi}}{\sum_{j=1}^{N} e^{zi}} \quad (4)$$

Where z is the vector of raw outputs from the neural network

The value of e ≈ 2.718

2.3.4. Model training and testing

In the context of deep learning, training and testing are critical phases for developing and evaluating models. Training involves using a labeled dataset to teach the model to recognize patterns and make predictions, while testing assesses the model's performance on unseen data to determine its accuracy and suitability for real-world applications. In this study, the DL models were trained on monthly streamflow data from 1991 to 2008 and tested on subsequent data. Performance measures, such as comparing predicted streamflow to observed data using specific metrics (RMSE, MAE, NSE and R^2), were used to evaluate the accuracy and reliability of the models. These measures help determine how well the models generalize to new data and their effectiveness in streamflow prediction tasks.

3. Results and Discussion

3.1. Results

This study applied three DL models (MPL, ED-DLSTM, and CNN-ED-DLSTM) in Python to simulate floods in the Kulfo watershed. MSE was used as the cost function to optimize performance. The best

hyperparameters, determined through multiple iterations, are in Table 3. Monthly predicted and observed flow hydrographs are shown in Figures 7 and 8.

Table 3| Ranges of model parameters used in optimization.

Parameter	**Range**	**Applicable Models**
Conv1D Layer	16-128	CNN-ED-DLSTM
Learning Rate	[0.1, 0.01, 0.001, 0.0001]	All models (CNN-ED-DLSTM, ED-DLSTM, MLP)
Number of LSTM Units	16-256	CNN-ED-DLSTM, ED-DLSTM
Number of MLP Layers	1-4	MLP

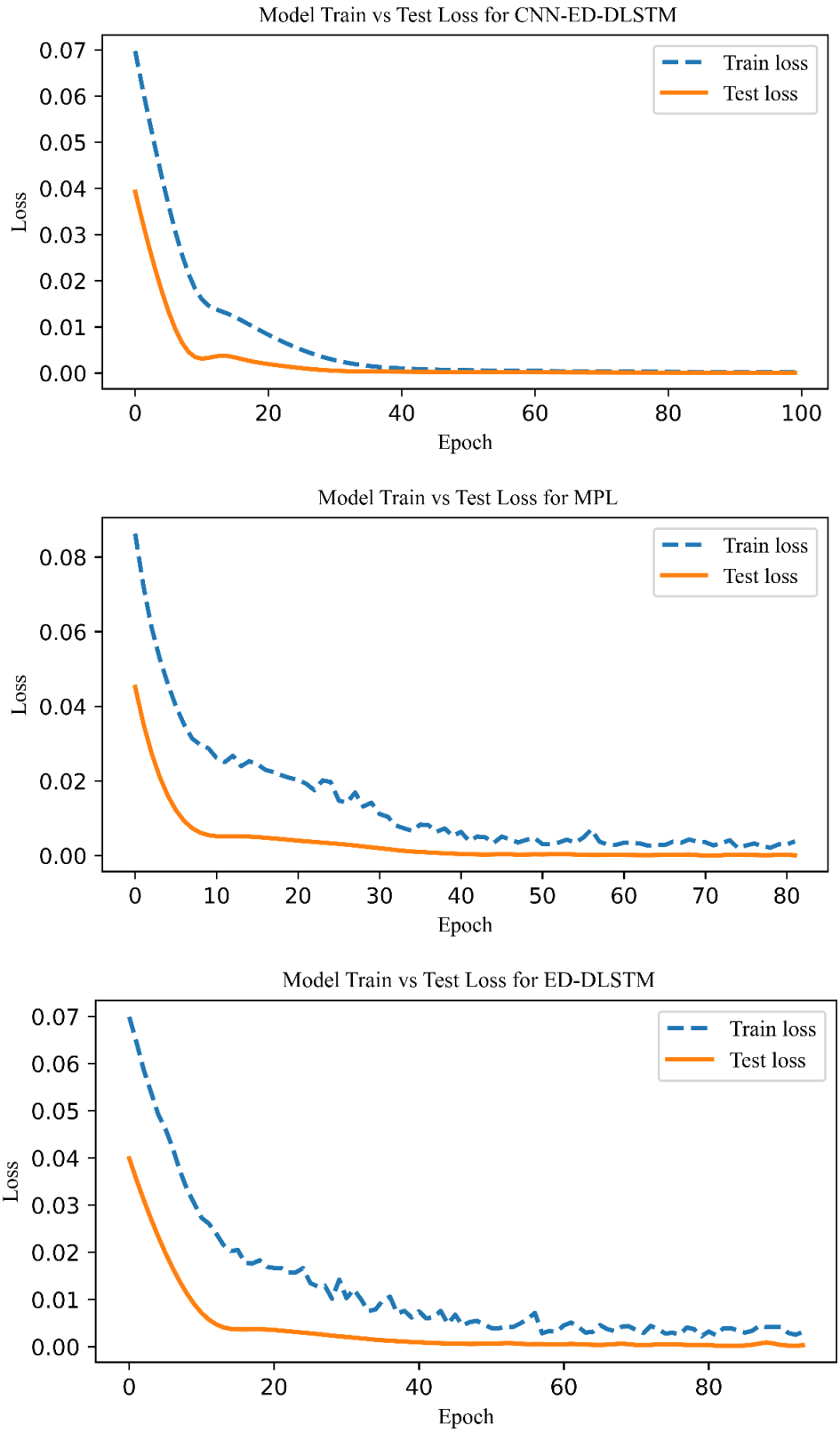

Figure 6 | Training and test loss function of the optimized models.

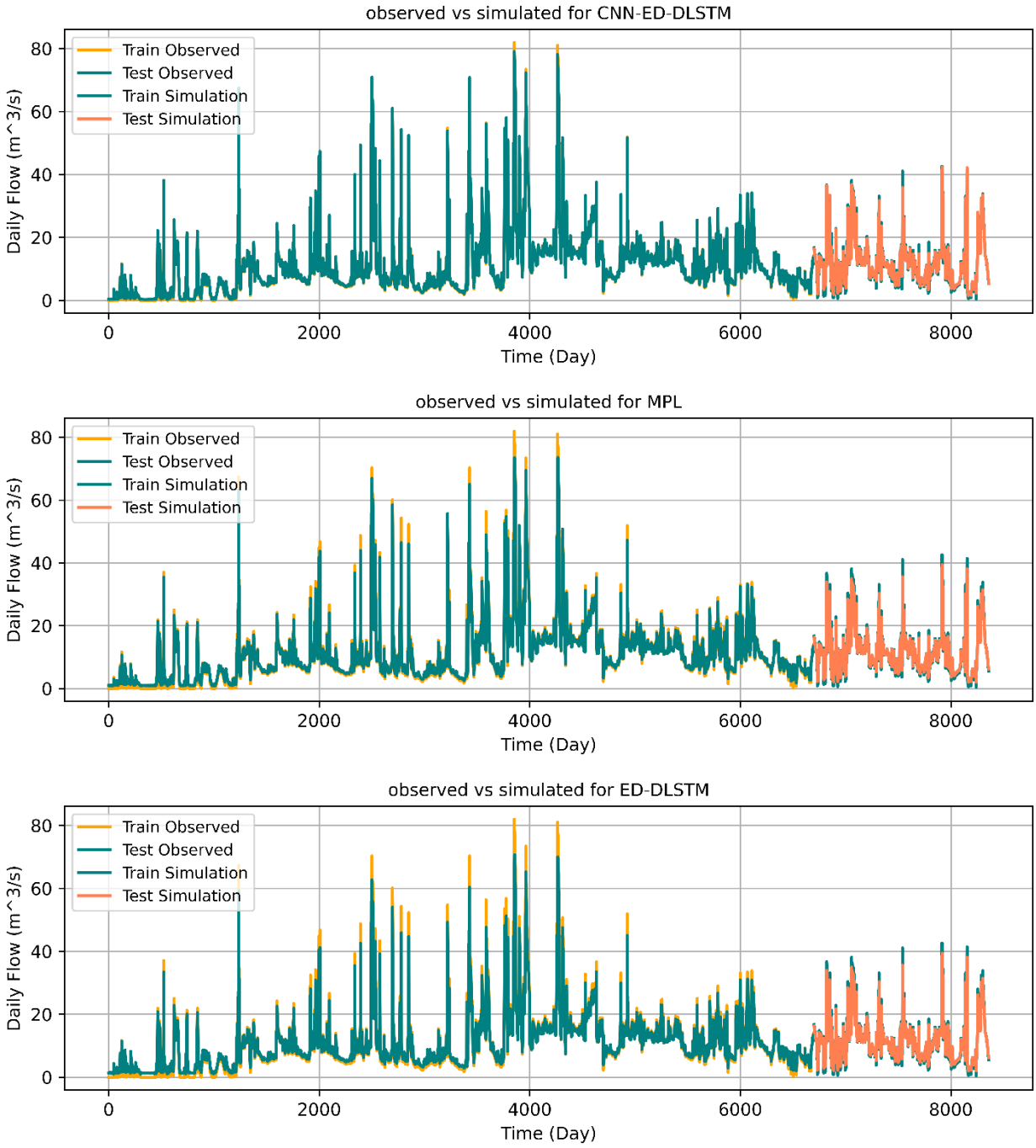

Figure 7| Comparison of observed and predicted flow hydrograph for daily simulation

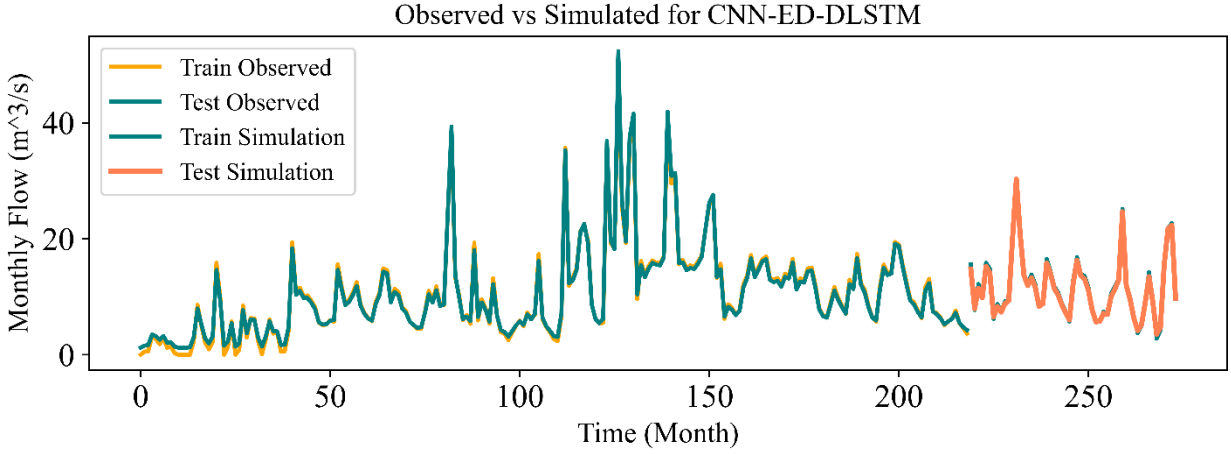

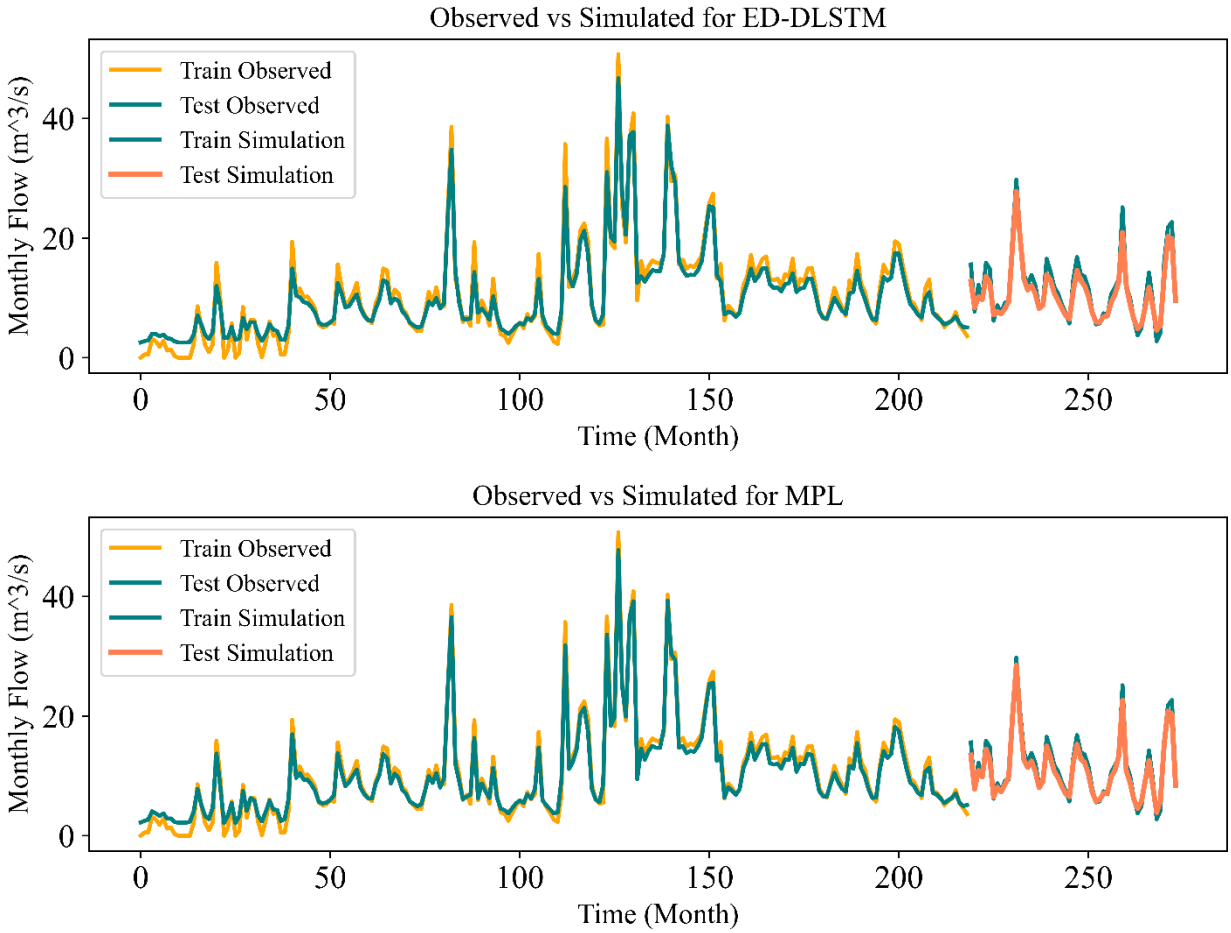

Figure 8| Comparison of observed and predicted flow hydrograph for monthly simulation

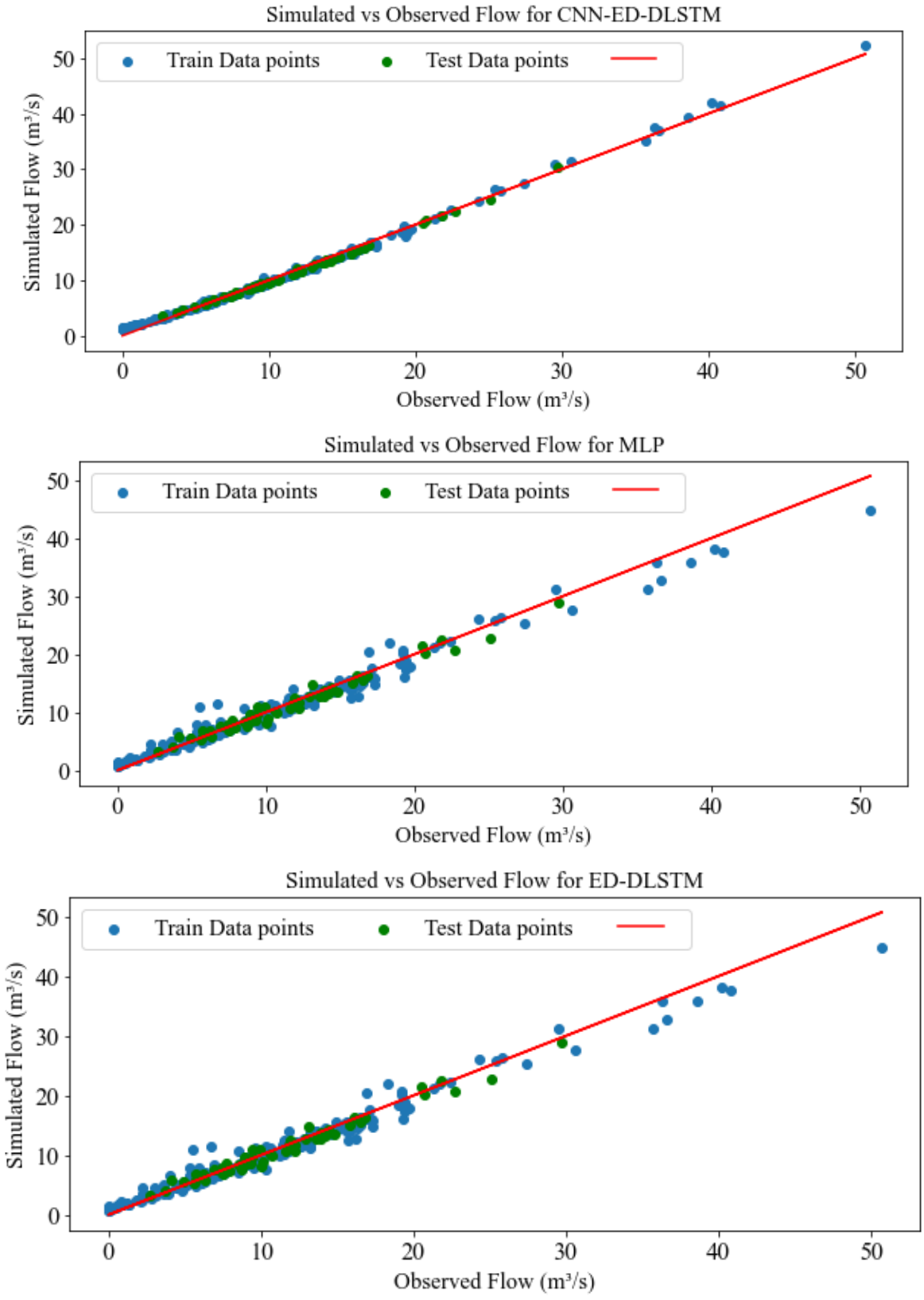

Figure 9 | Scatter plot for employed DL models

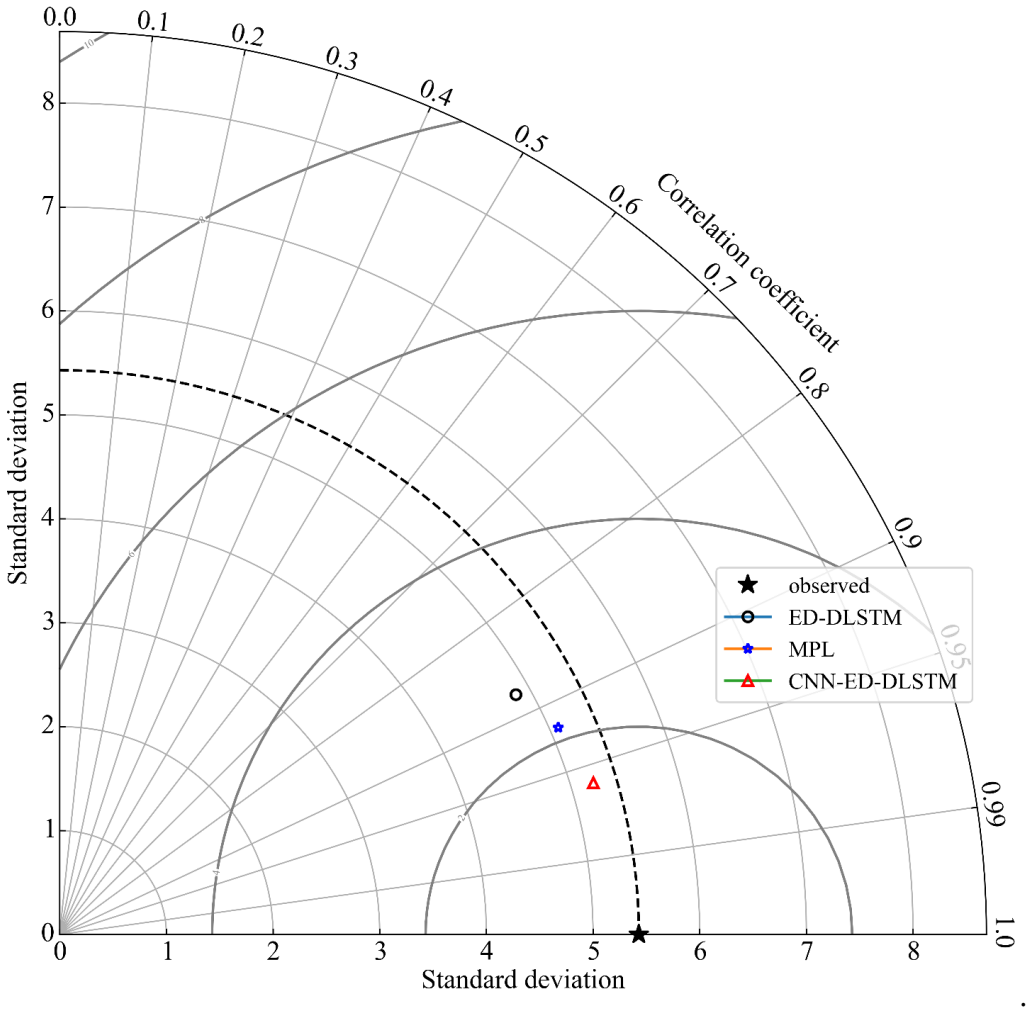

Figure 10 | Taylor diagram displays the standard deviations and correlation coefficient between observed and predicted hydrograph for the proposed models.

Table 4| Performance of DL Model for Kulfo watershed.

	Testing Period			
Model name	MAE	RMSE	NSE	R^2
MPL_1	5.13	3.01	0.87	0.89
MPL_2	4.64	2.94	0.88	0.91
MPL_3	4.12	2.87	0.90	0.93
MPL_4	4.05	2.52	0.92	0.94
$ED\text{-}DLSTM_1$	5.91	4.11	0.84	0.86
$ED\text{-}DLSTM_2$	5.95	4.12	0.83	0.86
$ED\text{-}DLSTM_3$	5.53	3.81	0.85	0.87
$ED\text{-}DLSTM_4$	4.74	3.12	0.87	0.88
CNN-ED-DLSTM1	3.34	2.32	0.93	0.95
$CNN\text{-}ED\text{-}DLSTM_2$	3.13	2.11	0.94	0.95
$CNN\text{-}ED\text{-}DLSTM_3$	3.04	1.62	0.94	0.96
$CNN\text{-}ED\text{-}DLSTM_4$	2.85	1.41	0.96	0.97

This study gathered daily discharge data from Kulfo station and daily rainfall data from five gauging stations, covering 22 flood events from 1991 to 2013.

Table 5| Collected flood events with their predicted values for Kulfo Watershed.

Event No.	Time	Observed (m^3s^{-1})	MPL (predicted)	ED-DLSTM (Predicted)	CNN-ED-DLSTM model (predicted)

1	1997/11/26	70.32	67.76	65.88	68.89
2	2001/8/9	81.95	77.78	74.56	79.34
3	2001/8/11	78.32	76.21	74.54	77.06
4	2001/8/13	77.42	75.74	74.38	76.03
	…	…	…	…	…
19	2002/9/24	81.04	77.09	86.90	79.97
20	2002/9/25	79.67	77.34	76.88	78.82
21	2002/9/27	77.42	73.76	75.12	76.32
22	2002/10/3	87.29	85.67	80.36	86.45

3.2. Discussion

This study highlights the significant potential of deep learning models, particularly CNN-ED-DLSTM, in flood simulation and prediction. By leveraging 1D CNNs for spatial feature extraction and LSTMs for long-term temporal dependencies, CNN-ED-DLSTM effectively captures key flood dynamics, including variations in flow patterns, peak discharge, and recession trends, enhancing the accuracy of flood simulation. Numerical metrics, loss curves, and scatter plots confirm its superior predictive performance, demonstrating a high degree of agreement with observed flood discharge data. Compared to alternative models, CNN-ED-DLSTM outperforms both MLP and ED-DLSTM, showcasing its ability to model complex hydrological patterns. However, while MLP is a simpler model, it often generalizes well and achieves competitive accuracy, making it a viable alternative in certain cases. ED-DLSTM, despite its advanced architecture, sometimes underperforms due to overfitting, computational demands, or sensitivity to hyperparameter tuning [15]. The study also emphasizes the importance of input data selection and lag times, with precipitation emerging as the most influential predictor. Scenario 4, which prioritizes precipitation, achieved the best performance, highlighting the necessity of carefully chosen input variables for accurate flood simulation. The findings underscore the need for further research to refine these models, optimize hyperparameters, and evaluate performance across different temporal scales and climatic regions. Incorporating high-resolution spatial and temporal data could further enhance predictive accuracy. In conclusion, CNN-ED-DLSTM's hybrid architecture provides a robust framework for flood simulation, offering a powerful tool for hydrological modeling and flood risk management. Future studies should focus on improving model generalizability and adapting these techniques to real-time forecasting applications in flood-prone regions.

4. Conclusion

The study highlights the strong potential of deep learning models, particularly CNN-ED-DLSTM, for accurate flood simulation. By integrating 1D CNNs for feature extraction and LSTMs for capturing long-term temporal dependencies, CNN-ED-DLSTM effectively models complex flood dynamics, including base flow, rising limbs, peak discharge, and recession limbs. Its hybrid architecture enables robust processing of precipitation and runoff data, leading to superior predictive performance compared to ED-DLSTM and MLP. While MLP demonstrates good generalization in some cases, CNN-ED-DLSTM's ability to combine spatial and temporal features makes it a more powerful tool for flood forecasting. The study underscores the importance of input selection, with precipitation emerging as a key factor in improving simulation accuracy. Additionally, it highlights that model performance can vary depending on complexity, with simpler models sometimes offering better generalization. Future research should focus on refining these models across diverse temporal scales and climatic regions, integrating high-resolution data to enhance their applicability in flood risk management and early warning systems.

Declaration of interests

The authors declare that they have no known competing financial interests.

Research Support

The research received no external financial or non-financial support.

Data Availability Statement

The data will be available on request.

REFERENCES

Y. Lin, D. Wang, Y. Meng, W. Sun, and J. Qiu, "Journal of Hydrology : Regional Studies Bias learning improves data driven models for streamflow prediction," *J. Hydrol. Reg. Stud.*, vol. 50, p. 101557, 2023, doi: 10.1016/j.ejrh.2023.101557.

N. Bhatia, L. Sharma, S. Srivastava, N. Katyal, and R. Srivastav, "Streamflow Decomposition Based Integrated ANN Model," vol. 2013, no. January, pp. 15–19, 2013.

R. Curve *et al.*, "Journal of Hydrology : Regional Studies Streamflow Simulations Using Machine Learning Models at Various Temporal Scales Under Rating Curve Uncertainty Conditions in Southern Ethiopia".

S. Duan, P. Ullrich, and L. Shu, "Using Convolutional Neural Networks for Streamflow Projection in California," vol. 2, no. September, pp. 1–19, 2020, doi: 10.3389/frwa.2020.00028.

T. Song, W. Ding, J. Wu, H. Liu, H. Zhou, and J. Chu, "Flash flood forecasting based on long short-term memory networks," *Water (Switzerland)*, vol. 12, no. 1, 2020, doi: 10.3390/w12010109.

E. B. Wegayehu and F. B. Muluneh, "Short-Term Daily Univariate Streamflow Forecasting Using Deep Learning Models," *Adv. Meteorol.*, vol. 2022, 2022, doi: 10.1155/2022/1860460.

J. Ji, C. Choi, M. Yu, and J. Yi, "Comparison of a data-driven model and a physical model for flood forecasting," *WIT Trans. Ecol. Environ.*, vol. 159, pp. 133–142, 2012, doi: 10.2495/FRIAR120111.

V. Atashi, R. Kardan, H. Taheri Gorji, and Y. Lim, *Comparative Study of Deep Learning LSTM and 1D-CNN Models for Real-time Flood Prediction in Red River of the North, USA*. 2023. doi: 10.1109/eIT57321.2023.10187358.

H. Huang *et al.*, "Improving the explainability of CNN-LSTM-based flood prediction with integrating SHAP technique," *Ecol. Inform.*, vol. 84, p. 102904, 2024, doi: https://doi.org/10.1016/j.ecoinf.2024.102904.

S. Mathewos, T. Yisihak, T. Kumar, N. Bekele, M. Legesse, and M. Arja, "Heliyon Comparative analysis in selecting best irrigation method to maximize tomato yield from various irrigation approaches in water scarce regions," *Heliyon*, vol. 10, no. 7, p. e28746, 2024, doi: 10.1016/j.heliyon.2024.e28746.

V. Te Chow, D. R. Maidment, L. W. Mays, and L. W. M. Ven Te Chow, David R. Maidment, "Applied Hydrology Chow 1988.pdf." pp. 1–294, 1988. [Online]. Available: http://ponce.sdsu.edu/Applied_Hydrology_Chow_1988.pdf

H. Apaydin, H. Feizi, M. T. Sattari, and M. S. Colak, "Comparative Analysis of Recurrent Neural Network," pp. 1–18.

S. P. Van, H. M. Le, D. V. Thanh, T. D. Dang, H. H. Loc, and D. T. Anh, "Deep learning convolutional neural network in rainfall-runoff modelling," *J. Hydroinformatics*, vol. 22, no. 3, pp. 541–561, 2020, doi: 10.2166/hydro.2020.095.

A. Zeroual, M. Meddi, and A. A. Assani, "Artificial Neural Network Rainfall-Discharge Model Assessment Under Rating Curve Uncertainty and Monthly Discharge Volume Predictions," *Water Resour. Manag.*, vol. 30, no. 9, pp. 3191–3205, 2016, doi: 10.1007/s11269-016-1340-8.

M.-C. Popescu, V. Balas, L. Perescu-Popescu, and N. Mastorakis, "Multilayer perceptron and neural networks," *WSEAS Trans. Circuits Syst.*, vol. 8, 2009.

A. Al Bataineh, D. Kaur, and S. Jalali, "Multi-Layer Perceptron Training Optimization Using Nature Inspired Computing," *IEEE Access*, vol. 10, p. 1, Jan. 2022, doi: 10.1109/ACCESS.2022.3164669.

M. Waqas and U. Humphries, "A Critical Review of RNN and LSTM Variants in Hydrological Time Series Predictions," *MethodsX*, vol. 13, Sep. 2024, doi: 10.1016/j.mex.2024.102946.

I.-F. Kao, Y. Zhou, L.-C. Chang, and F.-J. Chang, "Exploring a Long Short-Term Memory based Encoder-Decoder Framework for Multi-Step-Ahead Flood Forecasting," *J. Hydrol.*, vol. 583, p. 124631, 2020, doi: 10.1016/j.jhydrol.2020.124631.

J. Han *et al.*, "Integrating Convolutional Attention and Encoder–Decoder Long Short-Term Memory for Enhanced Soil Moisture Prediction," *Water*, vol. 16, p. 3481, Dec. 2024, doi: 10.3390/w16233481.

A. Sagheer, H. Hamdoun, and H. Youness, "Deep lstm-based transfer learning approach for coherent forecasts in hierarchical time series," *Sensors*, vol. 21, no. 13, pp. 1–23, 2021, doi: 10.3390/s21134379.

Theme 2

Renewable Energy

Theme 3

Irrigation and Drainage

Enhancing Tomato Productivity in Sodic-Saline Soils Using Mulching and Gypsum Amendment: Yield Prediction via Machine Learning Approach

Birara Gebeyhu*[1], Woinshet Habite[1]

[1]Faculty of Water Resources and Irrigation Engineering, Arba Minch Water Technology Institute, Arba Minch University, Arba Minch, Ethiopia.

*Corresponding author: biraragebeyhu@gmail.com

Abstract

Tomato production in Lake Abaya western shore, Ethiopia, was constrained by saline-sodic soil conditions, yet appropriate mitigation strategies are rarely implemented. The study aims to evaluate the effects of mulching and gypsum as sodic-saline soil amendments on tomato productivity and to assess the performance of Random Forest (RF) machine learning techniques in predicting tomato yield though evaluating coefficients of determination (R^2), Nash–Sutcliffe coefficient of efficiency (NSE), root mean square error (RMSE) and treatments were control (T1), mulching (T2), gypsum (T3), and combination of mulching and half level gypsum (T4). Soil samples were collected to 60cm for physicochemical analysis, while irrigation and soil moisture were measured in-field. Percentage of exchangeable sodium was decreased by 42.3% (T2), 38.1% (T3), and 43.8% (T4) and soil pH also reduced by 15.1% (T2), 1.1% (T3), and 14% (T4) compared with T1. Soil electrical conductivity was decreased by **0.31 ds/m (**T2), **0.10 ds/m** (T3), and **0.24 ds/m** (T4). Land productivity was improved by 8.7% (T2), 0.7% (T3), and 24.8% (T4), compared to T1 and where water productivity also increased by 30.9% (T2) and 41.8% (T4). RF identified irrigation as most influential (T1: 50%, T2: 40%, T3: 45%, T4: 35%), followed by temperature (25–32%). The mean R^2, NSE and RMSE of the RF model were 0.87, 0.87 & 1.08ton/ha (T1), 0.88, 0.89 & 1.18ton/ha (T2), 0.90, 0.91 & 0.94ton/ha (T3), and 0.92, 0.94 & 1.12ton/ha (T4), respectively. Gypsum and mulching enhance agricultural resilience in salinity-affected areas, while the Random Forest model accurately predicts tomato yield.

Keywords; *Gypsum; Land Productivity; Machine learning; Mulching*

1. Introduction

Tomato (Solanum lycopersicum) is a widely cultivated and economically significant vegetable crop grown worldwide, including Ethiopia (Leogrande et al., 2012). Nevertheless, tomato production is affected by several factors such as soil salinity, and sodicity (Lioubimtseva, 2010). Tomato under saline conditions endure osmotic pressure-induced water stress, salt-induced mineral toxicity stress (Tanveer et al., 2019), and mineral equilibrium imbalances (Ram et al., 2017). Implementing effective soil amendments like straw mulching (Abd El-Mageed et al., 2016) and gypsum application (Hanson & May, 2011) are important to improve tomato yield in saline sodic soil. Gypsum provides essential nutrients calcium and sulfur, improving sodic soils by replacing sodium with calcium and enhancing soil structure, water infiltration, and root development (Watts & Dick, 2014). Application of organic such as straw also be beneficial in increasing fertility (Abid et al., 2020) and organic matter content (Walche et al., 2023).

Machine learning algorithms such as Random Forest (RF)**,** has demonstrated remarkable success in predicting agricultural parameters such as crop biomass, and yield under the response of straw mulching and gypsum application (Paithane, 2023). Random Forest (RF) is an ensemble learning method that builds multiple regression decision trees during training and outputs the average prediction for regression problems (Mohammadi et al., 2024). These algorithms is particularly effective due to their ability to handle large, non-linear, and heterogeneous datasets (Inoue, 2020).

The pumped irrigation scheme in western shore of Lake Abaya faces saline-sodic soil issues, (Setegn et al., 2022) and that may limiting tomato production in the area. Irrigation waters sources of pumped irrigation scheme from Lake Abaya was too alkaline with an average pH of 8.66 and electric conductivity of 1.25ds/m (Oba, 2017). To mitigate this saline sodic problem of irrigation scheme, proper saline sodic amendments were not evaluated to increase tomato production in the area. The small hold farmer in the area also have not an idea about saline sodic amendments strategies. Potential of random forest model to forecast tomato yields under response of mulching and gypsum saline-sodic soil amendment not properly evaluated. Addressing these gaps is important for improving soil management and ensuring sustainable tomato cultivation. Therefore, this research was conducted to evaluates effects of straw mulching, gypsum, and their combination on tomato productivity in saline-sodic soils and to assess the performance of Random Forest machine learning algorithms to predict yield under these treatments. The significance of this finding lies in improving tomato productivity in sodic-saline soils using mulching and gypsum while demonstrating Random Forest's accuracy in predicting yield.

2. Material and Methods

2.1. Study area description

The study area was located between 6°09'0"N to 6°11'0"N latitude and 37°41'0"E to 37°42'0"E longitude, at an elevation of around 1203 meters above sea level. The area was irrigated using water from Lake Abaya, with tomatoes being the most widely cultivated crop, followed by onions, peppers, and cabbage. Average monthly temperature of 24.4°C and annual rainfall of 934.9 mm. The soil at the site was classified as silty clay with an average bulk density of 1.28 g/cm³. Field capacity and permanent wilting point were 38.5% and 26.8%, respectively and the basic infiltration rate of study area was 0.06mm/min.

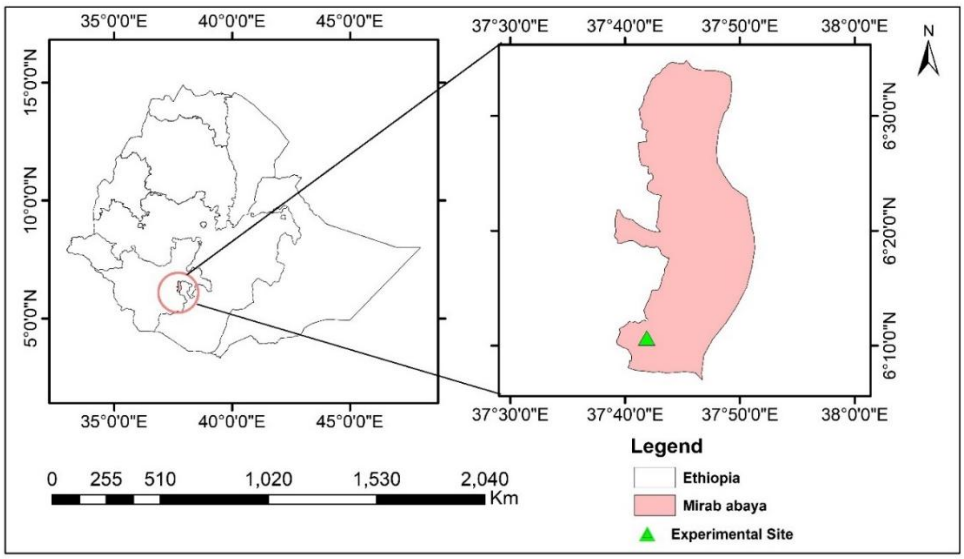

Figure 2: Study area location map

2.2. Experimental plot design

Experiments were conducted at on the western shore of Lake Abaya, using straw mulch and gypsum treatments. The experiment followed a randomized complete block design with three replications and four treatments: control (T1), mulching (T2), gypsum (T3), and mulching with half gypsum (T4). The application rate of straw mulch and gypsum were 15tons/ha and 14.5ton/ha, respectively and both gypsum and mulch were applied at time of tomato transplanting date. Tomatoes were the experimental crop, irrigated via furrow irrigation with full water application. Plot size was 3.75m², with 0.75m furrow

spacing and 5m furrow length (Figure 2). The total experimental area was 156.25m². The experiment conducted from January 7 to April 10, 2023, and December 25, 2023, to April 5, 2024. The source of irrigation water was Lake Abaya, and it was diverted to the farm using a pump system.

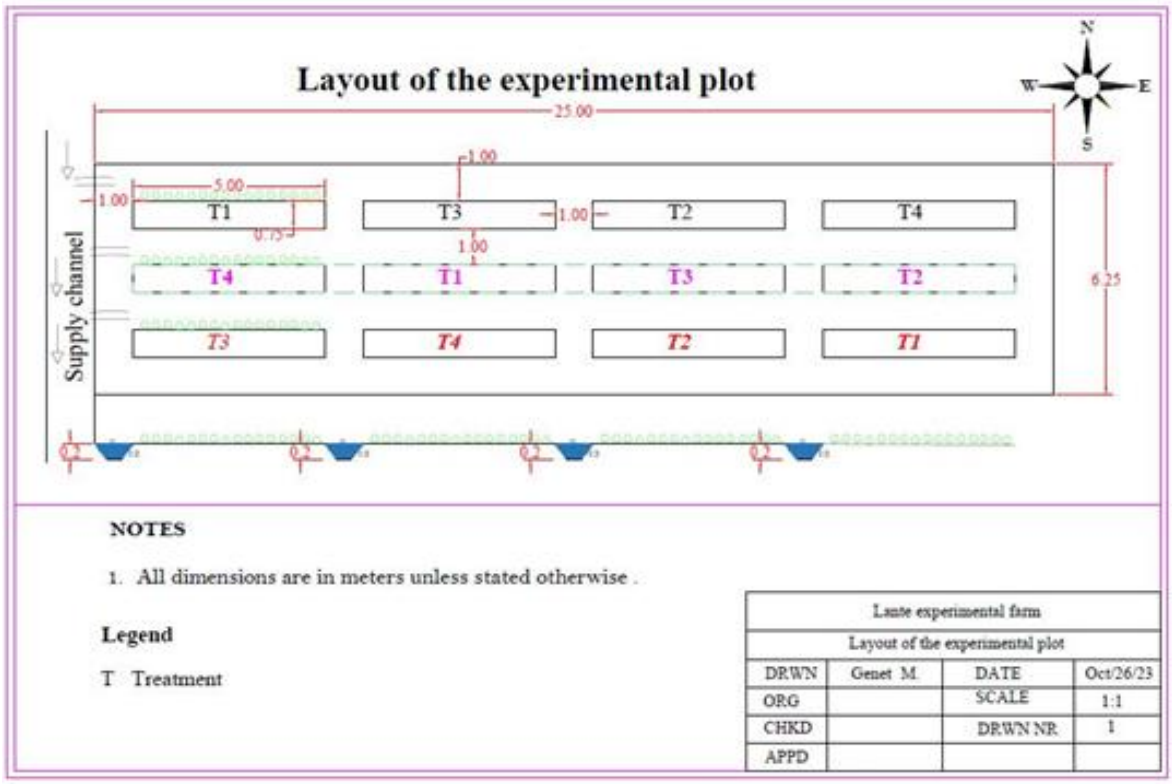

Figure 3: Alignment of the experimental plot

2.3. Soil physiochemical properties

Soil samples were collected using a composite method at 60cm depth with 20cm intervals from experimental plots and dried at 105°C for 24 hours. Soil texture was analyzed using a hydrometer test, while permanent wilting point θ_{pwp} and field capacity (θ_c) were evaluated using pressure plate apparatus. Soil electrical conductivity and pH of experimental site were measured using EC and pH meters at1:2.5 soil-to-water ratio. Exchangeable potassium and sodium were measured using a flame photometer after extracting using ammonium acetate where calcium and magnesium via EDTA titration method. Soil moisture at time of irrigation (θ_t) was monitor using calibrating Time Domain Reflectometry. Amount of gypsum requirement, exchangeable sodium perecentage (ESP) and irrigation required were estimated by Eq 1, Eq 2, and Eq 3, respectively.

$$\text{Gypsum requirement } \left(\frac{\text{ton}}{\text{ha}}\right) = 1.72 * \text{CEC} * \frac{ESP_{in} - ESP_f}{100} \quad (1)$$

$$\text{ESP } (\%) = \frac{ExchNa +}{\text{CEC}} * 100 \quad (2)$$

$$\text{Irrigation requierd (mm)} = \sum_{i=1}^{n} \left(\frac{\theta_c - \theta_t}{100}\right) * d_i \quad (3)$$

Where: CEC is sum of exchangeable cations (Ca^{2+}, Mg^{2+}, Na^{+}, and K^{+}), ESP_{in} is the initial ESP (%) of the soil to be amended, ESP_f is the final ESP (%) after treatment, and d_i is soil depth in i^{th} layer of soil.

2.4. Productivity and economic analysis

Land and water productivity are important elements in longer-term and strategic water resources planning (Ahmed et al., 2017). Water and land productivity of the experiments were evaluated through Eq 4 &5. The net return can be calculated by deducting total cost from gross return after (Fan et al., 2023) in using Eq 6. The gross return was calculated by multiplying the market price at the time of harvesting by the marketable tomato yield and benefit-cost ratio also calculated by using Eq 7.

$$\text{Water productivity} = \frac{\text{Yield (kg)}}{\text{Water supply } (m^3)} \quad (4)$$

$$\text{Land Productivity} = \frac{\text{Yield (ton)}}{\text{Irrigated land (ha)}} \quad (5)$$

$$Net\ return\ \left(\frac{ETB}{ha}\right) = Gross\ return\left(\frac{ETB}{ha}\right) - total\ cost\left(\frac{ETB}{ha}\right) \quad (6)$$

$$Benefit\ cost\ ratio = \frac{Gross\ return\ \left(\frac{ETB}{ha}\right)}{Total\ cost\ \left(\frac{ETB}{ha}\right)} \quad (7)$$

Random forest machine learning

Features like irrigation, temperature, humidity, wind speed, gypsum, and straw mulching were used to predict tomato yield across treatments. Biomass data from two years were collected for training (Year 1) and testing (Year 2) the model. The training dataset was used to build and optimize the models, while the testing set allowed for an evaluation of the model performance. Number of trees during train process were fixed according to (Belgiu & Dra, 2016) using griding search techniques and the search range for number of tree (Ntree) was from 10 to 200 and random sample was 42 that was commonly used in worldwide. Based on (Prasad et al., 2006), bootstrap sample sets, denoted as X_i (where i represents the bootstrap iteration, constrained to the range [1, ntree], were randomly drawn with replacement from the original training dataset. Data points not included in X_i for a given bootstrap sample are referred to as out-of-bag (OOB) data as show in Figure 3 and the green subset was prediction and the remaining subset were out of bag data.

$$Y = \frac{1}{T}\sum_{i}^{T} h_t(x) \quad (8)$$

Where: y is predicted value, T is number of decision trees, ht(x) is prediction value from the t^{th} decision tree, x is input feature.

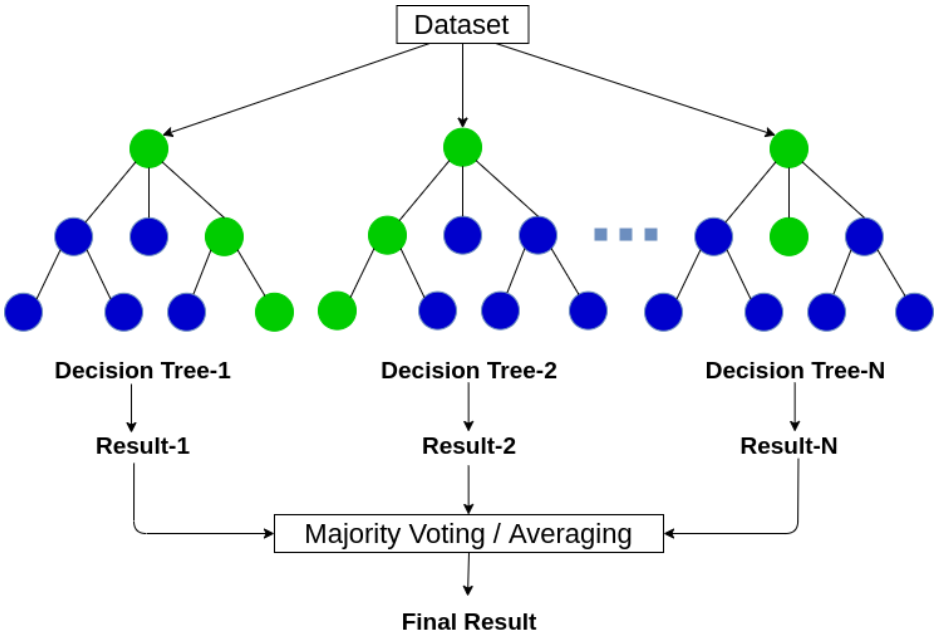

Figure 4:Schematic structure of random forest model for this study

Model performance indicators such as root means square error (RMSE)and Nash–Sutcliffe coefficient of efficiency (NSE) were estimated based on (Soomro et al., 2019).

$$\text{RMSE} = \sqrt{\frac{1}{\text{n}}\sum_{\text{i=1}}^{\text{n}}(\text{S s} - M_o)\text{\^{}2}} \quad (9)$$

$$\text{NSE} = 1 - \frac{\sum_{\text{i=1}}^{\text{n}}(\text{S s} - M_o)\text{\^{}2}}{\sum_{\text{i=1}}^{\text{n}}(M_o - M_{oav})^2} \quad (10)$$

Where S_s, M_o, and M_{oav} were predicting value, measured values and mean of measured values, respectively, and n is the number of observations.

3. Result and Discussion

3.1. Effects of treatment on irrigation water

The total seasonal crop water requirement of tomatoes was 378mm under non-mulching and 333.02mm under soil mulching practices. Compared to previous findings, this value is lower than the 395.5mm reported by (Maingi et al., 2020), for non-mulched tomatoes but higher than the 343.23mm reported by (Affessa, 2022) for the Arba Minch area. Differences in water requirements are influenced by climate, soil type, crop variety, and agricultural practices (Ewaid et al., 2019). Straw mulching was saved about 13.2% of soil water by reducing surface evaporation. Surface-applied straw mulch increased soil water by 4.4%, while buried straw increased it by only 0.9% (X. Song et al., 2020), showing that surface mulch is more effective. Mulching supports sustainable agriculture in water-limited areas by improving soil moisture retention and reducing irrigation needs (El-Beltagi et al., 2022).

3.2. Effects of treatment on exchangeable cation

Under T1, exchangeable sodium (Na^+), magnesium (Mg^{2+}), and calcium (Ca^{2+}) were increased (Figure 4). The alkaline content Lake Abaya water 44.28meq/L Na^+, 2.8 meq/L Mg^{2+}, and 2.2 meq/L Ca^{2+} (Setegn, 2022) that may was cause of increasing cation of soil in the current study. Conversely,

potassium decreased in T1 and T3 due to plant uptake and the lower K content in silt clay soils compared to clay soils (Ghiri & Hashemi, 2015). Straw mulching in T2 and T4 increased exchangeable potassium through nutrient release from decomposing straw, enhancing K levels by 6.64–18.54% (Li et al., 2014). Decomposition also promotes chelation that increasing leaching process of Mg^{2+} and Ca^{2+} (Xu et al., 2016), and accelerates saline-sodic leaching by 7.3% (M. Li et al., 2023). The competitive adsorption of K^{+}, Ca^{2+}, and Mg^{2+} further influenced their availability (Ranjbar & Jalali, 2017). At harvest, Na^{+} decreased by 48.2% (T2), 40.4% (T3), and 48.9% (T4), aided by straw mulching and gypsum, which reduce soil Na^{+} by up to 66.7% while increasing Ca^{2+} and Mg^{2+} (Saeed & Ahmad, 2009). Straw mulch also increases humic acid carbon by 26.5% % (X. Chen et al., 2020) and promotes Na^{+} replacement with H^{+} (Paramisparam et al., 2021), forming sodium sulfate and improving soil structure (Choudhary & Kharche, 2018).These research shown the aids of straw mulching and gypsum in managing soil cation balance and fertility.

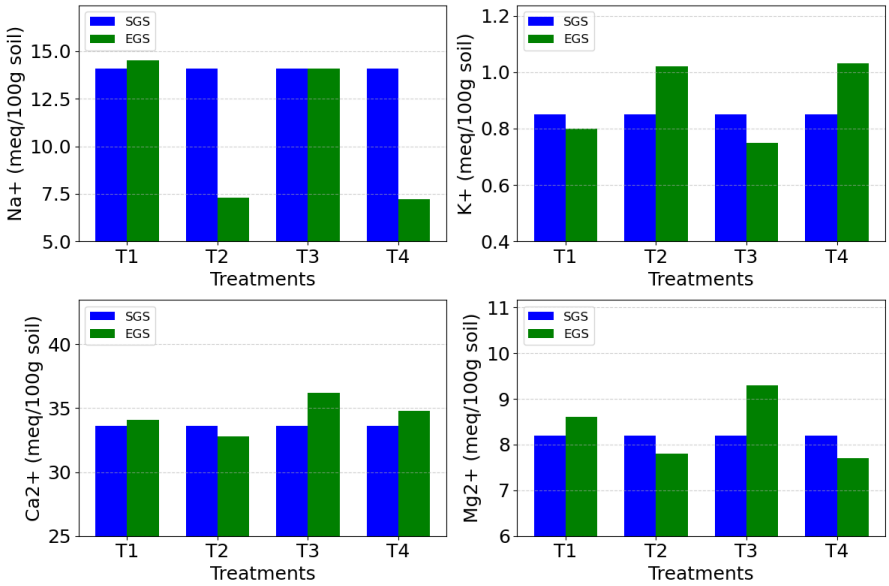

Figure 5:Exchangeable cation for each treatment

Notes: SGS and EGS were stand for starting of growing season, and end of growing season, respectively.

The total cation exchange capacity and exchangeable sodium percentage of the soil were 56.7 meq/100g and 24.8%, respectively. These values were higher than those reported in the Central Rift Valley, where average values were 41.4meq/100g and 39.4%, respectively (Kiflu, 2021), indicating site-specific variability due to differences in alkalinity sources. As noted by Daba and Qureshi (2021), soils with exchangeable sodium percentages above 15% are considered sodic, confirming high sodicity in the study area. By the end of the season, exchangeable sodium percentage decreased by 42.3% (T2), 38.1% (T3), and 43.8% (T4) compared to T1, with the highest reduction under T4 (Figure 5). This aligns with (X. Song et al., 2020), who reported a 33% reduction using straw mulching. Surface straw mulching reduced the sodium absorption ratio by 21.5%, more effectively than straw burial (7.4%). Similarly, (Y. Zhang et al., 2020), found that applying 100% gypsum reduced sodium levels by 70.5%.

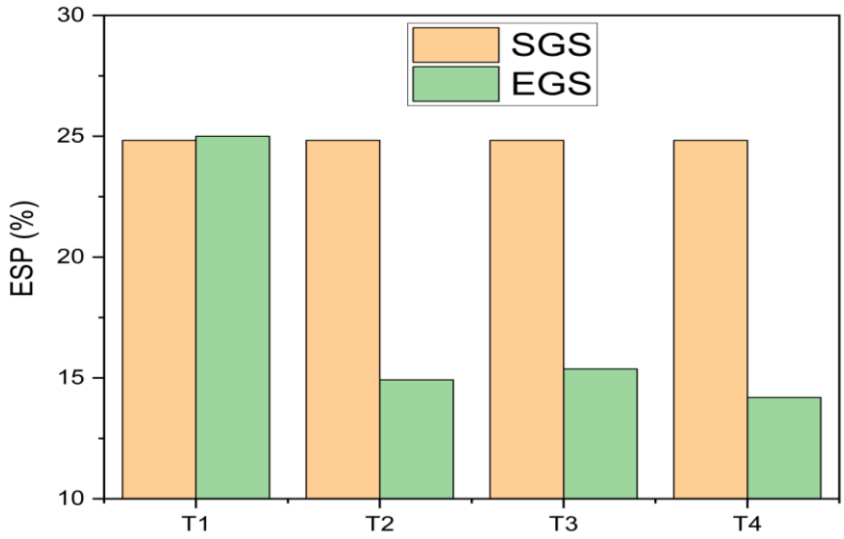

Figure 6: Exchangeable sodium percentage for each treatment

3.3. Soil pH, electric conductivity, and organic matter and carbon

At the experimental site, soil pH levels exhibited reductions in treatments T2 (15.1%), T3 (1.1%), and T4 (14%) compared to T1 (Figure 6). Organic mulches tend to slightly acidify soil during decomposition (Mbukwa et al., 2023), leading to decreased pH in treatments 2 and 4. Gypsum application, being a neutral salt (Dubrovina et al., 2021), showed less significant impact on soil pH in T3 compared to T1. However, it facilitated leaching of alkaline salts, contributing to a slight pH reduction in T3 (Tavakkoli & Mcdonald, 2021). Comparatively, pH values at the end of the growing season did not significantly differ between T1 and T3, indicating gradual changes with prolonged alkaline irrigation. Lake Abaya water pH was reported as 8.7 (Oba, 2017), and 8.5 (Setegn, 2022). Higher gypsum application rates resulted in greater soil pH reductions, with values dropping from 8.48 to 8.3 at 2.5 tons/ha and further to 8.26 at 5 tons/ha (Tavakkoli & Mcdonald, 2021). Application of 100% gypsum can lower pH from 8.29 to 7.98 (Bekele et al., 2020), similar to the pH decrease observed in T3 from 8.6 to 8.5 in the current study.

Straw mulching reduced soil bulk density (Z. Zhang et al., 2022), and promoted soil salt leaching through increased pore space (Kun et al., 2023). Electrical conductivity decreased by 59.6% (T2), 19.2% (T3), and 46.2% (T4) by the end of the tomato growing period (Figure 6). Application of 100% gypsum reduced soil electrical conductivity from 2.9 to 2.6ds/m (Zhao et al., 2019), while in T3, it was decreased from 0.52 to 0.42ds/m. Mulching aids in reducing soil electrical conductivity in saline soils by conserving water, leaching salts, and regulating soil temperature (Abd El-Mageed et al., 2016). The greatest reduction in electrical conductivity was observed in T4, compared to T2, due to these effects. Available soil organic matter increased by 8.6% (T1) and 11.1% (T4), and decreased by 4.9% (T1) and 3.7% (T3) (Figure 6), showing a similar trend for soil organic carbon. Straw mulch application increased soil organic matter by 3% in agricultural land (Qin et al., 2022), contrasting with a higher increase of 21.69% reported in other studies by (Maomao et al., 2014). Variations in organic matter effects from straw mulching are influenced by geographical, environmental, and soil factors (Changliang Du, 2022).

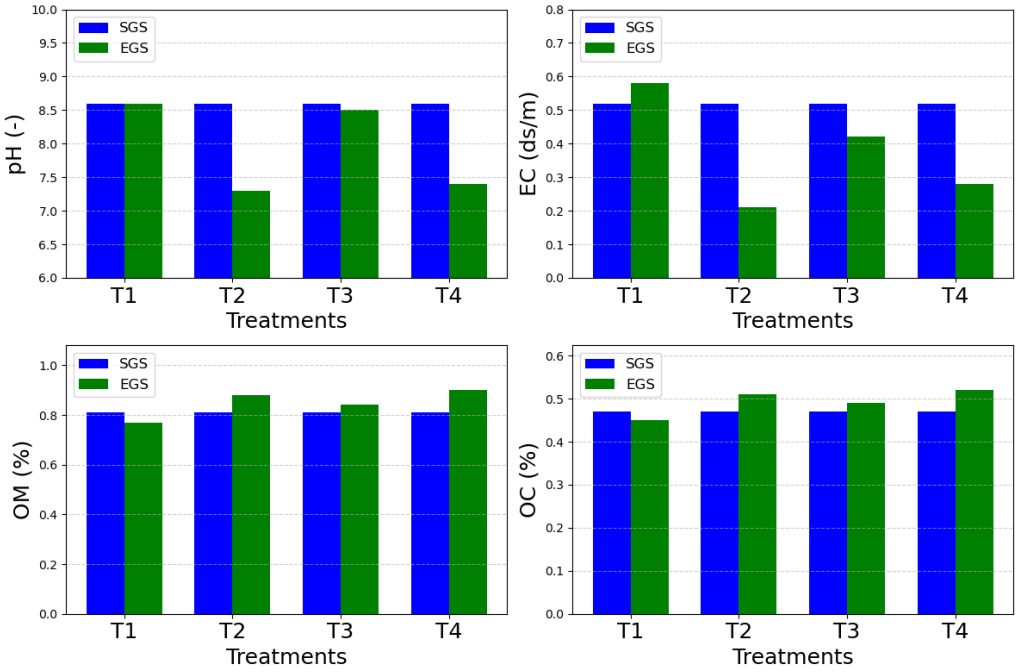

Figure 7: Soil electric conductivity (EC), pH value, organic matter (OM) and organic carbon (OC) for each treatment

3.4. Crop productivity, and benefit-cost ratio

Land productivity was improved by 8.7% (T2), 0.7% (T3), and 24.8% (T4) compared to T1 and where water productivity also increased by 30.9% (T2) and 41.8% (T4) (Figure 7). The highest land and water productivity was observed under T4, indicating the positive effect of combined straw mulching and regulated irrigation. These results align with studies such as (Zhou et al., 2009), who reported a 31% increase in water productivity due to mulching, and Mendonça et al. (2021), who recorded 41 tons/ha land productivity under full irrigation with mulching. Although the current productivity values are lower than the optimal benchmarks of 45–60tons/ha (Doorenbos and Kassam, 1986), the observed increases highlight the role of improved water management and mulching practices. Variations in productivity are likely influenced by location-specific factors such as soil type, salinity, climate, and farming practices, as supported by (Abd El-Mageed et al., 2016). The economic analysis revealed that T4 had the highest net return and benefit-cost ratio (B:C), with improvements of 81.8% in net return and 43.7% in B:C ratio compared to T1 (Figure 7). T2 also showed strong performance, with a 47.8% increase in net return and a 10.5% increase in B:C ratio compared to T1. T3 had moderate improvements, with a 10.0% increase in net return and a 6.9% increase in B:C ratio compared to T1. Based on (Kifle, 2019), tomato net returns under full irrigation in southern Ethiopia were higher compared with value of current study.

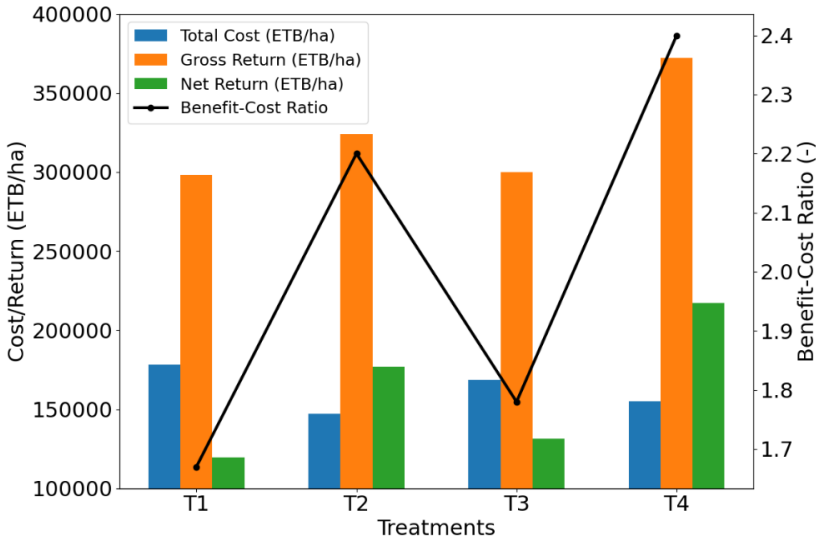

Figure 8: Total cost, gross return, net return and benefit cost ratio.

3.5. Feature importance and model performance

The Random Forest model recognized irrigation as the most influential factor for predicting tomato biomass across all treatments, contributing over 50% in T1 and remaining dominant in T2–T4 (Figure 8). Temperature was consistently the second key variable, followed by straw mulch in T2 (20%) and gypsum in T3 (18%). Wind speed and humidity had minimal and equal influence in all cases. These results highlight the primary role of water management and temperature in biomass prediction, with soil amendments offering additional benefits under specific treatments.

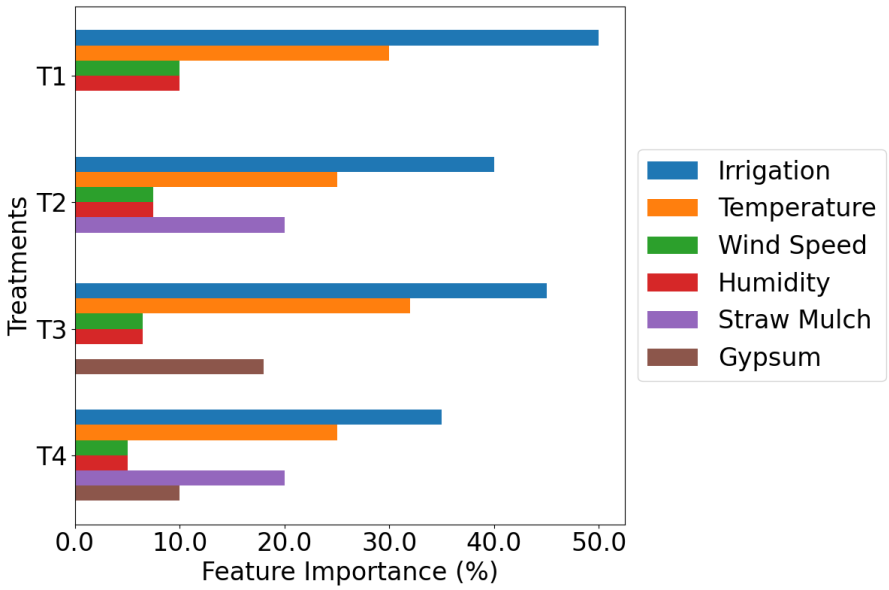

Figure 9: Random Forest perecentage of feature importance for predicting tomato biomass

For T1 (control), the random forest model achieved an R^2 of 0.88 (train) and 0.86 (test), an RMSE of 1.01 ton/ha (train) and 1.15 ton/ha (test), and an NSE of 0.87 (train) (Figure 9a) and 0.86 (test) (Figure 9b), indicating strong agreement between observed and predicted biomass values. Similarly, for T2 (straw mulching**)**, the R^2 improved to 0.89 (train) (Figure 9c) and 0.87 (test) (Figure 9d), while the RMSE increased slightly to 1.15 ton/ha (train) and 1.20 ton/ha (test), and the NSE rose to 0.90 (train) and 0.88 (test). The best performance was observed for T4 (half level gypsum + straw mulching)**,** where

the RF model achieved the highest R^2 of 0.92 (train) (Figure 9g) and 0.91 (test) (Figure 9h), an RMSE of 1.11 ton/ha (train) and 1.12 ton/ha (test), and an NSE of 0.95 (train) and 0.93 (test). For T3 (Gypsum**)**, the RF model also performed well, with an R^2 of 0.91 (train) (Figure 9e) and 0.89 (test) (Figure 9f)**,** RMSE of 0.93 ton/ha (train) and 0.95 ton/ha (test**)**, and NSE of 0.92 (train) and 0.90 (test)**.** Random forest models have demonstrated strong predictive performance in similar studies. RF model achieved an R^2 of 0.88, RMSE of 2.7 ton/ha, and NSE of 0.85 for tomato biomass prediction (Dey et al., 2024), and an R^2 of 0.85, RMSE of 3.2 ton/ha, and NSE of 0.83 (Y. Chen et al., 2021). These results are consistent with the current study, except for slight differences in RMSE values. Based on (Mancer et al., 2024), the R^2 for the random forest model predicting tomato biomass without mulching was 0.89, higher value of current study (T1). According to (J. Song, 2021), the RF model performed better during training than testing, as it learns from known patterns. This aligns with the current study, where accuracy decreased when tested on unseen data.

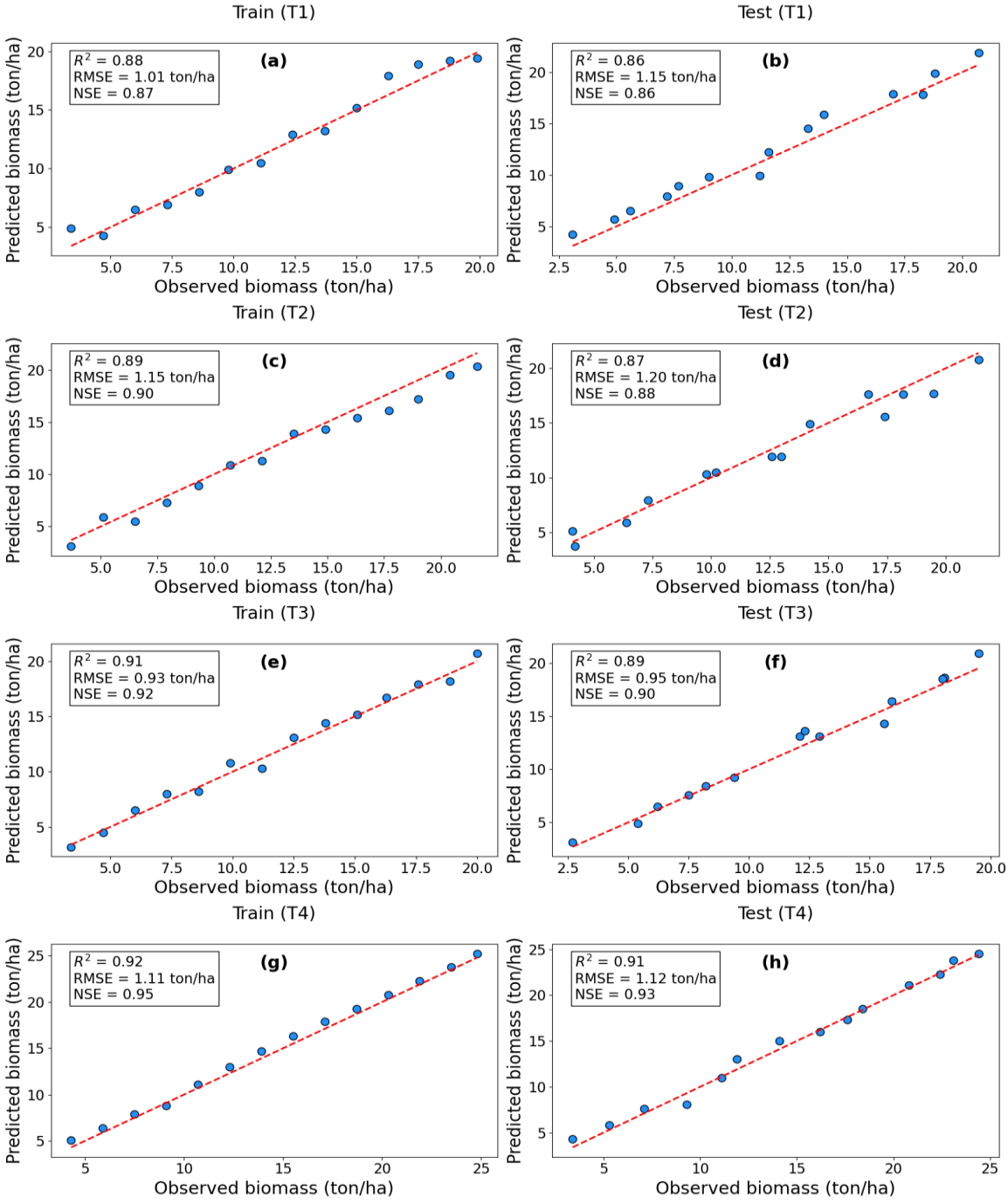

Figure 10: Performances of Random Forest model for each treatment during model train and test

4. Conclusion

The study conducted on the Western shore of Lake Abaya has provided substantial evidence that soil salinity and sodicity, a major impediment to agricultural productivity, can be effectively managed through the application of gypsum and the adoption of soil mulching. The significant reduction in exchangeable sodium percentage and soil pH, as well as the decrease in soil electric conductivity in treatments involving gypsum, mulching, and their combination, clearly indicates that these interventions have a positive impact on soil quality. Remarkably, the combination of mulching and half level of gypsum (T4) yielded the most favorable results, with a marked increase in tomato land and water productivity compared to the control group (T1). The Random Forest model showed improved performance in predicting tomato biomass under mulching and gypsum treatments, with the highest accuracy observed under the combined treatment (T4). These findings highlight the value of using mulching and half-level gypsum to restore soil health and call for supportive policies to promote sustainable productivity in saline-affected agricultural areas.

Declaration of interests

The authors affirm that there are no financial conflicts of interest or affiliations that could have influenced the outcomes of this work.

Acknowledgments

We sincerely thank the Water Resources Research office of Arba Minch University for their vital assistance in facilitating access to the experimental sites, financial support, and provision of necessary laboratory equipment.

References

Abd El-Mageed, T. A., Semida, W. M., & Abd El-Wahed, M. H. (2016). Effect of mulching on plant water status, soil salinity and yield of squash under summer-fall deficit irrigation in salt affected soil. *Agricultural Water Management*, *173*, 1–12. https://doi.org/10.1016/j.agwat.2016.04.025

Abid, N., Ansari, A., & Singh, S. (2020). *Contaminants in Agriculture*.

Affessa, M. (2022). *Assessment of stage-wise de cit furrow irrigation on tomato crop production at Arba minch , Ethiopia*.

Ahmed, N. U., Mahmud, N. U., Zaman, M. A. U., Ferdous, Z., & Halder, S. C. (2017). Effect of different salinity level on tomato (Lycopersicon esculentum) production under climate change condition in Bangladesh. *Annual Research and Review in Biology*, *13*(3). https://doi.org/10.9734/ARRB/2017/33613

Belgiu, M., & Dra, L. (2016). Random forest in remote sensing : A review of applications and future directions ˇ gut. *ISPRS Journal of Photogrammetry and Remote Sensing*, *114*, 24–31. https://doi.org/10.1016/j.isprsjprs.2016.01.011

Changliang Du, L. L. and Z. E. (2022). Effects of Straw Mulching and Reduced Tillage on Crop Production and Environment : A Review. *Water*, *14*(6), 1–15. https://doi.org/https://doi.org/10.3390/w14162471

Chen, X., Wu, J., & Opoku-kwanowaa, Y. (2020). E ff ects of Returning Granular Corn Straw on Soil Humus Composition and Humic Acid Structure Characteristics in Saline-Alkali Soil. *Sustainability*, *12*(3).

Chen, Y., Guerschman, J., Shendryk, Y., Henry, D., & Harrison, M. T. (2021). Estimating tomsto Biomass Using Sentinel-2 Imagery and Machine Learning. *Remote Sens*, *13*(4).

Choudhary, O. P., & Kharche, V. K. (2018). Soil Salinity and Sodicity. *Soil Science*, *September*.

Dey, B., Ferdous, J., & Ahmed, R. (2024). Machine learning based recommendation of agricultural and horticultural crop farming in India under the regime of NPK , soil pH and three climatic variables. *Heliyon*, *10*(3), e25112. https://doi.org/10.1016/j.heliyon.2024.e25112

Doorenbos and Kassam. (1986). Yield Response to Water: FAO Irrigation and Drainage Paper 33. In *FAO (Food and Agriculture Organization)*.

Dubrovina, T. A., Losev, A. A., Karpukhin, M. M., Vorobeichik, E. L., Dovletyarova, E. A., Brykov, V. A., Brykova, R. A., Ginocchio, R., & Carolina, Y. (2021). Chemosphere Gypsum soil amendment in metal-polluted soils — an added environmental hazard. *Chemosphere*, *281*, 1–9. https://doi.org/10.1016/j.chemosphere.2021.130889

El-Beltagi, H. S., Basit, A., Mohamed, H. I., Ali, I., Ullah, S., Kamel, E. A. R., Shalaby, T. A., Ramadan, K. M. A., Alkhateeb, A. A., & Ghazzawy, H. S. (2022). Mulching as a Sustainable Water and Soil Saving Practice in Agriculture: A Review. *Agronomy*, *12*(8), 1–31. https://doi.org/10.3390/agronomy12081881

Ewaid, S. H., Abed, S. A., & Ansari, N. Al. (2019). Crop Water Requirements and Irrigation Schedules for Some Major Crops in Southern Iraq. *Water*, *11*(4), 1–12.

Fan, Y., Wang, X., Chen, R., Dang, H., & Liu, H. (2023). *applied sciences Differences in Water Consumption and Yield Characteristics among Winter Wheat (Triticum aestivum L .) Varieties under Different Irrigation Systems*.

Ghiri, M. N., & Hashemi, S. (2015). Archives of Agronomy and Soil Science Potassium release from sand , silt and clay fractions in calcareous soils of southern Iran. *Archives of Agronomy and Soil Science*, *December 2012*. https://doi.org/10.1080/03650340.2011.591384

Hanson, B., & May, D. (2011). Drip Irrigation Salinity Management for Row Crops. *Drip Irrigation Salinity Management for Row Crops*. https://doi.org/10.3733/ucanr.8447

Inoue, Y. (2020). Soil Science and Plant Nutrition Satellite- and drone-based remote sensing of crops and soils for smart farming – a review. *Soil Science and Plant Nutrition*, *66*(6), 798–810. https://doi.org/10.1080/00380768.2020.1738899

Kifle, T. (2019). *Evaluation of Irrigation Regime on Tomato (Lycopersicon Esculentum), at Hadero Tunto Zuria Woreda, Ehiopia*. *19*(6).

Kiflu, A. (2021). *Gypsum and Water Level Effects on Central Rift Valley Sodic Soils of Ethiopia*. *December 2020*. https://doi.org/10.3923/ijss.2021.20.25

Kun, Á., Simon, B., & Boz, C. (2023). Effect of Mulching on Soil Quality in an Agroforestry System Irrigated with Reused Water. *Agronomy*, *13*(6), 1–12. https://doi.org/10.3390/agronomy13061622

Leogrande, R., Lopedota, O., Montemurro, F., Vitti, C., & Ventrella, D. (2012). *and yield of tomato m er ci al us e on m al*. *7*. https://doi.org/10.4081/ija.2012.e8

Li, J., Lu, J., Li, X., Ren, T., Cong, R., & Zhou, L. (2014). Dynamics of Potassium Release and Adsorption on Rice Straw Residue. *PLoS ONE*, *9*(2), 1–9. https://doi.org/10.1371/journal.pone.0090440

Lioubimtseva, E. (2010). Global Food Security and Grain Production Trends in Central Eurasia: Do Models Predict a New Window of Opportunity? *National Social Science Journal*, *41*(1), 154–165.

Maingi, S., Ndiiri, J., & Mati, B. (2020). *Estimation of Crop Water Requirements for Garden Pea , Sweet Pepper and Tomato using the CropWAT Model in Maragua Watershed , Murang ' a County , Kenya*. *5*, 112–123.

Mancer, M., Terrissa, L. S., & Ayad, S. (2024). Machine Learning-Based Prediction of Tomato Yield in Greenhouse Environments. *Proceedings of the International Conference on Emerging Intelligent Systems for Sustainable Development (ICEIS 2024)*. https://doi.org/10.2991/978-94-6463-496-9

Maomao, H., Xiaohou, S., & Yaming, Z. (2014). Effects of Different Regulatory Methods on Improvement of Greenhouse Saline Soils , Tomato Quality , and Yield. *The Scientific World Journal*.

Mbukwa, D., Gui, R., & Deng, S. (2023). Effect of Soil Organic Mulching Combined with Aeration Treatment on Soil Quality , Nutrients Content , and Lei Bamboo Shoot Production. *Agriculture*, *13*(3).

Mohammadi, Z., Taghizadeh-mehrjardi, R., & Khosravani, P. (2024). Random Forest-Based Soil Moisture Estimation Using Sentinel-2 ,. *Remote Sens.Ing*, *16*.

Oba, B. T. (2017). Physicochemical Analysis of Water Collected from Lake Chamo. *International Journal of Applied and Natural Sciences*, *6*(1), 69–76.

Paithane, P. M. (2023). Research Article Random Forest Algorithm use for Crop Recommendation. *Journal of Engineering and Technology for Industrial Applications*, 34–41.

Paramisparam, P., Ahmed, O. H., Omar, L., Ywih, H., Johan, P. D., & Hamidi, N. H. (2021). Co-Application of Charcoal and Wood Ash to Improve Potassium Availability in Tropical Mineral Acid Soils. *Agronomy*, *11*(10), 1–30.

Prasad, A. M., Iverson, L. R., & Liaw, A. (2006). Newer Classification and Regression Tree Techniques : Bagging and Random Forests for Ecological Prediction. *Ecosystems*, *9*, 181–199. https://doi.org/10.1007/s10021-005-0054-1

Qin, T., Wang, L., Zhao, J., Zhou, G., Li, C., Guo, L., & Jiang, G. (2022). Effects of Straw Mulching Thickness on the Soil Health in a Temperate Organic Vineyard. *Agriculture*, *12*(11), 1–15.

Ram, J., Ortuño, M. F., Bernal-vicente, A., Diaz-vivancos, P., Sanchez-blanco, M. J., & Hernandez, J. A. (2017). *Plant Responses to Salt Stress : Adaptive Mechanisms*. 1–38. https://doi.org/10.3390/agronomy7010018

Ranjbar, F., & Jalali, M. (2017). Communications in Soil Science and Plant Analysis Calcium , Magnesium , Sodium , and Potassium Release during Decomposition of Some Organic Residues. *Communications in Soil Science and Plant Analysis*, *43*, 645–659. https://doi.org/10.1080/00103624.2012.644005

Saeed, R., & Ahmad, R. (2009). Vegetative growth and yield of tomato as affected by the application of organic mulch and gypsum under saline rhizosphere. *Pak. J. Bot.*, *41*(6), 3093–3105.

Setegn, Y. A. (2022). *Impact of irrigation with Lake Abaya water on soil quality – southern Rift Valley* ,. *17*(7). https://doi.org/10.2166/wpt.2022.070

Setegn, Y. A., Kassa, K., Dagalo, S., & Tsegaye, D. (2022). Impact of irrigation with Lake Abaya water on soil quality – southern Rift Valley, Ethiopia. *Water Practice and Technology*, *17*(7), 1433–1444. https://doi.org/10.2166/wpt.2022.070

Song, J. (2021). The Random Forest Model Has the Best Accuracy Among the Four Pressure Ulcer Prediction Models Using Machine Learning Algorithms. *Risk Management and Healthcare Policy*, *14*, 1175–1187.

Song, X., Sun, R., Chen, W., & Wang, M. (2020). *Effects of surface straw mulching and buried straw layer on soil water content and salinity dynamics in saline soils*. *68*(December 2019), 58–68.

Soomro, K. B., Alaghmand, S., Shahid, M. R., Andriyas, S., & Talei, A. (2019). *evaluation of aquacrop model in simulating bitter gourd water*. https://doi.org/10.1002/ird.2395

Tanveer, K., Gilani, S., Hussain, Z., Ishaq, R., Adeel, M., & Ilyas, N. (2019). Effect of salt stress on tomato plant and the role of calcium. *Journal of Plant Nutrition*, 1–8. https://doi.org/10.1080/01904167.2019.1659324

Tavakkoli, E., & Mcdonald, G. K. (2021). Field applications of gypsum reduce pH and improve soil C in highly alkaline soils in southern Australia ' s dryland cropping region. *British Society of Soil Science*, 1–12. https://doi.org/10.1111/sum.12756

Walche, A., Haile, W., Kifu, A., & Tsegaye, D. (2023). Assessment and Characterization of Agricultural Salt-Affected Soils around Abaya and Chamo Lakes , South Ethiopia Rift Valley. *Applied and Environmental Soil Science*.

Watts, D. B., & Dick, W. A. (2014). *Sustainable Uses of FGD Gypsum in Agricultural Systems: Introduction*. https://doi.org/10.2134/jeq2013.09.0357

Xu, P., Sun, C., Ye, X., Xiao, W., Zhang, Q., & Wang, Q. (2016). Ecotoxicology and Environmental Safety The effect of biochar and crop straws on heavy metal bioavailability and plant

accumulation in a Cd and Pb polluted soil. *Ecotoxicology and Environmental Safety*, *132*, 94–100. https://doi.org/10.1016/j.ecoenv.2016.05.031

Zhang, Y., Yang, J., Yao, R., Wang, X., & Xie, W. (2020). Short-term effects of biochar and gypsum on soil hydraulic properties and sodicity in a saline-alkali soil. *Pedosphere: An International Journal*, *30*(5), 694–702. https://doi.org/10.1016/S1002-0160(18)60051-7

Zhang, Z., Zhang, Z., Feng, G., Lu, P., Huang, M., & Zhao, X. (2022). Biochar Amendment Combined with Straw Mulching Increases Winter Wheat Yield by Optimizing Soil Water-Salt Condition under Saline Irrigation. *Agriculture*, *12*(10).

Zhao, Y., Wang, S., Li, Y., Zhuo, Y., & Liu, J. (2019). Effects of straw layer and fl ue gas desulfurization gypsum treatments on soil salinity and sodicity in relation to sun fl ower yield. *Geoderma*, *352*(1), 13–21. https://doi.org/10.1016/j.geoderma.2019.06.004

Zhou, L., Li, F., Jin, S., & Song, Y. (2009). Field Crops Research How two ridges and the furrow mulched with plastic film affect soil water , soil temperature and yield of maize on the semiarid Loess Plateau of China. *Field Crops Research*, *113*, 41–47. https://doi.org/10.1016/j.fcr.2009.04.005

Deep Learning for Temporal Uncertainty Reduction in SMAP-Derived Soil Moisture Predictions in Kulfo Watershed, Ethiopia.

Demiso Daba Dugassa*[1], Aschalew Cherie Workneh[2], Babur Tesfaye Yersaw[2], Getachew Enssa Sedeta[2], Mulusew Bezabih Chane[1], Sintayehu Yadete Tola[3], Sufiyan Abdulmenan Ousman[1], Zelalem Anley Birhan[4]

[1]Faculty of Hydraulic and Water Resources Engineering, Water Technology Institute, Arba Minch University, P. O. Box 21, Arba Minch, Ethiopia
[2]Faculty of Water Resources and Irrigation Engineering, Water Technology Institute, Arba Minch University, P. O. Box 21, Arba Minch, Ethiopia
[3]Faculty of Water Supply and Environmental Engineering, Water Technology Institute, Arba Minch University, P. O. Box 21, Arba Minch, Ethiopia
[4]Faculty of Meteorology and Hydrology, Water Technology Institute, Arba Minch University, P. O. Box 21, Arba Minch, Ethiopia
*Corresponding Author: Email: demisod390@gmail.com

Abstract

Precise soil moisture estimation is critical for irrigation scheduling, crop yield forecasting, and water resource management, especially in semi-arid regions like the Kulfo watershed, Ethiopia, where water availability is highly climate-dependent. However, temporal uncertainty in soil moisture predictions remains a significant challenge when relying on satellite data. To address this, a deep learning framework was developed using satellite data from the Soil Moisture Active Passive (SMAP) mission, with time-series data processed in Google Earth Engine (GEE) and converted into 3D arrays using the Geospatial Data Abstraction Library (GDAL). Ten models were evaluated: a baseline long short-term memory (LSTM) model (non-uncertainty-aware) and nine uncertainty-aware models (five deep ensemble models, Monte Carlo Dropout (MC Dropout), and Quantile Regression models), all developed using Keras/TensorFlow. Using baseline LSTM model as a reference, the Deep Ensemble Model achieved a 94.51% reduction in temporal uncertainty, followed by the MC Dropout model with a 41.79% reduction. Among the Quantile Regression models, the 5th percentile model reduced uncertainty by 40.58%, while the 50th and 95th percentile models achieved reductions of 24.02% and 19.15%, respectively. The Deep Ensemble and MC Dropout models demonstrated excellent performance, with RMSE values of 0.131 and 0.345, respectively, and R^2 values of 0.993 and 0.949, indicating strong predictive accuracy. This study demonstrates that coupling an LSTM-based model with the deep ensemble method effectively reduces temporal uncertainty in SMAP-derived soil moisture predictions, offering a promising approach for improving soil moisture forecasting in data-limited regions.

Keywords: *Deep Learning; Kulfo Watershed; LSTM; SMAP; Soil Moisture; Uncertainty Reduction.*

1. Introduction

Soil moisture is a fundamental variable in hydrological processes, influencing water availability, agricultural productivity, and climate interactions (Vereecken et al., 2015). The Soil Moisture Active Passive (SMAP) mission provides valuable global soil moisture estimates, yet these data are subject to inherent uncertainties arising from sensor limitations and retrieval algorithms (Entekhabi et al., 2010). These uncertainties can propagate through hydrological models, affecting the precision of studies such as drought monitoring and yield forecasting (Dorigo et al., 2017; Famiglietti et al., 2011). The challenge is particularly acute in regions like Ethiopia's Kulfo watershed, where complex topography and climatic variability amplify prediction errors, undermining water management and agricultural planning (Fan et al., 2019; Engda et al., 2011).

Despite the significance of soil moisture for hydrological and agricultural systems, previous studies in the watershed have primarily focused on land use and land cover changes (Yirgu et al., 2020), soil

erosion mapping (Jothimani et al., 2020; Kassie et al., 2020), analyzing the impact of soil and water conservation on watershed hydrology (Mekonnen et al., 2016), hydrological extreme characteristics (Yisehak et al., 2020), climate variability, and their impacts on hydrological processes (Gudeta et al., 2018).

Additionally, a research done have mapped soil erosion-prone sub-watersheds using drainage morphometric and weighted sum approaches (Jothimani et al., 2022), assessed soil loss via remote sensing and GIS, and applied Soil and Water Assessment Tool (SWAT) based DEM analysis for soil and water conservation (Ayana et al., 2022). While these studies contribute to a broader understanding of environmental processes in the watershed, there is a noticeable gap in research specifically addressing temporal uncertainty in remotely sensed soil moisture data.

Soil moisture prediction is challenged by temporal variability in environmental factors, which complicates retrieval processes and introduces uncertainties (Zhou et al., 2024; Mohseni et al., 2023; Peng et al., 2023). In the Kulfo watershed, seasonal rainfall patterns, diverse land cover, and varied terrain create a dynamic soil moisture regime. Traditional (Conventional) models fail to capture these temporal dynamics, leading to discrepancies between SMAP predictions and actual soil moisture conditions (Dorigo et al., 2017). Land cover change and topographic factors further contribute to inconsistencies in SMAP predictions, making it difficult for agricultural communities to plan irrigation and predict crop yields (Tilahun et al., 2024; Lee et al., 2024; Sharma et al., 2024). Recent advances in deep learning, particularly Long Short-Term Memory (LSTM) networks, have demonstrated potential in modeling temporal dependencies in hydrological data, mainly in refining remotely sensed data by capturing temporal dependencies (Choi et al., 2022; Reichstein et al., 2019). However, despite the proven effectiveness of LSTM in time-series analysis (Arwansyah et al., 2024), their application in quantifying and mitigating SMAP's temporal uncertainty in the watershed is remarkably underexplored; indeed, no research has directly addressed this issue.

The hypothesis of this study is that; uncertainty-aware deep learning models, such as LSTM-based architectures, can reduce temporal uncertainty in SMAP-derived soil moisture. To test this hypothesis, a deep learning framework was developed and implemented in Python using TensorFlow. A baseline LSTM model was implemented to predict temporal soil moisture without uncertainty reduction techniques, while keeping the available SMAP uncertainty as it is. To reduce temporal uncertainty, nine uncertainty-aware variants of the LSTM model were developed by integrating it with Monte Carlo Dropout (MC Dropout), five Deep Ensemble approaches, and three Quantile Regression techniques. Their capacity to reduce uncertainty was quantified relative to the Baseline LSTM model, which lacks uncertainty estimation.

These models leveraged SMAP data spanning from 2017 to 2021 and auxiliary variables (rainfall, temperature, SMAP uncertainty) to improve predictions (EARTH2OBSERVE, 2017). Hence, this research quantifies the reduction in uncertainty, which contributes to enhanced hydrological modeling, water resource management, and agricultural decision-making in the Kulfo watershed. Furthermore, this approach addresses a significant literature gap and provides valuable insights into reducing uncertainty in satellite-derived soil moisture data, with potential applications for similar regions worldwide.

2. Materials and Methodology

2.1. Study area

This research was conducted in the Kulfo watershed, located within the Rift Valley Lakes Basin of Southern Ethiopia. The watershed extends from 37°20'0"E to 37°40'0"E longitude and 6°5'0"N to 6°15'0"N latitude, covering total area of 493km². Its landscape is shaped by variations in elevation, ranging from 1,171 to 3,565 meters amsl.

The landscape shifts from flat plains in the southern and southeastern regions to gently undulating terrain (See Figure 11). The central area features rolling hills, which become steeper and more dissected with ridges and peaks, influencing local hydrology. The highest areas are marked by steep slopes and exposed

bedrock. The soil composition varies with elevation; the upper regions predominantly feature orthic acrisols, while the lower areas are characterized by dystric nitisols. These soil types impact soil erosion processes, with the steep slopes in the upper regions experiencing higher erosion rates due to the erodibility of orthic acrisols (Yirgu et al., 2020; Kassie et al., 2020).

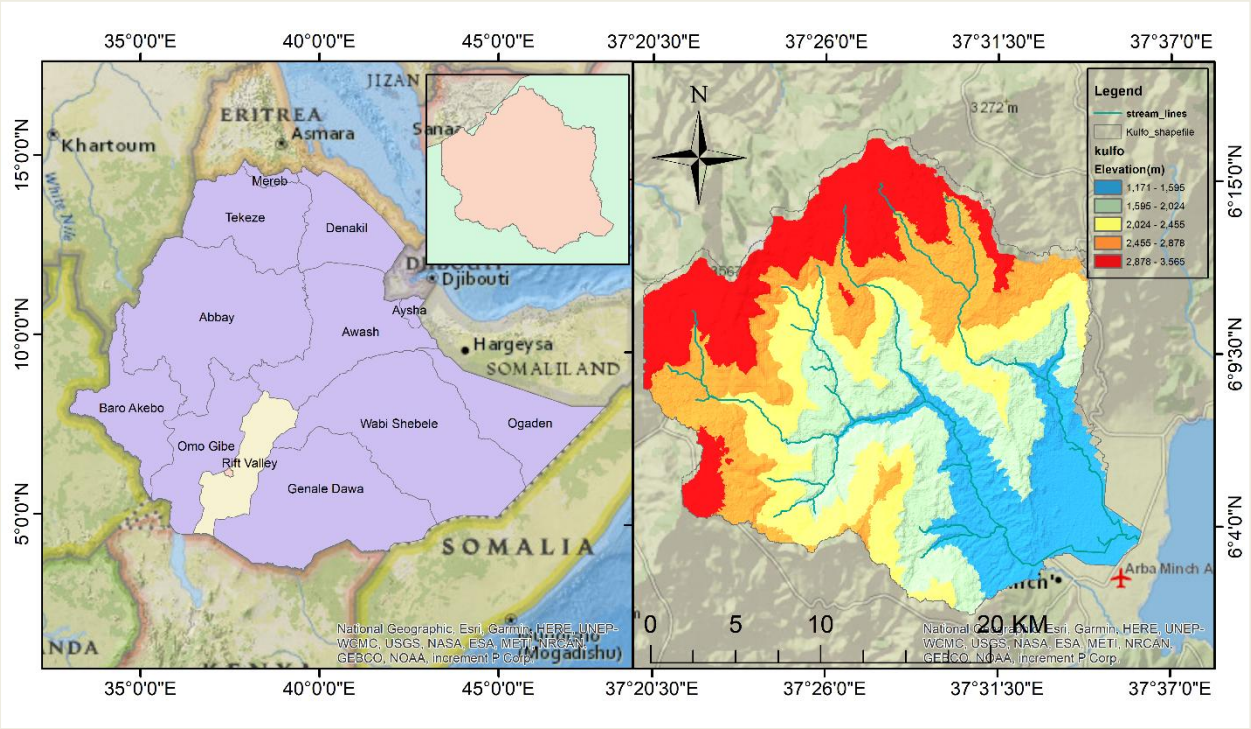

Figure 11: Location of the Study Area: Elevation, and Terrain Overview

2.2. Data collection and preprocessing

The dataset for this study was obtained using custom JavaScript code executed within Google Earth Engine (GEE) for the study area. It spans from 2017 to 2021 and includes precipitation, temperature, soil moisture, and uncertainty (Table 2). Precipitation data were sourced from CHIRPS at a 0.05° (~5 km) spatial resolution, temperature data from ERA5 at 0.25° (~25 km), and soil moisture and uncertainty from SMAP at 25 km resolution, which was then reprojected to 1 km. All datasets have a daily temporal resolution and were clipped to the study area.

To further assess the reliability of the data, NASA's Goddard Space Flight Center (GSFC) provides uncertainty estimates as part of the SMAP soil moisture product. This uncertainty is visualized in Figure 12 as a 3D plot, which shows the spatial distribution of the soil moisture and its associated uncertainty across the study area. The plot serves to illustrate how the uncertainty varies there. This is a key issue addressed in the study, as reducing uncertainty is essential for improving the reliability of soil moisture predictions.

Table 2: Data (Variable) Sources and Resolutions

Data Type	Source	Spatial Resolution
Precipitation	CHIRPS (Climate Hazards Group Infrared Precipitation with Station data)	0.05° (~5 km)
Temperature	ERA5 (ECMWF Reanalysis 5th Generation)	0.25° (~25 km)
Soil Moisture	SMAP (Soil Moisture Active Passive)	25 km (reprojected to 1 km)

Uncertainty	SMAP (Soil Moisture Active Passive)	25 km (reprojected to 1 km)

With this understanding of the data and its uncertainty, preprocessing steps were applied to prepare the dataset for modeling. To generate watershed-scale daily representations from the gridded satellite data, spatial averaging was performed. Each grid cell in the satellite dataset corresponds to a defined portion of the watershed and contains daily values for the selected variables. For each variable, all grid cells located within the watershed boundary were identified, and their values were averaged to compute a single mean value for each day.

This procedure transformed the distributed, high-resolution gridded data into a single daily value representing the overall condition of the watershed. The averaging process ensured consistency in spatial coverage and reduced potential biases introduced by local anomalies. The resulting daily averages were then stored and exported as GeoTIFF files. This step organized and converted the raw satellite observations into a structured time series format suitable for input into the deep learning model used in this study.

To ensure comparability across precipitation, maximum and minimum temperatures, soil moisture, and its uncertainty, the data were normalized to a 0–1 range using Min-Max scaling. This step helped improve the model's performance by enhancing training efficiency.

The data were then structured into a 3D array using the GDAL library, where each band represented a specific variable: precipitation (Band1), maximum temperature (Band2), minimum temperature (Band3), SMAP soil moisture (Band4), and SMAP uncertainty (Band5) (Figure 12). Each variable was subsequently flattened into 1D arrays, forming a feature matrix (X) for model inputs and a target vector (y) for soil moisture prediction. This preprocessing set the stage for the next step in model development.

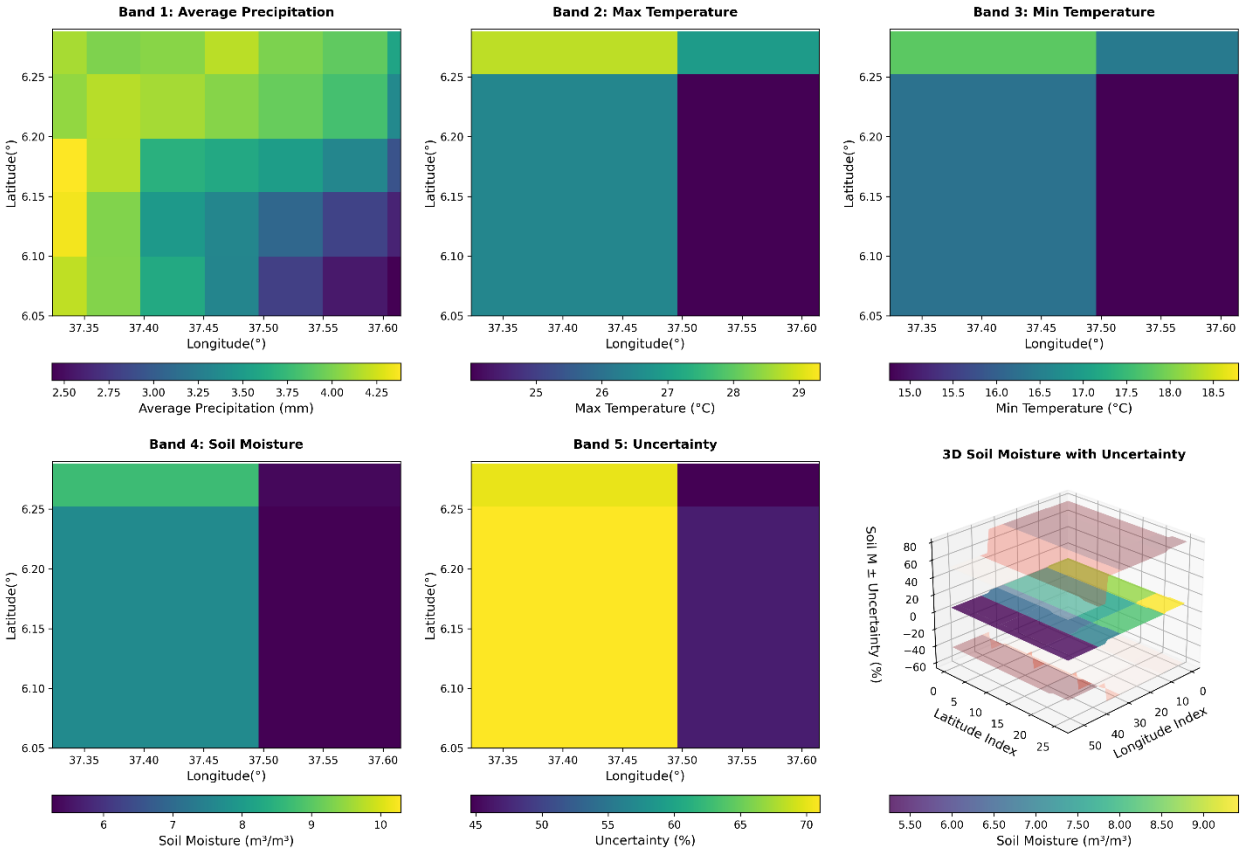

Figure 12: Band-wise Representation of Precipitation, Temperature, Soil Moisture, and Uncertainty, with 3D Visualization of SMAP Uncertainty for Temporal Uncertainty Reduction.

2.3. Deep learning model development

This study employs ten deep learning models (Baseline LSTM, five Deep Ensemble, MC Dropout, and three Quantile Regression models) to predict SMAP soil moisture, focusing on reducing uncertainty in the predictions. As shown in Figure 13, input parameters precipitation, min/max temperature, and SMAP soil moisture uncertainty are processed through these models.

The Baseline LSTM model captures temporal dependencies without uncertainty estimation, keeping available uncertainty. The Deep Ensemble model, consisting of five independently trained LSTM models, averages their predictions to reduce uncertainty. The MC Dropout model applies dropout during training and inference to introduce uncertainty. The Quantile Regression models predict the 5th, 50th, and 95th percentiles, providing uncertainty bounds. Each model operates independently, and their outputs are compared to evaluate uncertainty reduction.

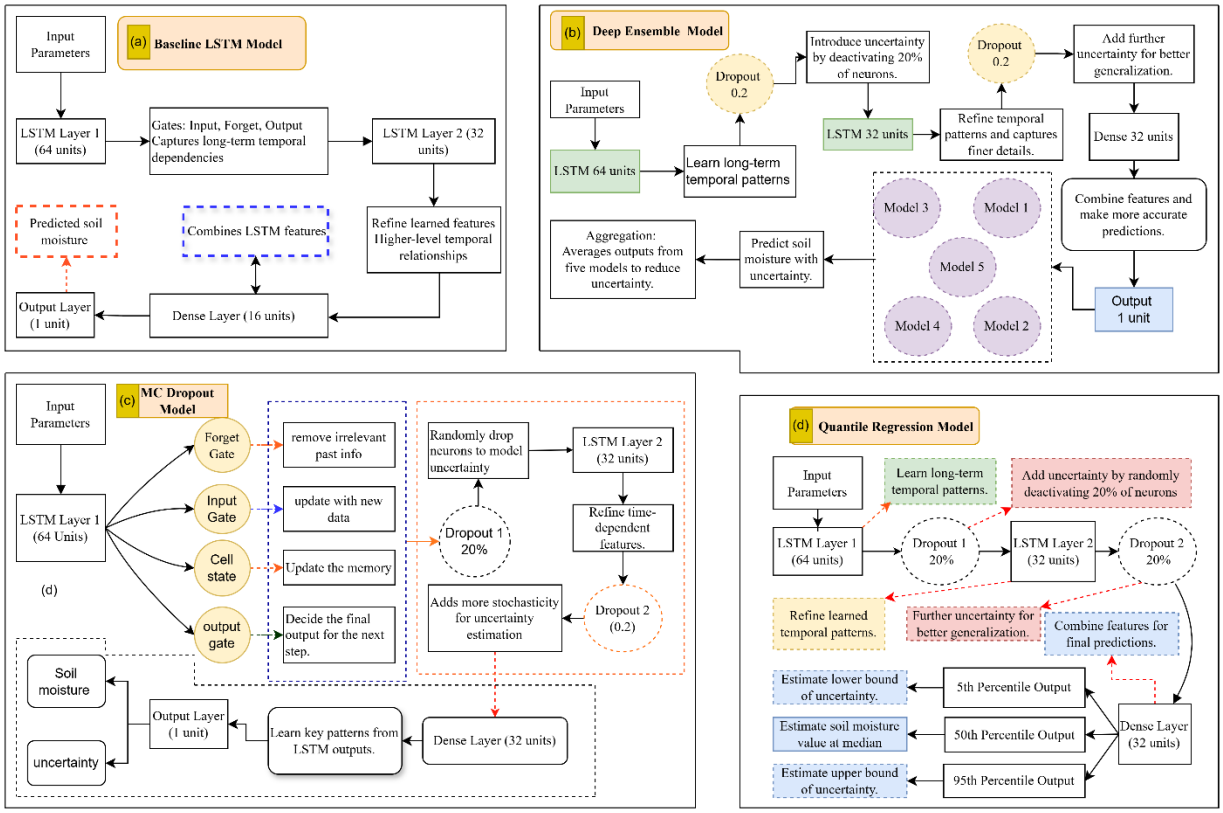

Figure 13: Overview of Deep Learning Models for Soil Moisture Prediction: Architectures and Algorithms for Baseline LSTM (a), Deep Ensemble (b), MC Dropout (c), and Quantile Regression (d) in this Study

2.3.1. Baseline LSTM model development

The Baseline LSTM model consists of two LSTM layers and a dense output layer. The first LSTM layer, with 64 units, is designed to capture long-term temporal dependencies in the input data. The second LSTM layer, with 32 units, refines the features learned by the first layer, focusing on higher-level temporal relationships. A dense output layer, consisting of a single unit, provides the predicted soil moisture value.

The model's performance is optimized using the Adam optimizer with a learning rate of 0.001, and Mean Squared Error (MSE) is used as the loss function during training. For a detailed breakdown of the model architecture and parameters (Table 3). The model is trained using the Adam optimizer (Yang, 2024; Dereich et al., 2025), with the learning rate and parameter tuning enhancing convergence during training.

Table 3: Detailed architecture and parameter summary of deep models (Arrows (↔) denote shared parameters between paired models; Slashes (/) indicate unique parameters)

Baseline LSTM model		**Quantile Regression Model**		**Param #** (Shared/Unique)
Layer (type)	**Output Shape**	**Layer (type)**	**Output Shape**	
Lstm_1 (LSTM)	(None, 64)	Lstm_1 (LSTM)	(None, 64)	17,664 ↔
Dropout (Dropout)	(None, 64)	Dropout (Drop)	(None, 64)	0 ↔
Lstm_2 (LSTM)	(None, 32)	Dense_1 (Dense)	(None, 32)	2,080 ↔
Dense (Dense)	(None, 1)	Dense_2 (Dense)	(None, 1)	33 ↔
Deep Ensembled Model		**MC dropout Model**		**Param #** (Shared/Unique)
Layer (type)	**Output Shape**	**Layer (type)**	**Output Shape**	
Lstm_1 (LSTM)	(None, 64)	Lstm_1 (LSTM)	(None, 1, 64)	17,664 ↔
Dropout (Dropout)	(None, 64)	Dropout (Dropout)	(None, 1, 64)	0 ↔
LSTM_2 (LSTM)	(None, 32)	Lstm_2(LSTM)	(None, 32)	16,768 / 12,416
Dense (Dense)	(None, 32)	Dropout (Drop)	(None, 32)	2,080 / 0
Dense_1 (Dense)	(None, 1)	Dense_1 (Dense)	(None, 1)	33 ↔
Parameter Summary				
Model	**Total Params**	**Trainable**	**Non-Trainable**	**Optimizer**
Baseline LSTM	59,333	19,777	0	39,556
Quantile Regression	59,333	19,777	0	39,556
Deep Ensembled	59,333	19,777	0	39,556
MC Dropout	90,341	30,113	0	60,228

The optimizer adapts the learning rate based on the first and second moments of the gradients, combining the advantages of AdaGrad and RMSProp, which is particularly useful for regression tasks involving noisy data and sparse gradients (Zaznov et al., 2024). The learning rate, beta values, and epsilon were fine-tuned for improved convergence during training, as demonstrated in previous studies (Biswas et al., 2025; Gour et al., 2024). The model contains a total of 59,333 parameters, with 19,777 being trainable and 39,556 dedicated to optimizer settings.

2.3.2. Deep ensemble model development

The Deep Ensemble model consists of two LSTM layers, two Dropout layers, a Dense layer, and a final output layer. Five models, each with the same architecture, are used to improve prediction accuracy and reduce uncertainty (Eteifa et al., 2025; Wang et al., 2024). For architecture details, see Table 3. The first LSTM layer, consisting of 64 units, captures temporal dependencies using the ReLU activation function.

A Dropout layer with a rate of 0.2 is applied after each LSTM layer to prevent overfitting, while the second LSTM layer, with 32 units, refines the features learned by the first layer. The Dense layer, with 32 units, integrates the features, and the final Dense unit outputs the predicted soil moisture value.

The model is optimized using the Adam optimizer with a learning rate of 0.001, and Mean Squared Error (MSE) is used as the loss function during training. The Adam optimizer adjusts the learning rate based on the first and second moments of the gradients, making it effective for regression tasks with noisy data and sparse gradients (Yang, 2024; Dereich et al., 2025; Zaznov et al., 2024; Biswas et al., 2025; Gour et al., 2024). Each model contains 59,333 parameters, and the total number of parameters for the ensemble is 296,665. Predictions from the ensemble models are aggregated by averaging, enhancing stability by combining the strengths of multiple models, which results in more accurate and reliable predictions (Bourdais & Owhadi, 2024).

2.3.3. MC dropout model development

The MC Dropout model consists of two LSTM layers, two Dropout layers, and a final Dense output layer. The detailed architecture and parameter summary of the model are presented in Table 3. The first LSTM layer, with 64 units, captures temporal dependencies in the input data, extracting relevant patterns for soil moisture prediction (Liu et al., 2024). A 20% Dropout layer follows, mitigating overfitting by deactivating a proportion of neurons during training, enhancing generalization (Li et al., 2024).

The second LSTM layer, with 32 units, refines the learned representations, followed by another 20% Dropout layer to introduce additional regularization and prevent overfitting (Bérchez-Moreno et al., 2024; Raghuvanshi, 2024; Hu, 2024). The final Dense output layer with a single unit generates the soil moisture prediction with uncertainty estimation. The model is optimized using the Adam optimizer with a learning rate of 0.001, and the Mean Squared Error (MSE) is used as the loss function during training. The model has a total of 90,341 parameters, of which 30,113 are trainable, while the remaining 60,228 parameters belong to the optimizer. The model does not include any non-trainable parameters.

2.4. Quantile regression models (5th, 50th, 95th percentiles) development

The quantile regression models were designed to predict soil moisture values at specific percentiles (5th, 50th, and 95th), offering an effective approach for estimating uncertainty in the predictions (Cheung et al., 2024). Each model follows the same architecture with two LSTM layers, one Dropout layer, one Dense layer, and a final Dense output layer.

The first LSTM layer, consisting of 64 units, captures temporal dependencies in the input data. A 20% Dropout layer is applied after the first LSTM layer to mitigate overfitting by randomly deactivating neurons during training, improving generalization (Li et al., 2024). The second LSTM layer, with 32 units, refines the features extracted by the first LSTM layer. A Dense layer with 32 units combines these features and prepares them for the final prediction.

The output layer, consisting of a single unit, generates the predicted soil moisture values at the 5th, 50th, and 95th percentiles, providing a measure of uncertainty in the predictions. The model is optimized using the Adam optimizer, with a learning rate set to 0.001, and the Mean Squared Error (MSE) loss function is used during training to ensure effective convergence and accurate predictions. The model architecture contains a total of 59,333 parameters, with 19,777 trainable parameters, and 39,556 parameters dedicated to the optimizer (refer Table 3 for detail).

2.5. Model training and data splitting

The dataset was split into three subsets: 70% for training, 15% for validation, and 15% for testing. This division allows the model to be trained on a substantial portion of the data while ensuring that validation and testing occur on unseen data, providing insights into the model's generalization ability and performance. For each model, the training process was carried out over different numbers of epochs. The Baseline LSTM, Deep Ensemble models, and Quantile Regression models were each trained for 50

epochs. The MC Dropout model was trained for 100 epochs. The training set was used to fit the models, while the validation set was employed to tune hyperparameters and prevent overfitting, with performance evaluated on the test set. Monitoring validation metrics during training allowed adjustments to be made iteratively to avoid overfitting (Sivakumar et al., 2024; Gangu et al., 2024). By this approach, the models are well-trained, preventing overfitting and improving generalization for real-world applications.

2.6. Uncertainty quantifications, predictions and model evaluation

Following the model architectures outlined in the deep learning development section, uncertainty in soil moisture predictions was quantified using nine different approaches: Five Deep Ensemble Models, MC Dropout, and Three Quantile Regressions. For the Deep Ensemble model, five independently initialized LSTM models were trained. The final prediction was computed by averaging the outputs of these models, and the uncertainty was quantified as the standard deviation of the individual model predictions, capturing epistemic uncertainty. This approach follows established ensemble learning techniques (Lakshminarayanan et al., 2017).

MC Dropout was applied by keeping dropout active during the inference phase. The model was run for 100 stochastic forward passes per input sample. The final prediction was taken as the mean of these 100 passes, with uncertainty quantified as the standard deviation of the predictions. This method aligns with the approach proposed by Gal and Ghahramani (2016) for capturing uncertainty during model inference.

In Quantile Regression, separate models were trained to predict the 5th, 50th, and 95th percentiles of soil moisture. The model outputs at these percentiles represented the lower, median, and upper bounds of uncertainty, respectively. This technique enabled the generation of prediction intervals, with uncertainty represented by the range between the 5th and 95th percentiles. This method has been widely used for uncertainty estimation in regression tasks (Koenker & Hallock, 2001).

The baseline model, which does not incorporate any uncertainty reduction techniques, was used as a reference for uncertainty quantification. To assess the effectiveness of uncertainty reduction, the percentage reduction in uncertainty compared to the baseline model was calculated by:

$$\text{Uncertainty Reduction} = \frac{\text{Std. Dev.(Baseline)} - \text{Std. Dev.(Model Predictions)}}{\text{Std. Dev.(Baseline)}} \times 100\% \quad (1)$$

Where:

- Std. Dev. (Baseline): represents the standard deviation of predictions from the baseline.
- Std. Dev. (Model Predictions): represents the standard deviation of predictions from the uncertainty-aware models.

The performance of the deep learning models is evaluated by comparing their soil moisture predictions with SMAP-derived soil moisture values, which are used as reference for assessment.

Model performance was evaluated using Root Mean Squared Error (RMSE) to quantify prediction error and R^2 to assess how well the model explained the variance in the soil moisture observations. Predictions were visualized using line plots, where true soil moisture values were compared to model predictions. Shaded regions around the predicted values represented the quantified uncertainty, illustrating the confidence bounds for each model.

2.7. Feature importance and model interpretability

Feature importance analysis was conducted using permutation and gradient-based methods for methods for selected models with uncertainty quantification or complex architectures.

Table 4: Summary of Feature Importance Methods Applied to Models for Permutation and Gradient-Based Importance Analysis ((✗) indicates not applied, (✓) indicates applied)

Model	Permutation Importance	Gradient-Based Importance
Baseline LSTM	✗	✗
Deep Ensemble	✓	✓
MC Dropout	✗	✓
Quantile Regression	✗	✗

For the Deep Ensemble, permutation importance was calculated by shuffling features in the validation set and measuring performance degradation. Gradient-based importance was computed by averaging gradients of predictions with respect to input features across the ensemble models. For MC Dropout, gradient-based importance was computed using TensorFlow's GradientTape with dropout enabled during inference, averaging absolute gradients over multiple samples. Permutation importance was not applied to MC Dropout due to computational cost (Table 4)

2.8. Software and Tools

This study utilizes Keras with TensorFlow to develop the LSTM model to predict soil moisture, with a primary focus on reducing temporal uncertainty in the predictions. Keras with TensorFlow is employed for building and training the LSTM model, while Dropout is applied to estimate and quantify uncertainty. Environmental data is processed using GDAL, and data manipulation is handled by NumPy. For data preprocessing and splitting, Scikit-learn is used, and the model's performance and uncertainty are visualized through Matplotlib (Table 5).

Table 5: Software and Tools used in this study

Software/Tool	Purpose
Keras with TensorFlow	Building and training the Long Short-Term Memory model.
GDAL (Geospatial Data Abstraction Library)	Reading and processing GeoTIFF files containing environmental data (precipitation, temperature, SMAP soil moisture and its uncertainty).
NumPy	Data manipulation and array handling, especially when combining and preprocessing data.
Scikit-learn	Preprocessing (MinMaxScaler for normalization) and splitting data into training, validation, and test sets.
Matplotlib	Visualizing predictions and uncertainty to analyze the model's performance.

3. Results and Discussion

3.1. Model Performance Evaluation

Table 6 summarizes the performance of deep learning models in predicting soil moisture across training, validation, and test datasets using RMSE (lower is better) and R^2 (higher is better). The Baseline

LSTM achieved strong performance across all datasets. Its test RMSE was 0.137, with an R^2 of 0.992 meaning it explains over 99.2% of soil moisture variation. Training (RMSE = 0.153) and validation (RMSE = 0.155) results were equally consistent, confirming its ability to model temporal dependencies in soil moisture data, aligning with studies that highlight LSTMs' efficacy in sequential environmental forecasting (Hu, 2024; Zhou, 2025; Pu et al., 2025).

The Deep Ensemble improved slightly on the Baseline LSTM's test performance, achieving the lowest RMSE (0.131) and highest R^2 (0.993). While its training (RMSE = 0.154) and validation (RMSE = 0.155) errors were marginally higher than the LSTM's, its stronger test result suggests better generalization. This aligns with recent findings showing that combining multiple models (ensembles) often enhances predictive performance in environmental forecasting (Soni et al., 2024; Tang et al., 2024; Mahaveerakannan, 2024).

In contrast, the MC Dropout model struggled. Its test RMSE (0.345) was over twice as high as the Baseline LSTMs, and its training (RMSE = 0.448) and validation (RMSE = 0.4840) errors showed large gaps. While its test R^2 (0.949) improved compared to training, the overall variability indicates challenges in balancing randomness (for robustness) with accuracy a known issue in soil moisture modeling (Fu et al., 2024; Zeevi et al., 2024).

The Quantile Regression approach lagged significantly, with the 5th and 50th percentiles yielding negative R^2 values (−0.5194 and −0.0703) and high RMSE (1.871 and 1.570). Even its best-performing 95th percentile (RMSE = 0.979, R^2 = 0.584) fell short of deep learning benchmarks, reflecting inherent limitations in capturing nonlinear soil moisture dynamics. These results reflect limitations of traditional methods in capturing soil moisture's complex, time-dependent behavior (Cheung et al., 2024; Xu, 2023; Park et al., 2021).

Table 6: Performance and Uncertainty Evaluation of Deep Learning Models for Soil Moisture Prediction (RMSE, R^2, and Uncertainty Across Training, Validation, and Test Datasets.

Model	**Dataset**	**RMSE**	**R^2**	**Uncertainty**
Baseline LSTM	Training	0.153	0.989	1.488
	Validation	0.155	0.990	1.568
	Test	0.137	0.992	1.507
Deep Ensemble	Training	0.154	0.989	0.050
	Validation	0.155	0.990	0.049
	Test	0.131	0.993	0.049
MC Dropout	Training	0.448	0.910	0.889
	Validation	0.484	0.906	0.885
	Test	0.345	0.949	0.898
Quantile Regressions	**Dataset**	**RMSE**	**R^2**	**Uncertainty**
5th Percentile	All datasets	1.871	-0.519	0.931
50th Percentile	All datasets	1.570	-0.070	1.157

95th Percentile	All datasets	0.979	0.584	1.216

3.2. Predictive Accuracy and Uncertainty Reduction

Figure 14 illustrates the trade-offs between predictive accuracy (RMSE), correlation coefficient (CC), and uncertainty across models using a Taylor Diagram. The Baseline LSTM achieved the highest correlation with a reference data (CC = 0.996), confirming its strong ability to replicate soil moisture trends. However, it exhibited high uncertainty (1.488–1.568), a limitation also noted in LSTM-based soil moisture studies (Sankalp et al., 2025).

The Deep Ensemble balanced accuracy and uncertainty reduction more effectively. While its correlation coefficient (CC = 0.995) was slightly lower than the Baseline LSTM's, it achieved the lowest test RMSE (0.131) and drastically reduced uncertainty (0.049–0.050). This aligns with findings that ensemble methods improve reliability in environmental modeling by aggregating diverse predictions (Han et al., 2024).

MC Dropout demonstrated a distinct strength in uncertainty quantification, with values ranging from 0.889 to 0.898 significantly lower than the Baseline LSTM but higher than the Deep Ensemble. Its predictive accuracy (RMSE = 0.345, CC = 0.982), though weaker than the top models, reflects a deliberate trade-off common in stochastic regularization methods (Zeevi et al., 2024, 2025). Prior studies suggest this balance can be optimized for applications prioritizing uncertainty awareness over peak accuracy (Fu et al., 2024).

Quantile Regression underperformed in all metrics. With RMSE = 1.570 and uncertainty = 1.157 for the 50th percentile, it struggled to match even the weakest deep learning model. These results reinforce critiques of traditional quantile methods in dynamic systems like soil moisture, where nonlinearity and temporal dependencies dominate (Xu, 2023; Cheung et al., 2024).

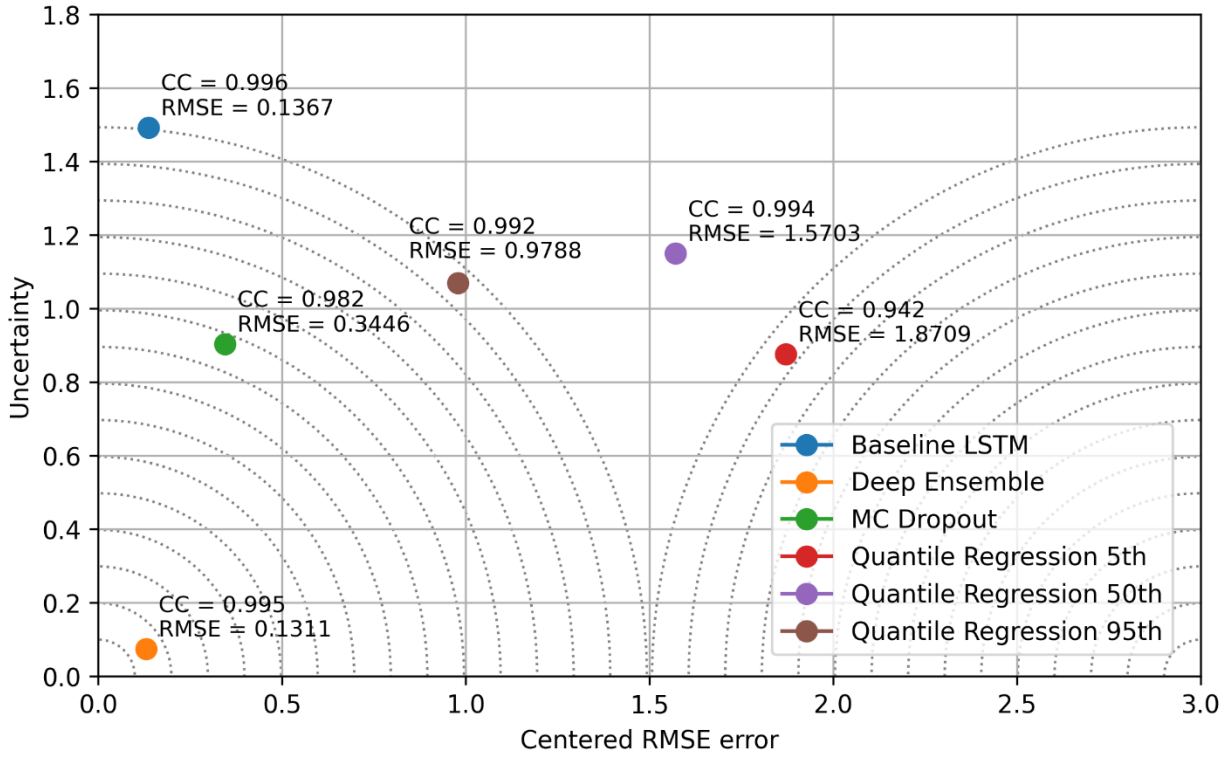

Figure 14: The relationship between the correlation coefficient and prediction accuracy.

3.3. Uncertainty Assessment in Soil Moisture Prediction Models

The uncertainty assessment across all models reveals significant differences in predictive confidence, critical for evaluating reliability in real-world applications as tabulated in Table 6.

The Baseline LSTM had high uncertainty across all datasets (1.48–1.57), suggesting variability in its predictions despite strong accuracy metrics. This aligns with critiques of standalone LSTMs lacking integrated uncertainty quantification, where complex temporal patterns can inflate prediction variance (Hoang, 2024). Deep Ensemble, in contrast, achieved near-identical low uncertainty (0.049–0.050), reflecting exceptional stability. By aggregating predictions from diverse subnetworks, it reduces errors and stabilizes predictions; a strategy proven effective in environmental science (Zhu et al., 2024).

MC Dropout demonstrated moderate uncertainty reduction (0.88–0.90), balancing stochastic regularization with partial error mitigation. While its uncertainty values exceeded the Deep Ensemble's, they underscore MC Dropout's utility as a lightweight uncertainty-aware tool, particularly where computational efficiency is prioritized (Zeevi et al., 2025; Fu et al., 2024).

Quantile Regression showed percentile-dependent uncertainty, with the 5th percentile performing best (0.931) and values rising sharply for the 50th (1.157) and 95th (1.216). This pattern highlights its struggle to model extreme soil moisture values; a known limitation in nonparametric methods applied to volatile environmental systems (Zeevi et al., 2024).

3.4. Impact of Uncertainty Reduction on Prediction Accuracy

Figure 15 illustrates uncertainty impacts in the validation dataset. The Deep Ensemble method consistently provided the most precise predictions, closely matching SMAP values and showing minimal uncertainty.

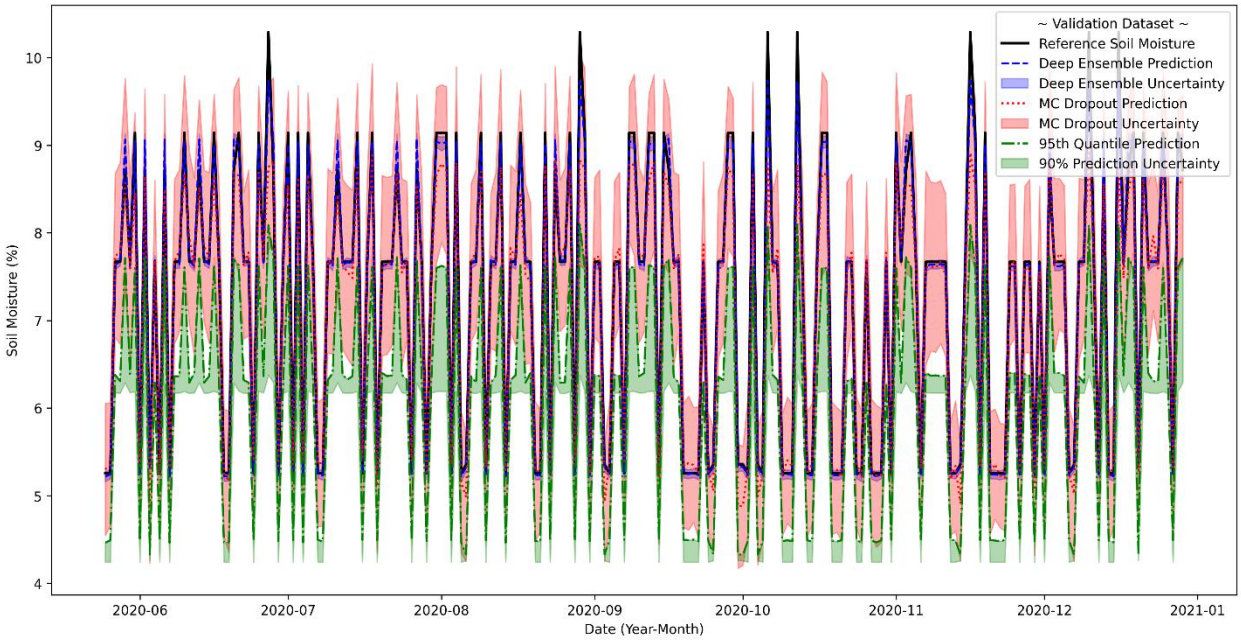

Figure 15: Impact of Uncertainty Reduction on Soil Moisture Prediction Accuracy (Validation Dataset).

This supports the effectiveness of ensemble methods in reducing uncertainty, as noted by Abulawi et al. (2024) and Jin et al. (2024). In contrast, the MC Dropout method, while also reliable, exhibited slightly higher uncertainty due to the randomness introduced by dropout layers, as highlighted by Matyushin et al. (2024).

Despite this, MC Dropout remains effective in uncertainty quantification, although it does not achieve the same stability as the Deep Ensemble. Quantile regression models, especially at the 95th and 50th percentiles, show more variability, leading to larger uncertainty ranges.

Previous studies suggest that quantile regression is more unstable, particularly when predicting extreme values (Xu, 2023; Mai, 2024). Higher percentiles often produce less accurate predictions due to noise

and outliers, while the 5th percentile model showed the most uncertainty, reinforcing that lower percentile result in more uncertain predictions (Mai, 2024).

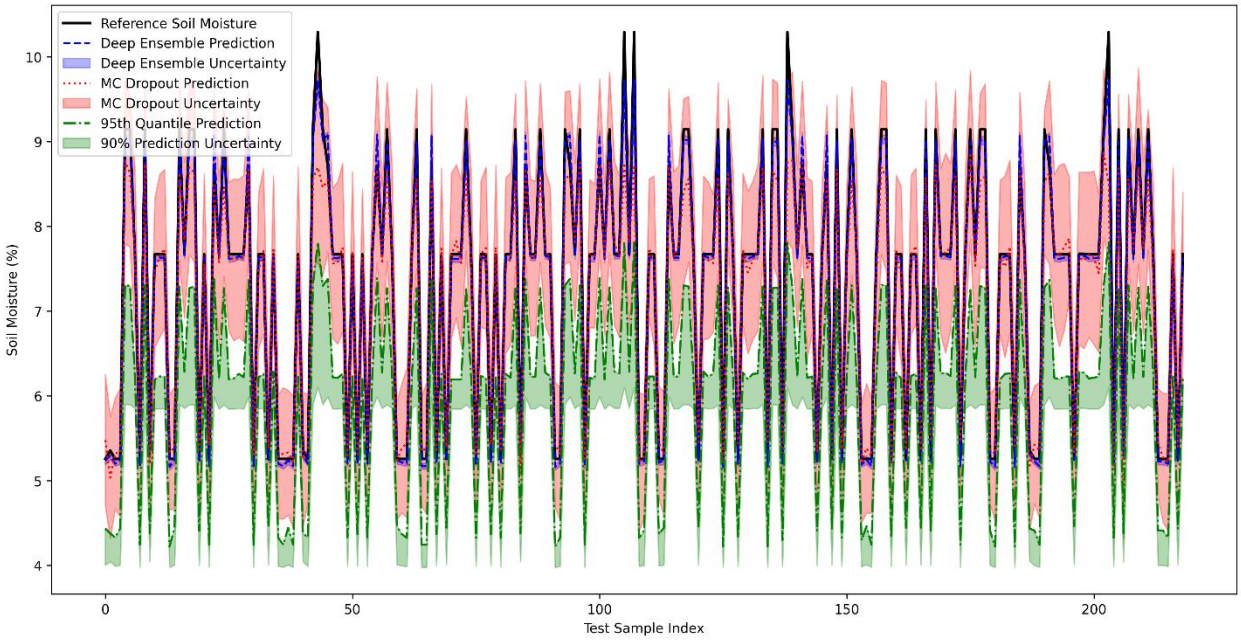

Figure 16: Impact of Uncertainty Reduction on Soil Moisture Prediction Accuracy (Test Dataset)

A similar trend is seen in Figure 16, which presents the test dataset. The Deep Ensemble method consistently outperforms other models in terms of accuracy and uncertainty management. It effectively captures SMAP values with minimal uncertainty, showcasing its robustness. In contrast, while MC Dropout performs well, it exhibits slightly higher uncertainty levels.

The Quantile Regression models, especially at the 95th and 50th percentiles, demonstrate broader uncertainty regions, indicating greater variability and reduced reliability. The 5th Percentile model shows the highest uncertainty and largest deviation from true values, marking it as the least accurate. Although the Deep Ensemble method excels in both accuracy and uncertainty quantification, MC Dropout and Quantile Regression can still provide valuable insights, especially in situations where managing uncertainty is crucial (Karimzadeh & Lima, 2024; Papacharalampous et al., 2024; Baño-Medina, 2023; Yang & Yee, 2023).

3.5. Uncertainty Quantification in Soil Moisture Prediction Models

As shown in Figure 17, Deep Ensemble model significantly reduced uncertainty, outperforming both the Baseline LSTM and MC Dropout models. The Baseline LSTM exhibited an uncertainty width of 1.50, while the Deep Ensemble reduced this value to 0.049, a 94.51% improvement. This underscores the effectiveness of ensemble methods in enhancing predictive reliability, aligning with previous studies that highlight their role in improving soil moisture predictions (Sankalp et al., 2025; Cheemakurthi, 2024).

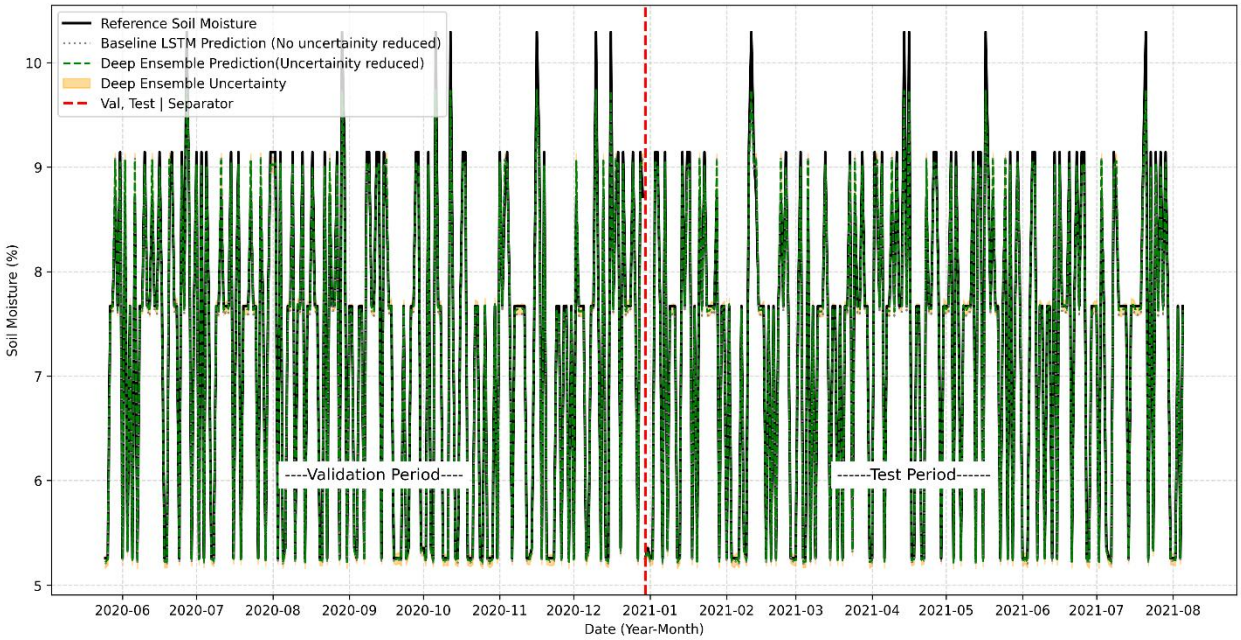

Figure 17: Uncertainty Reduction in the Deep Ensemble Model for Validation and Test Datasets

In comparison, Figure 18, reveals that the MC Dropout method also reduced uncertainty but to a lesser extent. Its uncertainty width decreased by 41.79% (from 1.50 to 0.88).

Although MC Dropout provides a practical approach for uncertainty estimation, its residual variability suggests that ensemble techniques offer superior precision. This aligns with prior observations that MC Dropout, despite its utility, lacks the stability of ensemble-based strategies (Sankalp et al., 2025).

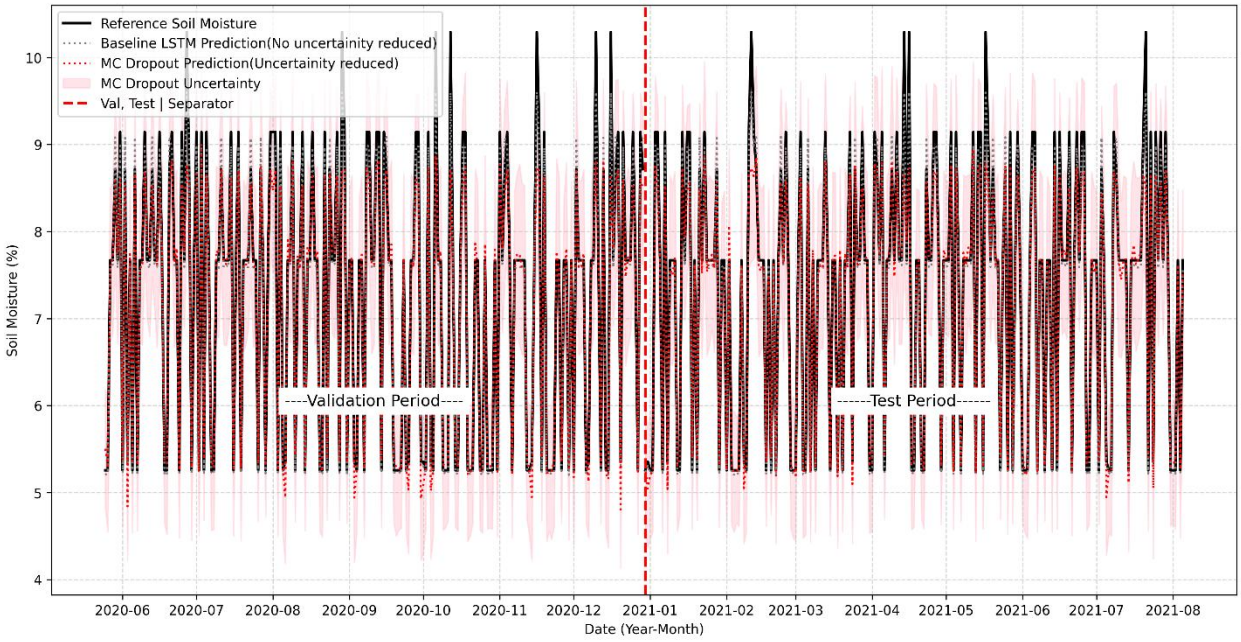

Figure 18: Uncertainty Reduction in the MC Dropout Model for Validation and Test Datasets

Notably, while Quantile Regression models also reduced uncertainty with the 5th, 50th, and 95th Percentile models achieving reductions of 40.58%, 24.02%, and 19.15%, respectively their uncertainty ranges remained broader than those of both models. This highlights a key limitation of Quantile Regression compared to more advanced techniques.

The Deep Ensemble model's improved uncertainty quantification is valuable for applications like drought forecasting, where precise predictions aid timely decision-making. Its integration into

environmental monitoring can further benefit agriculture and water resource management (Du et al., 2024; Han et al., 2024; Rau et al., 2024).

3.6. Feature Importance and Model Interpretability

Feature importance for four climatic variables such as precipitation, maximum temperature, minimum temperature, and uncertainty was assessed for Deep Ensemble and MC Dropout models. The results of permutation and gradient-based analyses are summarized in Table 7**.**

Permutation importance analysis for Deep Ensemble model revealed that uncertainty had the greatest influence on model performance, with a score of 2.0778, emphasizing the model's reliance on uncertainty quantification for reducing prediction uncertainty. Maximum temperature and minimum temperature were also significantly impactful, with scores of 0.3983 and 0.3770, respectively. Precipitation had the least impact, scoring 0.0033.

Table 7: Comparison of Feature Importance Using Permutation and Gradient-Based Methods for Deep Ensemble and MC Dropout Models

Features	Deep Ensemble		MC Dropout
	Permutation Importance	Gradient-Based Importance	Gradient-Based Importance
Feature 0: Precipitation	0.0033	0.0674	0.0611
Feature 1: Max Temp	0.3983	0.2291	0.1511
Feature 2: Min Temp	0.3771	0.3456	0.2001
Feature 3: Uncertainty	2.0778	0.0842	0.1091

In the gradient-based analysis, minimum temperature emerged as the most influential feature, scoring 0.3456. Maximum temperature followed with a score of 0.2291, while uncertainty had a lower gradient-based importance of 0.0842, suggesting that uncertainty's role is more integrated in reducing prediction uncertainty rather than directly influencing the gradient-based decision process. Precipitation remained minimally important.

For the MC Dropout model, the gradient-based importance analysis revealed that minimum temperature had the greatest impact, scoring 0.2001, followed by uncertainty with a score of 0.1091. Maximum temperature and precipitation had lower scores, reflecting their limited impact on uncertainty reduction. These findings are consistent with previous research that highlighted the significant role of temperature-related features and uncertainty in soil moisture prediction. For instance, Taneja et al. (2021) and Yamaç et al. (2020) show that temperature variables, especially minimum temperature, are among the most important for predicting soil moisture.

Additionally, uncertainty has been identified as a critical factor in improving prediction reliability, as noted by Yang et al. (2023) and Zeevi et al. (2025). Previous work on MC Dropout by Sun et al. (2023) aligns with the current findings, showing that uncertainty plays a moderate role in prediction but is less influential compared to temperature features. The results for precipitation being the least important are consistent with earlier studies by Taneja et al. (2021), which found that while precipitation influences soil moisture, its role in prediction is secondary compared to temperature and uncertainty.

In both the Deep Ensemble and MC Dropout models, minimum temperature was the most influential feature. Uncertainty played a critical role in reducing prediction uncertainty for Deep Ensemble, with a higher permutation importance score. However, its gradient-based importance was lower, indicating its

primary role in uncertainty reduction. Precipitation was the least impactful feature in both analyses. These results align with and extend previous research, confirming the key roles of temperature and uncertainty in enhancing soil moisture prediction.

4. Conclusion

This study investigated temporal uncertainty reduction in SMAP-derived soil moisture predictions within the Kulfo watershed, Ethiopia, using ten custom-coded deep learning models. The Baseline LSTM model, designed to predict soil moisture and capture the uncertainty inherent in SMAP data, served as the reference point. This model does not incorporate additional uncertainty quantification techniques, reflecting the uncertainty already present in SMAP data. Nine uncertainty-aware models were developed to improve this: five Deep Ensemble models, the MC Dropout model, and three Quantile Regression models. These models were specifically designed to reduce uncertainty in the predictions by incorporating advanced uncertainty quantification techniques.

The uncertainty assessment showed that the Deep Ensemble models significantly reduced uncertainty, with values around 0.05 across training, validation, and testing, achieving a reduction of 94.51% relative to the Baseline LSTM. The best-performing Deep Ensemble model demonstrated high predictive accuracy ($R^2 = 0.99$, RMSE = 0.131, and CC= 0.995) in the test dataset. In contrast, the MC Dropout model achieved moderate uncertainty reduction, with values ranging from 0.89 to 0.90, reducing uncertainty by 41.79% compared to the Baseline LSTM, and a correlation coefficient of 0.9823.

The Quantile Regression models showed increasing uncertainty at higher percentiles, with values ranging from 0.93 at the 5th percentile to 1.22 at the 95th percentile, reducing uncertainty by 40.58%, 24.02%, and 19.15%, respectively. However, they exhibited weaker performance with lower R^2, higher RMSE, and exhibits a weaker correlation coefficient compared to the other models. Feature importance analysis revealed that minimum temperature was the most influential variable in predicting soil moisture and reducing uncertainty, particularly in the Deep Ensemble and MC Dropout models. In contrast, precipitation had a minimal impact.

The study proves that the LSTM-based model coupled with the Deep Ensemble method, which integrates the forecasts from five independent models, effectively reduces temporal uncertainty in SMAP-derived soil moisture predictions. Furthermore, the MC Dropout and Quantile Regression Models were helpful for uncertainty quantification, while the efficiency of the models was lower than that of the ensemble model. This makes it the most effective strategy for improving soil moisture predictions in data-limited regions.

This study effectively reduced temporal uncertainty in SMAP soil moisture predictions using deep learning models. Future research should integrate ground-based observations with satellite data to enhance the reliability of uncertainty-aware models. Investigating hybrid deep learning approaches may improve prediction accuracy and reduce uncertainty. Besides, refining the Deep Ensemble model and incorporating more environmental variables could optimize performance, particularly in data-limited regions.

Acknowledgments

We express our sincere gratitude to the CHIRPS, ERA5, and SMAP datasets providers, which were critical in supplying the necessary data for our study.

AI use in writing

The author used AI tools to enhance language in parts of the manuscript. All content was reviewed and edited, and the author takes full responsibility for the submitted work.

Declaration of Interests

The authors declare no conflict of interest.

References

Abdar, M., Pourpanah, F., Hussain, S., Rezazadegan, D., Liu, L., Ghavamzadeh, M., Fieguth, P., Cao, X., Khosravi, A., Acharya, U. R., Makarenkov, V., & Nahavandi, S. (2021). A review of uncertainty quantification in deep learning: Techniques, applications and challenges. *Information Fusion, 76*, 243–297 https://doi.org/10.1016/j.inffus.2021.05.008.

Abulawi, Z., Hu, R., Balaprakash, P., & Liu, Y. (2024). Bayesian optimized deep ensemble for uncertainty quantification of deep neural networks: A system safety case study on sodium fast reactor thermal stratification modeling. arXiv. https://doi.org/10.48550/arxiv.2412.08776

Arwansyah, A., Suryani, S., Sy, H., Alam, S., Piu, S., Usman, U., Tamsir, N., & Djafar, I. (2024). Deep sequence models for time series data: A comparative study and parameter fine-tuning approach. *2024 International Conference on Electrical Engineering and Computer Science (ICEECS)*, 703–709. https://doi.org/10.1109/eecsi63442.2024.10776052

AutoDEUQ: Automated Deep Ensemble with Uncertainty Quantification. (2022). *2022-26th International Conference on Pattern Recognition (ICPR)*. https://doi.org/10.1109/icpr56361.2022.9956231

Ayana, M. T., Bizuneh, Y. K., Koshuma, A. E., Workneh, A. C., Ali, B. M., & Lohani, T. K. (2022). Developing a DEM and Elucidating through SWAT to Conserve Soil in Kulfo Watershed of Rift Valley Basin, Ethiopia. *Applied and Environmental Soil Science*. https://doi.org/10.1155/2022/7702739

Baño-Medina, J. (2023). Deep ensembles to improve uncertainty quantification of statistical downscaling models under climate change conditions. arXiv. https://doi.org/10.48550/arXiv.2305.00975

Behzadipour, F., Ghaseminezhad, M., Abdanan Mehdizadeh, S., Taki, M., Khalili Moghadam, B., & Zare Bavani, M. R. (2023). Predictions of greenhouse soil moisture using artificial neural network and wireless network sensing. *Iranian Journal of Biosystems Engineering, 53*(4), 341–356. https://doi.org/10.22059/ijbse.2023.341992.665482

Bérchez-Moreno, F., Fernández, J. C., Hervás-Martínez, C., & Gutiérrez, P. A. (2024). Fusion of standard and ordinal dropout techniques to regularise deep models. *Information Fusion*. https://doi.org/10.1016/j.inffus.2024.102299

Biswas, S., Dey, S., & Nath, S. (2025). Learning Rate Tuner with Relative Adaptation (LRT-RA): Road to Sustainable Computing. *AppliedMath, 5*(1), 8. https://doi.org/10.3390/appliedmath5010008

Bourdais, T., & Owhadi, H. (2024). Model aggregation: Minimizing empirical variance outperforms minimizing empirical error. arXiv. https://doi.org/10.48550/arxiv.2409.17267

Cheemakurthi, S. K. M. (2024). Reducing model uncertainty: Optimized ensemble methods for high-stakes prediction tasks. *Deleted Journal, 12*(1), 247–257. https://doi.org/10.36676/dira.v12.i1.147

Cheung, J., Rangarajan, S. S., Maddocks, A., Chen, X., & Chandra, R. (2024). Quantile deep learning models for multi-step ahead time series prediction. arXiv. https://doi.org/10.48550/arxiv.2411.15674

Choi, J., Won, J., Jang, S., & Kim, S. (2022). Learning Enhancement Method of Long Short-Term Memory Network and Its Applicability in Hydrological Time Series Prediction. *Water (Switzerland)*. https://doi.org/10.3390/w14182910

Dereich, S., Jentzen, A., & Riekert, A. (2025). Averaged Adam accelerates stochastic optimization in the training of deep neural network approximations for partial differential equation and optimal control problems. arXiv. https://doi.org/10.48550/arxiv.2501.06081

Dorigo, W., Wagner, W., Albergel, C., Albrecht, F., Balsamo, G., Brocca, L., Chung, D., Ertl, M., Forkel, M., Gruber, A., Haas, E., Hamer, P. D., Hirschi, M., Ikonen, J., de Jeu, R., Kidd, R., Lahoz, W., Liu, Y. Y., Miralles, D., … Lecomte, P. (2017). ESA CCI Soil Moisture for improved Earth system understanding: State-of-the art and future directions. *Remote Sensing of Environment*. https://doi.org/10.1016/j.rse.2017.07.001

Du, J., Kimball, J. S., Jencso, K. G., Hoylman, Z., Brust, C., Ketchum, D., Xu, Y., Lü, H., & Sheffield, J. (2024). Machine-learning based multi-layer soil moisture forecasts—An application case study of the Montana 2017 flash drought. *Water Resources Research, 60*(10). https://doi.org/10.1029/2023wr036973

EARTH2OBSERVE. (2017). Final report summary - Global Earth Observation for integrated water resource assessment (Grant agreement ID: 603608). European Commission. https://cordis.europa.eu/project/id/603608

Engda, T. A. et al. (2011). Watershed Hydrology of the (Semi) Humid Ethiopian Highlands. In A. M. Melesse (Ed.), *Nile River Basin* (pp. 51–72). Springer. https://doi.org/10.1007/978-94-007-0689-7_7

Entekhabi, D., Njoku, E. G., O'Neill, P. E., Kellogg, K. H., Crow, W. T., Edelstein, W. N., Entin, J. K., Goodman, S. D., Jackson, T. J., Johnson, J., Kimball, J., Piepmeier, J. R., Koster, R. D., Martin, N., McDonald, K. C., Moghaddam, M., Moran, S., Reichle, R., Shi, J. C., … Van Zyl, J. (2010). The soil moisture active passive (SMAP) mission. *Proceedings of the IEEE*. https://doi.org/10.1109/JPROC.2010.2043918

Eteifa, S., Shafik, A. K., Eldardiry, H., & Rakha, H. (2025). Deep learning ensemble approach for predicting expected and confidence levels of signal phase and timing information at actuated traffic signals. Preprints. https://doi.org/10.20944/preprints202501.1203.v1

Fan, Y., Clark, M., Lawrence, D. M., Swenson, S., Band, L. E., Brantley, S. L., Brooks, P. D., Dietrich, W. E., Flores, A., Grant, G., Kirchner, J. W., Mackay, D. S., McDonnell, J. J., Milly, P. C. D., Sullivan, P. L., Tague, C., Ajami, H., Chaney, N., Hartmann, A., … Yamazaki, D. (2019). Hillslope Hydrology in Global Change Research and Earth System Modeling. *Water Resources Research*. https://doi.org/10.1029/2018WR023903

Fu, Z., Fujita, N., & Terada, Y. (2024). Enhancing reliability in model-based DL reconstruction: A systematic study of MC dropout for uncertainty quantification. *Proceedings of the International Society for Magnetic Resonance in Medicine... Scientific Meeting and Exhibition*. https://doi.org/10.58530/2024/2818

Gal, Y., & Ghahramani, Z. (2016). Dropout as a Bayesian approximation: Representing model uncertainty in deep learning. *Proceedings of the 33rd International Conference on Machine Learning (ICML), 48*, 1050–1059. https://arxiv.org/abs/1506.02142

Gangu, K., Tayal, S., Mishra, R., Voola, P. K., Kavuri, S. N., & Mehra, A. (2024). An analysis on performance scale and model validation in machine learning. *2024 International Conference on Computing, Communication, and Intelligent Systems (IC3IS)*, 1107–1113. https://doi.org/10.1109/ic3i61595.2024.10828707

Gour, S., Wazir, S., Nafis, M. T., & Parveen, S. (2024). Optimizing hyperparameters in neural networks using genetic algorithms. In *Advances in Artificial Intelligence* (pp. 106–116). Informa. https://doi.org/10.1201/9781003518587-9

Gudeta Nega Demmissie, Tamene Agugna Demissie, Fayera Gudu Tufa. (2018). Predicting the Impact of Climate Change on Kulfo River Flow. *Hydrology*, *6*(3), 78-87. https://doi.org/10.11648/j.hyd.20180603.11

Han, J., Jian, H., Chen, X., Wang, J., Zhu, J., Li, X., Yan, Y., & Li, Q. (2024). Integrating convolutional attention and encoder–decoder long short-term memory for enhanced soil moisture prediction. *Water, 16*(23), 3481. https://doi.org/10.3390/w16233481

Hassan, H., Sakr, F., Salem Al Jawazneh, F. Y., Alsmadi, M. K., Gomaa, I., & Abdallah, S. (2024). Data-driven weather prediction: Integrating deep learning and ensemble models for robust weather forecasting. *Journal of Cybersecurity and Information Management, 15*(2), 260–284. https://doi.org/10.54216/jcim.150220

Hoang, M. L. (2024). Prediction uncertainty of deep neural network in orientation angles from IMU sensors. *Sensors and Actuators, 129–148*. https://doi.org/10.2174/9789815313055124010009

Hu, J. (2024). A high-performance stock prediction system leveraging LSTM neural networks. *Applied and Computational Engineering, 114*(1), 65–72. https://doi.org/10.54254/2755-2721/2024.18219

Jin, H., Akhavan Aghdam, M., Medikonduru, S. N. C., Wei, W., Wang, X., Zhang, W., & Wu, Y. (2024). Effective diversity optimizations for high accuracy deep ensembles. *2024 IEEE Conference on Cognitive and Computational Aspects of Situation Management (CogMI)*, 278–287. https://doi.org/10.1109/cogmi62246.2024.00044

Jothimani, M., Abebe, A., & Dawit, Z. (2020). Mapping of soil erosion-prone sub-watersheds through drainage morphometric analysis and weighted sum approach: a case study of the Kulfo River basin, Rift valley, Arba Minch, Southern Ethiopia. *Modeling Earth Systems and Environment*. https://doi.org/10.1007/s40808-020-00820-y

Jothimani, M., Getahun, E., & Abebe, A. (2022). Remote sensing, GIS, and RUSLE in soil loss estimation in the Kulfo river catchment, Rift valley, Southern Ethiopia. *Journal of Degraded and Mining Lands Management*. https://doi.org/10.15243/jdmlm.2022.092.3307

Karimzadeh, M., & Pires de Lima, R. (2024). Model ensemble with dropout for uncertainty estimation in binary sea ice or water segmentation using Sentinel-1 SAR. ESS Open Archive. https://doi.org/10.31223/x51t34

Kassie, A. E., Amare, D. G., & Sulla, G. G. (2020). Soil erosion estimation and watershed prioritization in Kulfo watershed, Ethiopia. *Journal of Natural Sciences Research, 10*(1), 1–12. https://doi.org/10.7176/JNSR/10-1-01

Koenker, R., & Hallock, K. (2001). Quantile regression. *Journal of Economic Perspectives, 15*(4), 143–156. https://doi.org/10.1257/jep.15.4.143

Lakshminarayanan, B., Pritzel, A., & Blundell, C. (2017). Simple and scalable predictive uncertainty estimation using deep ensembles. *Advances in Neural Information Processing Systems (NeurIPS), 30*. https://arxiv.org/abs/1612.01474

Lee, S., Lim, K. J., & Kim, J. (2024). Analysis of effects of spatial distributed soil properties and soil moisture behavior on hourly streamflow estimate through the integration of SWAT and LSM. *Sustainability*. https://doi.org/10.3390/su16041691

Li, T. (2024). Investigating spatial-temporal variability of soil moisture in agricultural catchments. *Journal of Hydrology, 15*(1). https://doi.org/10.14311/dis.fsv.2024.022

Li, X., Zhang, Z., Li, Q., & Zhu, J. (2024). Enhancing soil moisture forecasting accuracy with REDF-LSTM: Integrating residual en-decoding and feature attention mechanisms. *Water, 16*(10), 1376. https://doi.org/10.3390/w16101376

Liu, Y. S., Shen, L., Zhu, X., Xie, Y., & He, S. (2024). Spectral data-driven prediction of soil properties using LSTM-CNN-attention model. *Applied Sciences, 14*(24), 11687. https://doi.org/10.3390/app142411687

Mahaveerakannan, R. (2024). Ensemble deep learning for enhanced human microbiome-based disease prediction: A comprehensive analysis on public datasets. *2024 International Conference on Computing, Communication, and Intelligent Systems (IC3IS)*, 1–4. https://doi.org/10.1109/csitss64042.2024.10816874

Mai, T. T. (2024). A sparse PAC-Bayesian approach for high-dimensional quantile prediction. arXiv. https://doi.org/10.48550/arxiv.2409.01687

Matyushin, D. D., Burov, I. A., & Sholokhova, A. Yu. (2024). Uncertainty quantification and flagging of unreliable predictions in predicting mass spectrometry-related properties of small molecules using machine learning. *International Journal of Molecular Sciences, 25*(23), 13077. https://doi.org/10.3390/ijms252313077

Mekonnen Seka, A., & Kemal Mohammed, A. (2016). Evaluation of impacts of Soil and water Conservation on Watershed hydrology of Kulfo River Using Hydrological SWAT Models, SNNPR. *International Journal of Scientific & Engineering Research*.

MEKONNEN, Y. I. (2020). Land Use/Land Cover Dynamics and its Environmental Impacts in Kulfo Watershed, Gamo Highlands, South Western Ethiopia. Journal of Geography, Environment and Earth Science International. https://www.academia.edu/59916745.

Mohseni, F., Jamali, S., Ghorbanian, A., & Mokhtarzade, M. (2023). Global soil moisture trend analysis using microwave remote sensing data and an automated polynomial-based algorithm. *Global and Planetary Change*. https://doi.org/10.1016/j.gloplacha.2023.104310

MC Dropout Based Active Learning for Deep Learning in Structural Simulation. (2024). *Proceedings of the ASME 2024 43rd International Conference on Ocean, Offshore and Arctic Engineering*. https://doi.org/10.1115/omae2024-126087

Papacharalampous, G., Tyralis, H., Doulamis, N., & Doulamis, A. (2024). Uncertainty estimation in spatial interpolation of satellite precipitation with ensemble learning. arXiv. https://doi.org/10.48550/arxiv.2403.10567

Park, Y., Maddix, D. C., Aubet, F.-X., Kan, K. K. W., Gasthaus, J., & Wang, Y. (2021). Learning quantile functions without quantile crossing for distribution-free time series forecasting. arXiv. http://arxiv.org/pdf/2111.06581.pdf

Patel, M., & Shah, A. (2024). Feature importance in machine learning with explainable artificial intelligence (XAI) for rainfall prediction. *ITM Web of Conferences, 65*, 03007. https://doi.org/10.1051/itmconf/20246503007

Peng, C., Zeng, J., Chen, K. S., Li, Z., Ma, H., Zhang, X., Shi, P., Wang, T., Yi, L., & Bi, H. (2023). Global spatiotemporal trend of satellite-based soil moisture and its influencing factors in the early 21st century. *Remote Sensing of Environment*. https://doi.org/10.1016/j.rse.2023.113569

Pu, X., Zhang, J., Wang, F., & Xue, S. (2025). A novel prediction model of grounding resistance based on long short-term memory. *AIP Advances, 15*(1). https://doi.org/10.1063/5.0248514

Raghuvanshi, K. P. (2024). A systematic literature review on the role of LSTM networks in capturing temporal dependencies in data mining algorithms. *International Journal for Science Technology and Engineering, 12*(10), 1219–1224. https://doi.org/10.22214/ijraset.2024.64761

Rau, K., Eggensperger, K., Schneider, F., Hennig, P., & Scholten, T. (2024). How can we quantify, explain, and apply the uncertainty of complex soil maps predicted with neural networks? *Science of The Total Environment, 944*, 173720. https://doi.org/10.1016/j.scitotenv.2024.173720

Reichstein, M., Camps-Valls, G., Stevens, B., Jung, M., Denzler, J., Carvalhais, N., & Prabhat. (2019). Deep learning and process understanding for data-driven Earth system science. *Nature*. https://doi.org/10.1038/s41586-019-0912-1

Sankalp, S., Sahoo, B. B., Gupta, S. K., Bhushan, M., Majhi, R. K., & DT, S. (2025). A deep learning approach to predict surface soil wetness and its uncertainty analysis over the Tel River Basin, India. *Clean-Soil Air Water, 53*(1). https://doi.org/10.1002/clen.70003

Sharma, S., Swami, D., & Joshi, N. (2024). The puzzle of soil moisture: Unravelling its dynamics in a watershed with complex physiographic features. SSRN. https://doi.org/10.2139/ssrn.4692856

Sheffield, J., & Wood, E. F. (2008). Global trends and variability in soil moisture and drought characteristics, 1950-2000, from observation-driven simulations of the terrestrial hydrologic cycle. *Journal of Climate*. https://doi.org/10.1175/2007JCLI1822.1

Sivakumar, M., Parthasarathy, S., & Padmapriya, S. (2024). Trade-off between training and testing ratio in machine learning for medical image processing. *PeerJ, 10*, e2245. https://doi.org/10.7717/peerj-cs.2245

Soni, V., Yadav, H., Semwal, V. B., & Tripathi, S. (2024). Improving human activity recognition in smart healthcare with ensemble deep learning. *IETE Journal of Research*, 1–15. https://doi.org/10.1080/03772063.2024.2434579

Sun, T., Yin, B., & Bohté, S. (2023). Efficient uncertainty estimation in spiking neural networks via MC dropout. In *Artificial Neural Networks and Machine Learning – ICANN 2023* (pp. 393–406). Springer. https://doi.org/10.1007/978-3-031-44207-0_33

Tang, B., Senlin, L., & Zhao, C. (2024). Predicting the performance of students using deep ensemble learning. *Journal of Intelligence, 12*(12), 124. https://doi.org/10.3390/jintelligence12120124

Tilahun, A., Atnafu Zewude, W., & Ersuncho, B. (2024). Satellite remote sensing for the evaluation of the impact of watershed management on surface soil moisture in the Kulfo watershed, Ethiopia. Research Square. https://doi.org/10.21203/rs.3.rs-5214529/v1

Vereecken, H., Huisman, J. A., Hendricks Franssen, H. J., Brüggemann, N., Bogena, H. R., Kollet, S., Javaux, M., Van Der Kruk, J., & Vanderborght, J. (2015). Soil hydrology: Recent methodological advances, challenges, and perspectives. *Water Resources Research*. https://doi.org/10.1002/2014WR016852

Wang, G., Huang, X., Li, Y., Wang, H., Zhang, X., & Qiu, J. (2024). Conv-ELSTM: An ensemble deep learning approach for predicting short-term wind power. *IET Renewable Power Generation*. https://doi.org/10.1049/rpg2.13159

Wang, H., Ma, C., Almakky, I., Reid, I. R., Carneiro, G., & Yaqub, M. (2024). Rethinking weight-averaged model-merging. arXiv. https://doi.org/10.48550/arxiv.2411.09263

Xu, M. (2023). Quantile regression model and its application research. *Academic Journal of Science and Technology, 7*, 34–38. https://doi.org/10.54097/vt1qpm59

Yang, L. (2024). Theoretical analysis of Adam optimizer in the presence of gradient skewness. *International Journal of Applied Science, 7*(2), 27. https://doi.org/10.30560/ijas.v7n2p27

Yang, S., & Yee, K. (2023). Towards reliable uncertainty quantification via deep ensembles in multi-output regression task. *Engineering Applications of Artificial Intelligence, 107871*. https://doi.org/10.1016/j.engappai.2024.107871

Yirgu, T., Yihunie, Y., Assele, A., & Wogayehu, T. (2020). Land Use/Land Cover Dynamics and its Environmental Impacts in Kulfo Watershed, Gamo Highlands, South Western Ethiopia. *Journal*

of Geography, Environment and Earth Science International. https://doi.org/10.9734/jgeesi/2020/v24i230197

Yisehak, B., Adhena, K., Shiferaw, H., Hagos, H., Abrha, H., & Bezabh, T. (2020). Characteristics of hydrological extremes in Kulfo River of Southern Ethiopian Rift Valley Basin. *SN Applied Sciences*. https://doi.org/10.1007/s42452-020-3097-1

Zaznov, I., Badii, A., Dufour, A., & Kunkel, J. (2024). AdamZ: An enhanced optimisation method for neural network training. arXiv. https://doi.org/10.48550/arxiv.2411.15375

Zeevi, T., Staib, L. H., & Onofrey, J. A. (2025). Enhancing uncertainty estimation in semantic segmentation via Monte-Carlo frequency dropout. arXiv. https://doi.org/10.48550/arxiv.2501.11258

Zeevi, T., Shwartz-Ziv, R., LeCun, Y., Staib, L. H., & Onofrey, J. A. (2024). Rate-In: Information-driven adaptive dropout rates for improved inference-time uncertainty estimation. arXiv. https://doi.org/10.48550/arxiv.2412.07169

Zhao, H., Zhao, H., & Zhang, C. (2024). Reconstructing SMAP-derived 1-km soil moisture dataset using DINEOF+ algorithm. *2024 IEEE International Conference on Agro-Geoinformatics*, 1–5. https://doi.org/10.1109/agro-geoinformatics262780.2024.10661101

Zhou, N., Hong, J., Cui, W., Wu, S., Bing, X., & Kou, X. (2024). Analysis of spatial-temporal variability and heterogeneity of soil moisture. *2024 3rd International Conference on Smart Grid and Renewable Energy (SGRE)*. https://doi.org/10.1145/3661725.3661732

Zhou, Y. (2025). Analysis of stock prediction model based on LSTM. *Advances in Economics, Management and Political Sciences, 152*(1), 42–47. https://doi.org/10.54254/2754-1169/2024.19430

Zhu, L., Mo, Y., & Cheng, Y. (2024). Uncertainty qualification for deep learning-based elementary reaction property prediction. *Journal of Chemical Information and Modeling*. https://doi.org/10.1021/acs.jcim.4c01358

Zignol, F., Lidberg, W., Greiser, C., Larson, J., Hoffrén, R., & Ågren, A. (2024). Controls on spatial and temporal variability of soil moisture across a heterogeneous boreal forest landscape. EGUsphere. https://doi.org/10.5194/egusphere-2024-2909

Evaluation of Irrigation Water Application Practices Using DSSAT-CROPGRO Model Under Varying Water Level for Peanut Crop at Arba Minch, Ethiopia

Asres Getnet Workie*[1] and Yohannes Smeneh Ketsela[1]

[1]Arba Minch University Water Technology Institute, Department of water resources and irrigation engineering, Ethiopia.

*Corresponding email: asresgetnet21@gmail.com

Abstract

Inadequate water management and resources significantly impact peanut crop productivity. Implementing water-saving irrigation strategies and cultivating water-stress-resistant varieties can address these challenges. This study, conducted at Arba Minch University demonstration farmland, aimed to evaluate the effect of deficit irrigation on Werer-962 and local peanut varieties under four irrigation levels: 100% (V1T1, V2T5), 80% (V1T2, V2T6), 60% (V1T3, V2T7), and 40% (V1T4, V2T8) of Soil Moisture Depletion (SMD) and assessed the performance of the DSSAT-CROPGRO model in predicting peanut yield components, using coefficients of determination (R^2) and root mean square error (RMSE) for two seasons (December–April 2022 and November–March 2023). Data for climate, soil, crop management, and others were collected from field, laboratory, FAO references, and publications for model calibration and validation. Werer-962 yields were 41.6 q ha^{-1} (V1T1), 38.3 q ha^{-1} (V1T2), 30.2 q ha^{-1} (V1T3), 22.3 q ha^{-1} (V1T4), and local peanut variety were 39.5 q ha^{-1} (V2T5), 35.9 q ha^{-1} (V2T6), 27.8 q ha^{-1} (V2T7), 20.7 q ha^{-1} (V2T8). Higher yields were obtained under full irrigation, and decreasing at lower water levels for both varieties. Werer-962 better than the local variety, with water productivity ranged from 0.65 kg m^{-3} (V1T1) – 0. 74 kg m^{-3} (V1T3) and 0.62 kg m^{-3} (V2T1) –0.68 kg m^{-3} (V2T7) for the local variety. The DSSAT-CROPGRO model demonstrated strong predictive accuracy (+RMSE: 0.04; R^2: 0.96). The study concludes that this model is effective tool for determining irrigation depth and schedules and implementing deficit irrigation strategies could save up to 36.3% of water while maintaining satisfactory peanut yields.

Keywords: *Crop yield; Deficit irrigation; Soil moisture depletion; Water management; Irrigation scheduling*

1. Introduction

Water is the main input resource for peanut agricultural production during a period of inadequate rainfall (Xia et al., 2020). To balance the scarcity of water and the required food necessity, effective water use, and proper water management are very crucial (Reta et al., 2024). Proper water management techniques help to enhance crop yields and water use efficiency in the area of water scarcity (Setu et al., 2023). Use an effective irrigation water management approach to improve irrigation efficiency and water productivity (Ulsido & Alemu, 2014). Using irrigation water rather than waiting for rainfall is important to increasing peanut crop yields and ensuring food security for farmers to maintain a stable and reducing the risk of crop failures due to drought (Tebebal & Ayana, 2015).

Deficit irrigation (DI) is the application of irrigation below crop evapotranspiration (ETc) and conserving irrigation water while maintaining a reasonable yield level (Yohannes et al., 2017). Implementing deficit irrigation techniques helps to enhance peanut crop yields and water use efficiency in water stress areas (Yemane Gebreselassie, Mekonen Ayana, 2015). Estimating appropriate irrigation scheduling is crucial to applying the right amount of water at the right time to promote plant growth and achieve high-quality yields (Gebeyhu et al., 2024). Measure the soil moisture status is essential for both planning irrigation schedules and accurately refilling soil moisture to required levels (Hassen et al., 2019). The soil moisture contents determined based on the percentage depletion of available soil water in the root zone and it is important for water savings and increasing crop productivity (Naab et al., 2015).

Peanut is an important legume cash crop for farmers typically grown in semi-arid regions and the recommended soil water depletion factor of this crop is 0.5 (Allen et al., 1998). It requires good aeration and drainage for optimal growth and it is successful in warm climates with sufficient sunlight, simply this crop is a heat-loving crop(Wedajo, 2017). Spacing for the plant to plant is 10 cm and row spacing for the center to center is 60 cm, the total growing period is 140 - 160 days (Halder et al., 2017).

Water productivity would be affected by different levels of water application to the crop in the field (Bekchanov, 2024). Improving water use and effectively managing water implies high water use efficiency without significant yield effects (Greaves & Wang, 2017).The water productivity of peanut crops done by (Hassen et al., 2019) and (Metin et al., 2022) ranged from 0.23 to 0.45 kg/m^3 and 0.39 to 0.61 kg/m^3 respectively. The recommended water productivity values suggested by (Doorenbos J., 1979) ranged from 0.6 to 0.8 kg/m^3.

In Ethiopian agriculture, the Aqua Crop model stands out as the most suitable crop simulation model (Yemane Gebreselassie, Mekonen Ayana, 2015). However, the Decision-support systems for agro technology transfer (DSSAT) model is the potential tool for designing water-efficient strategies and testing for accurate prediction of water deficit effects on crop production (Alderman., 2020). It can accurately simulate biomass, yield, and water distribution in the root zone of a crop in a uniform area of land (Malik et al., 2016).

Furthermore, some experiments were conducted on common crops in the study area such as field experimentation based simulation of yield response of maize crop to deficit irrigation using the Aqua Crop model by (Yemane Gebreselassie, Mekonen Ayana, 2015), Assessment of soil mulching field management, and deficit irrigation effect on productivity of watermelon varieties, and aqua crop model validation by (Gebeyhu & Markos, 2023) and evaluation of water productivity under furrow irrigation for onion Crop by (Asres et al., 2022). This study proposes a novel approach to address the challenges of inadequate water management and limited irrigation water resources in peanut production by integrating deficit irrigation practices with the DSSAT-CROPGRO model. By combining experimental results with advanced crop modeling, the research establishes a framework for improving peanut yields in water-scarce areas. The study also provides practical recommendations for enhancing productivity and water use efficiency, contributing to sustainable agricultural practices in Ethiopia.

2. Materials and Methods

2.1. Location of the experimental site

The experimental site was located about 455 km from the capital city, Addis Abeba, in southern Ethiopia. Its coordinates were found at 6°4'2.44" N latitude and 37°34'0.77" E longitude. More precisely, the experiment was carried out on Arba Minch University's demonstration farmland, which is situated in the Arba Minch Zuria woreda district as shown in Figure 1 below. In the study area, the crops that were mainly grown were mangoes, bananas, maize, onions, tomatoes, watermelons, papaya, and peanuts.

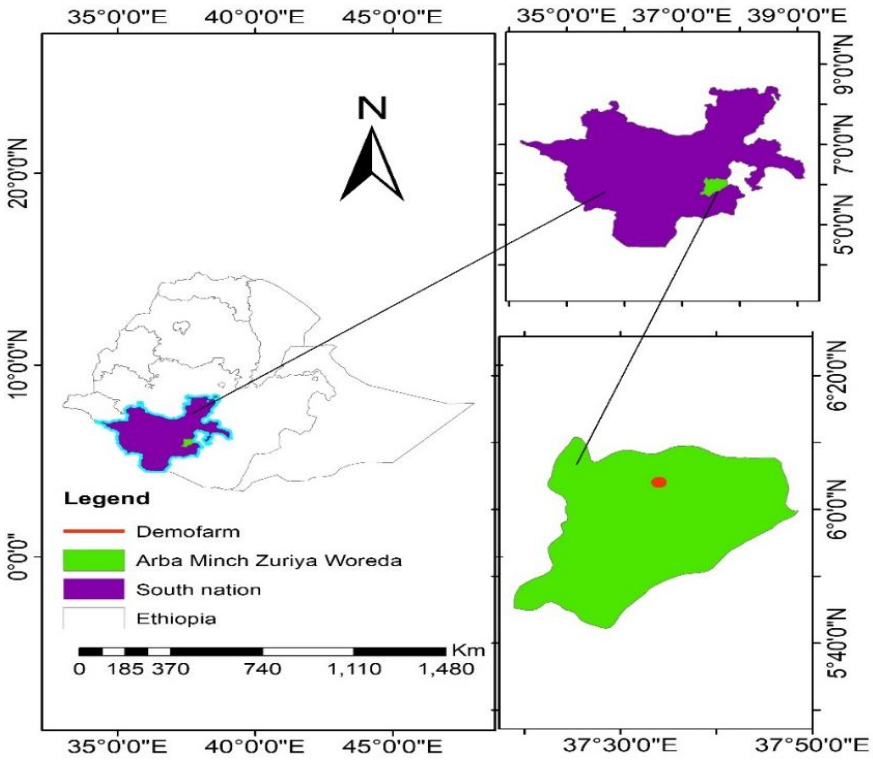

Figure 19: Map of the study area

2.2. Physical properties of soil

Soil texture is the leading physical property of soil in fixing irrigation water applications(Islam & Singh, 2022). It was determined by the hydrometer method (Abera et al., 2019). 5 g Sodium Hexametaphosphate a dry powder dispersion agent was added to the sample and mixed by an electronic shaker to identify the percentage of clay, silt, and sand. At the 40-second hydrometer reading, the temperature was reading and the percentage of (clay + silt) was recorded. After 2 hours, the temperature was again reading; the percentage of clay was noted, and silt was estimated, finally, subtracting the sum of clay and silt from 100% yielded the percentage of sand.

To determine the bulk density, undisturbed soil samples were collected and oven-dried for 24 hours at 105ºC to get the dry weight of the soil the procedure was suggested by (Panagos et al., 2024). The bulk density of the soil was computed using Equation (2.1)

$$\rho_b = \frac{M_S}{V_t} \tag{2.1}$$

Where: ρ_b = soil bulk density (g/cm^3), Ms= mass of solid and V_t = Volume of a soil sample (cm^3).

Field capacity (FC) and permanent wilting point (PWP) are vital for the determination of the soil water holding capacity (Li et al., 2019). Using a pressure plate apparatus, FC and PWP were measured in the laboratory at 1/3 and 15 atmospheric pressure, respectively.

Infiltration test was conducted using the double-ring Infiltrometer which is a simple device for determining the rate of water penetration into the soil which was suggested by (Zhou et al., 2019).

2.3. Treatments, Experimental Design, and Field Layout

The experiment was conducted in two consecutive years (2022 and 2023) with 4 treatments within three replications as shown in Table 1 below. The treatments consisted of four water levels (100%, 80%, 60%, and 40%) of available soil water which was regulated through the stage.

Table 8:Treatment for different water levels

Varieties	Treatment	Water Level at different stage				Deficit levels
		I	D	M	L	
Werer-962 peanut	V_1T_1	100	100	100	100	No deficit (Control)
	V_1T_2	100	80	80	80	20% deficit at D, M&L
	V_1T_3	100	60	60	60	40% deficit D,M&L
	V_1T_4	100	40	40	40	60% deficit D,M&L
Local peanut	V_2T_5	100	100	100	100	No deficit (Control)
	V_2T_6	100	80	80	80	20% deficit at D, M&L
	V_2T_7	100	60	60	60	40% deficit D,M&L
	V_2T_8	100	40	40	40	60% deficit D,M&L

**Description* *I= initial stage, D= development stage, M= middle stage, L = late-stage, and T=treatments*

2.3. Irrigation water management and application

The amount of irrigation water application was decided based on the current soil moisture status in the crop root zone (Gebeyhu et al., 2024). The crop root zone water depletion from the field capacity was determined for each treatment. According to (Zhang et al., 2023) described that irrigation was applied when root zone water depletion nearly reached to manage the allowable depletion of the available water in the root zone.

Irrigation water was measured using a partial flume The Parshall flume is a flow measurement device that gauges a depth (head) at a precise point on the upstream side (Patra et al., 2022), irrigators can easily calculate the flow by gauging the depth at this location. Before the water was diverted through the field furrow, the flume was installed. The amount of water required for given treatment plots was determined based on equation (2.2) in that the volume is equal to the depth of water required at the particular time multiplied by the area of the plot for a particular treatment. Similar procedures have been followed to supply the required amount of water in each plot and irrigation treatments throughout the crop season. The time of irrigation was recorded with a stopwatch to control the amount of water to be applied for each treatment. After estimating the amount of water delivered to a particular plot, the time of application was calculated by Equation (2.2)

$$Ti = \frac{V}{Q} \tag{2.2}$$

Where; Ti = time of irrigation(s), V = volume of irrigation water (liter), and Q = discharge or critical flow rate (l/s).

The critical flow rate should be non-scouring or non-silting at time of irrigation in the furrow (Shonka & Guchie, 2023). The maximum non-scouring or non-silting flow rate was estimated by equation (2.3)

$$\mathrm{Q_{max}} = \frac{\mathrm{C}}{\mathrm{S_o}} \tag{2.3}$$

Where; Q_{max} = Maximum non-erosive stream or non-silting flow rate (L/sec); S_o = Slope of the furrow in direction of flow (m/m); C = Empirical coefficient for the particular soil type and furrow shape. The range of values for the empirical coefficient (C) can vary widely based on the specific

characteristics of the soil and furrow shape. For example, different soil types, such as sandy loam, clay loam, or silt loam, may have different coefficients due to their varying levels of permeability and susceptibility to erosion.

2.4. Soil moisture content analysis

. Soil moisture depletion (SMD) is the difference between the field capacity and the actual moisture present in the crop root zone at any time before irrigation (Elsheikh et al., 2012)and (Berhe et al., 2022). The soil moisture depletion near management allowable depletion is the amount of water needed to bring the soil in the root zone up to field capacity (Nayak et al., 2016). Management allowable depletion of the available soil water is the percentage of the available soil water that can be depleted between irrigations without serious plant moisture stress (Gebeyhu & Markos, 2023). The amount of moisture in the plant root zone was estimated by soil moisture sensors or a time dominates reflectometer (TDR). It is easy to use and monitor soil moisture content, however, it needs calibration to be accurate (Mekonnen et al., 2022). Therefore, calibration is needed by using the gravimetric method. For the determination of gravimetric water content, soil samples were taken through the root depths with a standard sampler placed in an oven-dry machine at 105°C, and kept it 24 hours in the laboratory. The sample was determined by weight and the procedure was described by (TokováLucia et al., 2019). It was calculated by equation (2.4)

$$\theta_g = \frac{M_w}{M_S} \times 100 \tag{2.4}$$

The relation between volumetric water content and gravimetric water content was estimated by the equation (2.5).

$$\theta_V = \frac{\theta_g}{\rho_w} \times \rho_b \tag{2.5}$$

Where: θ_g = Gravimetric water content (%), M_w = mass of water in a soil sample (g), M_S = mass of dry soil (g), θv = volumetric moisture content (%), ρ_b = soil bulk density (g/cm^3), and ρ_w is water density (1 g/cm^3). Figure 4 shows the calibration of the TDR instrument using the gravimetric (laboratory) method.

2.5. Estimation of irrigation scheduling

Determination of irrigation scheduling is important for both water savings and improved crop yields. Soil moisture depletion (SMD) is the difference between field capacity and the actual moisture in the soil root zone at any given time before irrigation and it is the amount of water required to bring the soil in the root zone to field capacity (Mateos & Luck, 2017). It can be calculated by the equation (2.6).

$$\text{Soil Moisture depleation } (mm) = \frac{(\theta_C - \theta_i) \times R_d}{100} \tag{2.6}$$

Where:- θ_C= Volumetric moisture content at field capacity (%), θ_i = volumetric moisture content before irrigation (%), R_d = Root depth at different growth stages (mm).

The root depth was measured before the irrigation of the crop at the tagged plant to determine the depth of water applied. The effective root zone depth was determined by (Kumar, 2018). It was calculated by equation (2.7) as a function of time.

$$RD = RD_m[0.5 + 0.5\sin(3.03t_r - 1.47)] \tag{2.7}$$

Where; RD= Rooting depth(cm) at the time, RDm = Maximum expected rooting depth (cm), 100 cm for peanut, tr = Relative time (t/tm), and tm = Time to attain physiological maturity (Days after sowing),

2.6. Crop productivity (CP)

It is a measure of the yield of crops that can be obtained from a given area of land and soil quality, climate, water availability, and the use of agricultural inputs such as fertilizers and pesticides influence it (Wedajo, 2017). High crop productivity means that a piece of land can produce a large quantity of

yields while using relatively few resources. It is expressed by kg ha^{-1}, q ha^{-1}, or t ha^{-1}, and the yields of crops from specific land can be estimated by the equation (2.8).

$$CP = \frac{Grain\ yield\ (kg)}{Area(ha)} \quad (2.8)$$

2.7. Water productivity (WP)

Water productivity is expressed as the ratio of crop yield and water used during the crop season, and it is expressed as units of kg m^{-3} (Kumari et al., 2017). It was calculated by equation (2.9)

$$WP = \frac{Y}{ETa} \quad (2.9)$$

Where: WP = water productivity (Kg m^{-3}), ETa = Actual Evapotranspiration (mm)

2.8. Crop yield and water use relationship

The yield response factor was done using the crop water production function suggested by (Holzapfel & Godoy-faundez, 2020). The relationship was expressed by equation (2.10).

$$1 - \frac{Ya}{Y_m} = K_y(1 - \frac{ET_a}{ET_m}) \quad (2.10)$$

Where; ETa is the actual evapotranspiration that was effectively utilized by each deficit treatment (mm), ETm is the maximum evapotranspiration that was effectively utilized by control treatment(mm), Ky is the yield response factor, Ya is the actual harvested yield obtained from each deficit treatment (kg ha^{-1}), and Ym is the maximum harvested yield obtained from the control treatment (kg ha^{-1}).

2.9. DSSAT- CROPGRO model description

DSSAT Model is a Decision Support System for Agro technology Transfer tool (Jones et al., 2003). Using daily weather, soil characteristics, crop management, and cultivar/species factors, the DSSAT-CROPGRO model simulates the soil nitrogen (N) balance, water balance, yield, Biomass, and leaf area index of peanuts with great precision(Subramanian et al., 2021). The soil water balance equation was used to calculate the DSSAT- CROPGRO model to evaluate the yield reduction caused by water deficits (Hoogenboom et al., 1992). The model evaluates the soil water balance using the equation (2.11)

$$S = P + I - ET - R - D \quad (2.11)$$

Where: S = the amount of resultant soil water (storage); P = precipitation; I = irrigation; ET = evapotranspiration from soil and plants; R = runoff; and D = drainage from the profile. The values of drained upper limit (field capacity) and drained lower limit (wilting point)

2.9.1. Model input parameters

According to (Alderman., 2020) the minimum required data is needed to run the DSSAT simulation model, crop management data include planting date and type, row and plant spacing, number of rows per plot, number of plants per row, plot dimension, harvesting date, and methods. Meteorological data include daily maximum and minimum temperature, solar radiation, rainfall, wind speed, and relative humidity (%). Soil profile data include soil color, slope, permeability, soil texture, bulk density, organic carbon, nitrogen, phosphorus, field capacity, and permeant wilting point of the soil layer. The experimental data file consists of the experimental code and name, treatment combinations, tillage operations and land preparation, irrigation and water management amount, fertilizer and pesticide application, and environmental modifications. The experiment code is the agreement of the file identification system to provide information on the institute, site, planting year, experiment number, and crop type.

2.9.2. Model calibration and validations

The model was calibrated using the experimental data on grain yield, dry matter, and maximum leaf area index. The first crop season of 2022 was used for model calibration. The model was validated for

four treatments of irrigated crops, i.e., 100%, 80%, 60%, and 40% of the water applied. For validation, the model was run independently for each treatment of the second crop period in 2023. According to (Metin et al., 2022) the performance of the model during calibration and validation was done by equation (2.12).

$$RMSE = \sqrt{\frac{\sum_{i=1}^{n}(Oi-Pi)^2}{N}} \quad (2.12)$$

$$R^2 = \left(\frac{\sum_{i=1}^{n}(Oi-Oav)*(Pi-Pav)}{\sqrt{\sum_{i=1}^{n}(Oi-Oav)^2}*\sqrt{\sum_{i=1}^{n}(Pi-Pav)^2}} \right)^2 \quad (2.13)$$

Where; RMSE = Root-mean-square error, R^2 = coefficient of determination, o_i = Measured values, O_{av} = Average measured value, P_i = simulated value, P_{av} = average simulated value and N = numbers of sample

3. Results and Discussion

3.1. Soil physiochemical properties

According to the USDA triangular soil classification system, the dominant soil type in the study area was clay (table 2). The average bulk density in the experimental area was 1.36 g/cm$^{3.}$ According to (Panagos et al., 2024) the result of bulk density was found within the reasonable range. The organic matter of the current study area was recorded from 2.64% - 4.02% with average values of 3.4%. According to the previous researchers (Islam & Singh, 2022) and (Chaudhari et al., 2013), the organic matter content of the experimental area shows a good result, indicating a high level of fertility, and the soil is well-suited for cultivation; it is grouped under agricultural soil. The topsoil had lower pH levels and more organic matter. The pH levels in topsoil are lower since topsoil is rich in organic matter, and the decomposition of organic matter will result in the generation of more organic acid, reducing the pH of topsoil.

.The saturated hydraulic conductivity of the corresponding soil type was determined by the SPAW model by using organic matter and particle size distribution as an input and its average value of 3.4mm/hr. The field capacity and permanent wilting point at different depths were measured and summarized in Table 2 which shows the value of parameters found within the reasonable range as mentioned by (Li et al., 2019)

Table 2: Soil physiochemical properties

Soil depth(cm)	% sand	% silt	% clay	Texture	ρb (g/cm^3)	OM (%)	ECe (dsm^{-1})	pH (-)	FC (%Vol)	PWP (%Vol)
0-30	32	27.5	40.5	Clay	1.34	4.02	0.16	7.2	39.1	18.8
30-60	24.6	34.2	41.2	Clay	1.35	3.35	0.14	7.6	39.3	19.2
60-90	23.4	34.1	42.5	Clay	1.39	2.64	0.12	8.12	41.5	20.2
Average	26.7	27.5	40.5	Clay	1.36	3.4	0.14	7.6	40	19.4

3.2. Irrigation depth and scheduling

In the current study, a total of 11 irrigations were applied during the first growing season and 8 irrigations were applied during the second growing season as shown in Figure 2.

According to (Doorenbos ., 1979) and (Zhe et al., 2020) peanut crops typically require a total water depth of 500-700mm, with an average irrigation interval ranging from 6 to 14 days. In this research, the total depth of water used by crops during the first season was 620 mm at the control level and 340mm

at the lower deficit level. Similarly, during the second season of experiment, the total depth of water used by crops was 625 mm at the control level and 350 mm at the lower deficit level. The average soil moisture depletion in this study reached to the management allowable limit within 6-12 days. This finding found within this recommended range.

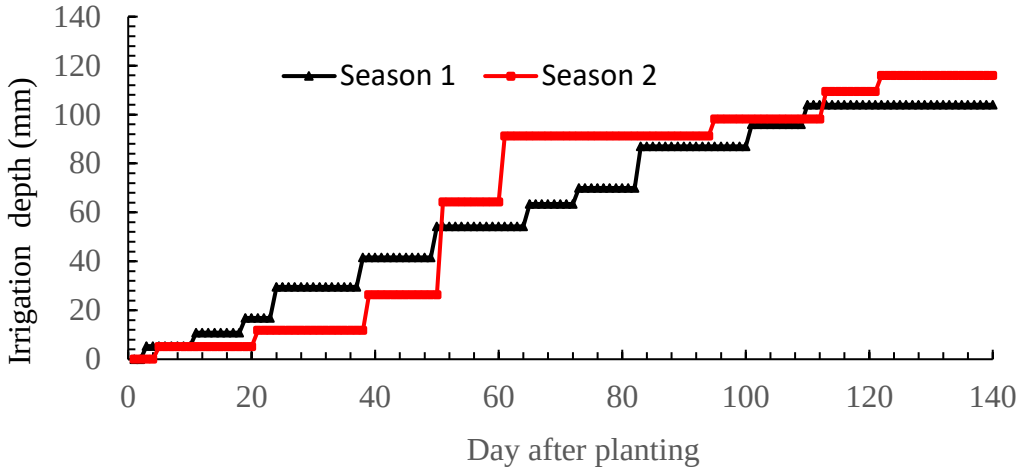

Figure 2: Irrigation scheduling

3.3. Effects of deficit irrigation on crop productivity

3.3.1. Average dry biomass under different water level

During the growing season, the Werer 962 variety exhibited a predominantly vertical growth habit, which is advantageous for efficient light interception and could potentially enhance photosynthetic activity. In contrast, the local varieties have a horizontal growth pattern, which is potentially beneficial for ground cover and soil moisture conservation. These growth behaviors significantly influenced biomass accumulation. Werer 962 provided biomass yield ranging from 126.65 q ha^{-1} under control treatment to 73.8 q ha^{-1} under the lower water level (table 3). The local varieties recorded lower biomass yields, ranging from 118 q $ha^{-1}$to 63.4 q ha^{-1} across the same water levels.

This difference suggests that Werer 962 possesses drought resilience and resource-use efficiency, enabling it to maintain higher productivity even under water stress. The study conducted by Fikre et al., (2012) investigated that, an average biomass ranging from 62.2 q ha^{-1} to 85.04 q ha^{-1}. Comparing these findings with the current study, higher values were observed under full water levels.

Table 3: Average dry biomass under varying water level

Variety	Treatments	Average DBM (q ha^{-1})
Peanut Werer 962	V1T1	126.65
	V1T2	113.75
	V1T3	83.8
	V1T4	73.75
Peanut Local	V2T5	118
	V2T6	104.2
	V2T7	74.3
	V3T8	63.4

3.3.2. Average grain yield of peanut crop under different water level

Under full irrigation conditions (control treatments), the Werer 962 variety outperformed the local variety, achieving an average yield of 41.6 q ha^{-1} compared to 39.5 q ha^{-1} for the local variety (figure3). This indicates the Werer 962 better adaptation that enhances water use efficiency and productivity.

As the level of deficit irrigation increased, both varieties exhibited a marked decline in yield, though the degree of reduction varied slightly between them. At the lowest water application level (V1T4 for Werer 962 and V2T8 for the local variety), the yields declined to 22.3 q ha^{-1} and 20.7 q ha^{-1}, respectively (figure 3). This translates to a yield reduction of 46.3% for Werer 962 and 47.6% for the local variety, relative to their control treatments.

At moderate deficit levels, a slightly lower yield reduction was observed in the Werer 962 variety. For instance, at V1T2, Werer 962 experienced a 7.8% reduction, which is slightly better than the 9.1% reduction seen in the local variety at V2T6. Similarly, at more severe deficit levels (V1T3 and V2T7), the yield reductions were 27.4% and 29.8%, respectively. in general, the results indicated that Werer 962 demonstrated a superior yield compared to the local variety across all treatments and the consumptive use of water decreases, the percentage of yield reduction increases. According to (Fereres & Soriano, 2007). as the consumptive use of water decreases, and the percentage of yield reduction increases (Fereres & Soriano, 2007). According to other previous researcher (Metin et al., 2022) got a grain yield of 53 quintal/ha at the control level and 27 q ha^{-1} at the low deficit level. A similar study was conducted in Southern Ethiopia by (Wedajo, 2017). According to (Doorenbos ., 1979) under irrigation and high level of management, the expected grain yields was ranged 35 q ha^{-1} - 45 q ha^{-1}. Based on the above scholars our results were found within a reasonable and acceptable range

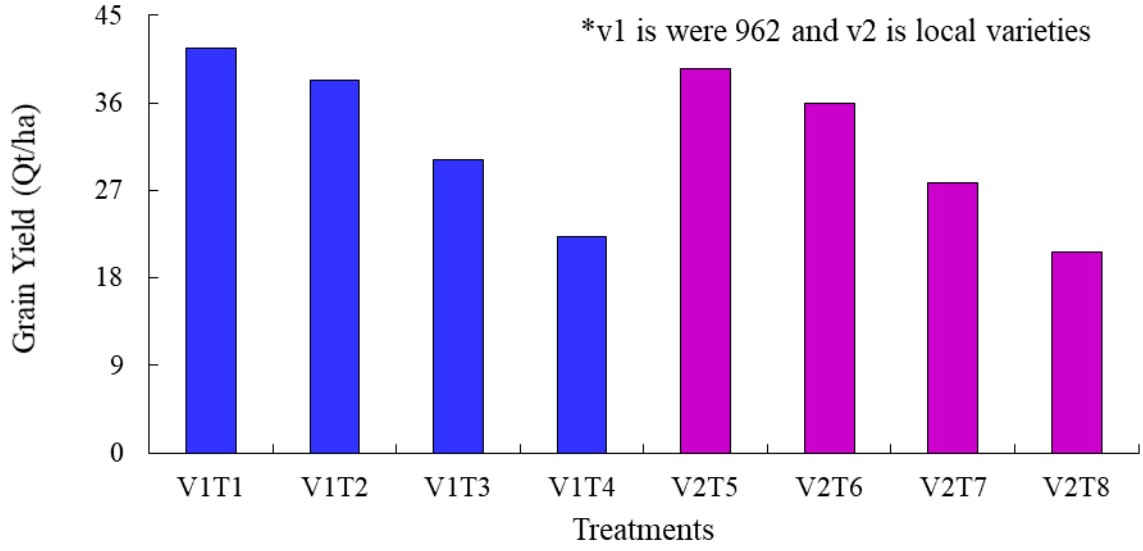

Figure 3: Observed average grain yield

3.4. Effect of deficit irrigation on water productivity of peanut crop

The average water productivity for Werer-962, ranged from 0.65 kg m^{-3} under treatment V1T1 to a maximum of 0.74 kg m^{-3} under treatment V1T3 and the local variety exhibited water productivity values ranging from 0.62 kg m^{-3} under V2T5 to 0.68 kg m^{-3} under V2T7 (figure 4).

Interestingly, treatment V1T4 for Werer-962 showed a decline in water productivity compared to the control (V1T1). The average for V1T4 was 0.65 kg m^{-3}, slightly lower than the control value of 0.67 kg m^{-3}. Similarly, the local variety under treatment V2T8 recorded an average of 0.62 kg m^{-3}, lower than the control treatment V2T5, which yielded 0.64 kg m^{-3}.

This trend suggests that treatments V1T4 and V2T8 did not improve water productivity. A reasonable explanation for this decline is that the crops under these treatments exposed to water stress, which

limited their growth and yield potential, thereby reducing their water productivity. The lower values reflect the sensitivity of both Werer-962 and the local variety to water availability.

The water productivity of peanut crops values compared to previous peanut research conducted by(Hassen et al., 2019) ranged from 0.23 to 0.45 kg m^{-3} and (Metin et al., 2022) ranged from 0.39 to 0.61 kg m^{-3} while our results yielded higher average values (ranging from 0.65 to 0.74 kg/m^3). Furthermore, we compared the current results to the recommended water productivity values provided by (Doorenbos J, 1979) ranging from 0.6 to 0.8 kg m^{-3}. The results indicated Werer 962 and local peanut crop varieties provided higher compared to previous studies and meeting the recommended values.

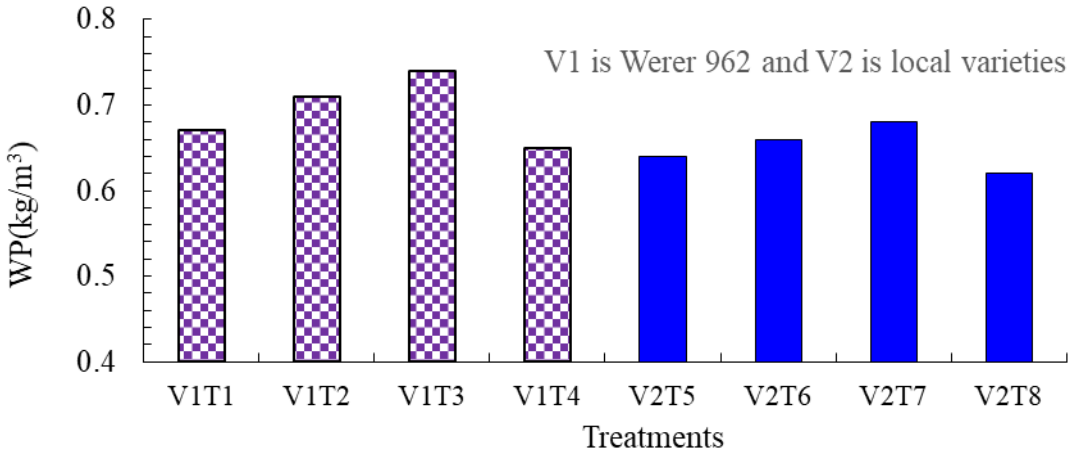

Figure 4: Water productivity at Various water levels

3.5. Analysis of yield response factor

The yield response factor for the Werer 962 variety to water stress to the Arba Minch climatic condition ranges from 1.02–1.06. Similarly, the determined value of the yield response factor for the local variety to water stress to similar climatic conditions ranges from 1.06–1.08. This result indicated that both peanut varieties are sensitive to water stress at lower water levels, with highly reduced yield and the yield response factors of the two peanut varieties were different; that is, the K_y of local was greater than the K_y of Werer 962. The message of this result was that the local peanut crop variety was more sensitive to water stress than the Werer 962 peanut variety.

The average yield reduction factor (Ky) value for Treatment (V1 T1, V1T2, and V1T3) and (V2T5, V2T6, V2T7) was less than 1 while the maximum average Ky value for treatment (V1T4) and V2T8 was 1.04 and 1.07 which is greater than 1 (table 4). The results of previous research work (Thiyagarajan et al., 2016) the value of Ky ranged from 0.45 – 1.72.. Our results indicated that the treatments of lowest water level the crop was under moisture stress at treatment).

Table 4: Crop yield response factor at different water levels.

Treatment	Yield response factor (Ky)	
	Season -1	Season -2
V1T1	0.00	0.00
V1T2	0.58	0.62
V1T3	0.80	0.82
V1T4	1.02	1.06
V2T5	0.00	0.00
V2T6	0.68	0.71

V2T7	0.85	0.91
V2T8	1.06	1.08

3.6. DSSAT model performance Evaluation

The model validation was conducted across four irrigation treatments: V1T1 (100% soil moisture depletion, SMD), V1T2 (80% SMD), V1T3 (60% SMD), and V1T4 (40% SMD) (Figure 5).

The simulated grain yields under these treatments closely aligned with the observed yields, demonstrating the model's reliability in capturing the crop response to varying irrigation levels. However, some discrepancies were noted between the two growing seasons. In season 1, the observed grain yields slightly exceeded the simulated values, whereas in season 2, the model overestimated the yields compared to field observations.

. In season 1, the coefficient of determination (R^2) was 0.97, with a root mean square error (RMSE) of 0.05, indicating an excellent fit. In season 2, the model maintained strong performance with an R^2 of 0.95 and an RMSE of 0.03. The previous study by Subramanian et al. (2023) reported that the CROPGRO model performance metrics R^2 were 0.77 during calibration and 0.729 during validation for peanut crops. The high R^2 values and low RMSE indicate a strong agreement between simulated and observed yields. The high R^2 values and low RMSE indicate a strong agreement between simulated and observed yields.

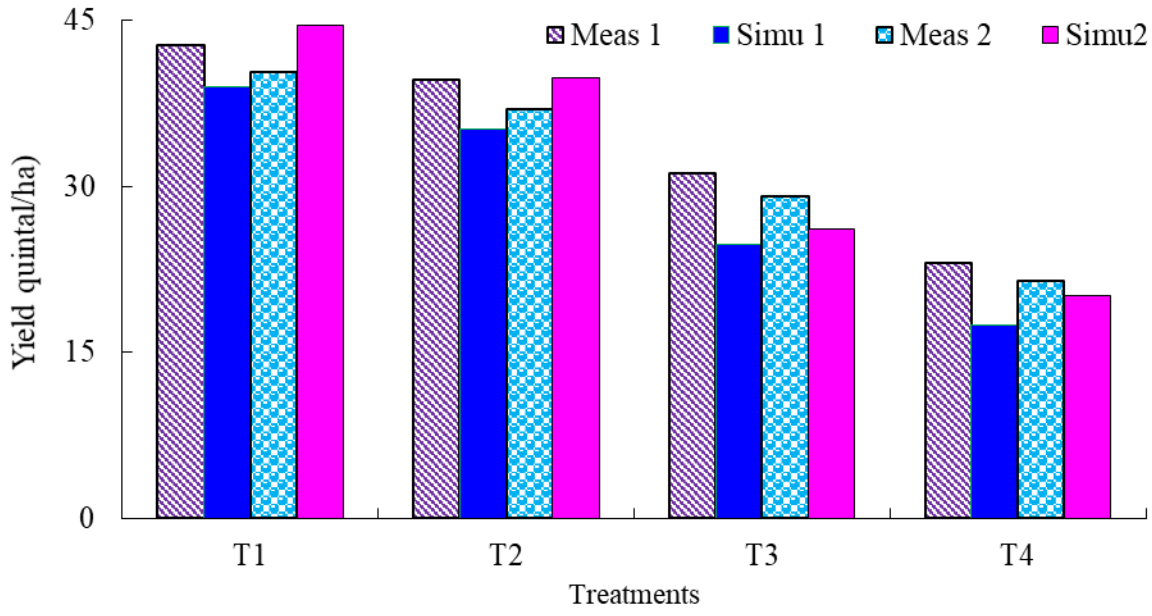

*1 and 2 represent the Year 2022 and 2023 respectively

Figure 5: Measured and simulated grain yield

3.6.1. Comparison of measured and simulated dry biomass of peanut crop

The highest dry biomass yield was observed during the first experimental season, reaching 129.2 quintals per hectare. In contrast, the second experimental season recorded the 124.1 quintals per hectare. This variation occurs due to the significant impact of water levels on biomass production. In the first season (2022), the coefficient of determination (R^2) was 0.88 and the root mean square error (RMSE) was 0.06. Similarly, during the second season (2023), the R^2 was 0.86 and the RMSE was 0.052, indicating a good level of accuracy in the model's predictions and the results indicated a good agreement between the observed and simulated values. The performance metrics of the CROGRO model reported by (Metin et al., 2022) has been reviewed. Their findings reveal an RMSE of 0.025 and an R^2 of 0.9, further confirming the credibility and strength of the model's performance in simulating biomass

dynamics. Overall, we observed a strong agreement between the simulated and measured values of peanut crop biomass. Figure 6 below shows the dry biomass for both crop seasons.

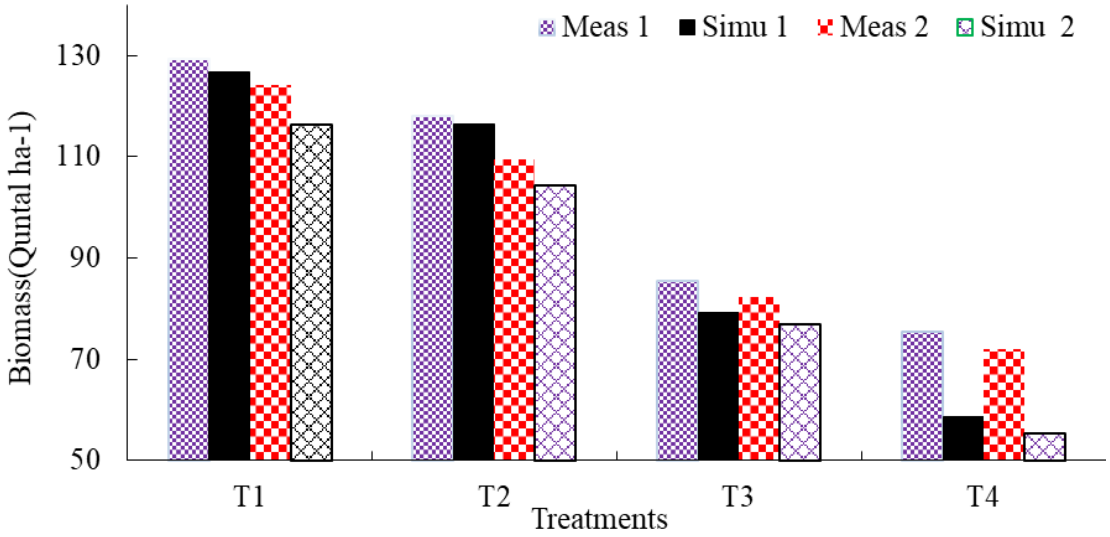

*1 and 2 represent the Year 2022 and 2023 respectively

Figure 6: measured and simulated dry biomass

4. Conclusion

Effectively managing irrigation water enhances peanut crop productivity, increases water savings, and reduces water wastage. Implementation of deficit irrigation practices with less crop water stress in water-scarce regions can achieve up to 38.5 % of water savings and enhance water productivity without significant peanut crop yield reduction. However, a 40% irrigation water level (V1T4 and V2T8) saves more than 50 % of water with a highly significant yield reduction of up to 47% for variety V1 and V2. Due to this reason, this water level is not recommended for the study area and similar agro-ecological zones due to resulting crop water stress. The grain yield and water productivity of Werer 962 peanut variety is a high-yield provider compared to the local crop variety across all irrigation treatments due to its resistance to water stress. The study recommended the widespread adoption of Werer-962 peanut variety rather than local peanut to Arba Minch farmers and the region having similar climatic conditions to increase crop yields, improve water productivity. The DSSAT-CROPGRO model performance indicator showed that a good agreement was found between measured and simulated grain yield and biomass. Researchers and policymakers would be better for using this model for effective water management, to predict the water deficit effect on peanut crop productivity, and to integrate it with agricultural practices for decision-making. This study contributes to implementing deficit irrigation strategies for peanut crop production in water-shortage areas, adapt Werer- 962 peanut crop variety to the Arba Minch climate, and utilizing the DSSAT-CROPGRO model techniques under different irrigation water levels to predict yield.

Author contribution statement

Asres Getnet; Yohannes Smeneh: Conceived and designed the experiments, Performed the experiments, Analyzed and interpreted the data; Contributed reagents, materials, analysis tools or data; Wrote the paper.

Data availability statement

Data availability will be made on formal request.

Additional information

No additional information is available for this paper.

Declaration of interests

The authors declare that they have no known competing financial interests or personal relationships that could have appeared to influence the work reported in this paper.

Acknowledgments

We express our gratitude to Arba Minch University Water Resources Research for their invaluable support in securing the experimental sites and providing essential laboratory materials.

REFFERENCE

Abera, A., Verhoest, N. E. C., Tilahun, S. A., Alamirew, T., Adgo, E., Moges, M. M., & Nyssen, J. (2019). Performance of small-scale irrigation schemes in Lake Tana Basin of Ethiopia: technical and socio-political attributes. *Physical Geography*, *40*(3), 227–251. https://doi.org/10.1080/02723646.2018.1516445

Alderman., P. D. (2020). A comprehensive R interface for the DSSAT Cropping Systems Model. *Computers and Electronics in Agriculture*, *172*. https://doi.org/10.1016/j.compag.2020.105325

Allen, R. G., Pereira, L. S., Raes, D., Smith, M., & Ab, W. (1998). *Crop evapotranspiration - Guidelines for computing crop water requirements - FAO Irrigation and drainage paper 56 By*. 1–15.

Asres, L. A., Singh, P., Derebe, M. A., & Yersaw, B. T. (2022). *Evaluation of Water Productivity under Furrow Irrigation for Onion (Allium cepa L .) Crop*. *2022*.

Bekchanov, M. (2024). Conveyance efficiency and irrigation water productivity under varying water supply conditions in arid lowlands of Central Asia. *Agricultural Water Management*, *293*. https://doi.org/10.1016/j.agwat.2024.108697

Berhe, G. T., Baartman, J. E. M., Veldwisch, G. J., Grum, B., & Ritsema, C. J. (2022). Irrigation development and management practices in Ethiopia: A systematic review on existing problems, sustainability issues and future directions. *Agricultural Water Management*, *274*. https://doi.org/10.1016/j.agwat.2022.107959

Bertino, A. M. P., Faria, R. T. De, Coelho, A. P., & Neto, A. C. (2023). Peanut crop yield under full and deficit irrigation in the reproductive phase1. *Agricultural and Environmental Engineering*, *27*(11), 900–909.

Chaudhari, P. R., Ahire, D. V, Ahire, V. D., Chkravarty, M., & Maity, S. (2013). Soil Bulk Density as related to Soil Texture, Organic Matter Content and available total Nutrients of Coimbatore Soil. *International Journal of Scientific and Research Publications*, *3*(1), 2250–3153. www.ijsrp.org

Doorenbos J., and K. A. H. (1979). *Yield Response to water*.

Elsheikh, E. R. A., Schultz, B., Haili, A. M., & Adam, H. S. (2012). Effect of deficit irrigation on yield and yield components of sunflower on gezira clay soil, Sudan. *WIT Transactions on Ecology and the Environment*, *168*, 369–378. https://doi.org/10.2495/SI120321

Fereres, E., & Soriano, M. A. (2007). Deficit irrigation for reducing agricultural water use. *Journal of Experimental Botany*, *58*(2), 147–159. https://doi.org/10.1093/jxb/erl165

Gebeyhu, B., Dagalo, S., & Muluneh, M. (2024). Soil moisture-based irrigation interval and irrigation performance evaluation : In the case of lower kulfo catchment , Ethiopia. *Heliyon*, *10*(16). https://doi.org/10.1016/j.heliyon.2024.e36089

Gebeyhu, B., & Markos, G. (2023). Assessment of soil mulching field management , and deficit irrigation effect on productivity of watermelon varieties , and AquaCrop model validation. *Heliyon*, *9*(11). https://doi.org/10.1016/j.heliyon.2023.e21632

Greaves, G. E., & Wang, Y. (2017). Yield response , water productivity , and seasonal water production functions for maize under deficit irrigation water management in southern Taiwan. *Plant Production Science*, 1–13. https://doi.org/10.1080/1343943X.2017.1365613

Halder, D., Kumar, R., Kumar, R., & Kheroar, S. (2017). Evaluation of the CROPGRO-Peanut model in simulating appropriate sowing date and phosphorus fertilizer application rate for peanut in a subtropical region of eastern India. *The Crop Journal*, *5*(4), 317–325. https://doi.org/10.1016/j.cj.2017.02.005

Hassen, J. M., Adugna, W. T., Sori, N. A., Borena, F. R., & Tufa, K. N. (2019). Determination of Optimal Soil Moisture Depletion Level for Groundnut at Amibara , Middle Awash , Ethiopia. *International Journal of Novel Research in Life Sciences*, *6*(5), 53–56.

Holzapfel, E. A., & Godoy-faundez, A. (2020). *Estimation of Yield Response Factor for Each Growth Stage under Local Conditions Using AquaCrop-OS*. *April*. https://doi.org/10.3390/w12041080

Hoogenboom, G., Jones, J. W., & Boote, K. J. (1992). Modeling growth, development, and yield of grain legumes using soygro, pnuogro, and beangro: a review. *Transactions of the American Society of Agricultural Engineers*, *35*(6), 2043–2056. https://doi.org/10.13031/2013.28833

Islam, R., & Singh, B. (2022). Stabilisation of soil organic matter : interactions between clay and microbes. *Biogeochemistry*, *160*(2), 145–158. https://doi.org/10.1007/s10533-022-00956-2

Jones, J. W., Hoogenboom, G., Porter, C. H., Boote, K. J., Batchelor, W. D., Hunt, L. A., Wilkens, P. W., Singh, U., Gijsman, A. J., & Ritchie, J. T. (2003). The DSSAT cropping system model. In *European Journal of Agronomy* (Vol. 18, Issues 3–4). https://doi.org/10.1016/S1161-0301(02)00107-7

Konlan, S, Sarkodies-Addo, J,. Asare, E and Kombiok, M. J. (2012). Groundnut (Arachis hypogaea L .) varietal response to spacing in the Guinea savanna agro-ecological zone of Ghana : Growth and yield. *AGRICULTURE AND BIOLOGY JOURNAL OF NORTH AMERICA*, *4*(3), 324–335. https://doi.org/10.5897/AJAR12.1313

Kumar, J. (2018). *Profile wise soil moisture extraction pattern of wheat and maize*. 773–780.

Kumari, M., Singh, O. P., & Meena, D. C. (2017). Crop Water Requirement, Water Productivity and Comparative Advantage of Crop Production in Different Regions of Uttar Pradesh, India. *International Journal of Current Microbiology and Applied Sciences*, *6*(7), 2043–2052. https://doi.org/10.20546/ijcmas.2017.607.242

Li, X., Shao, M., & Zhao, C. (2019). *Estimating the field capacity and permanent wilting point at the regional scale for the Hexi Corridor in China using a state-space modeling approach*. 3805–3816.

Malik, W., Dechmi, F., & Isla, R. (2016). DSSAT MODEL AS A TOOL FOR WATER AND NITROGEN MANAGEMENT IN INTENSIVE IRRIGATED AREAS : CALIBRATION AND VALIDATION. *International Modelling Symposium*.

Mateos, L., & Luck, J. D. (2017). *Field Characterization of Field Capacity and Root Zone Available Water Capacity for Variable Rate Irrigation*.

Mekonnen, Z., Sintayehu, G., Hibu, A., & Andualem, Y. (2022). Performance Evaluation of Small-Scale Irrigation Scheme: a Case Study of Golina Small-Scale Irrigation Scheme, North Wollo, Ethiopia. *Water Conservation Science and Engineering*, *7*(4), 491–503. https://doi.org/10.1007/s41101-022-00157-w

Metin, S., Ishfaq, S., Muhammad, A., Amiri, E., & Tekin, S. (2022). Growth and productivity assessments of peanut under different irrigation water management practices using CSM -

CROPGRO - Peanut model in Eastern Mediterranean of Turkey. *Environmental Science and Pollution Research*, *29*, 26936–26949. https://doi.org/10.1007/s11356-021-17722-w

Naab, J. B., Boote, K. J., Jones, J. W., & Porter, C. H. (2015). Field Crops Research Adapting and evaluating the CROPGRO-peanut model for response to phosphorus on a sandy-loam soil under semi-arid tropical conditions. *Field Crops Research*, *176*, 71–86. https://doi.org/10.1016/j.fcr.2015.02.016

Nayak, T. R., Choudhary, M. K., & Pandram, V. K. (2016). Modelling the Crop Water Requirement Using CROPWAT: A Case Study of Samrat Ashok Sagar (Halali) Project Command. *India Water Week*, *April*. https://doi.org/10.13140/RG.2.1.4831.0164

Panagos, P., Rosa, D. De, Liakos, L., Labouyrie, M., Borrelli, P., & Ballabio, C. (2024). Agriculture , Ecosystems and Environment Soil bulk density assessment in Europe. *Agriculture, Ecosystems and Environment*, *364*(October 2023), 108907. https://doi.org/10.1016/j.agee.2024.108907

Patra, S. K., Poddar, R., Pramanik, S., & Id, A. G. (2022). *Crop and water productivity and profitability of broccoli (Brassica oleracea L . var . italica) under gravity drip irrigation with mulching condition in a humid sub-tropical climate*. 1–19. https://doi.org/10.1371/journal.pone.0265439

Reta, B. G., Hatiye, S. D., & Finsa, M. M. (2024). *Assessment of Irrigation Water Management Performance Indicators and Mitigation Measure in Arba Minch Irrigation*. *2024*.

Setu, T., Legese, T., Teklie, G., & Gebeyhu, B. (2023). Effect of furrow irrigation systems and irrigation levels on maize agronomy and water use efficiency in Arba Minch ,Southern, Ethiopia. *Heliyon*, *9*(7). https://doi.org/10.1016/j.heliyon.2023.e17833

Shonka, T. G., & Guchie, and G. (2023). Performance Evaluation of Field Water Application at Tendaho Sugar Estate, Ethiopia. *Irrigation & Drainage Systems Engineering*, *6*(3). https://doi.org/10.4172/2168-9768.1000199

Subramanian, T., Pazhanivelan, S., Sudarmanian, N. S., & Kaliaperumal, R. (2021). Calibration and Validation of DSSAT CROPGRO Peanut Model for Yield and Yield Attributing Characters of Groundnut Varieties in Northern Agro- Climatic Zone of Tamil Nadu. *International Journal of Environment and Climate Change*, *11*(11), 207-215,. https://doi.org/10.9734/ijecc/2021/v11i1130535

Subramanian Thirumeninathan , Sellaperumal Pazhanivelan, S. K. R., , Ramalingam Kumaraperumal, G. S., & Mohan, and R. (2023). Integrating SAR Sentinel-1A and DSSAT CROPGRO Simulation Model for Peanut Yield Gap Analysis. *Agronomy*, *13*, 1–21.

Tebebal, M., & Ayana, M. (2015). Hydraulic Performance Evaluation of Hare Community Managed Irrigation Scheme, Southern, Ethiopia. *International Research Journal of Engineering and Technology(IRJET)*, *02*(08), 901–909.

Thiyagarajan, G., Ranghaswami, M. V, Rajakumar, D., & Kumaraperumal, R. (2016). Deficit Irrigation Effects on Groundnut (Arachis hypogaea L .) with Micro Sprinklers. *Madras Agricultural Journal ·*, *97*(3), 40–42. https://doi.org/10.29321/MAJ.10.100338

TokováLucia, Igaz Dušan, A., & Elena Aydin. (2019). Measurement of Volumetric Water Content by Gravimetric and Time Domain Reflectometry Methods at Field Experiment with Biochar and N Fertilizer. *Acta Horticulturae et Regiotecturae 2*, *November*, 61–64. https://doi.org/10.2478/ahr-2019-0011

Ulsido, M. D., & Alemu, E. (2014). Irrigation Water Management in Small Scale Irrigation Schemes: the Case of the Ethiopian Rift Valley Lake Basin. *Environmental Research, Engineering and Management*, *67*(1), 4–15. https://doi.org/10.5755/j01.erem.67.1.6240

Wedajo, G. (2017). Performance Evaluation of Ground Nut Varieties in Lowland Areas of South Omo , Southern Ethiopia. *International Journal of Research Studies in Science, Engineering and Technology [IJRSSET]*, *4*(2), 6–8.

Xia, G., Wu, Q., Chi, D., Chen, J., & Wang, S. (2020). Enhancing water productivity while improving peanut kernel quality by water regulation under different nitrogen LEVELS. *Irrigation and Drainage*, 86–94. https://doi.org/10.1002/ird.2394

Yemane Gebreselassie, Mekonen Ayana, K. T. (2015). Field experimentation based simulation of yield response of maize crop to deficit irrigation using AquaCrop model , Arba Minch , Ethiopia. *Journal of Agricultural Research*, *10*(4). https://doi.org/10.5897/AJAR2014.8703

Yohannes, D. F., Ritsema, C. J., Solomon, H., Froebrich, J., & van Dam, J. C. (2017). Irrigation water management: Farmers' practices, perceptions and adaptations at Gumselassa irrigation scheme, North Ethiopia. *Agricultural Water Management*, *191*(2017), 16–28. https://doi.org/10.1016/j.agwat.2017.05.009

Zhang, T., Zuo, Q., Ma, N., Shi, J., Fan, Y., Wu, X., Wang, L., Xue, X., & Ben-gal, A. (2023). Optimizing relative root-zone water depletion thresholds to maximize yield and water productivity of winter wheat using AquaCrop. *Agricultural Water Management*, *286*(June), 108391. https://doi.org/10.1016/j.agwat.2023.108391

Zhe Gu; Zhiming Qi; Rasika Burghate; Shouqi Yuan; Xiyun Jiao; and Junzeng Xu, A. M. As. (2020). Irrigation Scheduling Approaches and Applications : A Review. *Journal of Irrigation and Drainage Engineering ·*, *146*(6). https://doi.org/10.1061/(ASCE)IR.1943-4774.0001464

Zhou, W., Han, G., Liu, M., & Li, X. (2019). *Effects of soil pH and texture on soil carbon and nitrogen in soil pro fi les under different land uses in Mun River Basin , Northeast Thailand*. *October*. https://doi.org/10.7717/peerj.7880

Evaluating Surface Irrigation Suitability for Wheat Using Remote Sensing and AHP: A Case Study in East Shewa Zone, Oromia, Ethiopia.

Taye Teshome Terefe*[1], Belay Beko Legese[2], Selam Abebaw[3], Amanuel Kumsa Bojer[4]

[1]Department of Digital Image Processing, Space Science & Geospatial Institute, Addis Ababa, Ethiopia, email: tayegeo2013@gmail.com
[2]Department of Digital Image Processing, Space Science & Geospatial Institute, Addis Ababa, Ethiopia, email: belay46@gmail.com
[3]Department of Digital Image Processing, Space Science & Geospatial Institute, Addis Ababa, Ethiopia, email: selamabebawh@gmail.com
[4]Ethiopian Artificial Intelligence Institute, PO Box 40782, Addis Ababa, Ethiopia
*Correspondence: tayegeo2013@gmail.com

Abstract

Agriculture is the backbone of human survival and economic stability, especially in developing countries like Ethiopia, where it plays a vital role in providing livelihoods, ensuring food security, and contributing to the national economy. However, Ethiopia's agriculture is largely dependent on rainfall, making it highly vulnerable to the unpredictable effects of climate change. Irrigation has emerged as a crucial strategy for addressing this challenge and enhancing agricultural productivity, especially for important crops like wheat. This study utilizes advanced technologies such as Geographic Information Systems (GIS), remote sensing, and the Analytical Hierarchy Process (AHP) to pinpoint the best locations for irrigated winter wheat farming in the East Shewa Zone of Oromia, Ethiopia. It examines nine critical factors that influence wheat production: temperature, land use/cover, slope, elevation, soil type, texture, pH, drainage, and proximity to water sources. By using GIS-based AHP to analyze these factors and assign weights to each criterion, the study creates a map illustrating the area's suitability for wheat production. The results categorize the study area into five suitability levels: highly suitable (10.22%), moderately suitable (25.81%), marginally suitable (24.96%), unsuitable (3.39%), and permanently not suitable (35.63%). The model's accuracy was validated using the Receiver Operating Characteristics (ROC) method, achieving an impressive Area under the Curve (AUC) value of 0.896, or 89.6% accuracy. The findings indicate a significant opportunity to expand irrigation, particularly for wheat production in the East Shewa Zone, especially in regions deemed highly and moderately suitable. However, a considerable amount of land is classified as marginally suitable or unsuitable, highlighting the necessity for targeted interventions such as soil enhancement, improved drainage systems, and effective water management practices. This study offers a clearer understanding and a practical, data-driven framework for land use planning, providing valuable insights for policymakers and agricultural professionals. By identifying the best areas for wheat cultivation and addressing existing challenges, this research seeks to improve food security, boost agricultural productivity, and encourage sustainable farming practices in Ethiopia.

Keywords: *Irrigation, suitability, Receiver operating Characteristics, Weight overlay, Wheat*

1. Introduction

Around the world, farming is basic to keeping up human presence and implies of subsistence. For numerous individuals, it remains a noteworthy source of salary and nourishment security, having been one of the to begin with implies of subsistence. Among the most broadly developed crops are grain crops, such as corn, rice, and wheat, with wheat being the most broadly developed cereal in the world. Over 220 million hectares of wheat are developed each year over extend of climates (Shiferaw et al., 2013). Around the world, horticulture is fundamental to keeping up human life and providing implies

of subsistence. For numerous individuals, it proceeds to be a major source of pay and nourishment security, as it was one of the to begin with ways to make a living. Grain crops counting corn, rice, and wheat are among the most broadly developed crops; in truth, wheat is the most broadly developed cereal in the world. In a assortment of climates, more than 220 million hectares of wheat are developed every year (Shiferaw et al., 2013). In any case, a major deterrent to rural yield is the uneven precipitation that happens in numerous ranges. Water system frameworks have been put in put to increment efficiency and diminish reliance on rain-fed cultivating by empowering edit developing amid dry spells. In spite of making up as it were 17% of all agrarian regions, watered agribusiness accounts for around 40% of worldwide nourishment and agrarian generation, (FAO, 2003). This emphasizes how vital water system is to improving nourishment security and supporting agrarian economies.

In Africa, agriculture is the most important economic activity, providing livelihoods for the majority of the working population, contributing significantly to GDP, and generating income through exports. Despite its importance, agricultural practices in Africa are largely rain-fed, making them vulnerable to climate variability and change. Of the estimated 143.3 million hectares of cultivated land in Africa, only about 12.2 million hectares rely on irrigation (Firehiywet Girma et al., 2019). This low adoption of irrigation limits the potential for year-round crop production and exacerbates food insecurity in many regions. However, Africa has the potential to greatly boost agricultural output and attain food security with the right land suitability study and irrigation infrastructure investment.

Ethiopia, like many African nations, is heavily dependent on agriculture as a predominant source of employment, income, and food security. The agriculture sector contributes 34.1% to the GDP, employs 79% of the population, and generates 79% of foreign income (Benyam Tadesse et al., 2021). Ethiopia's diverse agroecological zones are favorable for cultivating a variety of crops, including wheat, which is essential for feeding its growing population. However, agricultural practices in Ethiopia are predominantly traditional, subsistence-based, and rain-fed, making them highly vulnerable to the spatial and temporal variability of rainfall (Azemeraw Wubalem, 2021). This variability often leads to declining crop productivity, food insecurity, and reduced foreign currency earnings, forcing the population to rely on foreign aid.

Irrigation is one of the key solutions to address food shortages in rain-fed agricultural systems. It can alleviate poverty, enhance food security, and increase farmers' incomes by enabling crop production during non-rainy seasons. In Ethiopia, traditional irrigation practices date back centuries, but modern irrigation systems were introduced in the early 1950s, primarily for sugarcane cultivation (Awulachew, S. B., et al. (2007). Recently, Ethiopia has recognized the potential for irrigated wheat production, with the government initiating an irrigated wheat program a few years ago under the leadership of Prime Minister Abiy Ahmed. This program aims to boost wheat productivity through irrigation farming, particularly during the dry season. However, current land use practices in Ethiopia, as in many developing countries, often lack proper suitability analysis. This highlights the urgent need for rational and efficient land use planning to maximize agricultural productivity and sustainability.

Land suitability analysis is a critical tool for identifying suitable areas for specific crops or land uses. It evaluates factors such as soil properties, topography, proximity to water sources, and land use/land cover to determine the most appropriate areas for irrigation and crop production (Abdel et al., 2016). For winter wheat, this analysis is often conducted using Geographic Information System (GIS)-based methods like the Analytical Hierarchy Process (AHP), which considers multiple criteria to determine suitability. By identifying optimal areas for irrigation, land suitability analysis can contribute to Ethiopia's food security and economic development. This research focuses on conducting a land suitability analysis for winter wheat production using GIS-based methods, aiming to identify optimal areas for irrigation and contribute to Ethiopia's food security and economic development.

2. Material and Methods

2.1. Description of study area

East Shewa (in Afaan Oromoo known as Shawaa Bahaa) is one of a zone in Oromia Regional State of Ethiopia. The zone is located at center of Oromia. This zone is bordered on the south by the West Arsi Zone, on the southwest by the Southern Nations, Nationalities and Peoples Region, on the west by Southwest Shewa Zone and Shegger city, on the northwest by North Shewa, on the north by the Amhara Region, on the northeast by the Afar Region, and on the southeast by Arsi; its westernmost reach is defined by the course of the Bilate River. The elevation is from 859m to 3000m above mean sea level. There are rivers and lakes in the study area. Awash and mojo rivers are among major rivers and Batu, koka, Bishoftu lakes and beseka lakes are also find in the study area. The capital city of east shoa zone is Adama city; serving as administration center of the zone.

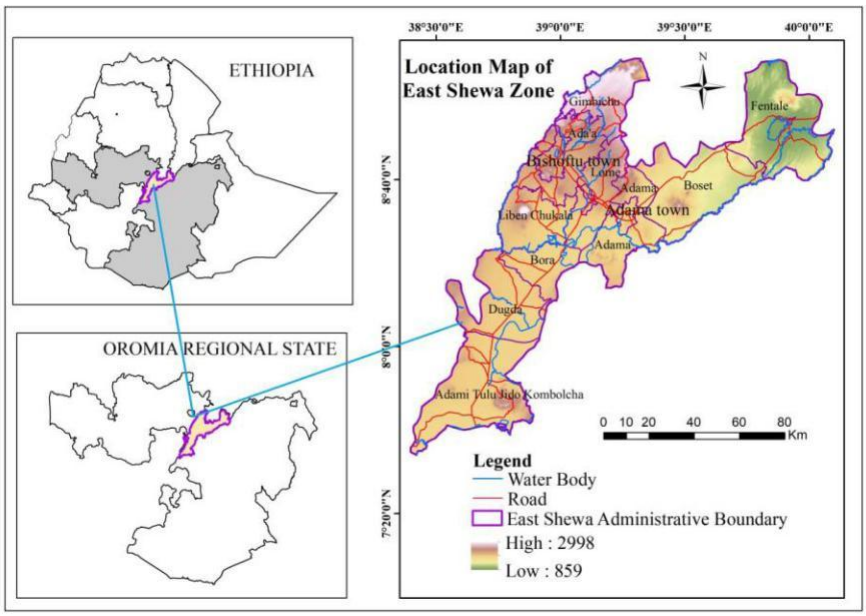

Figure 1. Location Map of East Shewa Zone, Oromia Regional State

2.2. Methods of data collection and sources

The datasets listed here provide a wealth of geospatial and environmental information, making them invaluable for detailed land use and land cover (LULC) studies. Landsat 8/9 imagery, available through the USGS Earth Explorer at a 30-meter resolution, is a key resource for mapping and analysing LULC patterns. Soil data, sourced from the ISRIC Soil Data Hub, offers insights into soil type, texture, pH, drainage, moisture, and depth, which is crucial for understanding land suitability and health. Elevation and slope data, derived from Digital Elevation Models (DEMs) also available on the USGS Earth Explorer, help in terrain analysis. Additionally, water body data from SSGI provides Euclidean distance measurements, useful for hydrological studies, while annual temperature data from the National Metrology adds a climatic dimension to the analysis.

The primary data was gathered via field observation and reconnaissance survey to identify key land cover and existing irrigated area. Also, by using GPS tool, 100 ground truth points are collected. Additionally, the x and y coordinates collected by local administrative are collected from each district found in the study area. Together, these datasets form a robust foundation for applications in agriculture, environmental monitoring, urban planning, and climate research, enabling informed decision making and sustainable resource management (Table 1).

Table 1. Data used and source

No	Data sets	Sources	Spatial resolution	Data variable
1	Landsat 8/9	https://earthexplorer.usgs.gov	30m	LULC
		https://www.isric.org/explore/isric-soil-data-		Soil Type, Soil texture, Soil PH,
3	Soil data's	hub	-	Soil drainage, Soil moisture,Soil Depth
4	DEM	https://earthexplorer.usgs.gov	30m	Elevation, Slope
5	Water Body	SSGI	-	Euclidean Distance
6	Temperature	National Metrology	-	Annual temperature
7	GTP	Field survey and Local admirations	X and Y coordinates	Validation

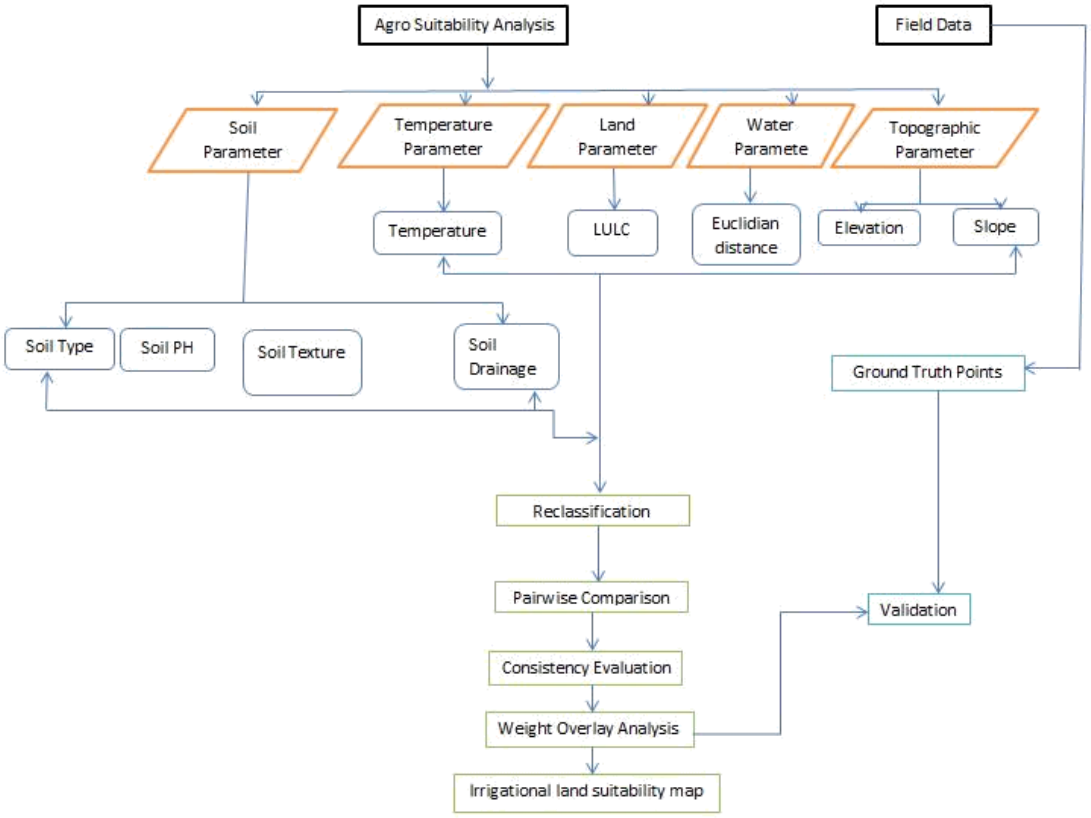

Figure 2: the methodology flow chart

2.3. Method of land suitability Evaluation

The suitability site map of winter wheat analysis is based on FAO (1976) land suitability classification Sultan D (2013). According to FAO, generally land suitability map is classified in to two classes i.e. Suitable (S) and not suitable (N). These suitable and unsuitable classes are further classified based on their benefits and limitations; suitable classified into three as highly suitable, moderately suitable, and marginally suitable whereas unsuitable class into two as currently not suitable and permanently not suitable

2.4. Analytical hierarchy process method (AHP)

GIS-based AHP is popular because of its capacity to integrate a large amount of heterogeneous data and the ease in obtaining the weights of a large number of criteria, and therefore, it has been applied in tackling a wide variety of decision-making problems (Y. Chen, 2010).

2.5. Land suitability parameters for surface irrigation particularly for wheat production.

2.5.1. Soil parameter

Based on its availability soil type, soil drainage, soil texture and soil PH are included in the study as a soil parameter. Soil type is one parameter that affects the growth and productivity of wheat production. Soil type in the study area includes Nitosols, Luvisols, Leptosols, Andosols, Cambisols, Vertisols, Solonchaks, Fluvisols, Regosols, Xerosols, Phaeozems. Soil type of the study area is classified and scaled into four land suitability classes that of highly suitable (Nitosols, Luvisols, Phaeozems), moderately suitable (Fluvisols, Vertisols, Cambisols), marginally suitable (Andosols, Xerosols, Regosols,) and unsuitable classes (Solonchaks, Leptosols) (Fig 6A). Luvisols are highly fertile soils,

making them well-suited for a wide range of agricultural activities. Studies by Worqlul et al. (2015) and Balew et al. (2021) classify them as highly suitable for crop production. Similarly, Nitisols have been recognized for their excellent agricultural potential (Girma et al., 2019), and Phaeozems are also considered highly suitable for farming (IUSS Working Group WRB, 2015). Moderately suitable soils include Cambisols, Vertisols, and Fluvisols, as identified by Worqlul et al. (2015) and Balew et al. (2021). While these soils can support crop growth, they may have limitations such as drainage issues or structural constraints that require proper management.

On the other hand, marginally suitable soils—such as Andosols (IUSS Working Group WRB, 2015), Regosols (Worqlul et al., 2015; Balew et al., 2021), and Xerosols (FAO, 1990) present more significant challenges for agriculture. These soils may have issues related to texture, nutrient availability, or moisture retention, making large-scale farming difficult without substantial soil amendments. Finally, some soils are considered unsuitable for crop production. These include Leptosols (Worqlul et al., 2015; Balew et al., 2021; IUSS Working Group WRB, 2015), which are often shallow and rocky, and Solonchaks which are affected by high salinity, making them largely unproductive for most crops.

Soil drainage significantly affects water availability, root health, and aeration, making it a crucial factor in agricultural suitability. Well-drained to moderately well-drained soils are classified as highly suitable, as they ensure adequate moisture while preventing waterlogging (Fig 4B). Imperfectly drained soils are considered moderately suitable, though they may require drainage improvements to prevent excess moisture stress USDIBR, 2021. Poorly drained or excessively drained soils are marginally suitable, as water stagnation or rapid percolation can hinder crop growth. Very poorly drained soils, which are prone to flooding, and excessively drained soils, which cause drought stress, are generally unsuitable for agriculture.

Soil texture is a key determinant of agricultural suitability, influencing water retention, drainage, aeration, and root penetration. Highly suitable soils typically include loam, sandy loam, or silt loam textures, as they provide a balanced combination of water-holding capacity and drainage (Fig 5B). Moderately suitable soils, such as clay loam and sandy clay loam, may require management practices to enhance aeration or moisture retention (FAO, 2006). Marginally suitable soils, including sandy or clayey soils, pose challenges due to excessive drainage or compaction, respectively. Soils with extremely sandy or heavy clay textures are generally unsuitable, as they can lead to drought stress or waterlogging, impairing plant growth (Hagos, Y. G., Mengie, M. A., Andualem, T. G., et al. (2022).

Soil pH is a critical factor in determining agricultural suitability, as it influences nutrient availability, microbial activity, and overall soil health (McFarland et al., 2015). The highly suitable pH range for most crops is 6.0–7.5 where nutrients are readily available. Moderately suitable soils fall within 5.5–6.0 and 7.5–8.5 though slight acidity or alkalinity may require amendments. Marginally suitable soils have pH levels of 5.0–5.5 or 8.5–9.0 (FAO, 2006), where toxicity or nutrient deficiencies can hinder plant growth. Soils with pH below 5.0 or above 9.0 are generally unsuitable due to extreme acidity or alkalinity, leading to severe nutrient imbalances and poor soil structure (Worku, D et.al (2024).

5

2.5.2. Temperature parameter

The optimum temperature for wheat grain development ranges from 15 to 25 °C (Asseng, S., Ewert, F., Martre, P., et al. (2015). Wheat is best grown in winter under irrigation with optimum day temperatures of between 15 – 20 °C. Based on this standard, temperature of the study area is classified and scaled into four land suitability classes that of highly suitable (15°C – 20°C), moderately suitable (14°C – 15°C and 20°C – 25°C), marginally suitable (13°C – 14°C), and unsuitable classes.

2.5.3. Land parameter

In land suitability site analysis land use land cover is a vital parameter employed in crop production produced via irrigation. This parameter is useful to indicate which kinds of land use/cover in the area relevant for crop production. Cropland was grouped as highly suitable (Azemeraw Wubalem, 2021); Grassland is assessed as moderately suitable. Woodland/Shrub/bush is classified as marginally suitable, because it required initial investment for land preparation. Forest/Barren land/Water body/Settlements are classified as not suitable.

Land use land cover of the study area is classified and scaled into four land a suitability class that is classified based on FAO principle as highly suitable (cropland), moderately suitable (there is no land cover), marginally suitable (shrub land), and unsuitable classes (Water body, urban, plantation, forest, bare land). Even though, it is classified in to four suitability class, there is no moderately suitable land use land cover in the study area for wheat production.

2.5.4. Water Parameter

Evaluation and determination of the distance of land to the water source is vital component in land suitability analyses for wheat crop in winter season. According to Azemeraw Wubalem, 2021 the suitability classes' distances of land in km to water body classified as 0km – 5km optimum, 5 – 10km moderate, and 10km – 20km marginal and greater than 20km low. According to the above scientific standard, the suitability classes of land distance to water body classified as into 0km to 2km highly suitable, 2km to 4km moderately suitable, 4km to 6km marginally suitable, and greater than 6km unsuitable for winter season crop production via irrigation.

2.5.5. Topographic parameter

Slope is one factor in land suitability analysis for crop production via irrigation. Wheat production prefers slopes less than 8% for the highest productivity (Endalkachew Fekadu and Ajanaw Negese, 2020). It affects land preparation, irrigation operation, production costs, soil depth, and erosion (Azemeraw Wubalem, 2021 cited USDIBR, 2003. Suitability classes of slope (in percent) classified as 0% – 2% optimum, 2% – 5% moderate, 5% – 8% marginal and greater than 8% low. (Azemeraw Wubalem, 2021 cited Mandal et al, 2017,). Based on the above scientific, slope (generated from DEM) parameter is classified and rescaled into 4 land suitability classes as highly suitable (0% – 2%), moderately suitable (2% – 5%), marginally suitable (5% – 8 %) and unsuitable (> 8%) using the GIS tool.

Studies have shown that wheat performs best at elevations between 1,800 and 2,500 masl Ortiz, R., et al. (2008). Accordingly, the elevation of the study area is classified and scaled into four land suitability classes that of highly suitable (2000m – 2500m), moderately suitable (1500m – 2000m, 2500m – 2998m), marginally suitable (1400m – 1500m), and unsuitable classes (859m – 1400m) (fig 4A).

2.6. Validation method

After developing the irrigation suitability map for the East Shewa zone, it was crucial to assess the accuracy of the result in this study. To do this, we compared the suitability map generated using the AHP model with a reference map. For validation, we used the Receiver Operating Characteristics (ROC) method, which helps evaluate how well a model differentiates between suitable and unsuitable areas.

The Area under the Curve (AUC) score, which goes from 0 to 1, is the foundation of the ROC analysis. A perfect model has a score of 1, whereas a random model receives a score of approximately 0.5. A higher AUC denotes a more dependable model. We examine the ROC curve, a graph that compares the True Positive Rate (TPR) against the False Positive Rate (FPR) at various thresholds, to acquire a better understanding of this. TPR, sometimes referred to as recall, indicates how successfully the model detects appropriate irrigation zones. It is computed by dividing the total number of actual appropriate areas (True Positives + False Negatives) by the number of accurately anticipated suitable areas (True Positives). On the other hand, FPR measures how often the model mistakenly classifies unsuitable areas as suitable. It is calculated by dividing the number of incorrect positive predictions (False Positives) by the total actual unsuitable areas (False Positives + True Negatives).

By contrasting expected suitability probability with actual suitability data, ROC analysis is a popular method for evaluating model reliability. In a typical ROC curve, the top-left corner represents an ideal model (TPR = 1, FPR = 0), with TPR on the Y-axis and FPR on the X-axis. Although it is uncommon to obtain a perfect score, the model performs better at differentiating between irrigation regions that are appropriate and those that are not, the closer the AUC value is to 1 (Ayele et al. (2024).

3. Results and Discussions

3.1. Results

3.1.1. Establishing the criterion/factors weight value

In this study, a GIS-based AHP as a multicriteria evaluation approach was used to identify suitable irrigation land for wheat. Nine irrigation determinant factors i.e. slope degree, elevation, distance to water, soil type, soil texture, soil PH, soil drainage, temperature and LULC were employed for suitability analysis. As shown in Table 6, the relationship between factors and land suitability for surface irrigation was determined using 9 × 9 pairwise comparison matrix (Table 7). For this study, nine governing factors such as soil factors (soil texture, soil drainage, soil type, and soil PH), land use and land cover, topographic factors (slope and elevation), and Water factor (distance to water body) were considered. The weight of every factor was calculated from the normalized table by the average sum of the row of the matrix (Table 7). The relative significance of every factor is summarized in Table 7. Distance from a water source (31%), slope (27.5%), soil type (11.9%), LULC (7.7%), soil PH (6.9%), and soil drainage (4.6%), soil texture (4.5%) has scored high weight criteria and they are the foremost important factors in determining suitable lands for surface irrigation followed by temperature and (2.9%), and elevation (2.8%).

The Analytic Hierarchy Process (AHP) commonly relies on expert evaluations for its rating system, making it highly effective for assessing complex challenges such as irrigation suitability. However, variations in

individual expert opinions can introduce cognitive biases, uncertainty, and subjectivity. Therefore, analysing the spatial relationships between irrigation suitability factors and optimal irrigation locations is essential. In this study, spatial analysis of each parameter, along with field observations, was integrated into the expert judgment process. As presented in Table 5, the pairwise comparison matrix for the factors and sub-factors, along with their relative weights, was determined using the Saaty (2001) methodology. The consistency ratio (CR) was calculated for all factors and remained 7.4% which is below 10% indicating that the assigned weights were appropriate and reliable.

Table 5 Criteria prioritization with weights and rankings.

Criteria	Priority	rank
Distance to water	31.0%	1
Slope	27.5%	2
Soil type	11.9%	3
LULC	7.7%	4
Soil PH	6.9%	5
Soil drainage	4.6%	6
Soil texture	4.5%	7
Temperature	2.9%	8
Elevation	2.8%	9

Table 6 The pairwise comparison matrix.

Criteria	Distance to water	Slope	LULC	Soil type	Soil drainage	Soil PH	Soil texture	Temperature	Elevation
Distance to water	1	2.00	7.00	4.00	7.00	5.00	5.00	5.00	5.00
Slope	0.50	1	7.00	3.00	7.00	5.00	7.00	7.00	7.00
LULC	0.14	0.14	1	0.33	3.00	1.00	4.00	3.00	3.00
Soil type	0.25	0.33	0.33	1	3.00	3.00	3.00	3.00	3.00
Soil drainage	0.14	0.14	0.33	0.33	1	1.00	1.00	1.00	1.00
Soil PH	0.20	0.20	1.00	0.33	1.00	1	3.00	2.00	5.00
Soil texture	0.20	0.14	0.25	0.33	1.00	0.33	1	3.00	3.00
Temperature	0.20	0.14	0.33	0.33	0.33	0.50	0.33	1	1.00
Elevation	0.20	0.14	0.33	0.33	0.50	0.20	0.33	1.00	1

3.1.2. Analysis of criterion used for potential irrigation site

Land suitability analysis is a fundamental system to identify the natural resource potentials and limitations of a given area that could help to provide decisions on the farming. In this project, the major criterion used for winter wheat site analysis are like water body, soil type, soil drainage, soil texture, soil PH land use land cover, temperature and topography (slope, elevation).

Table 7 Land suitability parameters class area summary.

Parameter	Land suitability	Parameter class	Area (ha)	Area%
Euclidean Distance	S1	0km – 2km	227018.25	23.20
	S2	2km – 4km	180038.07	18.40
	S3	4km – 6km	151221.24	15.45
	N	>6km	420222.78	42.94
Slope	S1	0%–2%	457223.58	46.70
	S2	2%–5%	167047.56	17.06
	S3	5%–8%	109837.8	11.22
	N	>8%	244810.62	25.00
Elevation	S1	200m – 2500m	124,721.50	12.74
	S2	150m – 2000m, 250m – 2998m	602,989.23	61.62
	S3	140m – 1500m	34,184.79	3.49
	N	859m – 1400m	216,658.30	22.14
Soil Drainage	S1	Well	455749.11	50.28
	S2	Moderate	242557.65	26.76
	S3	Imperfect	117026.91	12.91
	S4	poor	90978.39	10.04
Temperature	S1	15°C – 20°C	673,140.6	68.822
	S2	14°C – 15°C&20°C – 25°	303,841.63	31.065
	N	No data	1,102.14	0.113
Soil Texture	S1	Loam, Silt loam, Clay loam	109440.45	12.07
	S2	Sandy loam, Silty clay loam	797028.75	87.9
	S3	Sandy, Silty, Clay	29.88	0.003
Soil Type	S1	Nitosols, Luvisols and Phaeozems	227539.17	24.16
	S2	Fluvisols, Vertisols and Cambisols	471871.71	50.11
	S3	Andosols, Xerosols and Regosols	152012.7	16.14
	N1	Solonchaks and Leptosols	60794.73	6.46
	N2	No data	29428.65	3.12
Soil PH	S2	6.5 – 7.5	677,813.31	69.28
	S2	7.5 – 8.5 and 5.5 – 6.4	236,466.99	24.17
	N	10 or less than 5.5	64,049.22	6.54
LULC	S1	Cropland	613,909.1	62.75
	S2	Grassland	123,292.4	12.602
	N	Forest/Barren	241,139.60	

		land/Water body/Settlements		24.648

3.1.2.1. **Euclidean distance to the water**.

Land distance to water source generated for the study area using Euclidean distance tool of ArcMap software. Highly and moderately suitable class of land distance from water resource is covered about 23.20% and 18.40 of land respectively. Whereas, marginally suitable and unsuitable class of land distance from water resource is covered about 15.45% and 42.94% of land respectively (Table 7).

3.1.2.2. Slope.

Highly and moderately suitable class of slope is covered about 46.70% and 17.06% of land respectively. Marginally suitable and unsuitable class of slope land is covered about 11.22% and 25.00% of land respectively (Table 7).

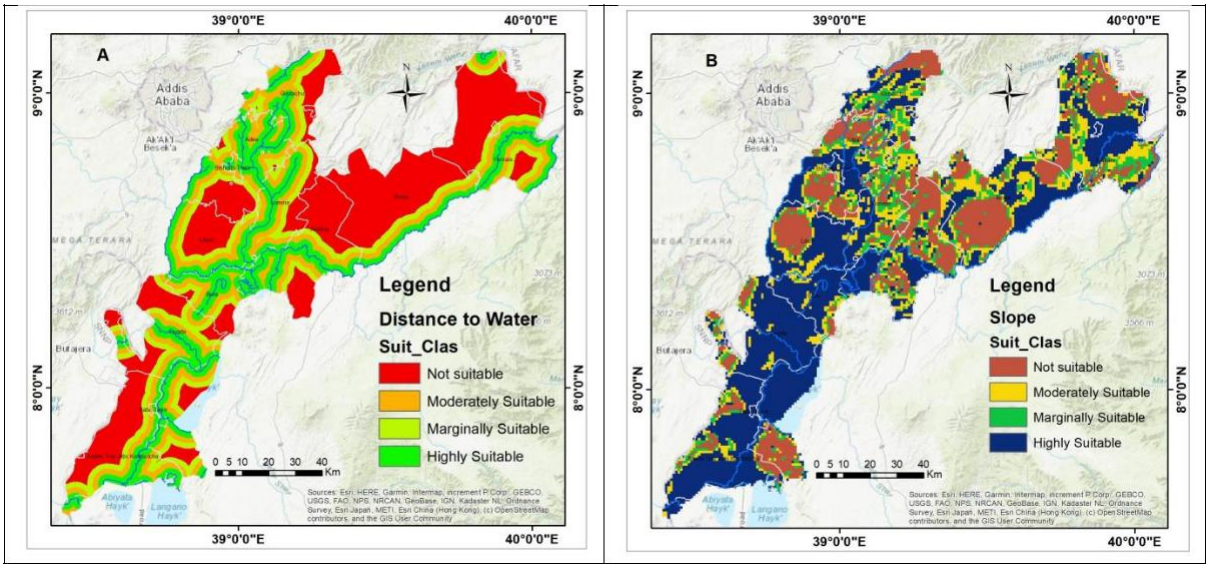

Figure 3 Factor A is distance to water body and B is slope

3.1.2.3. Elevation. The highly and moderately suitable class of elevation is covered about

124,721.5 and 602,989.23 hectare of land respectively. Furthermore, marginally suitable and unsuitable class of elevation is covered about 34,184.79 and 216,658.3 hectare of land respectively (Table 7).

3.1.2.4. **Soil Drainage**.

In the study area, highly suitable drainage conditions cover **50.28%** of the total land, offering favorable conditions for most crops. Moderately suitable soils account for **26.76%**, where drainage management may be needed. Marginally suitable soils drainage makes up 12.91%**,** and unsuitable soils cover 10.04% of the region. (Table 7).

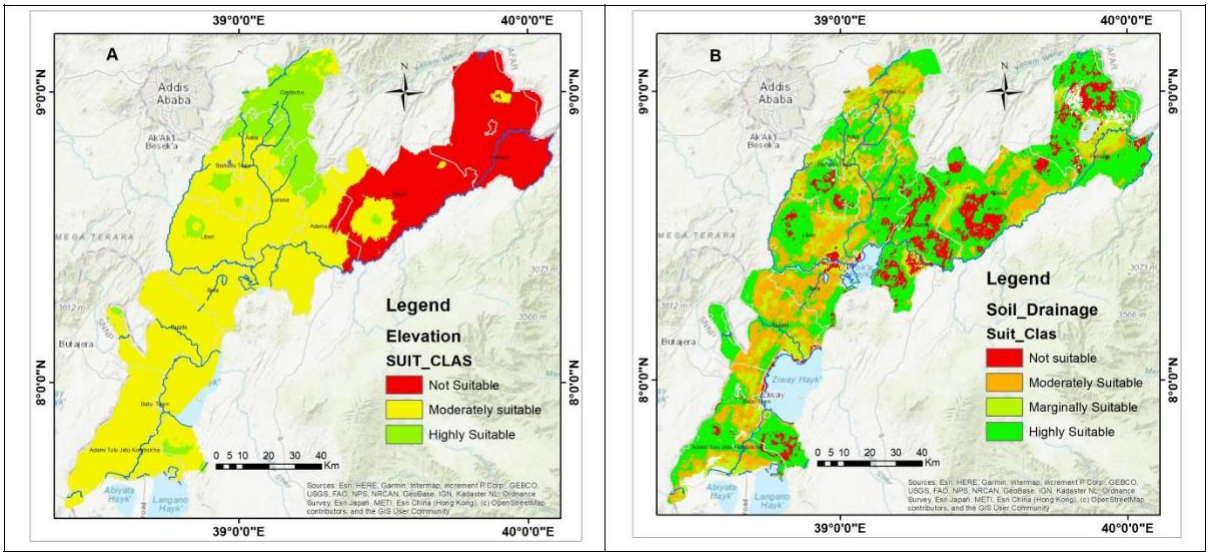

Figure 4 Factor A is elevation and factor B is soil drainage

3.1.2.5. **Temperature.**

The highly suitable, moderately suitable and unsuitable class of temperature in the study area is covered about 673,140.6, 303,841.63 and 1,102.14 hectare of land respectively (Table 7).

3.1.2.6. Soil Texture.

In the study area, highly suitable soil textures cover approximately **12.07%** of the total land, providing optimal conditions for most crops. Moderately suitable soils account for **87.92%**, where minor interventions may enhance productivity. Marginally suitable is very small present coverage which is less than 0.005% (Table 7).and there is no unsuitable soil texture in the region.

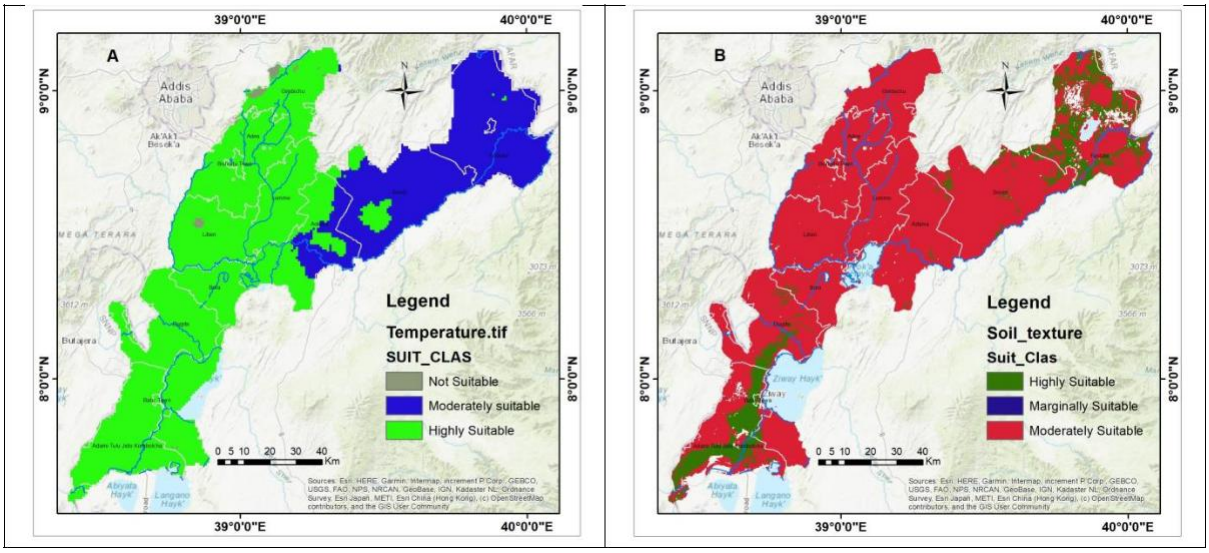

Figure 5. Factor A temperature and factor B soil texture

3.1.2.7. Soil Type.

In the study area, highly suitable soils cover approximately 24.16% of the total land area, while moderately suitable soils account for 50.11%**.** Marginally suitable soils make up 16.14%**,** and unsuitable soils cover 6.46% of the region. Additionally, soil data is unavailable for 3.12% of the study area (Table 7).

3.1.2.8. Soil PH.

In the study area, *highly suitable* soil pH covers approximately *69.28%* of the total land, indicating optimal conditions for most crops (Fig 6B). *Moderately suitable* soil pH accounts for *24.17%***,** where minor adjustments may be needed to improve fertility. The remaining *6.54%* of the area falls under the *unsuitable* category, where extreme acidity or alkalinity could severely limit agricultural productivity (Table 7).

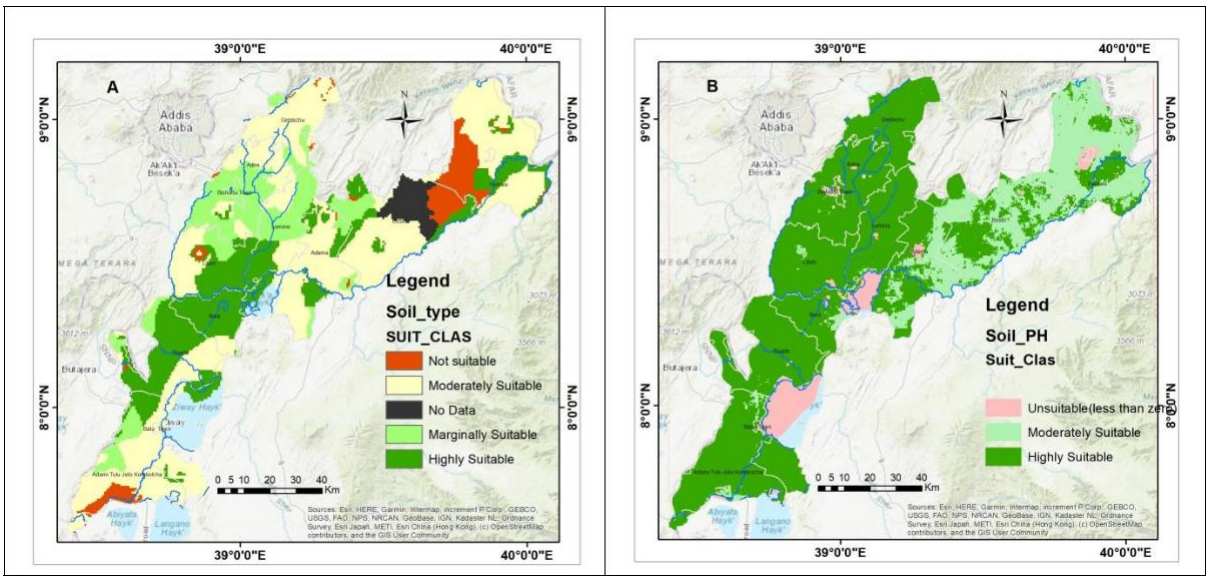

Figure 6 Factor A soil Type and Factor B is soil PH

3.1.2.9. Land use land cover.

In land suitability site analysis land use land cover is a vital parameter employed in crop production produced via irrigation. This parameter is useful to indicate which kinds of land use/cover in the area relevant for crop production. According to FAO, some of land cover suitable for agricultures is.

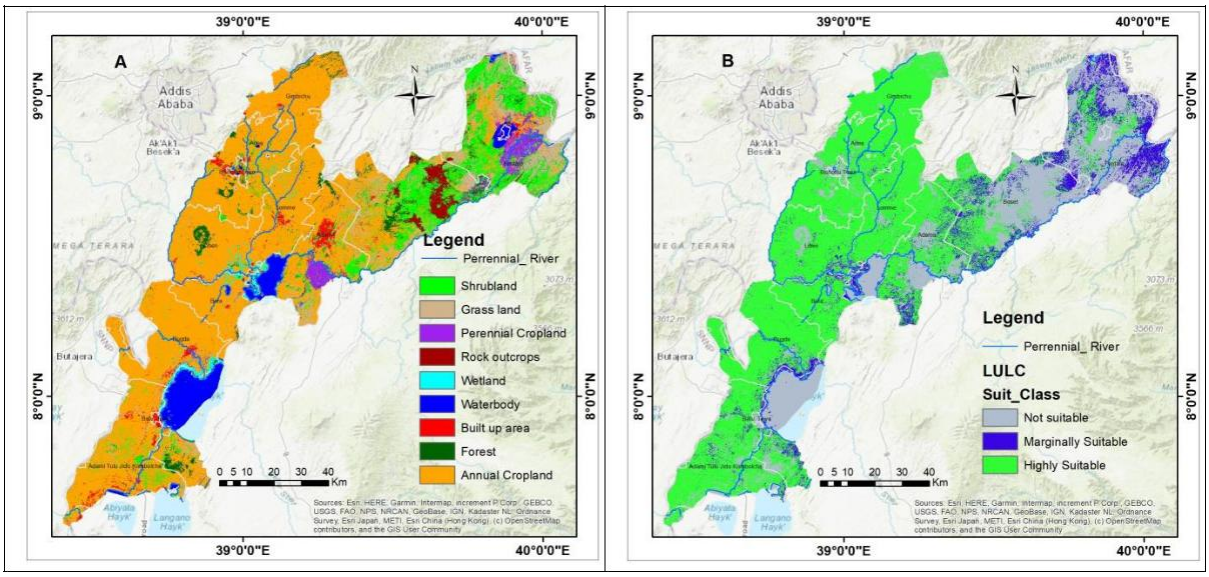

Figure 7 A is LULC classes and B is LULC suitability level

The highly suitable class of land use land cover is covered about 62.75% of the area. Furthermore, marginally suitable class of land use land cover is covered about 12.60% of the region and while, unsuitable class of land use land is covered about 24.65% (Table 7).

3.1.3. Land suitability map for surface irrigation

In order to locate the suitability of the study area for irrigated wheat cultivation, thematic maps of each reclassified factors are overlaid together. GIS permits the user to derive knowledge from different sources of spatial parameters in order to assess land suitability site (Safwan Mohammed, et.al 2020. Finally, after evaluated the consistency condition (has to accepted) of the weighted criteria, the land suitability class is generated using ―weight overlay‖ methods in ArcGIS by applying the following equation

$$S = \left[\sum_{i=1}^{n} Wi * Xi\right] \Pi cj \qquad (3)$$

(Safwan Mohammed, et.al 2020)

Where: S: Suitability index, wi: Weight of criterion i, xi: Rank of criterion i, cj: Boolean value of limited or restricted criterion, n is number of criteria or parameter.

The East Shewa Zone, located in the Oromia regional state, exhibits significant potential for irrigated wheat production through the utilization of irrigation methods and the abundant water resources available, such as lakes and perennial rivers. The area boasts a substantial extent of highly suitable land, encompassing approximately 10.22% (100056.06 hectares) of the total land area (fig 8). This favorable land presents an ideal opportunity for maximizing winter wheat yields (Tolera, A.M., et al 2023). This highly suitable land offers favorable conditions for cultivating winter wheat, indicating its potential for supporting productive

agricultural activities. The presence of water resources such as lakes and perennial rivers in the area enables the implementation of irrigation mechanisms, further enhancing the suitability for winter wheat cultivation.

Moreover, the region also comprises a considerable portion of moderately suitable land; accounting for approximately 25.81% (252767.88 hectares) (table 8). While not as optimal as the highly suitable land, this category still offers suitable conditions for cultivating winter wheat, albeit with potential limitations or restrictions that need to be addressed. The FAO's Land Suitability Classification defines the 'Moderately Suitable' (S2) class as land with limitations that reduce productivity or require increased inputs compared to 'Highly Suitable.

However, it is important to note that a significant portion of the East Shewa Zone's land is classified as marginally suitable, covering about 24.96% (244468.8 hectares) of the area (table 8). The Food and Agriculture Organization (FAO) defines "Marginally Suitable" (Class S3) land as having limitations that are severe enough to significantly reduce productivity or benefits, or to increase the inputs required for sustained use, making the expenditure only marginally justified. In the context of winter wheat cultivation, utilizing marginally suitable land may lead to reduced yields and higher production costs due to factors such as suboptimal soil conditions, inadequate drainage, or unfavorable climate. Therefore, while cultivation is possible, it may not be economically viable without significant investments in land improvement and management practices.

On the other hand, a substantial proportion of the land, approximately 3.39% (33169.32 hectares), is classified as unsuitable or temporarily not suitable for winter wheat cultivation (table 15). According to FAO 1976 temporarily not suitable (N1) can be improved for agriculture with interventions. The remaining 35.63% (348946.91 hectare) of the region is permanently not suitable (N2) (table 8). Severe limitations (e.g., rocky terrain, lakes, poor soil) make it unfit for cultivation.

Considering the favorable and moderately suitable land, as well as potential improvements in management practices, the East Shewa Zone in Oromia presents a promising opportunity for expanding winter wheat production. By harnessing the available water resources and implementing appropriate strategies, such as efficient irrigation mechanisms, this region can contribute significantly to meeting the demand for winter wheat and bolstering food security in the area. However, careful consideration must be given to the limitations associated with marginally suitable and unsuitable land to ensure sustainable and effective agricultural practices in the region.

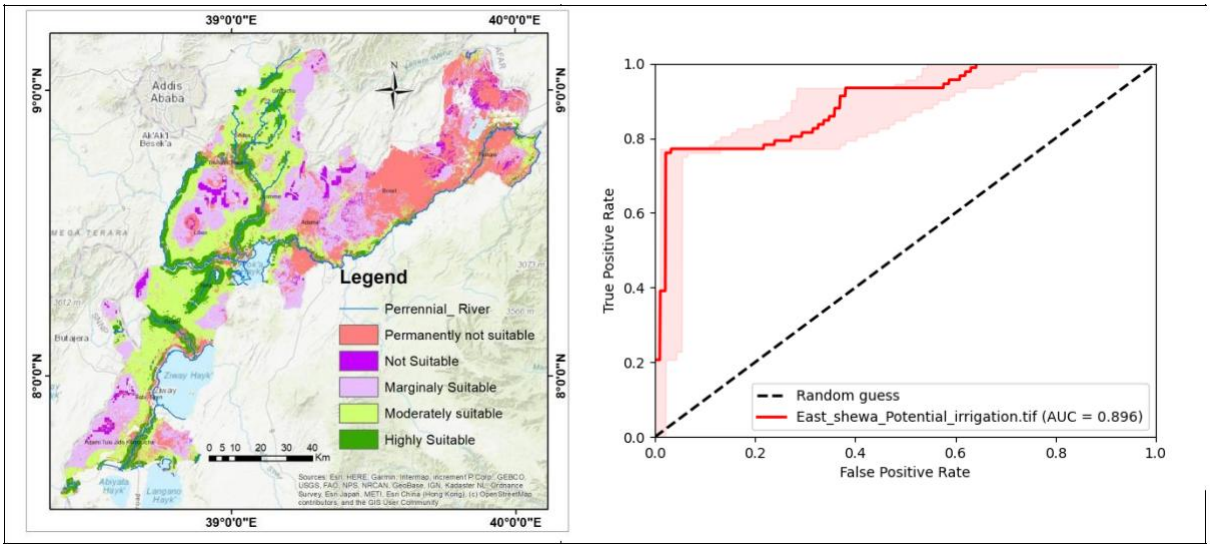

Figure 8. Irrigational Wheat Suitability Level Map and *Figure 10 validation graph of suitability level using AUC method*

Table 8 Suitability level

Suitability level	**Area (Ha)**	**%**
Permanently Not suitable	348946.91	35.63
Not Suitable	33169.32	3.39
Marginally Suitable	244468.8	24.96
Moderately Suitable	252767.88	25.81
Highly Suitable	100056.06	10.22
Total	979408.97	100.00

3.1.4. Validation of land suitability

To validate the precision rate of weight overlay model in east shewa zone, using the AUC method, the total irrigation suitability observed were 100 points used for validation of models. Therefore, 100 points were collected using the Global Position System GPS device during field visits and compared with five levels of susceptibility map. The ROC curve was created by plotting the cumulative percentage of suitability level in descending order on the X-axis against the cumulative percentage of irrigational suitablity on the Y-axis. Area under curve (AUC) value of accuracy curve was calculated and its value is 0.896. The analysis indicated that the global success rate of the suitability level map is 89.6% (Fig. 10).

AHP was solicited to derive priority scales of different suitability causative factors and sub-factors, through pairwise comparisons based on the expert judgments. From the spatial effectiveness of the generated

suitability map checked by AUC (89.6% of accuracy), it is seen that the used model yielded a good result for suitability mapping in east shewa zone zone **(**Ayele et al. (2024). Despite these encouraging results and the flexibility of the model, the main issue is that of causality related to landslides in our study area.

3.2. Discussion

The study on land suitability evaluation for surface irrigation in the Rift Valley Lakes Basin, Ethiopia, using GIS and the Analytic Hierarchy Process (AHP), provides a comprehensive framework for identifying suitable areas for irrigated wheat production. By integrating spatial analysis, expert judgment, and field observations, the research presents a robust methodology that can be applied to other regions with similar agro-ecological conditions.

This study highlights the effectiveness of combining GIS and AHP for land suitability evaluation. GIS enables the visualization and analysis of spatial relationships between various factors, while AHP provides a structured approach to weighting these factors based on expert judgment. This combination is widely recognized as a reliable method in land suitability assessment (FAO, 2021).

The reliability of the weighting process is confirmed by a consistency ratio (CR) of 7.4%, which falls below the acceptable 10% threshold (Saaty, 2008). However, the reliance on expert judgment introduces a degree of subjectivity. Differences in expert opinions can lead to cognitive biases, which may affect the accuracy of results. To address this, the study incorporates spatial analysis and field observations, an approach recommended by recent research (Zhang et al., 2023). By doing so, the study enhances objectivity and ensures the results are grounded in empirical data.

The study identifies nine key factors influencing land suitability for irrigation: slope, elevation, and distance to water, soil type, soil texture, soil pH, soil drainage, temperature, and land use/land cover (LULC). These factors align with global and regional studies on irrigation suitability (FAO, 2021; Azemeraw Wubalem, 2021).

Distance to Water is a crucial determinant, with land within 0–2 km classified as highly suitable, consistent with findings from (Worku, D et.al (2024). However, 42.94% of the study area is unsuitable due to its distance from water sources, underscoring the need for investment in irrigation infrastructure.

Slope plays a significant role, with 46.70% of the land having slopes between 0–2%, making it highly suitable for irrigation. This aligns with global recommendations that slopes below 8% are ideal for wheat cultivation. Steeper slopes require terracing or soil conservation measures, increasing production costs.

Soil Properties such as type, texture, pH, and drainage are also critical. The study finds Nitosols, Luvisols, and Phaeozems to be the most suitable, consistent with previous studies (Worqlul et al., 2015; Balew et al., 2021). However, 6.46% of the area is unsuitable due to poor soil conditions, such as Leptosols and Solonchaks. Soil amendments and management practices could improve marginally suitable soils.

Temperature in the study area falls within the optimal range (15–20°C) for wheat cultivation, covering 68.82% of the land. This finding is consistent with the optimal wheat-growing conditions reported by Porter, J. R., & Gawith, M. (1999).

Land Use/Land Cover analysis reveals that cropland makes up 62.75% of the highly suitable land, while 24.65% of the area is unsuitable due to forests, settlements, and water bodies. This highlights the need for careful land use planning to balance agricultural expansion with environmental conservation.

The study categorizes land suitability into five classes: highly suitable (10.22%), moderately suitable (25.81%), marginally suitable (24.96%), unsuitable (3.39%), and permanently not suitable (35.63%). The relatively small proportion of highly suitable land (10.22%) suggests that while the region has potential for irrigated wheat production, significant challenges remain. Expanding irrigation infrastructure, improving soil conditions, and adopting better land management practices could enhance the suitability of marginally suitable areas.

These findings align with similar studies. For example, Gebre and Melesse (2022) reported that only 12% of the Rift Valley Lakes Basin is highly suitable for surface irrigation. Studies in East Africa also highlight the limited availability of highly suitable land due to factors such as water scarcity, poor soil quality, and steep slopes (FAO, 2021; Azemeraw Wubalem, 2021).

To ensure the accuracy of the land suitability model, the study uses the Area under Curve (AUC) method, achieving an accuracy of 89.6%. This high level of precision demonstrates the effectiveness of the GIS-based AHP model in predicting land suitability. The AUC method is widely used in land suitability studies due to its ability to quantify predictive performance. The strong validation results suggest that this model could be effectively applied to other regions with similar conditions.

5 Conclusion

This study set out to identify the best areas for irrigated winter wheat production in the East Shewa Zone of Oromia, Ethiopia, using Geographic Information Systems (GIS), remote sensing, and the Analytical Hierarchy Process (AHP). By analyzing nine key factors including slope, elevation, proximity to water sources, soil properties, temperature, and land use the research provides a detailed assessment of land suitability. The results show that about 10.22% of the area is highly suitable for irrigated wheat farming, while 25.81% is moderately suitable. These regions have favorable conditions for wheat cultivation, especially with proper irrigation. However, a large portion of the land 24.96% marginally suitable and 35.63% unsuitable faces challenges such as poor drainage, unsuitable soil conditions, and extreme climate factors. Addressing these issues through targeted interventions could help unlock more agricultural potential in the region.

Beyond mapping land suitability, this study highlights how important it is to use data-driven approaches to improve agricultural productivity and food security. By pinpointing the most promising areas for wheat cultivation, the findings offer valuable guidance for policymakers, agricultural planners, and farmers. The combination of GIS, remote sensing, and AHP provides a powerful tool for making informed decisions about land use and resource management. However, the study also recognizes its limitations, such as potential data gaps, the subjectivity of expert input in the AHP process, and the absence of socio-economic factors. Future research should aim to address these gaps by considering climate change, soil degradation, and economic constraints. Expanding the scope to include other crops and regions could also enhance the relevance of this approach. Ultimately, this study underscores the East Shewa Zone's potential to boost Ethiopia's agricultural productivity through irrigated wheat farming. With strategic water management and

sustainable land use practices, the region can overcome existing challenges and contribute to national food security and economic growth.

Limitations

While this study provides valuable insights into land suitability for irrigated wheat farming, it is important to acknowledge certain limitations. The accuracy of the analysis depends on data quality, which may sometimes be outdated or incomplete, particularly regarding soil properties, temperature, and land use/land cover. Additionally, the Analytical Hierarchy Process (AHP) introduces some level of subjectivity, as expert judgment is used to assign weights to different factors. Efforts were made to minimize bias, but inherent subjectivity may still influence final classifications. The study also simplifies complex agricultural systems by focusing on a limited set of factors, leaving out socio-economic conditions, access to irrigation, and farmer practices key elements for real-world implementation. Furthermore, the analysis offers only a static snapshot based on current conditions, without accounting for evolving factors like climate change, soil degradation, or shifting land use patterns.

Beyond these methodological constraints, the study does not factor in economic and social realities, such as the cost of irrigation infrastructure or land tenure challenges, both of which can significantly influence the success of irrigated wheat farming. Additionally, potential environmental impacts such as water resource depletion, soil salinity, and biodiversity loss are not deeply explored, though they are essential for sustainable agricultural planning. Despite these limitations, this research lays a strong foundation for identifying suitable areas for irrigated wheat production. Addressing these constraints in future studies will help refine the approach, making it more accurate, practical, and sustainable for long-term agricultural development.

Feature constraints

Future research will consider additional criteria, such as socio-economic factors and localized climate models, to enhance the comprehensiveness of land suitability assessments for agricultural practices. Continued exploration into sustainable agricultural practices and innovative irrigation techniques is necessary for addressing challenges posed by climate change, aiming for long-term productivity and food security.

Acknowledgment

We would like to express our sincere gratitude to the Space Science and Geospatial Institute for their financial support, which has been crucial in facilitating this land suitability study. Our appreciation extends to the stakeholders in the east shewa Zone for their invaluable collaboration during field data collection and validation. Their insights and cooperation greatly enhanced the quality of our research.

Data Availability

Data will be made available on request.

Conflict of interest

The authors declare no conflict of interest.

Authors Contribution

Taye Teshome Terefe: Methodology, Formal analysis, Conceptualization, Mapping. Belay

Beko Legese: Investigation, Formal analysis, Conceptualization. Selam Abebaw: Methodology. Data curation. Amanuel Kumsa Bojer: Writing – review & editing, writing original draft.

Funding: Space science and geospatial institute

References

Abdel Rahman MAE, Natarajan A, Hegde R (2016) Assessment of land suitability and capability by integrating remote sensing and GIS for agriculture in Chamara janagar district, Karnataka, India. The Egyptian Journal of Remote Sensing Space Science, 19(1), 125–141. Doi: 10.1016/j. ejrs.2016.02.001.

Asseng, S., Ewert, F., Martre, P., et al. (2015). Rising temperatures reduce global wheat production. *Nature Climate Change, 5*(2), 143-147. https://doi.org/10.1038/nclimate2470

Awulachew, S. B., Yilma, A. D., Loulseged, M., Loiskandl, W., Ayana, M., & Alamirew, T. (2007). Water Resources and Irrigation Development in Ethiopia. International Water Management Institute (IWMI).

Ayele, N. A., Engda, E. M., Terefe, T. T., Leta, E., Reda, T. M., & Jothimani, M. (2024). Geospatial analysis of landslide susceptibility and safe relocation zones: Insights from recent disasters in Gofa Zone, Southern Ethiopia. Quaternary Science Advances, https://doi.org/ [DOI].

Azemeraw Wubalem, 2021. GIS-based Land Suitability Analysis for Surface Irrigation Using Analytical Hierarchy Process Method in East and West Bellessa, Northwestern Ethiopia. https://doi.org/10.21203/rs.3.rs-768423/v1

Balew, A., Nega, W., Legese, B., and Semaw, F. (2021). Suitable potential land evaluation for surface water irrigation using remote sensing and GIS–MCE in the case of rib– gumara watershed, Ethiopia. J. Indian Soc. Remote Sens. 49 (9), 2273–2290.

Benyam Tadesse, Yaregal Tilahun, Tilahun Bekele, Getachew Mekonen, 2021.Assessment of challenges of crop production and marketing in Bench-Sheko, Kaffa, Sheka, and West-Omo zones of southwest Ethiopia. https://doi.org/10.1016/j.heliyon.2021.e07319.

FAO (2006). Guidelines for Soil Description, 4th Edition. Food and Agriculture Organization of the United Nations.

FAO (2021). *Land Suitability Evaluation for Sustainable Agriculture*. Food and Agriculture Organization of the United Nations.

Firehiywet Girma, Kefelegn Getahun and Ajay Babu, 2019. Assessment of Physical Land Suitability for Surface Irrigation by using GIS and RS, In case of Loma District, South Western Ethiopia. International Journal of Current Research and Academic Review. https://doi.org/10.20546/ijcrar.2019.701.004.

Gautam Dadhicha, Parul R. Patel, Manik H. Kalubarme, 2017. Agriculture land suitability evaluation for wheat cultivation using geomatics for Patan District, India. Int. J. Agricultural Resources, Governance and Ecology, Vol. 13, No. 1, 2017.\

Girma, F., Getahun, K., & Babu, A. (2019). International Journal of Current Research and Academic Review. *Int. J. Curr. Res. Aca. Rev*, *7*(1), 32-45.

Huete, A. R. (1988). A soil-adjusted vegetation index (SAVI). Remote Sensing of Environment, 25(3), 295-309.

Jones, H. G. (2004). Irrigation scheduling: advantages and pitfalls of plant-based methods.

Journal of Experimental Botany, 55(407), 2427-2436.

McFarland, C. R., Huggins, D. R., Koenig, R. T., & Dean, A.(2015). Soil pH and implications for management: An introduction. Washington State University Extension Publication.

Mohamed A.E et.al. AbdelRahman, A. Natarajan, Rajendra Hegde, 2016. Assessment of land suitability and capability by integrating remote sensing and GIS for agriculture in Chamarajanagar district, Karnataka, India. The Egyptian Journal of Remote Sensing and Space Sciences (2016) 19, 125–141.

Ortiz, R., et al. (2008). Climate change: Can wheat beat the heat? *Agriculture, Ecosystems*

1 *Environment*, 126(1-2), 46-58.

Porter, J. R., & Gawith, M. (1999). Temperatures and the growth and development of wheat: a review. European Journal of Agronomy, 11(1), 23–36. https://doi.org/10.1016/S1161-0301(99)00047-8

Safwan Mohammed, Karam Alsafadi , Haidar Ali , Seyed Mohammad Nasir Mousavi , Samer Kiwan , Sami Hennawi , Endre Harsanyie , Quoc Bao Pham , Nguyen Thi Thuy Linh , Rawshan Ali , Duong Tran Anh & Van Nam Thai (2020): Assessment of land suitability potentials for winter wheat cultivation by using a multi criteria decision Support- Geographic information system (MCDS-GIS) approach in Al-

Yarmouk Basin (S syria), Geocarto International, DOI: 10.1080/10106049.2020.1790674

Saaty, T. L. (2008). Decision making with the analytic hierarchy process. *International Journal of Services Sciences*, *1*(1), 83-98. https://doi.org/10.1504/IJSSCI.2008.017590

Shiferaw, B., Smale, M., Braun, HJ. *et al*. Crops that feed the world 10. Past successes and future challenges to the role played by wheat in global food security. *Food Sec.* **5**, 291–317 (2013). https://doi.org/10.1007/s12571-013-0263-y

Sultan D (2013) Assessment of irrigation land suitability and development of map for the fogera catchment using GIS, South Gondar. Asian J Agric Rural Dev 3(1):7–17

Tolera, A. M., Haile, M. M., Merga, T. F., & Feyisa, G. A. (2023). Assessment of land suitability for irrigation in West Shewa Zone, Oromia, Ethiopia. *Applied Water Science*, *13*(4), 90. https://doi.org/10.1007/s13201-023-01883-9

USDIBR (United State Development of the Interior Bureau of Rec-lamation) (2003) Technical guidelines for irrigation suitability land classification. Technical Service Center Land Suitability and Water Quality Group, Denver, Colorado

Wondafrash Mulugeta1, Demeke Nigussie, Adamu Molla, Zewdie Bishaw, Chandrashekhar Biradar, 2021. Suitability analysis for scaling chickpea varieties in Ethiopia using multi-criteria evaluation and geographic information system (GIS). African Journal of Agricultural Research.

Worku, D., Boja, A., & Fantu, A. (2024). Evaluation of land suitability areas for irrigation using GIS and AHP-based tools in the case of Zenti River Catchment, Gofa district, Ethiopia. *Cogent Engineering*, *11*(1), 2345519. https://doi.org/10.1080/23311916.2024.2345519

Worqlul, A. W., Collick, A. S., Rossiter, D. G., Langan, S., and Steenhuis, T. S. (2015). Assessment of surface water irrigation potential in the Ethiopian highlands: The Lake Tana Basin. Catena 129, 76–85. doi:10.1016/j.catena.2015. 02.020

Y.G. Hagos, M.A. Mengie, T.G. Andualem, et al., Land suitability assessment for surface irrigation development at Ethiopian highlands using geospatial technology, Appl Water Sci 12 (2022) 98. https://doi.org/10.1007/s13201-022-01618-2.

Y. Chen, J. Yu, S. Khan, 2010. Spatial sensitivity analysis of multi-criteria weights in GIS-based land suitability evaluation. Environmental Modelling & Software. doi:10.1016/j.envsoft.2010.06.001

Zhang, Y., Li, F., Yang, X., Li, Z., & Wang, H. (2019). GIS and Remote Sensing Techniques for Crop Monitoring and Management. In Agricultural GIS Applications: Actionable Knowledge in Decision Making (pp. 153-183).

Theme 4

Water Supply and Sanitation

Assessing Groundwater Contamination from Landfill Leachate: Integration of Electrical Resistivity Tomography with Physiochemical Water Quality Analysis

Genzeb Yimech Melkamu*[1], Abhay Raj[2], Basant Yadav[3]

[1]Department of Water Resources Development and Management, Indian Institute of Technology, Roorkee-247667, India

*Corresponding author: genzebyimech2006@gmail.com

Abstract

Groundwater contamination occurs when pollutants migrate vertically or horizontally due to geogenic and anthropogenic factors. Solid waste disposal is a major source of groundwater pollution, with landfill leachate forming as rainwater infiltrates dumpsites and percolates through soil layers. Conducting non-invasive, cost-effective investigations using Electrical Resistivity Tomography helps map leachate plumes and assess groundwater contamination. This study analyses groundwater quality near a landfill using Electrical Resistivity Tomography. Electrical resistivity surveys were conducted from November 2023 to March 2024 in different directions to locate contaminant plumes and understand transport behaviours. Groundwater samples from nearby boreholes were collected and analysed to determine their chemical composition. The 2Directional ERT results revealed that leachate had migrated both spatially and vertically, contaminating the shallow aquifer. Low resistivity values (<10Ωm) indicated significant leachate infiltration. The presence of elevated concentrations of EC, TDS, Cd, Pb, Mn, and Al in groundwater samples confirmed the Electrical Resistivity Tomography findings. These analyses highlight the impact of landfill leachate on groundwater contamination. A strong correlation exists between geophysical investigations and hydro chemical analysis. The findings demonstrate that the landfill significantly affects the groundwater quality, posing risks to nearby water sources. The study provides insights into the extent of leachate infiltration and its consequences for groundwater sustainability.

Keywords: Electrical Resistivity Tomography (ERT); Landfill, Leachate; Groundwater Quality; Pseudo-section model

1. Introduction

Municipal solid waste (MSW) is a growing global challenge that negatively affects the environment, water quality, economic stability, and social equity. The generation of MSW is projected to reach 2.2 billion metric tons by 2025, driven by increasing urbanization and economic growth (Mosuro et al., 2017). In many developing countries, landfilling remains the primary waste disposal method. However, landfills pose environmental risks, particularly through leachate—a liquid formed when rainwater percolates through waste, carrying hazardous substances like organic matter, heavy metals, and chlorides (Bashir et al., 2009). Leachate infiltration into groundwater aquifers is a significant concern, contaminating water resources and affecting nearby communities (Danthurebandara et al., 2013). Studies show that groundwater contamination from leachate is most severe within 200 meters of a landfill, with impacts extending up to 1000 meters (Han et al., 2016). Monitoring leachate movement and spatial distribution is critical for mitigating its effects. Electrical Resistivity Tomography (ERT) has proven to be a cost-effective, non-invasive tool for mapping subsurface contamination. ERT uses the electrical conductivity of leachate to create 2D and 3D profiles, identifying areas affected by contamination (Feng et al., 2017).

Several studies have demonstrated the efficacy of ERT in landfill monitoring. For example, Meads et al. (2003) and Enikanselu (2008) used ERT to detect leachate-induced conductivity changes near landfills in Canada and Nigeria. Maurya et al. (2017) and Omolayo and Tope (2014) further confirmed its ability to identify polluted zones, correlating geophysical data with chemical analysis. Despite its proven effectiveness, there is a lack of studies integrating ERT with groundwater quality analysis, particularly near the Saliyar landfill. This study aims to fill this gap by combining ERT with laboratory analysis of groundwater samples to assess the extent of leachate contamination. It highlights the need for validation through well data, as ERT results can be influenced by factors like subsurface porosity and groundwater chemistry (Vega et al., 2003).

2. Materials and Methods

2.1. Description of study area

The study area is situated around the waste disposal site in Saliyar village, Haridwar district, Uttarakhand Pradesh, India and located between 29°53'N to 29°54'N and 77°51'E to 77°52'E. Saliyar landfill has been the only single and active open site for MSW disposal in Roorkee City since 1988. The region features a moderate subtropical to humid climate characterized by three distinct seasons: summer, followed by the rainy season, and then winter. The temperature typically increases in March, reaching a high of 29.10°C, and peaks in May at 44°C. The Saliyar landfills are roughly 7 km from the center of the city and get 3224 MT of solid waste monthly. The city produces roughly 104 Metric tons (MT) of municipal trash daily. The location of the study area with ERT profiles orientations is shown in Figure 1. The study area lies in the Himalayan foothills' Tarai zone near Roorkee, India, featuring Quaternary alluvial deposits of clay, sand, pebbles, and gravel. The topsoil (3–6 m thick) is sandy loam, underlain by an unconfined aquifer (3–27 m) and a deeper aquifer (~14 m), separated by a clay-gravel layer. The Solani River flows ~500 m southeast of the waste site, with groundwater movement following the gentle slope parallel to the river. This hydrogeological setting influences contaminant transport from the landfill towards the river (Devi et al., 2017). The lithology map of the study area is described in Figure 2.

2.2. Methods

A geophysical (ERT) method and hydro chemical analysis of water samples from wells and boreholes were used for the investigation of possible contamination of groundwater because of leachate infiltration from the landfill.

2.2.1. Electric resistivity tomography (ERT)

ER measures how strongly a material opposes the flow of electric current (Andrade, 2011). The purpose of electrical surveys is to determine the subsurface resistivity distribution by making measurements on the ground surface (Loke, 1997).

2.2.2. Data acquisition, processing, and inversion

The ERT analysis began with data collection using a Syscal Junior/R1 Plus Resistivity Meter and Wenner–Schlumberger configuration (Aydi et al., 2020), with electrode spacings from 2.4m to 10m for enhanced

sensitivity. RES2DINV software was used for modeling and interpretation (Loke, 2011). Processing included filtering unreliable data, topographic correction, and applying a smoothness-constrained least squares inversion (Oyeyemi et al., 2018; Yan et al., 2022). The subsurface was divided into prisms, and a finite element algorithm minimized differences between observed and calculated resistivity values (Ayolabi et al., 2015). The ERT lines were strategically laid out to cover the landfill and surrounding areas. The locations, length, orientation of the profile, spacing and number of electrodes were presented in Table 1.

Table 1. summary of obtained data from the ERT survey of ten profiles

Profiles	**Start point coordinates**	**Final point Coordinates**	**Number of Electrode**	**Electrode Spacing (m)**	**Length (m)**	**Orientation**
Profile-1	29° 54' 14" N	29° 53' 56" N	48	7	329	North-West
	77° 51' 54" E	77° 51' 13" E				
Profile-2	29° 53' 56" N	29° 53' 56" N	20	5	95	ES-NW
	77° 51' 14" E	77° 51' 13" E				
Profile-3	29° 54' 6" N	29° 53' 45" N	48	5	235	South-North
	77° 51' 57" E	77° 51' 43" E				
Profile-4	29° 54' 4" N	29° 54' 10" N	48	5	235	South-North
	77° 51' 49" E	77° 51' 55" E				
Profile-5	29° 54' 2" N	29° 54' 8" N	48	5	235	South-North
	77° 51' 52" E	77° 51' 57" E				
Profile-6	29° 54' 8" N	29° 54' 11" N	34	3	99	SW-EN
	77° 51' 53" E	77° 51' 54" E				
Profile-7	29° 54' 12" N	29° 54' 00" N	24	2.4	55.2	West -East
	77° 51' 54" E	77° 51' 16" E				
Profile-8	29° 54' 11" N	29° 54' 17" N	24	10	230	North-West
	77° 51' 55" E	77° 52' 2" E				
Profile-9	29° 54' 18" N	29° 54' 18" N	24	10	230	SW-EN
	77° 47' 18" E	77° 52' 5" E				
Profile-10	29° 54' 10" N	29° 54' 11" N	24	10	230	SW-EN
	77° 52' 6" E	77° 52' 3" E				

These results are relevant in imaging the causes of subsoil and groundwater contamination. They are discussed in terms of the inverse model resistivity concerning the corresponding depths of occurrence. A total of Ten (10) ERT profiles were taken in different directions of the landfill site as shown in Figure 1.

2.2.3. Physiochemical water quality analysis

Nine groundwater samples (5 samples from handpump wells and 4 samples from boreholes) were collected for chemical analysis within a 500m radius around the landfill area and proximally located near to the ERT lines as shown in Figure 3. The major elements like heavy metals, cations and anions including physical parameters were conducted in Soil and Water Quality laboratory of the Department of Water Resources

Development and Management (WRDM) and Institute Instrumentation Centre (IIC) of the Indian Institute of Technology, Roorkee.

2.2.4. Water quality index (WQI)

Suitability of groundwater can be assessed by using water quality index (Batabyal & Chakraborty, 2015; Li et al., 2010; Ramakrishnaiah et al., 2009; Saeedi et al., 2010). WQI were calculated by using standard recommended by Bureau of Indian Standard (BIS), 2012 for drinking purpose. To calculate the WQI, the weights for the physical and chemical parameters were determined with respect to the relative importance of the overall quality of the water for drinking water purposes (Balamurugan et al., 2020). The following steps are involved in WQI computing:

1. The maximum and minimum weight assigned is for each parameter from one to four based on the impact of the parameters on health.

2. The relative weights (Wi) are computed by the following equation:

$$W_i = w_i / \sum W_i \quad (1)$$

Where, W_i = Relative weight, w_i = Weight of each parameter, n= number of parameters.

3. Quality rating

$$q_i = (C_i / S_i) * 100 \quad (2)$$

Where, q_i=Quality rating for i_{th} parameter, C_i= Concentration of i_{th} parameter in groundwater sample, and S_i =desirable limit set by BIS.

4. Sub-index

$$SI_i = W_i * q_i \quad (3)$$

Where SI_i =the sub index, W_i = Relative weight, and q_i=Quality rating

5. Water quality index

$$WQI = \sum_{n=1}^{n} SI_i \quad (4)$$

According to WQI, groundwater is classified into five ranks, “Excellent water” to “Extremely poor water” (Li et al., 2010). The classification standards are listed in Table 2.

Table 2. classification standards of groundwater quality according to WQI

WQI	Rank	Water Quality
<50	1	Excellent water quality
50-100	2	Good water quality
100-150	3	Medium or average water quality
150-200	4	Poor water quality

>200	5	Extremely poor water quality

3. Results and Discussions

3.1. Physiochemical water quality analysis

Water quality parameters are measurable attributes that define the physical and chemical characteristics of water. These variables encompass physical parameters and chemical parameters, including heavy metals. The descriptive statistics of physicochemical parameters of the groundwater samples for this study like range, mean, standard deviation and the acceptable limit of BIS for drinking purpose of the groundwater quality samples were presented in Table 3.

Table 3: descriptive statistics of physicochemical parameters of the groundwater samples

Water Quality Parameters	**Range (ppm)**	**Mean**	**SD**	**WHO (2008)**	**BIS-2012 (Acceptable Limit)**	**Samples Exceeding WHO (2012)**	**Samples Exceeding BIS (2012)**
pH	6.98-7.365	7.14	0.15	6.5-8.5	6.5-8.5	0	0
TDS (ppm)	214.5-552	288.33	108.49	500.00	500.00	1	1
EC (µS/cm)	442.95-762.6	518.59	101.70	1000.00	400-1000	3	3
Fl (ppm)	0.022-0.32	0.21	0.09	0.50	1.00	0	0
Cl (ppm)	0.08-38.31	6.76	12.11	250.00	250.00	0	0
Br (ppm)	0.29-5.02	2.87	1.24	0.01	NA	9	0
Sulphate(ppm)	0.19-37.39	5.92	11.88	250.00	200.00	0	0
Nitrate (ppm)	0-11.58	1.37	3.83	3.00	45.00	0	0
Zn (ppm)	0.01-0.21	0.10	0.08	-	5.00	NA	0
Cd (ppm)	0.03-0.05	0.04	0.01	0.00	0.00	9	9
Ag (ppm)	0-0.1	0.01	0.00	-	0.10	NA	0
Cu (ppm)	0-0.01	0.01	0.00	2.00	0.05	0	3
Ni (ppm)	0.01-0.06	0.02	0.01	0.07	0.02	0	0
Fe (ppm)	0.07-0.12	0.08	0.02	-	0.30	NA	0
K (ppm)	2.12-6.09	2.88	1.24	-	-	NA	NA
Mg (ppm)	10.26-20.64	14.14	3.62	-	30.00	NA	0
Al (ppm)	0.05-0.09	0.06	0.01	-	0.03	NA	9

This study employed Electrical Resistivity Tomography (ERT) and hydro-chemical analysis to assess landfill leachate infiltration and its impact on groundwater quality near the Saliyar landfill, Roorkee, India. The key findings reveal significant contamination due to leachate migration, with low resistivity zones (<12Ωm) in ERT profiles (3–8) confirming leachate percolation into the aquifer. The plume appears to migrate toward the Solani River but does not reach the riverbank, as evidenced by higher resistivity values (13.6–17.4Ωm) in near-river profiles (9–10), suggesting dilution by river water.

Hydro-chemical analysis of groundwater samples indicated elevated levels of EC (>1000 µS/cm), TDS (>500 mg/L), and toxic metals (Cd, Pb, Mn, Al), exceeding permissible limits. The Water Quality Index (WQI) classified the groundwater as "average" to "poor," rendering it unsafe for drinking. Furthermore, the reliance on contaminated groundwater for sugarcane irrigation poses serious health and environmental risks, demanding immediate regulatory action.

To mitigate further contamination, proactive landfill management strategies, including leachate collection systems, impermeable liners, and continuous groundwater monitoring, must be implemented. This study highlights the urgent need for sustainable waste disposal practices and stricter enforcement of environmental policies to safeguard groundwater resources and public health in the region.

Several wells exceeded safe drinking water limits for heavy metals. Cadmium levels (0.04–0.05 ppm) in Wells 4,5,7,8,9 surpassed BIS/WHO standards (0.003 ppm). Lead concentrations (0.01–0.035 ppm) in Wells 1,2,5,7,8,9 exceeded the 0.01 ppm limit. Manganese (0.02–0.34 ppm) in Wells 1,5,8,9 also breached BIS guidelines (0.01 ppm). Figure 4(c) highlights these violations, indicating significant groundwater contamination, posing health risks. Urgent remediation is needed to ensure safe drinking water.

3.2. Classification of groundwater by water quality index (WQI)

WQI has been used for the classification of groundwater samples. WQI indicates degradation of water quality, and it also helps in the managing water resources for their varied usages. Standard for drinking purposes recommended by Bureau of Indian Standards (BIS) IS 10500:2012 has been used for calculation of WQI. Weights have assigned based on the significance of parameters in water quality assessment (Li et al., 2010). Overall weight has been assigned from 1 to 4 depending upon the impact of the parameter. The parameter having the higher impact has been assigned as 4 and the least impact assigned as 1. Relative weight has been calculated by assigning individual weights to the parameters and overall water quality has been computed for each parameter. On the basis of overall water quality index values of each sample, groundwater is categorized into five categories. The Assigned and relative weight for WQI computation is presented below in Table 4.

Out of 9 groundwater samples, 4 samples (44.4%) falling in the medium or average water quality, and 5 samples (55.5%) in poor water quality category. The groundwater samples of Well-5, Well-7, Well-8, and Well-9 are lies in the premise of landfill site and in the radius of <1 km from the landfill site. The calculated WQI results of the functional well are presented in Table 5.

Table 4. assigned and relative weight for WQI computation with BIS standards

Water Quality Parameters	**BIS (2012) IS0500:2012 (Ci)**	**Weight (wi)**	**Relative Weight (Wi)**
pH	6.5-8.5	1	0.04
TDS (ppm)	500	1	0.04
EC (µS/cm)	400-1000	2	0.08
Cl (ppm)	250	1	0.04
Sulphate(ppm)	250	1	0.04
Nitrate (ppm)	3	3	0.12
Zn (ppm)	5	1	0.04
Cd (ppm)	0.003	3	0.12
Cu (ppm)	0.05	2	0.08
Ni (ppm)	0.02	3	0.12
Fe (ppm)	0.3	4	0.16
Al (ppm)	0.03	3	0.12
		∑= 25	

Table 5. Computed WQI of the functional wells

Wells	Well-1	Well-2	Well-3	Well-4	Well-5	Well-6	Well-7	Well-8	Well-9
WQI	125.31	119.19	117.95	160.50	155.67	114.26	151.46	164.07	175.78

3.3. Electrical resistivity tomography results

The 2D ERT imaging of the subsurface which measures lateral and vertical variation with depth gave useful information on the subsurface related to the mapping the plume. The following ERT profiles represent the cross-sectional (vertical) surveys conducted around the landfill area. The results and discussions are organized according to the distance from the waste disposal site.

3.4. Longitudinal profiles

Profile-3 was conducted in the South-North direction of a landfill site, spanning a depth of 53m vertically from the ground surface and utilizing the Wenner-Schlumberger electrode configuration. The resistivity values lower than 10Ωm were observed, indicating the presence of leachate flow according to the same studies conducted by Moretto (2017) and Zaini (2022) in Brazil and Malaysia respectively. This area is downstream of the old landfill site, making the presence of leachate flow expected, as shown in Figure 5(a). Additionally, the leachate concentration increased towards the north of the profile. A study conducted by

Sudha et al. (2010) suggests the presence of saturated sandy loam, medium sand, and clay with pebbles throughout the traverse according to the lithology data of the area.

The inverse modelling of Profile-5, oriented south-north and extending 50m below the surface, provided insights into the subsurface near the landfill. Isolated high resistivity zones, likely linked to boulders or dry/unsaturated areas, were observed (Devi et al., 2017). A low resistivity zone, below 42Ωm, was consistent throughout the traverse, indicating leachate infiltration from the nearby landfill. Subsurface analysis revealed sandy loam composition, likely contributing to leachate migration into surrounding strata due to the landfill's proximity. Figure 5(b) presented the analysed pseudo-section model of Profile-5.

Profile-4, surveyed 30m downstream of the landfill, extended 50m below the surface in a south-north direction. The electrical resistivity values ranged from 1Ωm to 170Ωm, with low resistivity areas (less than 10Ωm) detected within 1.25m from the surface, indicating potential leachate infiltration threatening groundwater quality. The southern part of the traverse, close to the landfill, shows susceptibility to contamination, while the northern segment displays higher resistivity values (115Ωm to 170Ωm). Low resistivity zones, 140m to 200m from the site, at 6m depth, further confirm leachate migration through protective geological layers, supported by studies by Rao (2014) and Adhikary (2015). Figure 5(c) presented the pseudo-section model of Profile-5.

This inverse model traverse of Profile-1 was carried out to a depth of 70m from the ground surface, and the recorded resistivity values ranged from 2Ωm to 46Ωm in the direction from the North-West. The initial layer, extending from a depth of 1.75m to 14.1m, exhibited low resistivity anomaly values within the resistivity range of 2Ωm to 10Ωm horizontally at a total distance of 329m. The low resistivity suggests the infiltration of leachate near this profile section. The second layer has a resistivity value of 14Ωm to 26Ωm from a depth of 14m-20m. The lithology of the area at a given depth indicates the presence of medium sand (Sudha et al., 2010) in the vicinity. The groundwater table has been indicated at a depth of 17m with a resistivity value near 20Ωm. The depth to the groundwater level in most of the Roorkee area lies between 3.20m to 19.39m bgl. At certain places, the depth to the water table observed in tube wells rests between 11m and 18m bgl (District, 2022.). The interpreted mode of Profile-1presented in Figure 5(d).

Profile-8's ERT survey (48m depth, South-North orientation) revealed resistivity values of 11-39Ωm, with a distinct low-resistivity zone (11-13Ωm) at 5-10m depth, indicating leachate infiltration in sandy loam soil. A particularly conductive spot (<13Ωm) at 103m horizontal distance (2.5m depth) confirms leachate migration from the landfill (270m away), consistent with findings conducted by Ogilvy (2002) and Zaini (2022) The pseudo-section shows reduced leachate flow toward the Solani River. Groundwater levels in Roorkee range 3.20-19.39m bgl, with tube wells at 11-18m bgl (District, 2022) , suggesting potential aquifer contamination risks. The water table near the riverbank was raised to the surface at horizontal distance of 200m as shown in Figure 5(e).

3.5. Cross-sectional profiles

The following ERT profiles represent the lateral surveys conducted around the landfill area. The results and discussions are organized according to the distance from the waste disposal site.

Profile-2, located 10 to 20m southwest of the landfill site, extended 95m in length and reached a depth of 20m. Resistivity values ranged from 13Ωm to 39Ωm, with low resistivity consistently observed below 3m

depth. A leachate plume, showing resistivity values below 15Ωm, was detected at depths of 5m to 7.5m, and lateral distances of 50m to 80m. This suggests leachate migration within the profile (Chu et al., 2017; Giang et al., 2013; Moretto et al., 2017). Below the leachate zone, a contaminated groundwater region extended from 10m to 15m depth, showing a low resistivity anomaly. Figure 6(a) explains the pseudo-section resistivity model of Profile-2. Because the amount of resistivity values is directly correlated with the concentration of dissolved substances, zones with higher leachate accumulation also tend to have lower resistivity values as the higher concentration of ions and organic acids (Helene et al., 2020).

Profile-6, located 200m downstream from the Saliyar landfill, reached a depth of 22.1m. Resistivity values ranged from 7.4Ωm to 51.7Ωm, with a distinct pattern observed from 0.75m to 13m depth, across a 96m profile length. Small leachate plumes were detected between 69m to 96m, at depths of 0.75m to 4m. Low resistivity values near 8Ωm were observed 115m from the landfill. The subsurface lithology, as documented by Sudha (2010), consisting mainly of sandy loam and clayey soil, facilitates leachate percolation. These findings align with similar studies, confirming the potential contamination of groundwater by landfill leachate conducted by Camarero (2019) in Brazil. Figure 6(b) explains the pseudo-section resistivity model of Profile-6.

Profile-7, located 250m from the landfill, was investigated to a depth of 11.5m over a horizontal span of 55.2m. Resistivity values ranged from 9Ωm to 15Ωm, with areas showing values under 10Ωm, indicating potential landfill leachate infiltration. Leachate plumes were identified at depths of 0.6m to 1.8m, between 24m to 30m and 32m to 55.2m, and at depths of 4.45m to 9.4m from 10.8m to 18m as studied by Moretto (2017) and Olasunkanmi (2023). These low resistivity zones point to subsurface contamination from the landfill (Donohue et al., 2015).. The subsurface lithology, primarily sandy loam and clayey soil, supports leachate percolation. The interpreted model of Profile-7 presents in Figure 6(c).

Profile-9 was conducted 520m far away from the landfill site on the bank of the Solani River in the direction of SW to EW. The depth of the investigation reached 48m below the ground surface covering horizontal distance of 230m This profile has a resistivity of range 20Ωm to140Ωm. In the SW, EN and central segment of the profile, resistivity values ranging from 20Ωm to 30Ωm were distinguished at depths traversing 5m to 48m. These findings suggest the influence of saturation of water from the Solani River and the vegetative cover surrounding the profile area. It is understood in clear from inverse model of Profile-9 the infiltration of the leachate was ended up before reaching the bank of the river and can be seen from the previous Profile-8. Due to the distance far away from the landfill site there was no intrusion of leachate from the nearby landfill. Figure 6(d) describe the analysed pseudo-section model of ERT-9.

Profile-10's inverse modeling, conducted along a 230m SW-NE traverse in the Solani riverbed (depth: 52.3m), revealed subsurface resistivity ranging from 17.4Ωm to 158Ωm. Low values (17.4–158Ωm) indicate water-saturated zones, while high readings suggest boulders/unsaturated layers, typical of Himalayan foothills (Devi, 2017). The study, timed during the dry season for optimal data, aimed to assess groundwater dynamics and leachate spread near the landfill. Results highlight the riverbed's geological heterogeneity, aiding in understanding contaminant pathways and hydrological patterns. This profile is used as a reference for comparing with others to determine the extent of leachate infiltration into the subsurface, particularly at a considerable distance from the landfill site as shown in Figure 6(e).

3.6. Validation of ERT model and physiochemical analysis

To validate and check the resistivity models generated from ERT data, EC values of ground water samples were compared with the resistivity model for the test. Three groundwater samples namely Well-1, Well-5, and Well-8 were shown higher EC values among the other wells. Hence the EC values had been compared with the resistivity values of the pseudo section model of ERT profiles. According to the study conducted by Khaki et al. (2016) and Ogungbe et al. (2012), the electrical resistivity of contaminated aquifer with dissolved solids is less 20Ωm. A critical look at the resistivity-depth of pseudo-section model from Profile-3, Profile-4, Profile-5, Profile-6, Profile-7, and Profile-8 shows possible infiltration of leachate containing high concentration of dissolved solids to the subsurface environment. Generally, the results reflect high level of impact of leachate from the decomposed materials from the dumpsite, with resistivity value less than 10Ωm prevalent on the entire traverses of the ERT profiles. The presented values in Table 6 reveal that the groundwater samples exhibited significant EC values, aligning with the interpreted pseudo-section models of the ERT profiles.

Table 6. Electrical Conductivity (EC) values of selected groundwater sample around the landfill

Wells	**Well type**	**Electrical Conductivity (EC) in µS/cm**	**Electrical Conductivity (EC) in S/m**	**Electrical Resistivity (1/EC) in Ωm**
Well-1	Handpump	525.8	0.053	19.02
Well-5	Borewell	588.65	0.059	16.99
Well-8	Handpump	762.6	0.076	13.11

Notably, Well-1, Well-5, and Well-8 displayed EC measurements of 0.053 S/m, 0.059 S/m, and 0.076 S/m, respectively. Resistivity is the reciprocal of conductivity. Hence upon inversing the EC, obtain resistivity values of 19.02Ωm, 16.99Ωm, and 13.11Ωm, respectively. These notably low resistivity values serve as clear indicators of contamination and leachate infiltration into the aquifer originating from the landfill vicinity that validate the results of the ERT values nearby the area.

4. Conclusion

This study showcases the application of Electrical Resistivity Tomography (ERT) and hydro-chemical analysis to assess the extent of landfill leachate infiltration and its impact on groundwater quality near the Saliyar landfill, Roorkee, India. ERT profiles from Profiles 3 to 8 revealed low resistivity values (<12Ωm), indicating significant leachate infiltration. The leachate plume appears to flow towards the Solani River due to slope differences, but ERT-8 results suggest that it stops before reaching the riverbank. Profiles 9 and 10, located near the river, showed higher resistivity values (13.6Ωm and 17.4Ωm, respectively), signifying the saturation of subsurface water with river water. Hydro-chemical analysis of water samples from surrounding wells revealed elevated concentrations of parameters such as Electrical Conductivity (EC: >1000µS/cm), Total Dissolved Solids (TDS: >500mg/L), Cadmium (Cd: >0.003mg/L), Lead (Pb: >0.01mg/L), Manganese (Mn: >0.1mg/L), and Aluminum (Al: >0.03mg/L). The Water Quality Index (WQI) of the wells indicated "average" to "poor" drinking water quality. These results underscore the contamination of the aquifer by landfill leachate. Additionally, local sugarcane cultivation, which relies on groundwater for irrigation, is at risk of exposure to contaminated water, posing a significant health threat. Immediate regulatory measures and proactive management are essential to mitigate the environmental and health risks associated with landfill leachate.

Acknowledgments

The authors would like to acknowledge the Department of Water Resources Development and Management, Indian Institute of Technology, Roorkee, for providing support and facilities to conduct this study.

Conflict of Interest

The authors declare that there is no conflict of interest regarding the publication of this research.

References

Palmer, M. A., Bernhardt, E. S., Allan, J. D., Lake, P. S., Alexander, G., Brooks, S., ... & Sudduth, E. (2005). Standards for ecologically successful river restoration. Journal of applied ecology, 42(2), 208-217.

Ogundiran, O. O., & Afolabi, T. A. (2008). Assessment of the physicochemical parameters and heavy metals toxicity of leachates from municipal solid waste open dumpsite. International Journal of Environmental Science & Technology, 5, 243-250.

Kearey, P., Brooks, M., & Hill, I. (2002). An Introduction to Geophysical Prospecting 3rd edn, 262.

Meads, L. N., Bentley, L. R., & Mendoza, C. A. (2003). Application of electrical resistivity imaging to the development of a geologic model for a proposed Edmonton landfill site. Canadian Geotechnical Journal, 40(3), 551-558.

Omolayo, D., & Tope, F. J. (2014). 2D electrical imaging surveys for leachate plume migration at an old dump site in Ibadan south western Nigeria: A case study. International Journal of Geophysics, 2014.

Enikanselu, P. A. (2008). Detection and monitoring of dumpsite-induced groundwater contamination using electrical resistivity method. Pacific Journal of Science and Technology, 9(1), 254-262.

Maurya, P. K., Rønde, V. K., Fiandaca, G., Balbarini, N., Auken, E., Bjerg, P. L., & Christiansen, A. V. (2017). Detailed landfill leachate plume mapping using 2D and 3D electrical resistivity tomography-with correlation to ionic strength measured in screens. Journal of Applied Geophysics, 138, 1-8.

Abbaspour, K., Matta, V., Huggenberger, P., & Johnson, C. A. (2000). A contaminated site investigation: Comparison of information gained from geophysical measurements and hydrogeological modeling. *Journal of Contaminant Hydrology*, *40*(4), 365–380. https://doi.org/10.1016/S0169-7722(99)00055-8

Adhikary, P. P., Chandrasekharan, H., Dubey, S. K., Trivedi, S. M., & Dash, C. J. (2015). Electrical resistivity tomography for assessment of groundwater salinity in west Delhi, India. *Arabian Journal of Geosciences*, *8*(5), 2687–2698. https://doi.org/10.1007/s12517-014-1406-y

Andrade, R. (2011). Intervention of Electrical Resistance Tomography (ERT) in Resolving Hydrological Problems of a Semi Arid Granite Terrain of Southern India. In *JOURNAL GEOLOGICAL SOCIETY OF INDIA* (Vol. 78).

Aydi, A., Mhimdi, A., Hamdi, I., Touaylia, S., & Sdiri, A. (2020). Application of electrical resistivity tomography and hydro-chemical analysis for an integrated environmental assessment. *Environmental Nanotechnology, Monitoring and Management*, *14*(July), 100351. https://doi.org/10.1016/j.enmm.2020.100351

Balamurugan, P., Kumar, P. S., & Shankar, K. (2020). Dataset on the suitability of groundwater for drinking and irrigation purposes in the Sarabanga River region, Tamil Nadu, India. *Data in Brief*, *29*, 105255. https://doi.org/10.1016/j.dib.2020.105255

Bashir, M. J. K., Isa, M. H., Kutty, S. R. M., Awang, Z. Bin, Aziz, H. A., Mohajeri, S., & Farooqi, I. H. (2009). Landfill leachate treatment by electrochemical oxidation. *Waste Management*, *29*(9), 2534–2541. https://doi.org/10.1016/j.wasman.2009.05.004

Batabyal, A. K., & Chakraborty, S. (2015). Hydrogeochemistry and Water Quality Index in the Assessment of Groundwater Quality for Drinking Uses. *Water Environment Research*, *87*(7), 607–617. https://doi.org/10.2175/106143015x14212658613956

Brahmi, S., Baali, F., Hadji, R., Brahmi, S., Hamad, A., Rahal, O., Zerrouki, H., Saadali, B., & Hamed, Y. (n.d.). *Assessment of groundwater and soil pollution by leachate using electrical resistivity and induced polarization imaging survey, case of Tebessa municipal landfill, NE Algeria*. https://doi.org/10.1007/s12517-021-06571-z/Published

Camarero, P. L., Moreira, C. A., & Pereira, H. G. (2019). Analysis of the Physical Integrity of Earth Dams from Electrical Resistivity Tomography (ERT) in Brazil. *Pure and Applied Geophysics*, *176*(12), 5363–5375. https://doi.org/10.1007/s00024-019-02271-8

Chambers, J. E., Wilkinson, P. B., Kuras, O., Ford, J. R., Gunn, D. A., Meldrum, P. I., Pennington, C. V. L., Weller, A. L., Hobbs, P. R. N., & Ogilvy, R. D. (2011). Three-dimensional geophysical anatomy of an active landslide in Lias Group mudrocks, Cleveland Basin, UK. *Geomorphology*, *125*(4), 472–484. https://doi.org/10.1016/j.geomorph.2010.09.017

Choden, Y., & Sharma, M. P. (2019). Greenhouse gas estimation from municipal solid waste dump site in Roorkee (Uttrakhand), India. *IJRES*, *6*, 39–46. https://doi.org/10.33500/ijres.2019.06.004

Chu, Y., Liu, S., Wang, F., Cai, G., & Bian, H. (2017). Estimation of heavy metal-contaminated soils' mechanical characteristics using electrical resistivity. *Environmental Science and Pollution Research*, *24*(15), 13561–13575. https://doi.org/10.1007/s11356-017-8718-x

Danthurebandara, M., Passel, S. Van, & Nelen, D. (2013). *ENVIRONMENTAL AND SOCIO-ECONOMIC*. *April 2017*.

de la Vega, M., Osella, A., & Lascano, E. (2003). Joint inversion of Wenner and dipole-dipole data to study a gasoline-contaminated soil. *Journal of Applied Geophysics*, *54*(1–2), 97–109. https://doi.org/10.1016/j.jappgeo.2003.08.020

Devi, A., Israil, M., Anbalagan, R., & Gupta, P. K. (2017). Subsurface soil characterization using geoelectrical and geotechnical investigations at a bridge site in Uttarakhand Himalayan region. *Journal of Applied Geophysics*, *144*, 78–85. https://doi.org/10.1016/j.jappgeo.2017.07.005

District, H. (n.d.). *उ◆रांचल ◆ेत्र, दे हरादन ू Uttaranchal Region, Dehradun*.

Donohue, S., McCarthy, V., Rafferty, P., Orr, A., & Flynn, R. (2015). Geophysical and hydrogeological characterisation of the impacts of on-site wastewater treatment discharge to groundwater in a poorly productive bedrock aquifer. *Science of the Total Environment*, *523*, 109–119. https://doi.org/10.1016/j.scitotenv.2015.03.117

Ducut, J. D., Alipio, M., Go, P. J., Concepcion, R., Vicerra, R. R., Bandala, A., & Dadios, E. (2022). A Review of Electrical Resistivity Tomography Applications in Underground Imaging and Object Detection. In *Displays* (Vol. 73). Elsevier B.V. https://doi.org/10.1016/j.displa.2022.102208

Enikanselu, P. A. (2008). Detection and monitoring of Dumpsite-induced groundwater contamination using electrical resistivity method. *The Pac J Sci Technol*, *9*(1), 254–262.

Feng, S. J., Bai, Z. B., Cao, B. Y., Lu, S. F., & Ai, S. G. (2017). The use of electrical resistivity tomography and borehole to characterize leachate distribution in Laogang landfill, China. *Environmental Science and Pollution Research*, *24*(25), 20811–20817. https://doi.org/10.1007/s11356-017-9853-0

Fernández, D. S., Puchulu, M. E., & Georgieff, S. M. (2014). Identification and assessment of water pollution as a consequence of a leachate plume migration from a municipal landfill site (Tucumán, Argentina). *Environmental Geochemistry and Health*, *36*(3), 489–503. https://doi.org/10.1007/s10653-013-9576-1

Ganiyu, S. A., Badmus, B. S., Oladunjoye, M. A., Aizebeokhai, A. P., Ozebo, V. C., Idowu, O. A., & Olurin, O. T. (2016). Assessment of groundwater contamination around active dumpsite in Ibadan southwestern Nigeria using integrated electrical resistivity and hydrochemical methods. *Environmental Earth Sciences*, *75*(8), 1–19. https://doi.org/10.1007/s12665-016-5463-2

Gupta, N., Yadav, K. K., & Kumar, V. (2015). A review on current status of municipal solid waste management in India. In *Journal of Environmental Sciences (China)* (Vol. 37, pp. 206–217). Chinese Academy of Sciences. https://doi.org/10.1016/j.jes.2015.01.034

Han, Z., Ma, H., Shi, G., He, L., Wei, L., & Shi, Q. (2016). A review of groundwater contamination near municipal solid waste landfill sites in China. *Science of the Total Environment*, *569–570*(1), 1255–1264. https://doi.org/10.1016/j.scitotenv.2016.06.201

Helene, L. P. I., Moreira, C. A., & Bovi, R. C. (2020). Identification of leachate infiltration and its flow pathway in landfill by means of electrical resistivity tomography (ERT). *Environmental Monitoring and Assessment*, *192*(4). https://doi.org/10.1007/s10661-020-8206-5

Li, P. Y., Qian, H., & Wu, J. H. (2010). Groundwater Quality Assessment Based on Improved Water Quality Index in Pengyang County, Ningxia, Northwest China. *E-Journal of Chemistry*, *7*(S1), S209–S216.

Loke, M. H. (1997). *Electrical imaging surveys for environmental and engineering studies A practical guide to 2-D and 3-D surveys by*. www.abem.se

Loke, M. H. (2011). Electrical resistivity surveys and data interpretation. *Encyclopedia of Earth Sciences Series*, *Part 5*(0), 276–283. https://doi.org/10.1007/978-90-481-8702-7_46

Longe, E. O., & Balogun, M. R. (2010). Groundwater quality assessment near a municipal landfill, Lagos, Nigeria. *Research Journal of Applied Sciences, Engineering and Technology*, *2*(1), 39–44.

McLachlan, P., Chambers, J., Uhlemann, S., & Binley, A. (2020). Limitations and considerations for electrical resistivity and induced polarization imaging of riverbed sediments: Observations from laboratory, field, and synthetic experiments. *Journal of Applied Geophysics*, *183*, 104173. https://doi.org/10.1016/j.jappgeo.2020.104173

Meads, L. N., Bentley, L. R., & Mendoza, C. A. (2003). Application of electrical resistivity imaging to the development of a geologic model for a proposed Edmonton landfill site. *Canadian Geotechnical Journal*, *40*(3), 551–558. https://doi.org/10.1139/t03-017

Moretto, R. L., Siqueira Neto, A. C. de, Elis, V. R., & Miguel, M. G. (2017). Detection of leachate pockets in experimental cell of municipal solid waste with aid of geophysics. *Proceedings Sardinia 2017 / Sixteenth International Waste Management and Landfill Symposium*, *October*, 2–6.

Mosuro, G. O., Omosanya, K. O., Bayewu, O. O., Oloruntola, M. O., Laniyan, T. A., Atobi, O., Okubena, M., Popoola, E., & Adekoya, F. (2017). Assessment of groundwater vulnerability to leachate infiltration using electrical resistivity method. *Applied Water Science*, *7*(5), 2195–2207. https://doi.org/10.1007/s13201-016-0393-4

Mota, R., Monteiro Santos, F. A., Mateus, A., Marques, F. O., Gonçalves, M. A., Figueiras, J., & Amaral, H. (2004). Granite fracturing and incipient pollution beneath a recent landfill facility as detected by geoelectrical surveys. *Journal of Applied Geophysics*, *57*(1), 11–22. https://doi.org/10.1016/j.jappgeo.2004.08.007

Ogilvy, R., Meldrum, P., Chambers, J., & Williams, G. (2002). The Use of 3D Electrical Resistivity Tomography to Characterise Waste and Leachate Distribution within a Closed Landfill, Thriplow, UK. *Journal of Environmental and Engineering Geophysics*, *7*(1), 11–18. https://doi.org/10.4133/jeeg7.1.11

Ogundiran, O. O., & Afolabi, T. A. (2008). Assessment of the physicochemical parameters and heavy metals toxicity of leachates from municipal solid waste open dumpsite. *International Journal of Environmental Science and Technology*, *5*(2), 243–250. https://doi.org/10.1007/BF03326018

Olasunkanmi, N. K., Usman, Z. M., & Jimoh, A. A. (2023). Investigation of groundwater quality around municipal waste disposal site in Malete southwestern Nigeria. *Arabian Journal of Geosciences*, *16*(4). https://doi.org/10.1007/s12517-023-11359-4

Omolayo, D., & Tope, F. J. (2014). 2D electrical imaging surveys for leachate plume migration at an old dump site in Ibadan south western Nigeria: A case study. *International Journal of Geophysics*, *2014*. https://doi.org/10.1155/2014/879530

Oyeyemi, K. D., Aizebeokhai, A. P., & Attat, O. F. (n.d.). *Evaluation of Groundwater Pollution Near Municipal Solid Waste Landfill Site Using ERI Technique: A Case Study in Southwestern Nigeria*. www.neptjournal.com

Park, S., Yi, M. J., Kim, J. H., & Shin, S. W. (2016a). Electrical resistivity imaging (ERI) monitoring for groundwater contamination in an uncontrolled landfill, South Korea. *Journal of Applied Geophysics*, *135*, 1–7. https://doi.org/10.1016/j.jappgeo.2016.07.004

Park, S., Yi, M. J., Kim, J. H., & Shin, S. W. (2016b). Electrical resistivity imaging (ERI) monitoring for groundwater contamination in an uncontrolled landfill, South Korea. *Journal of Applied Geophysics*, *135*, 1–7. https://doi.org/10.1016/j.jappgeo.2016.07.004

Ramakrishnaiah, C. R., Sadashivaiah, C., & Ranganna, G. (2009). Assessment of water quality index for the groundwater in Tumkur taluk, Karnataka state, India. *E-Journal of Chemistry*, *6*(2), 523–530. https://doi.org/10.1155/2009/757424

Rao, G. T., Rao, V. V. S. G., Padalu, G., Dhakate, R., & Sarma, V. S. (2014). Application of electrical resistivity tomography methods for delineation of groundwater contamination and potential zones. *Arabian Journal of Geosciences*, *7*(4), 1373–1384. https://doi.org/10.1007/s12517-013-0835-3

Sudha, Tezkan, B., Israil, M., Singhal, D. C., & Rai, J. (2010). Geoelectrical mapping of aquifer contamination: A case study from Roorkee, India. *Near Surface Geophysics*, *8*(1), 33–42. https://doi.org/10.3997/1873-0604.2009049

Yan, Y., Yan, Y., Zhao, G., Zhou, Y., & Wang, Z. (2022). Combined ERT and GPR Data for Subsurface Characterization of Weathered Hilly Slope: A Case Study in Zhejiang Province, Southeast China. *Sustainability (Switzerland)*, *14*(13). https://doi.org/10.3390/su14137616

Zaini, M. S. I., Hasan, M., & Zolkepli, M. F. (2022). Urban landfills investigation for leachate assessment using electrical resistivity imaging in Johor, Malaysia. *Environmental Challenges*, *6*(August 2021), 100415. https://doi.org/10.1016/j.envc.2021.100415

Zhang, Q. Q., Tian, B. H., Zhang, X., Ghulam, A., Fang, C. R., & He, R. (2013). Investigation on characteristics of leachate and concentrated leachate in three landfill leachate treatment plants. *Waste Management*, *33*(11), 2277–2286. https://doi.org/10.1016/j.wasman.2013.07.021

Acidic Soil Amendment by Water Hyacinth Biochar for Production of Maize

Tizeta Debebe[1]

[1]Arba Minch University, Arba Minch Water Technology Institute, Faculty of Water Supply and Environmental Engineering

*Corresponding author: tizgen162@gmail.com

Abstract

This study investigates the effect of water hyacinth-derived biochar on maize growth in acidic soils, with the goal of identifying an optimal application rate for sustainable crop production. A pot experiment was conducted using varying biochar concentrations (0%, 5%, 10%, and 15%), and growth parameters such as plant height, leaf number, and dry biomass were measured alongside soil nutrient content. The results revealed that 10% biochar application significantly enhanced maize growth and biomass yield, with strong positive correlations observed between biochar-amended soil nutrients (total nitrogen, phosphorus, and potassium) and plant performance. However, a reduction in growth at 15% biochar indicates a potential threshold beyond which nutrient availability or soil structure may become limiting. These findings demonstrate the potential of transforming invasive water hyacinth into a valuable soil amendment that improves food production and supports sustainable land management. By promoting resource recycling and improving soil health, this approach contributes to multiple sustainable development objectives, offering a cost-effective and eco-friendly solution for regions facing soil degradation and food insecurity.

Keywords: Biochar, Water hyacinth, Maize growth, Soil amendment, Acidic soil, Sustainable agriculture, Soil fertility

1. Introduction

Water hyacinth (*Eichhornia crassipes*), an invasive aquatic weed, poses environmental challenges due to its rapid propagation and obstruction of water bodies. However, its high biomass production makes it a potential feedstock for biochar production(Masto et al., 2013). When applied as a soil amendment, water hyacinth biochar (WHB) can neutralize soil acidity, enhance cation exchange capacity, and improve soil organic matter content, thereby creating a more favorable environment for maize growth(Jutakanoke et al., 2023) and ultimately leading to a reduction of the biodiversity of the environment which it occupies(Ayanda et al., 2020) the weed does not discharge oxygen into the aquatic ecosystem (Tobias et al., 2019)thus it results in a decrease in the dissolved oxygen concentration of the water body. water hyacinth mats serving as breeding ground for vector organisms carrying malaria, bilharzia and river blindness(Gunnarsson & Petersen, 2007) and its management can assume serious environmental issue due to its high productivity (Gunnarsson & Petersen, 2007)(Masto et al., 2013).

Soil acidity is a major constraint to crop productivity, particularly in tropical and subtropical regions where leaching of essential nutrients and aluminum toxicity hinder plant growth(Regasa Gemada, 2021). Maize (*Zea mays*), a staple food crop, is highly sensitive to acidic soils, resulting in reduced yield and poor nutrient uptake(Tandzi et al., 2018). To mitigate soil acidity and enhance crop performance, various soil amendments, including biochar, have gained attention due to their ability to improve soil properties and fertility(Jemal et al., 2021).

This study explores the potential of water hyacinth biochar as an amendment for acidic soils in maize production. By evaluating its effects on soil properties and plant growth parameters, this research aims to provide a sustainable and eco-friendly approach to improving agricultural productivity while addressing water hyacinth invasion.

2. Materials and Methods

2.1. Study area

Arba Minch town is one of the emerging towns of Ethiopia which is located in Southern Nations, Nationalities and Peoples regional state of Ethiopia. Chencha Wereda is situated near Arba Minch, a prominent city in southern Ethiopia. The region is characterized by its highland and mountainous terrain, offering a unique environment compared to the lowland areas surrounding it. The area experiences a temperate climate due to its elevation, with cooler temperatures and more significant rainfall than the lowland areas. The Gircha Research Center is situated approximately 6 kilometers northwest of Chencha Woreda. The primary livelihood of the population is agriculture, with a focus on subsistence farming with producing enset (false banana),potatoes, barley, wheat, and a variety of fruits and vegetables (Tadesse et al., 2019)because many other crops are sensitive to acidic conditions (Rao et al., 1993)and may exhibit stunted growth, poor yields, or complete failure in highly acidic soils.

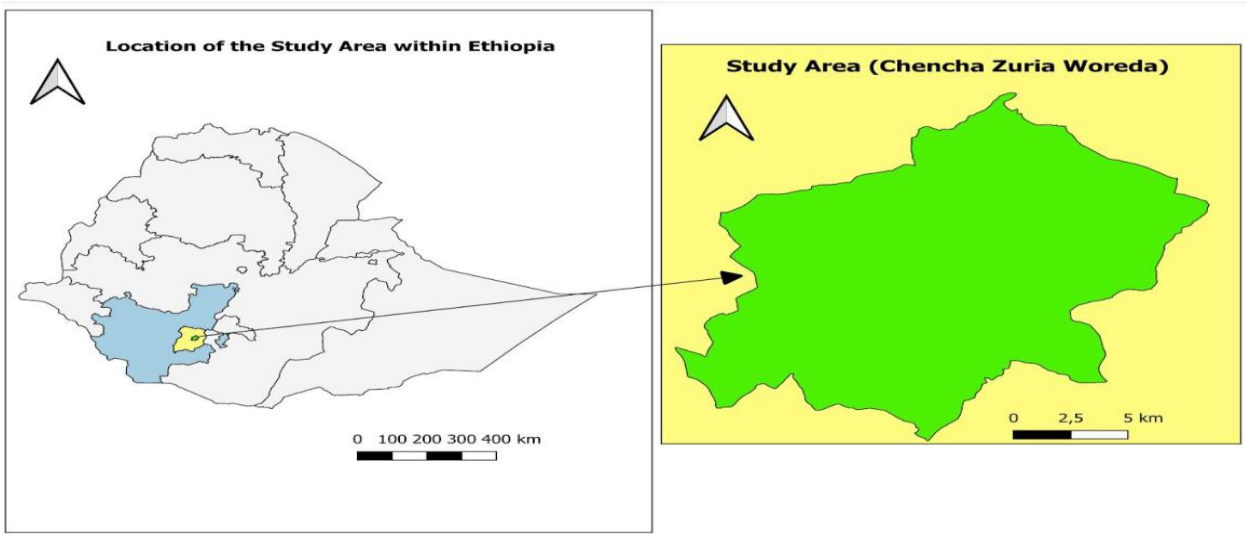

Figure 20: Location map of the study area

2.2. Biomass collection & biochar preparation from Water hyacinth

Water hyacinth biomass was collected from a densely infested area of Abaya Lake, specifically in Kola Shara Kebele. After collection, the biomass was transported manually to Arba Minch, near Sikela Stadium. The roots were removed, and the stems and leaves were thoroughly washed with tap water to eliminate unwanted debris, as illustrated in Figure 2. 1.

Figure 21: Removing the root & washing of water hyacinth

Following the cleaning process, the biomass was sun-dried and cut into small pieces (30–50 mm) following the method described by (Masto et al., 2013)(Zhang et al., 2016). The prepared biomass was then stored in a dry container for further processing. Biochar was produced from the dried water hyacinth under limited oxygen conditions using a 55 gallon cylindrical oil drum (85 cm height × 55 cm diameter)with reference & modification of (Balaguraviah Acharya Ranga et al., 2021). The drum was modified with 15 holes, each 4 cm in diameter, positioned at the bottom to regulate airflow. This setup simulated a simple pyrolysis process that could be easily adopted by farmers with minimal investment.

Figure 22: Preparation of biochar

Known quantity of sun dried water hyacinth was taken in the cylindrical oil drum with cover & chimney. The temperature was adjusted based on visual inspection of the color of the flame to obtain the required biochar quality.

2.3. Biochar characterization

Biochar yield

The yield was calculated as the ratio of the mass of biochar obtained (Mb) to the initial mass of dried biomass (Mi), expressed as a percentage:

$$Y_b(\%) = \frac{M_b}{M_i} * 100 \quad (1)$$

Moisture Content (MC)

Approximately 1.5 g of fresh biochar was placed in a pre-weighed crucible (Wc), and the combined weight was recorded as Wi. The sample was oven-dried at 105 °C for 24 hours, cooled in a desiccator, and reweighed (Wf). Moisture content was calculated as:

$$MC(\%) = \frac{Wi-Wf}{Wi} * 100 \quad (2)$$

Volatile Matter (VM)

A 20 g dried sample (Wd) was heated in a muffle furnace at 550 °C for 10 minutes under oxygen-limited conditions(Lin et al., 2025). After cooling, the residue was weighed (W550) and VM was determined as:

$$VM(\%) = \frac{Wd-W550}{Wd} * 100 \quad (3)$$

Ash Content

The same sample was combusted at 750 °C for 6 hours. After cooling, the remaining ash was weighed (W750) and ash content was calculated as:

$$\text{Ash}(\%) = (\frac{W_{550}-W_{residue}}{W_{550}} * 100 \quad (4)$$

Presence of functional groups

FTIR analysis was performed to identify functional groups in the biochar. The sample was finely ground and analyzed using an FTS 3000MX FT-IR spectrometer (Varian Instruments, Randolph, MA) over the 4000–600 cm^{-1} range. Each spectrum was averaged from 32 scans with background correction to minimize atmospheric interference. Characteristic peaks corresponding to hydroxyl (-OH), carbonyl (C=O), aromatic (C=C), and aliphatic (C-H) groups were identified to assess chemical composition and carbonization. Spectral data were further processed and visualized using SciDAVis 2.7 software.

Experimental Setup

Twenty pots were filled with equal amounts of acidic soil from Gircha Research Center (Chencha, Arbaminch) and planted with maize. Four treatments (0%, 5%, 10%, and 15% water hyacinth biochar) were applied, each in four replicates, following (X. Liu et al., 2020)Biochar was thoroughly mixed into the soil before planting. All pots received uniform irrigation, pesticide application, and sunlight exposure. The experiment ran until the maize reached its early reproductive stage.

2.3.1. Morphological analysis of maize plant

Leaf width and length, stack height & diameter, number of leaves on each maize shoot, were measured at the end of the experiment. The experiment was until the stage of early reproduction.

Figure 23: morphological analysis after ½ a month & 3 months of sowing

After morphological measurements, maize plants were carefully uprooted, and roots were washed to remove adhering soil. The entire biomass was chopped into smaller pieces, air-dried, and stored in labeled, separate bags for each treatment group, as illustrated in Figure 7.

Figure 24: Chopped & dried biomass

2.3.2. Soil sample collection, preparation and laboratory analysis

Representative soil samples were collected from each experimental pot at a depth of 15–25 cm, following the method of (Ahmed et al., 2020), to target the root zone of young maize plants and assess the biochar's impact on nutrient availability. Samples were properly labeled, air-dried, and transported to the Soil Testing Laboratory at the Abaya Campus of Arba Minch University for further analysis.

2.3.3. Soil macro nutrient (NPK) analysis

Total nitrogen (N) was determined using the Kjeldahl method (Bremner, 1960), available phosphorus (P) by the Bray-1 method (Aura, 1978), and exchangeable potassium (K) via ammonium acetate (NH_4OAc) extraction (Bazargan et al., n.d.,2024).Data were subjected to statistical analysis using ANOVA to assess significant differences and correlations between soil nutrient levels and maize growth responses. The pH and electrical conductivity (EC) of the soil before and after planting were determined at a soil (g) to deionized water (mL) ratio of 1:2.5(Yang et al., 2017). The pH and EC were determined from the suspension employing a calibrated pH meter and an EC meter.

3. RESULTS AND DISCUSSION

3.1. Biochar Characterization

3.1.3. Physicochemical properties

The water hyacinth biochar showed a **35% yield**, **6% moisture**, and **20% ash**, indicating efficient production and high mineral content. Its **30% volatile matter** reflects moderate carbonization at ~300–400 °C. With a **pH of 8.1** and **EC of 3.7 dS/m**, the biochar is slightly alkaline and nutrient-rich and ideal for improving acidic soils by enhancing pH, nutrient availability, and overall fertility.

3.1.4. Functional Groups and Their Role in Soil Amendment

The FTIR spectrum (Figure 9) of water hyacinth biochar shows key oxygen-containing functional groups. Broad peaks at **3200–3600 cm⁻¹** indicate **hydroxyl (-OH)** groups, enhancing moisture retention and CEC.

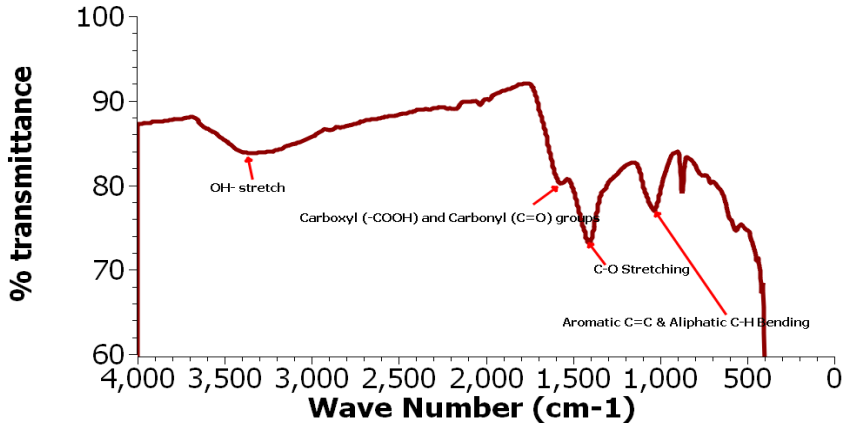

Figure 25: FTIR Spectrum of the Water Hyacinth Biochar

Peaks at **1600–1700 cm⁻¹** confirm **carboxyl and carbonyl** groups, aiding nutrient retention and heavy metal immobilization. Signals at **1000–1200 cm⁻¹** suggest **phenolic and ether** groups, promoting microbial activity and long-term stability. Peaks at **500–900 cm⁻¹** indicate **aromatic and aliphatic** structures, contributing to structural stability and potential carbon sequestration.

3.2. Effect of water hyacinth biochar on plant morphological parameters

Biochar application significantly improved maize growth, with optimal results at 10% biochar dose. Plant height, leaf number, leaf dimensions, and stem circumference all peaked at this level, with height reaching 104.20 ± 3.1 cm and dry mass 57.00 ± 2.7 g, over 3x higher than the control (15.60 ± 0.8 g). These improvements reflect enhanced soil fertility and structure.

Table 9: Changes in morphological parameters

Biochar dose (%)		Height of Stack(cm)	No of leaves (no)	Length of longest leaf (cm)	Stack Circumference (cm)	Width of longest leaf (cm)	Dry mass(g)
.0	Mean±SD	71.60±4.3	6.40±1.3	53.80±3.3	2.6800±0.09	4.620±0.2	15.60±0.8
.5	Mean±SD	87.60±2.1	10.60±1.1	80.00±2.7	3.7400±0.09	6.540±0.6	35.00±3.1
10	Mean±SD	104.20±3.1	12.40±0.6	92.80±2.2	4.5000±0.2	7.680±0.2	57.00±2.7
15	Mean±SD	80.40±2.2	8.80±0.4	71.40±1.7	3.3400±0.2	5.440±0.3	29.80±1.5
	Min	71.6	6.4	53.8	2.7	4.6	15.6
	Max	104.2	12.4	92.8	4.50	7.68	57.0

At 15%, most parameters declined—plant height dropped to 80.40 ± 2.2 cm, and dry mass to 29.80 ± 1.5 g—possibly due to nutrient imbalance or excess alkalinity. This suggests that while moderate biochar improves growth, higher doses may negatively affect plant development.

3.3. Effect on Soil Nutrient Availability

Water hyacinth biochar significantly improved soil nutrient availability. Available phosphorus (P) increased with biochar application, peaking at 2.01 ± 0.07 mg/kg at 10%, likely due to reduced fixation in acidic soil. Similarly, exchangeable potassium (K) reached its highest value (404.72 ± 12 mg/kg) at 10% biochar, enhancing nutrient uptake and plant growth.

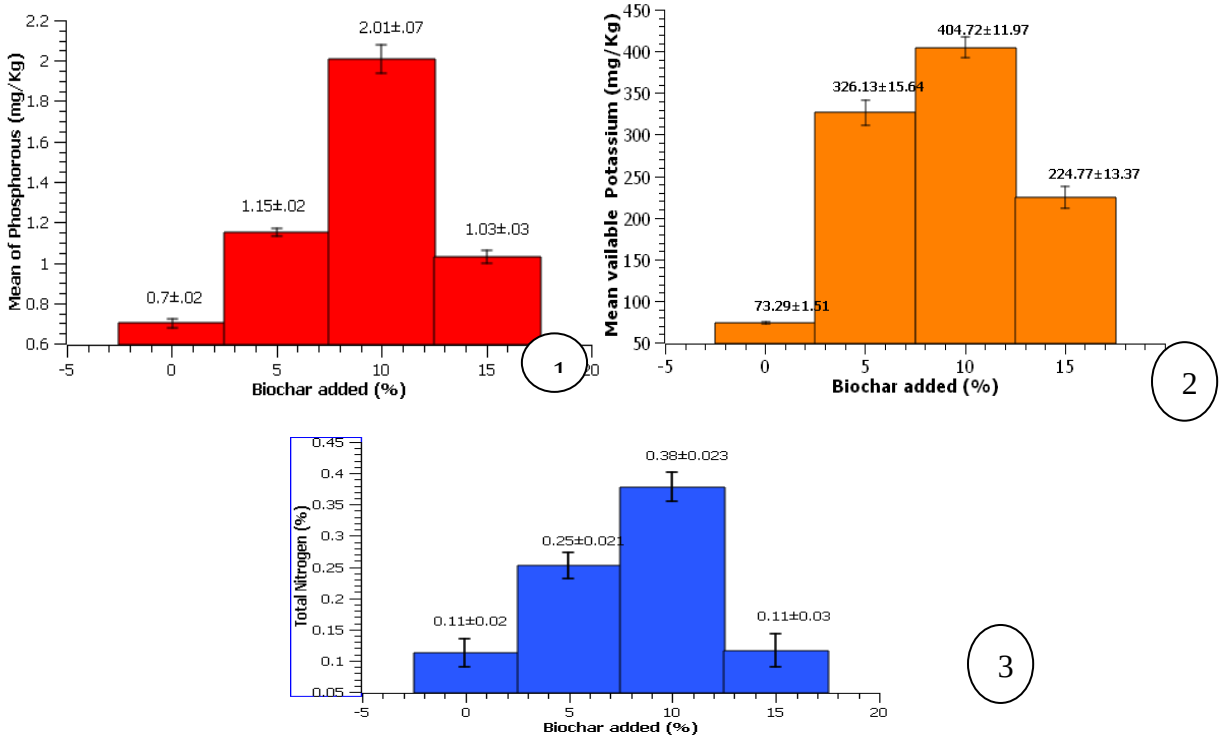

Figure 26: Mean +SD of Phosphorous (1), Potassium (2) and Total Nitrogen(3)

Total nitrogen (TN) also increased with biochar, from $0.11 \pm 0.02\%$ in the control to $0.38 \pm 0.02\%$ at 10%. However, at 15%, TN dropped sharply ($0.11 \pm 0.03\%$), possibly due to nutrient immobilization or microbial inhibition, indicating 10% as the optimum rate for N enhancement.

The alkaline nature of the water hyacinth biochar (pH 8.1) significantly raised soil pH across treatments. The control (pH 5.01 ± 0.06) confirmed the initial acidity. Biochar additions at 5%, 10%, and 15% increased soil pH to 6.36 ± 0.04, 6.55 ± 0.11, and 7.61 ± 0.22, respectively, highlighting its strong alkalizing effect and suitability for ameliorating acidic soils.

Strong, statistically significant ($p < 0.001$) positive correlations were observed between soil nutrients (P, K, and TN) and all plant growth parameters. Biomass weight showed the highest correlation with phosphorus ($r = 0.975$), while stalk circumference and leaf length were most strongly correlated with potassium ($r = 0.983$). These results indicate that improved nutrient availability directly influenced maize morphological development.

4. Conclusion

This study demonstrates that biochar produced from water hyacinth significantly enhances maize growth and soil quality in acidic soils. Application of biochar improved key morphological parameters, including plant height, leaf number, and dry biomass, with the 10% application rate yielding optimal results. At this dose, not only were total nitrogen (TN), available phosphorus (P), and potassium (K) markedly increased, but soil pH also improved significantly from 5.01 to 7.61 effectively neutralizing acidity and creating more favorable conditions for nutrient uptake and plant development.

The strong positive correlations between nutrient availability and growth parameters confirm biochar's potential to improve both chemical and physical soil properties. However, the decline in plant performance at 15% biochar indicates a possible saturation threshold, beyond which excessive amendment may lead to reduced soil aeration or nutrient imbalances, thereby emphasizing the importance of identifying optimal application rates.

Moreover, the study showcases a sustainable solution by transforming water hyacinth an invasive aquatic species into a beneficial agricultural input. This approach not only contributes to controlling ecological threats posed by the weed but also supports soil fertility restoration, aligning with broader sustainable development goals related to land degradation neutrality, food security, and climate-resilient farming.

In conclusion, water hyacinth biochar presents a cost-effective and eco-friendly soil amendment for improving crop production in acidic soils. Future research should focus on long-term field evaluations to assess its effects on soil microbial communities, water-use efficiency, nutrient cycling, and overall productivity in diverse agro-ecological zones.

Reference

Ahmed, F., Arthur, E., Liu, H., & Andersen, M. N. (2020). New Rootsnap Sensor Reveals the Ameliorating Effect of Biochar on In Situ Root Growth Dynamics of Maize in Sandy Soil. *Frontiers in Plant Science*, *11*(June), 1–12. https://doi.org/10.3389/fpls.2020.00949

Aura, E. (1978). Determination of available soil phosphorus by chemical methods. *Agricultural and Food Science*, *50*(4), 305–316. https://doi.org/10.23986/afsci.71982

Ayanda, O. I., Ajayi, T., & Asuwaju, F. P. (2020). Eichhornia crassipes (Mart.) Solms: Uses, Challenges, Threats, and Prospects. *Scientific World Journal*, *2020*. https://doi.org/10.1155/2020/3452172

Balaguraviah Acharya Ranga, D. N., Srinivasa Rao, C., Lavanya Kumari, P., Nataraja, K., Balaguraviah, D., Giridhara Krishna, T., & Reddi Ramu, Y. (2021). Biochar production through drum method and characterization for soil amendment qualities. *~ 544 ~ The Pharma Innovation Journal*, *10*(6), 544–551. http://www.thepharmajournal.com

Bazargan, K., Marzi, M., Sadat Hasheminasab, K., Shahbazi, K., & Akbar Zare, A. (n.d.). Optimizing ammonium acetate procedure for determining available potassium in Iranian calcareous soils, testing the concentration and contact time. In *Journal of Soil Science Society of Iran* (Vol. 1, Issue 1, pp. 125–136).

Bremner, J. M. (1960). Determination of nitrogen in soil by the Kjeldahl method. *The Journal of Agricultural Science*, *55*(1), 11–33. https://doi.org/10.1017/S0021859600021572

Gunnarsson, C. C., & Petersen, C. M. (2007). Water hyacinths as a resource in agriculture and energy production: A literature review. *Waste Management*, *27*(1), 117–129. https://doi.org/10.1016/j.wasman.2005.12.011

Irfan, M. (2017). Potential value of biochar as a soil amendment: A review. *Pure and Applied Biology*, *6*(4), 1494–1502. https://doi.org/10.19045/bspab.2017.600161

Jemal, K., -, A. Y., & 2021, U. (2021). Role of bio char on the amelioration of soil acidity. *Agrotechnology*, *10*(July), 212–217. https://www.researchgate.net/profile/Kedir-Ahmee/publication/353406424_Role_of_Bio_Char_on_the_Amelioration_of_Soil_Acidity/links/60fab5e00c2bfa282af63e67/Role-of-Bio-Char-on-the-Amelioration-of-Soil-Acidity.pdf

Jutakanoke, R., Intaravicha, N., Charoensuksai, P., Mhuantong, W., Boonnorat, J., Sichaem, J., Phongsopitanun, W., Chakritbudsabong, W., & Rungarunlert, S. (2023). Alleviation of soil acidification and modification of soil bacterial community by biochar derived from water hyacinth Eichhornia crassipes. *Scientific Reports*, *13*(1), 1–12. https://doi.org/10.1038/s41598-023-27557-9

Lin, G., Wang, Y., Wu, X., Meng, J., Ok, Y. S., & Wang, C. H. (2025). Enhancing agricultural productivity with biochar: Evaluating feedstock and quality standards. *Bioresource Technology Reports*, *29*, 102059. https://doi.org/10.1016/J.BITEB.2025.102059

Liu, Q., Liu, B., Zhang, Y., Hu, T., Lin, Z., Liu, G., Wang, X., Ma, J., Wang, H., Jin, H., Ambus, P., Amonette, J. E., & Xie, Z. (2019). Biochar application as a tool to decrease soil nitrogen losses (NH 3 volatilization, N 2 O emissions, and N leaching) from croplands: Options and mitigation strength in a global perspective. *Global Change Biology*, *25*(6), 2077–2093. https://doi.org/10.1111/gcb.14613

Liu, X., Wang, H., Liu, C., Sun, B., Zheng, J., Bian, R., Drosos, M., Zhang, X., Li, L., & Pan, G. (2020). Biochar increases maize yield by promoting root growth in the rainfed region. *Archives of Agronomy and Soil Science*, *0*(0), 1–14. https://doi.org/10.1080/03650340.2020.1796981

Masto, R. E., Kumar, S., Rout, T. K., Sarkar, P., George, J., & Ram, L. C. (2013). Biochar from water hyacinth (Eichornia crassipes) and its impact on soil biological activity. *Catena*, *111*, 64–71. https://doi.org/10.1016/j.catena.2013.06.025

Najmudeen, T. M., Arakkal Febna, M. A., Rojith, G., & Zacharia, P. U. (2019). Characterisation of Biochar from Water Hyacinth Eichhornia crassipes and the Effects of Biochar on the Growth of Fish and Paddy in Integrated Culture Systems. *Journal of Coastal Research*, *86*(sp1), 225–234. https://doi.org/10.2112/SI86-033.1

Olmo, M., Villar, R., Salazar, P., & Alburquerque, J. A. (2016). Changes in soil nutrient availability explain biochar's impact on wheat root development. *Plant and Soil*, *399*(1–2), 333–343. https://doi.org/10.1007/s11104-015-2700-5

Pandit, N. R., Mulder, J., Hale, S. E., Martinsen, V., Schmidt, H. P., & Cornelissen, G. (2018). Biochar improves maize growth by alleviation of nutrient stress in a moderately acidic low-input Nepalese soil. *Science of the Total Environment*, *625*, 1380–1389. https://doi.org/10.1016/j.scitotenv.2018.01.022

Rao, I. M., Zeigler, R. S., Vera, R., & Sarkarung, S. (1993). Selection and Breeding for Acid-Soil Tolerance in Crops. *BioScience*, *43*(7), 454–465. https://doi.org/10.2307/1311905

Regasa Gemada, A. (2021). Soil Acidity Challenges to Crop Production in Ethiopian Highlands and Management Strategic Options for Mitigating Soil Acidity for Enhancing Crop Productivity. *Agriculture, Forestry and Fisheries*, *10*(6), 245. https://doi.org/10.11648/j.aff.20211006.15

SHI, R. yong, LI, J. yu, NI, N., & XU, R. kou. (2019). Understanding the biochar's role in ameliorating soil acidity. *Journal of Integrative Agriculture*, *18*(7), 1508–1517. https://doi.org/10.1016/S2095-3119(18)62148-3

Tadesse, Y., Almekinders, C. J. M., Schulte, R. P. O., & Struik, P. C. (2019). Potatoes and livelihoods in Chencha, southern Ethiopia. *NJAS - Wageningen Journal of Life Sciences*, *88*, 105–111. https://doi.org/10.1016/j.njas.2018.05.005

Tandzi, L. N., Mutengwa, C. S., Ngonkeu, E. L. M., & Gracen, V. (2018). Breeding maize for tolerance to acidic soils: A review. *Agronomy*, *8*(6), 1–21. https://doi.org/10.3390/agronomy8060084

Tobias, V. D., Conrad, J. L., Mahardja, B., & Khanna, S. (2019). Impacts of water hyacinth treatment on water quality in a tidal estuarine environment. *Biological Invasions*, *21*(12), 3479–3490. https://doi.org/10.1007/s10530-019-02061-2

Wu, S., Zhang, Y., Tan, Q., Sun, X., Wei, W., & Hu, C. (2020). Biochar is superior to lime in improving acidic soil properties and fruit quality of Satsuma mandarin. *Science of the Total Environment*, *714*, 136722. https://doi.org/10.1016/j.scitotenv.2020.136722

Yadav, A., Ansari, K. B., Simha, P., Gaikar, V. G., & Pandit, A. B. (2016). Vacuum pyrolysed biochar for soil amendment. *Resource-Efficient Technologies*, *2*, S177–S185. https://doi.org/10.1016/j.reffit.2016.11.004

Yang, X., Lu, K., McGrouther, K., Che, L., Hu, G., Wang, Q., Liu, X., Shen, L., Huang, H., Ye, Z., & Wang, H. (2017). Bioavailability of Cd and Zn in soils treated with biochars derived from tobacco stalk and dead pigs. *Journal of Soils and Sediments*, *17*(3), 751–762. https://doi.org/10.1007/s11368-015-1326-9

Zhang, F., Wang, X., & Xionghui, J. (2016). *Ef fi cient arsenate removal by magnetite-modi fi ed water hyacinth*. *216*, 1–9. http://dx.doi.org/10.1016/j.envpol.2016.06.013

Disappearing Urban Stream: Aquatic Ecosystem Overthrow From Discharges by Stationary Concrete Batch Plants in the Fast-Urbanizing Addis Ababa

Getachew Dagnew Gebreeyessus*[1,2], Shemsu Jihad Abadura[1] & Ermias D. Woldemariam[1]

[1]Kotebe University of Education, P.O.Box 31248, Addis Ababa Ethiopia
[2]Africa Center of Excellence for Water Management, Addis Ababa University, P.O.Box 1176, Addis Ababa Ethiopia

*Corresponding author email: dagnew.getachew@kue.edu.et

Abstract

Concrete would be the most utilized material by humans accounting to its global use of 25x10^12–30x10^12 kilograms annually. A quantitative and qualitative evaluation of the concrete batch plants in Addis Ababa was performed by the current cross-sectional study. The batch plants are located typically in three sub cities of Addis Ababa and most are commissioned during the years 2020 and 2022. A snapshot of the chemical analysis of water samples from the streams located adjacent to these concrete producing plants indicated a pH of 11.4 ±1, total chemical oxygen demand of 10700 ±870 mg/l, SO_4^{2-} of 1325 ±60 mg/l, and NO_3^{2-} of 17.5 ±0.2 mg/l, which was found. The adjacent rivers are partly and disappointingly vanished. In fact, the regulatory and permit issues to those concrete batch plants are almost unavailable, worsening the aquatic environmental impact.

Keywords*: Aquatic, Concrete Batch Plants, Construction, Environmental Impact, River, Streams*

1. Introduction

Basically, our lives and livelihoods are directly or indirectly dependent on the natural and engineered environmental systems whereby healthy urban streams and ecosystems are vital to cities with provisions ranging from water to food and air temperature regulation (Ranta et al. 2021, Pandey and Ghosh 2023, Raquel Calapez et al. 2023). Likewise, urbanization and population growth demands fastened development accompanied by massive consumer productions. Unfortunately, the urban and industrial development activities are posing threats to the rivers and terrestrial ecosystems on a local and regional scale, if an environmental management system standard is not observed (Taylor and Owens 2009, Malmqvist and Rundle 2002). In spite of their huge positive implications, the rapid development activities and urbanization are abstracting the natural water on one side as raw material and are polluting back on the other side with resulting wastewater discharges signaling the unsustainability of not only the water bodies but also of other socioeconomic developments (Srinivasan et al. 2003, McMichael 2000). In order to ensure urban ecosystem sustainability, therefore, the anthropogenic effects on natural systems such as the urban rivers have to be minimized and if possible be avoided. For developing and fast-urbanizing sub-Saharan countries like Ethiopia, timely reconciling of the socioeconomic development activities with nature such as through avoiding water pollution in an integrated as well as adaptive approach appears demanding (Smith et al. 2013).

The centers of productivity, the natural water bodies that contribute to temperature regulation, water and food supply, the sites for the urbanites' recreation and more -the rivers, became open channels for wastewater flows and other kinds of waste dumping in Ethiopia's capital, Addis Ababa. These wastewaters are partly coming from industries that are unfairly commissioned along river banks and are poorly regulated already became

seriously concerning. Locally, a significant proportion (80-85%) of these industries are concentrated in and around Addis Ababa, accounting for over the 65% of the total national, that are discharging their process wastewater without proper treatment into adjacent streams or rivers (Yohannes and Elias 2017; Menbere and Menbere 2019).

A sector among those polluters is the construction industry. The huge expansion of the construction activities in Ethiopia, mainly concentrating in the capital, is heavily demanding for concrete supplies that consequently triggered the boom in concrete batch plants (CBPs) among other construction materials suppliers. Concrete is a type of construction material in which cement, aggregate, and admixture materials are mixed (Kim et al. 2016) and in fact it is the second most consumed material after water in the world (Gagg 2014). CBPs by process are connections of mechanical parts that are either mobile or fixed in a given area and are designed to weigh water, cement, aggregates, admixtures and introduce the ingredients into the mixer for producing a batch of concrete (Deligiannis and Manesis, 2008). Though concrete batching can be performed using either mobile or stationary mixers, this particular study focuses on the stationary CBPs in Addis Ababa of Ethiopia.

In its whole life cycle, concrete production has got environmental issues that include the generation of greenhouse gases, increased surface runoff following sand mining, urban heat island, and potential public health implications from toxic ingredients. These plants are mostly located adjacent to river passages thereby abstracting their water demand and dumping concrete residues, wash discharges and mixed wastewaters back to the rivers (Demissew 2020, Mulatu et al. 2018). Such expansion of CBPs are defeating aquatic ecosystems in the capital thereby resulting in the destruction of the aquatic biodiversity in addition to their visible particulate air pollution (Cooke et al. 2020). In spite of the rapid urbanization of Ethiopia and the booming of the construction industry, there is no such local study reporting on the environmental and public health impact (EPHI) of concrete production in general and the CBPs in particular.

In this regard, both the industrial practice and the context of the enabling environment are unclear. Research questions such as 1) are the CBPs in the city properly recorded, commissioned and monitored or regulated, 2) How are the byproducts and wastes from the CBPs impacting rivers nearby and 3) what are the views of nearby residents and the mandated instituions? Thus, the current study was aimed to explore on the aquatic environmental health impacts of CBPs with emphasis to streams in Addis Ababa using mix of methods. Consequently, the results found indicated the rapid increase of CBPs reaching to 95 and being among the 470 construction input suppliers in Addis Ababa city. While the area occupied by those process plants is considerably high and their location is environmentally sensitive, the mandate for issuance of permit to CBPs is diffused and little is known by the administrative and technical people there about CBPs. What makes it worse is that permit for the CBP business is issued by different public bodies such as the sub-city administrations, the trade and industry bureau, the bureau of mines etcetera. Contrarily, the EPHIs of CBPs is perhaps vivid witnessed by the water pollution in the areas, the rivers or streams clogging and the prevalent dust air pollution, which all demands the review of CBP permit issuance procedure. More importantly, clear mandates and guiding policy as well as strong regulatory mechanism are crucial to manage the situations.

1.1. Highlighting on concrete consumption contexts and concerns

Though concrete is not the only material of construction, it is the most consumed material after water (Gagg 2014). . According to People's Daily Online news, so far the largest concrete pour in a single project took place decades back during the construction of the three gorgeous dam of China, consuming 28 x10^6 m^3

followed by an earlier construction of the Itaipu hydropower station of Brazil that consumed an annual concrete pouring volume of 3.2 x10^6 m^3 (PDO 2001).

Ethiopia is among the least urbanized but fast urbanizing countries in the world, signaling on the potential expansion of infrastructure whereby construction projects that consume concrete are at stake (Ozlu et al. 2015). Urbanization brings both opportunities and challenges, especially that related to sustainable development through wise consumption of resources and environmental protection. Indeed, by 2050, 68% of world's population will live in urban areas and 90% of such growth are contributed by Asia and Africa (Terfa et al. 2019).

Addis Ababa, a fast-urbanizing city in Ethiopia, currently undergoes two kinds of transformations; an outward expansion and inner-city renovation with in fact attention is being given to rivers' restoration within the inner-city.

As fast urbanization brought construction of the high rise buildings for residences like those condominium houses and apartments, commercial centers, public and private institutions and roads as well as bridges and related structures, the massive consumption of concrete is inevitable. However, such consumption of concretes is resulting in public and environmental issues. From cement production, stone crushing, sand mining to water abstraction, the concrete industry poses environmental impacts that include, air pollution, water pollution, and increased runoffs (Babor et al. 2009).

In order to enjoy the full health, productivity, religious and socio-economic potentials of water bodies, including the urban rivers, countries, regions and international bodies have developed frameworks, policies, and strategies that consider rivers protection from pollution and restorations (UN Environment 2017, Speed et al. 2016, Savenije and Van der Zaag 2000, Wiering and Arts 2006). In this regard Ethiopia made some effort to restore urban rivers at least in selected cities like Addis Ababa and Jimma (Awoke et al. 2016). Unfortunate, in the absence of a strong legal and institutional frameworks to urban river protections, urbanization will have serious impact on the ecological integrity of the rivers and hence affecting urbanites as a consequence of pollution against benefitting from the privileges of healthy urban rivers (Beyene et al. 2009). Thus, studies that focus on inter-sectorial issues that include the construction, trade and environment will have great contributions in influencing policies, and contributing scientific information to stakeholders for their subsequent intervention as well as filling of existing knowledge gaps.

Furthermore, the abiotic environment is always interacting with the biotic environment; serving as a source and sink for various substances whereby it's proper management is mandatory, not just to enjoy the full resources but also to ensure sustainability in interactions (Barrow 2006, Lemly 1997, Wangai et al. 2016). Such physicochemical environment includes the aquatic environs where one of the most required, perhaps next to air/oxygen, need of humans is met-water. Such aquatic systems include rivers that are in continuous interaction with hydro-geochemical cycles so to keep a healthy and productive ecosystem (Mondal and Patel 2022). When it comes to urban settings, the importance of rivers is beyond the provision of ecosystem services such that recreational, transport, and other socioeconomic benefits are few to mention (Lundy and Wade 2011, Leal Filho et al. 2020, Ma et al. 2022). However, such ecosystems are under pressure following urbanization, industrialization and rapid population growth (Xiu et al. 2022), especially in developing countries like Ethiopia (Yohannes and Elias 2017, Koroso et al. 2021).

Such ecosystem services provisions are indispensible to social development (Xiu et al. 2022). Traditionally river health is measured using some physical, chemical and biological characteristics that are assumed to be

healthy for the ecosystem functioning and the protection of public health. For instance, the amount or concentration of the dissolved oxygen (DO) can be a good indicator. A related study describes a healthy river in the context of its social and ecosystem services whereby the social and natural functions of a river have to perform in balance. While quality is subjective and generic term, abundant and clean flow of rivers is suggested as a key parameter to river health as the environmental flows are very important to safeguard the river health (Liu and Liu 2008, Karr 1999). In fact, rivers and cities or urban setting are historic and their interaction is established (Phong 2015).

2. Materials and Methods

2.1. Study area description

Addis Ababa has an altitude ranging between 3000 m above sea level around Entoto Mountain to down to 2100 m above sea level around Akaki. This fast urbanizing city is incomparable the largest in the nation. Addis Ababa is plying the political and economic role of the country with an almost over 65% of the industries in the country are concentrated in and around it while it is undergoing huge vertical and horizontal expansion, currently it is renovating massively whereby high-rise building constructions are vivid everywhere. The context of the urban environment is concerning as the rapid population growth and urbanization of Addis Ababa has been putting tremendous pressures on the city's physical and biotic environment. River, soil, air and water pollution as a result of industrial wastes and even domestic wastes are becoming a growing concerns (UN Habitat 2013).

2.2. Study design, method and sampling

The current study has applied a cross sectional design whereby it has been conducted within two seasons of a year.

A mix of methods was applied to understand the environmental pressure mainly by CBPs on the urban streams, the quantitative context of CBPs, mandate and institutional circumstances as well as that of concrete consumptions. Based on initial observation and preliminary information, areas in Bole, Yeka and Akaki Kaliti sub cities were identified for investigating aquatic ecosystem impacts of CBPs in Addis Ababa, Ethiopia.

Regarding sampling, up on refined information regarding CBPs installations in the city, Bole sub city was selected as area of focus. Bole sub city is one of the eleven sub cities that is expansive and is a place where huge urban infrastructure are located that include Bole international airport and is perhaps most developed area of the city. Of those districts under Bole sub city, district 12 is relatively peripheral and is still expanding as it is not bounded spatially like other sub cities and most of the City's CBPs are located this particular district.

There are numerous CBPs adjacent to the tributary streams of the Akaki River. Most of the processing plants are functional at present. Within those CBPs in Bole district two located on both sides of a seasonal stream flowing through the Bole international airport catchment down to Akaki River were identified. The water sampling strategy is also presented (**Table 1)**. Further, residents around those plants were also interviewed systematically to get key information on the quality history and functionality trend of the streams.

Table 1. Sampling sites (US: Up Stream, DS: Down Stream, CBP1,2: Concrete batch plants 1 and 2 that face each other and the stream being in between)

Sites	Designation	Remarks
1	US (appx.100 m above CBP1,2)	Control

2	CBPs 1,2	Effluent effect
3	DS (appx.200 m below CBP1,2)	Dilution effect

At the CBPs sampling point (at Site – 2) process effluent and concrete wash wastewater are discharged directed to the stream. There were two additional sampling points arranged upward of the stream, namely Site – 1 (UP: upstream sampling site was located at an estimated distance of 100 m above effluent entering point) and Site – 3 (DS: downstream sampling site were located some 200 m after effluent entry point). Schematic representations of sampling sites are depicted (Figure 1).

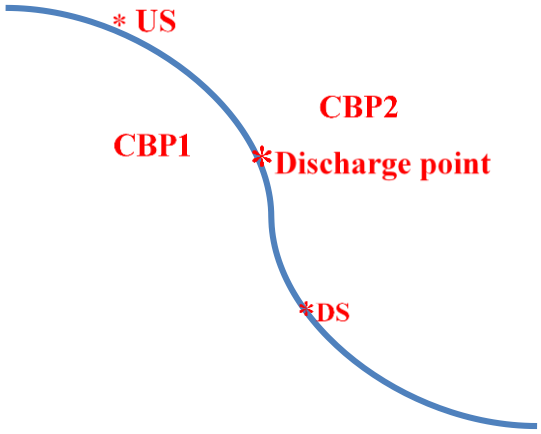

Figure 1: The water sampling points of the adjacent stream.

2.3. Data collection

2.3.1. Secondary data sources

Fundamentally, construction input manufacturers' data that include CBPs were searched from different stakeholders using official letter communications and visiting of websites. To this matter, several publicly mandated sectors such as Customs Authority of Ethiopia, Ministry of Trade and Industry of the country, Sub city Administrations and Personnel were contacted to gain access to relevant information. Fortunately, list of them and their attributes were collected from the Addis Ababa Environmental Protection Authority (AAEPA).

Scientific and technical reports were also accessed through various means and were reviewed for possible synthesis on the state of the art in concrete production and its lifecycle, consumption and their associated environmental concerns from a global to local scale.

2.3.2. Key informant interview

Six key informants were selected using purposive sampling techniques in order to gather detailed information through face-to-face interviews. The criteria of selection for informants were largely based on their closeness to CBPs. Interviews were taken place using questions prepared beforehand, which were crucial to the objective of the study and to support the information gained through the observation.

2.3.3. Observational checklist

Before site visits, observation checklists were prepared that contain relevant points with regard to CBPs in order to observe the different environmental characteristics of the study area. In this regard, the urban rivers

adjacent to CBPs were observed ideally sectioning the upstream, mid-stream and downstream contexts. The soil and other topographic context were also observed. In fact, the CBPs batching operation that include the input materials and chemicals were also included.

2.3.4. Physicochemical water sample analysis

Triplicate water/wastewater samples were collected from the three sampling points as indicated in figure one. All the water samples were collected using clean polyethylene plastic bottles, which were labeled on-site appropriately. The samples were stored in an ice box and got transported to AAEPA laboratory for analysis. Selected physicochemical parameter were analyzed according to accepted standard methods within the premises of the AAEPA laboratory that are comparable to other international standards (APHA; WWA & WEF 1999). The pH was tested using electrometric method, which was determined using a glass electrode and a reference electrode according to the USEPA-NERL: 150.1 (LaSota et al.). Sulfate was analyzed using Sulfaver 4 method, which was also accepted by USEPA for specified concentration range (Hatch Method 8051) and using DR/2010 (Mbui et al. 2016). The nitrate concentration was determined using spectrophotometry in a cadmium reduction method (Cortas and Wakid 1990). This colorimetric method involves the contact of nitrate in the sample with cadmium, which will then form red color in steps and the color is later measured at a wavelength of 543 nm using DR/2000 instrument. The total chemical oxygen demand (COD) was determined using USEPA Reactor Digestion Method (Xia et al. 2018).

2.4. Data analysis

The questionnaire and the checklist were cleaned and tested before data were collected. Experimental data were also obtained from AAEPA lab premise. Data were then entered into spreadsheet and mostly presented in a descriptive statists approach.

3. Results and discussion

3.1. Concrete production in Addis Ababa city: profile, environmental hygiene and mandate contexts

CBPs' appears environmentally critical and also demands consideration for its wider public health impacts. The sites of production evidenced solid pile of concrete waste that are thrown into adjacent streams and do block them and grey wastewater is forming large pool down slope of the site. The issue of concern with this particular construction input supplier begins with the issuance of the permit in the country or city. Though technically appears relevant, the offer of work permits to commission the CBPs in the capital of Ethiopia is not solely performed by the AAEPA. Permit is issued by different institutions at different levels, from federal to local, which may have a stake in the construction, trade and industry sectors. Though issuing permits and regulating pollution limits is environmentally critical, the mandate for permits is very much diffused (Novotny 2002). In the interest of uncovering the local context of large scale and static batch concrete production in the city, the current study managed to acquire quantitative information on such process plant profiles where their permit is offered (Chen et al. 2019, Jahiel 1998), by the AAEPA and therefore results may not be exhaustive. Interestingly, the acquired quantitative information is broader by scope in the context of construction works as it ranges from quarry sites to installation of batch concrete and asphalt making plants.

According to AAEPA there are around 470 construction input suppliers, including those batch concrete makers in and around the city since 2008. Indeed, some of them got revoked their permits, mainly due to the maturity of period as it has to be renewed. The construction input suppliers are categorized based on their product or service into white stone, black stone, crushers, sand, filler gravels, and the batching plants. The quarry sites

for these suppliers' range between one to 600 m^2 by occupancy and all are exclusively private entities. Based on the data accessed, it appears that the distribution of CBPs in the capital appear to be unequal most being concentrated mainly into two sub cities; Bole and Akaki Kaliti. This might be associated with the nearness to raw materials, the availability of land area and the relative intensity of constructions activities undergoing (**Table 2**). In fact, these two and Lemi Kura sub cities are not confined territorially and have better access to minerals and land.

Table 2. Lists concrete batch and asphalt plants and their location in Addis Ababa

CBPs	**Sub city**	**District**	**Year established**	**Shape area (m^2)**
CBP1	Akaki	11	2020	37948
CBP2	Bole	12	2020	10394
CBP3	Akaki	9	2022	26820
CBP4	Bole	12	2022	19502
CBP5	Bole	13	2020	16849
CBP6 (asphalt plant)	Bole	12	2022	28820
CBP7	Bole	12	2022	30646
CBP8	Lemi Kura	14	2022	14271

The installations of CBPs in the city are dated typically between 2020 and 2022, which is recent and the expansion of such emerging plants follows the construction boom. From table two it can be noted that, including the asphalt plant, majority of the batch plants are located within district 12 of Bole sub city where the current study has focused to delve into the environmental and public health implication with them, mainly focusing on urban stream pollution.

Table two also indicated that there exists a total of 9 CBPs built within three sub cities of Addis Ababa, occupying an area of 185248.8 m^2. This booming of large scale CBPs is unprecedented even in the country, demanding attention on the determination of its contexts in view of its public and environmental health whereby the issue of sustainability may ultimately be at stake. In this regard, a holistic overview of concrete mass production from the quarry to construction sites is necessary and that will be addressed in the life cycle section. The locations of those particular CBPs in a district within Bole sub city are indicated figure two with red line. As it can be seen from the figure the industries are concentrated to a certain corner of the city (Figure 2).

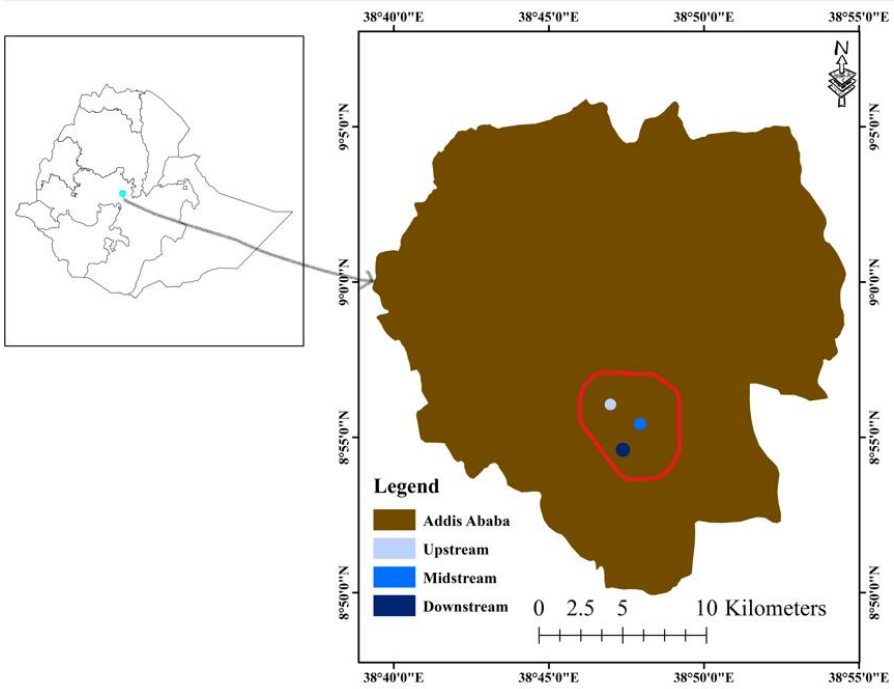

Figure 2: Map showing the area where the studies CBPs are located and water samples were collected (made using ArcGis tool).

It is unfortunate that most of the CBPs are located adjacent to seasonal and year-round streams. In fact, a passerby can just feel the extent of cement-mud run over by concrete carrying truck, the pile of concrete debris on river ways, all associated with the towers of CBPs. The detail of the environmental context of such plants is addressed in the section where checklist-based elucidation is depicted.

Thus, given the fact that the number of CBPs swiftly rose in just couple of years and there is diffused responsibility by the regulatory or competent authority, the operational conditions of those plants need urgent attention. If left as it is, greying and cementation of the urban streams where CBPs are adjacently located will not only be inevitable but also already become visible. These and the inner-city's streams wherein domestic wastes are channeled will make the city bad for living in. As a matter of fact, there lacks clear policy regarding wastewater management that does agree with the city's development policy. Indeed, lacking such environmental and public health conscious monitoring will undoubtedly result in failure to achieve the sustainable development goals that pushes for sound water and wastewater management and the lifecycle approach as stipulated by the United Nation (Sachs et al. 2019).

3.2. Life cycle perspective on concrete production and its environmental footprint

At first, it is difficult to say it life cycle since it is obvious that the produced concrete does not return back to either its parent component or rejoins the plants for reproduction thereby closing the loop. Rather, the fate of the produced concrete is either being a building or it is either dumped somewhere after demolishing. However, such analysis of input output conditions in concrete production are important for process improvements thereby explaining the environmental impacts of such process.

As a composite material of construction, concrete production in batch plants involves the use of water, cement, sand, gravel and additives for a batch of product. The aggregates, the belt conveyor as well as hoppers for the

raw materials are depicted in figure five, which is a photography taken during the field study on one of the CBPs in Addis Ababa. In the case of Addis Ababa, these raw materials are delivered by tracks and after the process specialized ready-mix concrete trucks deliver the mix to construction sites (Figure **3**).

Figure 3: A typical stationary concrete batch plant located in Addis Ababa.

Past studies indicated that concrete batching plants are normally located around a city so as to reduce transportation time and the average CO_2 emission due to batching is estimated at 0.0033 t CO_2-e/$m^3$of concrete produced (Flower and Sanjayan 2007). Of those models for life cycle assessment (LCA), include the one based on standard ISO 14044/2006, the Greenhouse gases, Regulated Emissions, and Energy use in Technologies (GREET) model is common and its derivation or extension are reported for concrete production LCA study such as in the United States by Hottle and colleagues that is published in 2022 (Hottle et al. 2022).

Indeed, in realizing cleaner production systems, studying the lifecycle of products has helped indicate where to intervene so to reduce environmental footprint while maintaining the desired quality of the product. This has become more interesting recently due to the need for an environmentally sustainable design. In this regard, studies have already determined the contribution of different processes and inputs for a portland cement-binded concrete production where the aggregate emission ranged 0.29 - 0.32 t CO_2-e/m^3 (Flower and Sanjayan 2007). Several studies have also identified environmental impacts related to concrete production of which particulate matter, as well as metals, dioxins, and furans resulting from fuel combustion are associated. In terms of water footprint, around 10% of the world's industrial water withdrawal is due to concrete production (Hottle et al. 2022).

Thus, based on literature it has already been determined that the following consumptions are applied per ton of concrete production:

- 143.94 kg to 150.73 kg of portland cement
- 89.90 liters to 101.85 kg of water

- Additive (Super-plasticizer for concrete that is considered as 1.5% of the amount of cement
- 14 kWh of electricity

Within the circular economy perspective, recycling of the construction and demolition wastes does not only reduce the extraction of the virgin raw natural materials and reduce waste generation and disposal, but also it showed huge energy saving. In fact, around 60% of the environmental impact of concrete production comes from the cement production in a cradle to grave scenario. Such reuse scenario has brought a significant reduction in fresh water ecotoxicity (63%) and water consumption reduction by 17%. Therefore, replacing raw materials, reuse of wasted same materials, changes in process efficiency and a dedicated policy as well as legislation appeared crucial for reducing impacts of concrete batch production based on LCAs (Cerchione et al. 2023).

3.3. Physicochemical characteristics of the concrete production wastewater

Wastewater samples were collected during the study to have an insight on the physicochemical nature of the concrete production wastewater, which is just released into the gorges of the stream where lastly it accumulates down slope forming a pool of the visually grey and grease-containing concrete wastewater. Table 3 presents the results of the quality analysis conducted within the premises of the AAEPA. From the table it appears quite clear that the pH (11.4±1) the total chemical oxygen demand (10700±870), SO_4^{2-}(1325±60), and NO_3^{2-} (17.5±0.2) concentrations measured in mg/l were incomparably high in mid-streams where the plants are located.

Table 3. Concrete production wastewater laboratory test results in different stream locations

Parameters	**Unit**	**Sampling locations**		
		Upstream	**Midstream**	**Downstream**
pH	-	7.35±(0.3)	11.4±(1)	11.06±(0.3)
Sulphate (SO_4^{2-})	mg/l	4±(0.2)	1325±(60)	300±(40)
Nitrate (NO_3^{2-})	mg/l	1.3±(0.02)	17.5±(0.2)	14±(2)
Chemical oxygen demand (COD)	mg/l	7±(0.2)	10700±(870)	30±(0.8)

As a matter of fact, the physical and chemical nature of concretes emanate from the characteristics of the inputs from which a batch of concrete is synthesized. That goes even back to the quarry sites property where excavating and crushing of stones, scraping the sands downstream and usually the Portland cement production. The pH of concrete wastewater is highly alkaline whereby Ca $(OH)_2$ is formed following the hydration of cement-mortar, a plastering composite (Mori et al. 1992, Wang et al. 2020). pH changes in water bodies obviously brings the changes in aquatic chemistry and the associated problems (Stumm and Morgan 2012). For instance, an increase in pH can result in the mobilization of metals' species in rivers and streams while altering their bioavailability and toxicity potentials (Foldvik et al. 2022). In fact, such phenomenon is associated with the death of living things in rivers that include fish. Indeed, for a normal aquatic functioning of rivers and streams the desired pH ranges between 6.5-8.5 (Scholz et al. 2011). Based on the result of this study, the upstream pH falls within the normal range.

The sulfate and nitrate concentration increase can also be associated with some organic pollution as well as inorganic ones. Unfortunately, such pollution of urban streams is compounded by the lack of connections to municipal services resulting in an unsafe water supply, sanitation and hygiene conditions. Since CBPs are

located adjacent to urban streams and underdeveloped areas of the city, they are not covered with municipal services. The employees in those plants as well as visitors may dispose wastes and perhaps excrete in the open field and in those stream gorges. Further, due to the blockage of the urban stream courses by concrete debris, the velocity of the stream flow and its surface are significantly diminished resulting in poor dilution capacity.

3.4. Checklists-based site survey of the concrete batch plants

A glimpse on the current status of CBPs, especially those located within Bole sub city of the capital has been conducted voluntarily and with pictorial evidences. The checking list includes variables of concern such as identifying problem related to site selection for those CBPs, noting the extent of destruction of the urban streams and the public health concerns basing expert views. The impression of the current batching practice is undoubtedly undesirable from an eco-centric perspective as it can be seen from the figures four and five. Indeed, sustainability is a concern in terms of the deterioration of the environmental resources that include water and sand for the same industry as well as other unrelated uses. The fact of the matter is that the leftover concrete, defective batch products, ready mix concrete delivery tracks as well as mixing and batching vat washing wastewater are simply discharged into the stream resulting in the cementation of the stream from its bed. Such cement conquest resulted in gray-dying of the streams where part of the natural hydrologic cycle is even possible interrupted and also exacerbating evaporation of the water as the surface area of the stream bed is artificially extended due to such dumping. Indeed, it has already been reported already that concrete is among the most damaging materials made by humans (Cooke et al. 2020).

Figure 4: A photographic view of one of the streams encroached by CBPs and its volume of water and color from upper side (Left) and the pool of concrete wastewater down stream of it (Right).

The public and environmental concerns do not end there; concrete batching also releases chemicals with the wastewaters. Even though < 5% by composition, admixture compositions that include accelerators, plasticizers and retarders constitute some of the eco-sensitive chemicals such as calcium chloride, calcium nitrate, sodium nitrate, pigments, lignosulfonate, and sodium gluconate. Hence, the release of such constituents into water ways will not be without damage. It has already been reported that concrete can interfere with the biogeochemical processes that occur in aquatic environments (Cooke et al. 2020).

Within an estimated length equivalent of a football field, three CBPs are located within district 12 of Bole sub city of capital that are owned by different companies where the occupancy time of the plants is different but very briefly in a span of two years. The two are just sited on each side of one of the rivers where the earliest one is located distances away and adjacent to the other stream. Such serial of establishments within a short distance in two years' time where two to three, largely seasonal, rivers flows does not just tell the demand for concrete to support the booming construction industry but also it informs about the need to pay attention, as early as possible, to the undesirable public and environmental consequences therein. Given the poor practices of post project realization environmental impact monitoring practices in the developing world, including Ethiopia, the graying of blue and green ecosystems is inevitable. Such local acts may not only bring local problems as the effect touches one of the global concerns-the integrated water resources management.

The picture in figure five was blue (left) before the establishment of an adjacent CBP and now has turned not to ice white but to concrete white (right). This evident environmental impact needs attention and corrective measure like restoring the topography and the river channel and ultimately the stream itself. As the country has provisions to expand ecotourism on one side and the concrete industry is imposing such kind of impacts, there need to be a coordinated and clear development policy based action. In fact, concrete wastewater has to be treated (de Paula et al. 2014) before discharge and this should be a primary task for the regulators to ensure if such industry do treat the wastes they release.

Figure 5: A photograph of surface change of an encroached urban stream, which is a year apart and the cemented gray layer is the place where stream used to flow (Right).

3.5. The key informant interview

In order to access technical and regulatory information several batch concrete production industry related institutions have been approached, especially those found in the two sub cities of the CBP locations, for possible key information interview. Unfortunately, the local administration staffs that are in charge of regulating such kind of industry and even personnel in charge of such regulatory and permit issuance activities such as those in the "Minerals" department did not have idea about CBPs and their EPHIs. Some were even being amazed by the orientation provided during field activities about CBPs. Ultimately, based on proximity to the subject of the study, six people were selected purposively. The selectees were three people from AAEPA, one from Bole sub city, one from Yeka sub city and one from the community adjacent to two CBPs studied. Table four summarized the major issues presented and the respective responses of those key informants.

Table 4. Presents the responses from the key informant interviews to selected questions regarding CBPs

Key question asked	**KIL***	**Key response**
Regarding major waste generated by the CBPs	AAEPA	Dust, wastewater and solid waste, light, alkaline water, excess noise, aggregate waste discharged to land and water
	Community	Dust, especially some time before, sediment
	Sub city	Aerosol, washed out cement and mixture
Common uses of urban streams	All	Sanitation like washing clothes, agricultural uses like farming and cattle watering, bathing, drinking and cocking
If any of them noted any change on streams nearby CBPs		Yes=4 (one from AAEPA, three from community and sub cities) No=2 (all from AAEPA
If the informants do think that CBP effluent can have EPHIs	ALL	Yes (n=6)
If there is any experience regarding effect fro question 4	ALL	Yes=1 (AAEPA) No=2 Reserved/do not know=3
If they do think CBPs release the wastes directly into urban streams without any treatment		Yes =4 (two from AAEPA) No=0 Reserved/do not know =2

KIL= key informants' location

Few have also described on the subsequent question that asks to explain the changes made to urban streams due to CBPs, one respondent from the community and one from AAEPA have explained it well. The later has technically explained the existing condition citing the dumping of sediments and construction materials into the urban stream gorges. The informant from the community nearby has told the real experience that people had been bathing, cattle watering, collecting grass, and even sand earlier times. But after CBPs came into operation, that all services of the streams ceased, noting that currently clear water is not flowing.

The key informants, especially from AAEPA, have criticized the current waste management practices by the CBPs and have expressed their concern for the environment. Furthermore, the community side witnesses dust particles have been engulfing visible nearby inhabitants and the church nearby for the reason the community is unaware until recently it stops. Yet, dust and cement particles are mostly there following loading unloading trucks movements.

Viewing at the range of the responses, it appears that the extent of being informed or aware about CBPs is so varied and that may prove the fact that there is still lack of participative decision making in issuing permits to those process plants during impact assessment study stages. This can result in uncoordinated action thereby hampering the interest with an environmentally conscious sustainable city realization. Relatively and as the position is expected, the respondents from the AAEPA are better aware of the magnitude of problem and the existing environmentally unfriendly practice by the CBPs. However, it also appeared that the same respondents missed to recognize the fact that the same organization was authorized to such mandate.

4. Conclusion

The existing operating conditions and hence the environmental performance of CBPs in Addis Ababa are environmentally unfriendly; the environmental health impact is evidenced by the complete alteration of fluvial

systems that needs urgent attention. The CBPs are producing massive solid and liquid waste that is large enough to clog the streams and form instead large ponds of grey cement-containing wastewater conquering the urban and perhaps vital streams to the level of distraction of natural environmental processes. The diffused and unclear responsibility and mandate of the regulatory sector has to be rectified as there is no clear mandate even to issue permits to those CBPs considering at least their environmentally unfair location. Clearly, the CBPs deteriorated the quality of urban streams, formed lagoon of concrete wastewater alarming the need for clear mandate as well as operational and accountability policy. Competent personnel within concerned regulatory or administrative body have to be there. Even, engaging the communities living around such sites should have involvement in either preliminary assessment or the continuous monitoring and evaluation of CBPs. Given the alarming deteriorating effects of CBPs in the city area, mapping the green infrastructure and ecosystem conditions and thereby determining the status as well as projecting the effect is very much important. Clear and specific state policy regarding the management of industrial wastes, including CBPs is demanding. Further in-depth study to elucidate the long-term environmental impact of CBPs that include the hydrogeological phenomena has to be studied.

Conflict of Interest

The authors declare that the review was conducted in the absence of any commercial or financial relationships that could be construed as a potential conflict of interest.

Author Contributions

GDG conceived the idea, crafted and drafted the manuscript. SJA reviewed and added more on the manuscript. EDW co-crafted & reviewed the manuscript.

Funding

There was no any source of funding for this research.

Acknowledgments

The current study would not have been realized without the kind of contribution such as internet, journals, books and library space by the Addis Ababa University.

Data availability

All data are included in the manuscript.

References

APHA; WWA & WEF, A. P. H. A. W. W. A. A. W. E. F., 1999. Standard methods for the examination of water and wastewater. *Solids.* USA: Amer Public Health Assn, 7.

AWOKE, A., *et al.* 2016. River water pollution status and water policy scenario in Ethiopia: raising awareness for better implementation in developing countries. *Environmental management,* 58, 694-706.

BABOR, D., PLIAN, D. and JUDELE, L. 2009. Environmental impact of concrete. *Buletinul Institutului Politehnic din lasi. Sectia Constructii, Arhitectura,* 55(4), 27.

BARROW, C., 2006. *Environmental management for sustainable development.* Routledge.

BEYENE, A., *et al.* 2009. Urban impact on ecological integrity of nearby rivers in developing countries: the Borkena River in highland Ethiopia. *Environmental monitoring and assessment,* 153, 461-476.

CERCHIONE, R., *et al.* 2023. Life Cycle Assessment of Concrete Production within a Circular Economy Perspective. *Sustainability,* 15(14), 11469.

CHEN, Q., WOOD, M. and ZHAO, J. 2019. Case study of the Tianjin accident: Application of barrier and systems analysis to understand challenges to industry loss prevention in emerging economies. *Process Safety and Environmental Protection,* 131, 178-188.

COOKE, S. J., *et al.* 2020. Overcoming the concrete conquest of aquatic ecosystems. *Biological Conservation,* 247, 108589.

CORTAS, N. K. and WAKID, N. W. 1990. Determination of inorganic nitrate in serum and urine by a kinetic cadmium-reduction method. *Clinical chemistry,* 36(8), 1440-1443.

DE PAULA, H. M., DE OLIVEIRA ILHA, M. S. and ANDRADE, L. S. 2014. Concrete plant wastewater treatment process by coagulation combining aluminum sulfate and Moringa oleifera powder. *Journal of Cleaner Production,* 76, 125-130.

DELIGIANNIS, V. and MANESIS, S. 2008. Concrete batching and mixing plants: A new modeling and control approach based on global automata. *Automation in Construction,* 17(4), 368-376.

DEMISSEW, A. 2020. Assessment on Cement Production Practice and Potential Cement Replacing Materials in Ethiopia. 12, 22-28.

FLOWER, D. J. and SANJAYAN, J. G. 2007. Green house gas emissions due to concrete manufacture. *The International Journal of Life Cycle Assessment,* 12, 282-288.

FOLDVIK, A., *et al.* 2022. Effects of Episodic Exposure to High-pH Water on Survival of Atlantic Salmon Eggs and Juveniles: Results from Laboratory and Field Studies. *Environmental Toxicology and Chemistry,* 41(3), 771-780.

GAGG, C. R. 2014. Cement and concrete as an engineering material: An historic appraisal and case study analysis. *Engineering Failure Analysis,* 40, 114-140.

HOTTLE, T., *et al.* 2022. Environmental life-cycle assessment of concrete produced in the United States. *Journal of Cleaner Production,* 363, 131834.

JAHIEL, A. R. 1998. The organization of environmental protection in China. *The China Quarterly,* 156, 757-787.

KARR, J. R. 1999. Defining and measuring river health. *Freshwater Biology,* 41(2), 221-234.

KIM, T., TAE, S. and CHAE, C. U. 2016. Analysis of Environmental Impact for Concrete Using LCA by Varying the Recycling Components, the Compressive Strength and the Admixture Material Mixing. *Sustainability,* 8(4), 389.

KOROSO, N. H., LENGOIBONI, M. and ZEVENBERGEN, J. A. 2021. Urbanization and urban land use efficiency: Evidence from regional and Addis Ababa satellite cities, Ethiopia. *Habitat International,* 117, 102437.

LASOTA, D. E., *et al.* Laboratory Manual for Chemical Analyses of Public Drinking Water.

LEAL FILHO, W., *et al.* 2020. Reviewing the role of ecosystems services in the sustainability of the urban environment: A multi-country analysis. *Journal of Cleaner Production,* 262, 121338.

LEMLY, A. D. 1997. Risk assessment as an environmental management tool: considerations for freshwater wetlands. *Environmental management,* 21(3), 343-358.

LIU, C. and LIU, X. 2008. Healthy river: Essence and indicators. *Acta Geographica Sinica,* 63, 683-692.

LUNDY, L. and WADE, R. 2011. Integrating sciences to sustain urban ecosystem services. *Progress in Physical Geography,* 35(5), 653-669.

MA, X., *et al.* 2022. Exploring the relationship between urbanization and water environment based on coupling analysis in Nanjing, East China. *Environmental Science and Pollution Research,* 29(3), 4654-4667.

MALMQVIST, B. and RUNDLE, S. 2002. Threats to the running water ecosystems of the world. *Environmental conservation,* 29(2), 134-153.

MBUI, D., *et al.* 2016. The state of water quality in Nairobi River, Kenya. *Asian Journal of Research in Chemistry,* 9(11), 579.

MCMICHAEL, A. J. 2000. The urban environment and health in a world of increasing globalization: issues for developing countries. *Bulletin of the world Health Organization,* 78, 1117-1126.

MENBERE, M. P. and MENBERE, T. P. 2019. Industrial wastes and their management challenges in Ethiopia. *Institutions,* 11(8), 1-6.

MONDAL, S. and PATEL, P. P., 2022. Incorporating Hydromorphological Assessments in the Fluvial Geomorphology Domain for Transitioning Towards Restorative River Science—Context, Concepts and Criteria. *Fluvial Systems in the Anthropocene: Process, Response and Modelling.* Springer, 43-75.

MORI, T., *et al.* 1992. Interactions of nutrients, moisture and pH on microbial corrosion of concrete sewer pipes. *Water Research,* 26(1), 29-37.

MULATU, D., HABTE, L. and AHN, J. W. 2018. The Cement Industry in Ethiopia. *Journal of Energy Engineering,* 27(3), 68-73.

NOVOTNY, V., 2002. *Water quality: diffuse pollution and watershed management.* John Wiley & Sons.

OZLU, M. O., *et al.* 2015. Ethiopia-Urbanization review: urban institutions for a middle-income Ethiopia. *Washington, DC: World Bank Group*.

PANDEY, B. and GHOSH, A. 2023. Urban ecosystem services and climate change: a dynamic interplay. *Frontiers in Sustainable Cities,* 5.

PDO, P. S. D. O., 2001. Concrete Pouring of Three Gorges Project Sets World Record. *https://web.archive.org.*

PHONG, L. 2015. The relationship between rivers and cities: influences of urbanization on the riverine zones–a case study of Red River zones in Hanoi, Vietnam. *WIT Transactions on Ecology and the Environment,* 193, 27-43.

RANTA, E., *et al.* 2021. Urban stream assessment system (UsAs): An integrative tool to assess biodiversity, ecosystem functions and services. *Ecological Indicators,* 121, 106980.

RAQUEL CALAPEZ, A., *et al.* 2023. Unveiling relationships between ecosystem services and aquatic communities in urban streams. *Ecological Indicators,* 153, 110433.

SACHS, J. D., *et al.* 2019. Six transformations to achieve the sustainable development goals. *Nature Sustainability,* 2(9), 805-814.

SAVENIJE, H. H. and VAN DER ZAAG, P. 2000. Conceptual framework for the management of shared river basins; with special reference to the SADC and EU. *Water policy,* 2(1), 9-45.

SCHOLZ, N. L., *et al.* 2011. Recurrent die-offs of adult coho salmon returning to spawn in Puget Sound lowland urban streams. *PLOS ONE,* 6(12), e28013.

SMITH, J., PEARCE, B. D. and WOLFE, M. S. 2013. Reconciling productivity with protection of the environment: Is temperate agroforestry the answer? *Renewable Agriculture and Food Systems,* 28(1), 80-92.

SPEED, R. A., *et al.* 2016. A framework for strategic river restoration in China. *Water International,* 41(7), 998-1015.

SRINIVASAN, S., O'FALLON, L. R. and DEARRY, A. 2003. Creating healthy communities, healthy homes, healthy people: initiating a research agenda on the built environment and public health. *American journal of public health,* 93(9), 1446-1450.

STUMM, W. and MORGAN, J. J., 2012. *Aquatic chemistry: chemical equilibria and rates in natural waters.* John Wiley & Sons.

TAYLOR, K. G. and OWENS, P. N. 2009. Sediments in urban river basins: a review of sediment–contaminant dynamics in an environmental system conditioned by human activities. *Journal of Soils and Sediments,* 9, 281-303.

TERFA, B. K., *et al.* 2019. Urban expansion in Ethiopia from 1987 to 2017: Characteristics, spatial patterns, and driving forces. *Sustainability,* 11(10), 2973.

UN ENVIRONMENT, 2017. A framework for freshwater ecosystem management. United Nations.

UN HABITAT, U. N. H., 2013. *State of the world's cities 2012/2013: Prosperity of cities.* Routledge.

WANG, J., *et al.* 2020. Test and simulation of cement hydration degree for shotcrete with alkaline and alkali-free accelerators. *Cement and Concrete Composites,* 112, 103684.

WANGAI, P. W., BURKHARD, B. and MÜLLER, F. 2016. A review of studies on ecosystem services in Africa. *International journal of sustainable built environment,* 5(2), 225-245.

WIERING, M. and ARTS, B. 2006. Discursive shifts in Dutch river management:'deep'institutional change or adaptation strategy? *Living rivers: trends and challenges in science and management,* 327-338.

XIA, J., *et al.* 2018. Hydrologic and water quality performance of a laboratory scale bioretention unit. *Frontiers of environmental science & engineering,* 12, 1-9.

XIU, Y., *et al.* 2022. Spatial–Temporal Variations of Water Ecosystem Services Value and Its Influencing Factors: A Case in Typical Regions of the Central Loess Plateau. *Sustainability,* 14(12), 7169.

YOHANNES, H. and ELIAS, E. 2017. Contamination of rivers and water reservoirs in and around Addis Ababa City and actions to combat it. *Environ Pollut Climate Change,* 1(116), 8.

Selection of Appropriate Sanitation Systems and Technology Options for Urban Context: A case of Kombolcha Town, Ethiopia

Seid Endris[1], Tewodrose Desale[1],*, Tigist Yimer[1], Almayehu Ali[1], Anteneh Yayeh[1], Nurye Mohammed[1] and Metafet Asmar1[7]

[1]Wollo University, Kombolcha Institute of Technology; P. O. Box 208, Kombolcha, Ethiopia;

*Corresponding Author: tewodrose0933@gmail.com

Abstract

Sustainable sanitation provision is challenging developing countries, especially sub-Saharan countries. Among those low-income sub-Saharan countries, Ethiopian towns and cities struggles with poor sanitation problems. The main objective of this research was to assess and select appropriate sanitation options for urban context of the town of Kombolcha, based on a comprehensive analysis of technical, environmental, social, economic, and institutional criteria. A multi-criteria decision analysis (MCDA) was used to assess and rank technology options to determine the most suitable solution for Kombolcha City. To gather information on the state of urban sanitation, a variety of methods has been employed, such as surveys, interviews, focus groups, observations, and document analysis. In this study, 243 households were approached which was a 97.94% response rate. Based on the result of our survey there were mostly five types of household toilets technologies in Kombolcha Town. These technologies included simple pit latrine with a slab which is 38.6%, cistern flush toilet (1.5%), pour/manual flush toilet (6.5%), VIP latrine (33.2%), and pit latrine without slab (20.2%). Similar ketenas or Kebeles (the smallest administrative unit within a town or city, typically functioning as a local government or community division) form were merged into groups. Consequently, 4 clusters of Kebeles were identified for the study with similar characteristics for sanitation technology option adaptation or intervention. The final weights of the selected criteria during pairwise comparison were environmental (37.3%), health (38.7%), technical (11.6%), economic (8.1%) and socio-culture (4.3%). Based on those main criteria the selected possible technology option for cluster 1 was “Pour Flush toilet connected to Twin Pits”, for cluster 2 “Pour flush toilet + sink and shower + watertight septic tank”, for cluster 3 “Flush toilet + sink and shower + simplified sewerage system” and for cluster 4 “Flush toilet + sink and shower + septic tank + solid free sewer system”. Moving forward, we recommend implementing pilot projects to test the selected sanitation technologies in the identified clusters. This will help evaluate their feasibility and effectiveness in improving urban sanitation. Collaboration with local government, sanitation experts, and community stakeholders will be crucial for successful implementation.

Keywords: Multi-Criteria Decision Analysis, Sanitation Technology, Pairwise Comparison

1. Introduction

Access to sanitation is considered a fundamental human right, rather than a luxury, for every individual. Adequate sanitation is widely recognized as the most crucial factor in public health, accessible to the global community (Velkushanova et al., 2021). The world still faces significant challenges in achieving adequate sanitation coverage for all. In 2017, the World Health Organization (WHO) estimated that 2.3 billion people lacked access to basic sanitation services, and 892 million people still practiced open defecation; consequently, the sanitation crisis remains a global concern (WHO & UNICEF, 2017). According to the CSAE et al., (2017) only 28.9% of Ethiopians had access to improved sanitation facilities. The situation is worse in rural areas,

where 34% of the population practice open defecation compared to 6% in urban areas. Sewerage connections are limited in urban areas, ranging from 0.4% to 6.6%, while there are no sewerage connections in rural area (Strande et al., 2014). The lack of institutional homes, shared responsibilities among authorities, unclear implementation approach, underfunding, and shortage of treatment facilities have all contributed to the country's poor sanitation coverage and increasing problems with environmental sanitation and sewage treatment (WHO & UNICEF, 2017)

Urban sanitation is a complex and multidimensional challenge that requires careful consideration of various factors, such as population density, land availability, environmental impacts, social preferences, economic costs, institutional capacities, and health risks (Hastuti et al., 2021). However, many urban areas lack adequate sanitation services and infrastructure, leading to poor hygiene, pollution, disease outbreaks, and reduced quality of life (Naznin, 2017). Sustainable sanitation provision is challenging developing countries, especially sub-Saharan countries. Among those low-income sub-Saharan countries, Ethiopian towns and cities struggles with poor sanitation problems. Ethiopia's sanitation problems stem from low priority, poverty, lack of resources, unclear institutional framework, and responsibilities (UNICEF/WHO, 2015).

However, there hasn't been much research on how to choose the best sanitation options in Ethiopian metropolitan areas, specifically the main issues and future possibilities in various urban slums. Therefore, it's imperative to offer strategies for choosing the best sanitation technologies for a specific community. Policymakers and responsible individuals can therefore offer potential answers for better and sustainable accomplishment by choosing the proper sanitation solutions for metropolitan settings. Therefore, the goal of this study was to determine the most environmental, technical, socio-culture, health and economic friendly sanitation option for Kombolcha City while considering a variety of sustainability criteria, such as social acceptance, technological and physical viability, economic and institutional considerations, as well as the preservation and improvement of both human health and the environment. The limitation of this study is the reliance on a single urban area (Kombolcha), which may not fully represent the diversity of sanitation challenges in other Ethiopian towns or regions with different socio-economic conditions. Additionally, while the study employed multiple data collection methods, including surveys, FGDs, and KIIs, the findings are based on qualitative assessments and may be influenced by participant biases. Moving forward, we suggest the implementation of pilot projects to test the selected sanitation technologies, especially in the identified clusters, to evaluate their feasibility and impact on improving urban sanitation. Collaboration with local government bodies, sanitation experts, and community stakeholders will be essential for successful implementation.

2. Methods

2.1 Study Area

The study was conducted in Kombolcha town which is located in South Wallo Zone of the Amhara Region, north-central part of Ethiopia (**Figure**). The town is about 377 km north of Addis Ababa (capital city of Ethiopia) and 505km from Bahr Dar City, the Amhara region capital The Kombolcha town Administration reports that the population of the town has increased to 143,637 as of 2018/19, including both rural and urban kebeles (the smallest administrative unit within a town or city, typically functioning as a local government or community division). Of this population, about 23 percent lives in rural areas and 77 percent in urban areas. The estimated population of the urban kebele is around 110,654, comprising of 50,860 women and 59,794 men. In terms of the age structure of the urban population of the city, 65.4% of the population is under the age of 15-64, 29.6% under the age of 14 and 5% over 65 years. Thus, the proportion of dependency due to age is 29.6% for children and 5% for elders. Thus, the age-dependency of the community is up to 34.6 percent (Kombolcha Town administration, 2018). The altitude ranges from 1842-1915 m above sea level. The mean annual rainfall varies from 725.1 mm to 1361.6 mm and the mean annual temperature varies from 18.7 to 20.9°C (Abegaz & Abera, 2020).

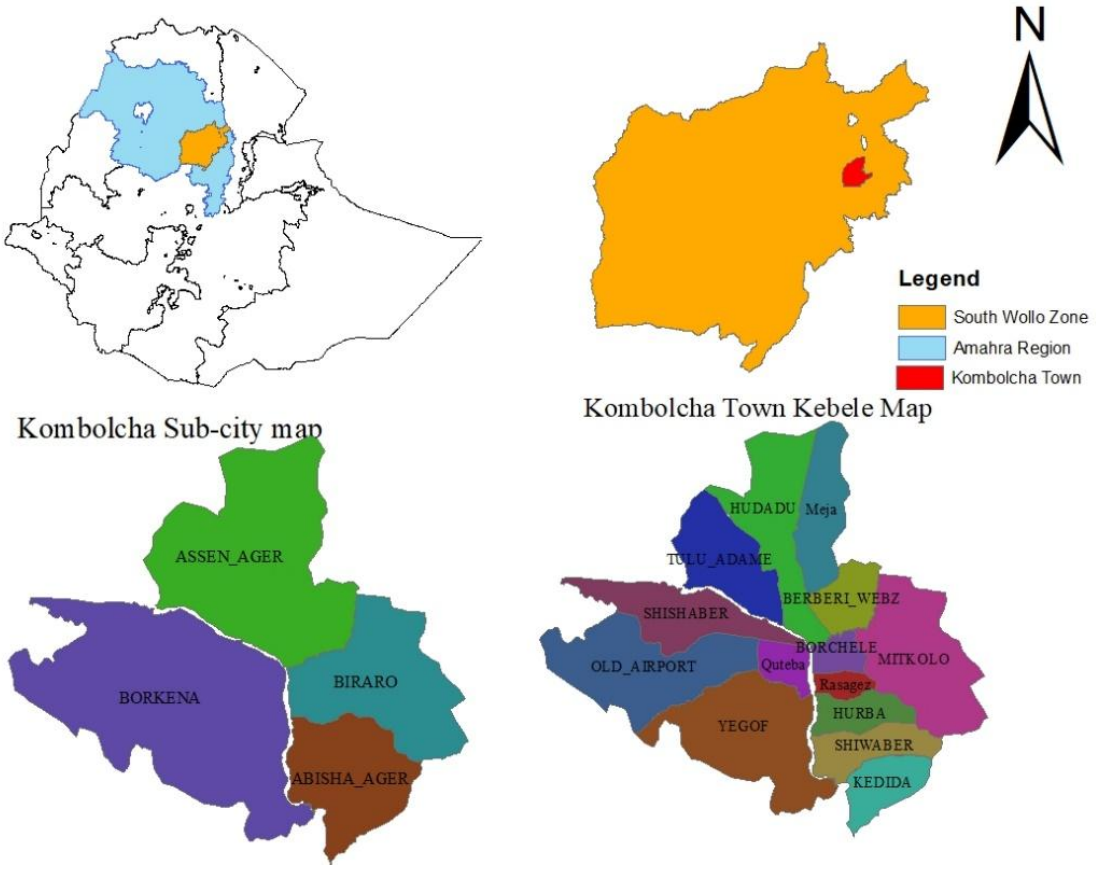

Figure 1: Location map of Kombolcha town

The housing conditions of the town fall under kebele rental, kuteba (tenants who live in government-owned houses or townhouses, often within urban settings), private rental and owner-occupied housing categories. The number of rental Kebele houses which is occupied by low-income households is about 379. The remaining number of private, kuteba and condominium houses are counted about 7722, 931 and 1545 respectively (Kombolcha Town administration, 2018).

A study conducted by Endris et al., (2024), shows that there are five different types of household toilet technologies used in Kombolcha town. These include cistern flush toilets, pour/manual flush toilets, Ventilated Improved Pit latrine (VIP), pit latrine with a slab and pit latrine without a slab. The research showed that the highest percentage of respondents, which was 56.4%, used a simple pit latrine with a slab. The remaining technologies were used as follows: cistern flush toilet (2.1%), pour/manual flush toilet (19.8%), VIP latrine (11.1%), pit latrine with slab (10.7%), and pit latrine without slab (10.7%). As of now, there is no updated data available on the toilet technology used in Kombolcha town, except for the 2007 census conducted by the CSA (CSA, 2007) that recorded the types of toilet facilities in the housing units. The survey revealed that out of the 15,261 housing units in Kombolcha town, 3505 (23%) did not have any toilet facility. Of the remaining, 861 (5.6%) had private or shared flush toilets, 1760 (11.6%) had VIP latrines, and 9129 (59.8%) had pit latrines. According to the definition provided by the health office department, unimproved toilet facilities are traditional latrines that are open pits and lack a roof (plastic roof), temporary/non-permanent wall, or wood slab, or any slab at all.

2.2. Research Design

The first step involved examining global trends and challenges in urban sanitation, particularly those relevant to developing countries. Partnering with Kombolcha officials, data on the city's current sanitation infrastructure, demographics, and environment were gathered. This data was essential for identifying potentially suitable sanitation systems such as sewers, on-site options, or decentralized treatment. Various technologies within these systems were evaluated based on their treatment efficiency, environmental impact, social acceptability, economic feasibility, and long-term sustainability (Fid et al., 2023). A multi-criteria decision analysis (MCDA) was used to assess and rank these options to determine the most suitable solution for Kombolcha City.

2.3. Data collection

The study employed two quantitative methods (a housing unit survey and field observation) alongside three qualitative approaches: key informant interviews (KII), focus group discussions (FGD), and a literature review. Conducting a literature review was essential to ensure the research was well-informed and comprehensive. Sources for the literature included relevant journals, conference proceedings, academic theses, reports from organizations and donors, official records, and maps from the administrative areas of Kombolcha town, as well as insights from key informants and sanitation professionals in the region, including resources from the Susana website (https://www.susana.org/en/#)". In this study, key informants of the Kombolcha Water Supply And Sanatioin System (WSSS) sanitation department head, Kombolcha town health department sanitation officer, and masons participating in toilet construction were consulted in person and via email based on the informant's available time to talk.

To complement the understanding gathered from the literature review, the research employed focus group discussions (FGDs) with various stakeholders in Kombolcha town. These FGDs strategically included community representatives, local government officials (policymakers), masons engaged in toilet construction, and sanitation experts. This approach facilitated a richer understanding of the sanitation challenges by fostering open discussions within each group, the FGDs revealed shared ideas and viewpoints. Besides these, two focus group discussions (FGD) were held with express from health office, sanitation office, urban planning and community representatives. The FGD topics also focused on obtaining data related to household practices, service levels, past interventions, risks, and other issues associated with fecal sludge management services.

Field observations involved targeted visits to key locations like existing sanitation facilities and areas facing sanitation challenges. Researchers meticulously documented the physical state of infrastructure, user behavior, and environmental factors impacting sanitation practices. Visual aids like photographs and videos were captured to support analysis. On the other hand, in a qualitative study, purposive sampling was conducted for stakeholder identification and key informant interview process. Appropriate checklists were established and 20 key informant interviews (KIIs) were conducted with different stakeholders from the government and non-government organizations.

The structured questionnaire for the household survey included open and closed-ended and fixed alternative questions. The structured questionnaire has taken a minimum of 40 minutes for each household survey.

Some of the data to be collected with the household questionnaire include:

- Current Sanitation situation: Understanding the types of sanitation households currently have and their level of satisfaction with them.
- Awareness of Options: Assessing households' knowledge of the different types of sanitation options available in their area.
- Factors Influencing Choice: Identifying the factors households consider when choosing a sanitation option, such as Cost, availability, ease of use, etc.
- Access and use: Examine all the challenges that households may face in accessing or using sanitation facilities.
- Interest in Alternatives: Measuring households' interest in learning more about alternative sanitation options that may be available to them.

2.4. Sampling Approach

The study employs stratified multistage sampling (probabilistic), and purposive sampling (nonprobability), methods to select representative samples and generate pertinent information from the target area households. Multistage sampling is an appropriate method to extract the desired information for the intended objectives of the study. Based on those considerations in addition to the purpose of the study and population size, a 95% confidence level, ±5% precision, and 80% proportion variability were adopted and the sample size was also determined using a proven scientific statistical formula (Singh et al., 2011).

n=([Np(1-p)])/([(e^2/(Z^2*(N-1) +p*(1-p)]))

Where, n = the required sample size, N = Total number of housing units

Z = standard normal deviation at the required confidence level that corresponds to a 95% confidence interval equal to 1.96, e = the level of statistical significance (Allowable error) (0.05), P = the proportion in the targeted population estimated to have characteristics being measured (from previous studies or studies in other comparable countries i.e. 0.8 from (Neilson, 2011).

According to Kombolcha town (2024), the total number of housing units is **17313**. Thus, based on the above formula, n=243 has been drawn for a reliable minimum sample size of households. Currently, Kombolcha town is divided into four Sub city with 14 administrative Kebeles which include both previous rural and urban kebele.

2.5. Characterization of the town and identification of homogeneous areas

Identifying homogenous areas within Kombolcha town to select suitable sanitation system technologies for each distinct area context based on three key contextual factors: physical, urban, and socioeconomic. By employing this multi-faceted approach, the research has identified homogenous areas within Kombolcha town based on their shared physical, urban, and socioeconomic characteristics. It has then recommended suitable sanitation system technologies for each specific cluster. This approach ensured that the selected sanitation systems were technically sound, culturally appropriate, financially sustainable, and feasible to implement and maintain in each area.

2.6. Determination of sanitation systems and technology options

Various sanitation system technologies are available and can evolve over time. These technologies can use improved on-site sanitation systems, small-piped systems (simplified and solid-free sewer), or conventional sewerage systems. The selection of the sanitation system and technologies in this study was based on a multi-faceted approach considering population demand, environmental constraints, local context, population density, and existing sanitation practices Through the combination of literature reviews on effective sanitation systems in similar developing countries and comparative analysis of case studies, this research identified potential sanitation system and technology alternatives. Finally, these alternatives have been evaluated for each distinct area or identified clusters within Kombolcha town, ensuring the chosen system(s) best suit the specific environmental and social contexts of each area.

2.7. Development of Main Criteria and Indicators (sub-criteria) list

A preliminary list of criteria and indicators was developed based on a review of international scientific literature that has been used to evaluate sanitation systems and technologies from previous similar studies and site visits to the identified homogenous area of Kombolcha town (**Table 10)**.

Table 10: - Criteria used for selecting technology option

Criterion	Sub-criterion	Objective
Environmental	Resource recovery	Maximize resource recovery (e.g., water, nutrients)
	Energy consumption	Minimize energy consumption required for operation and treatment process.
	Impact on ecosystem	Minimize negative impact on the surrounding environment (e.g., soil, water bodies).
Technical	Robustness	Ensure the system can function reliably under various operating conditions and withstand potential disruptions
	Complexity	Favor simpler systems with lower operation and maintenance demands
	Suitability	Select a system that is technically suitable for the local context (e.g., climate, soil conditions)
Economic	Capital costs	Minimize the initial investment required to construct and install the sanitation system.
	Operation and maintenance cost	Minimize the ongoing costs associated with operating and maintaining the system.
	Benefits	Maximize the long-term economic benefits associated with the system (e.g., reduced healthcare costs, improved productivity)
Socio-cultural	Acceptability	Ensure the sanitation system is culturally appropriate and accepted by the local community.
	Social equity	Promote equitable access to the sanitation system for all members of the community.

	Willingness to construct	Encourage community participation and willingness to contribute to the construction and management of the system
Health	Health benefit	Maximize the positive health outcomes associated with the sanitation system (e.g., reduced disease transmission).
	Pathogen exposure	Minimize the risk of exposure to harmful pathogens through the sanitation system.

2.8. Application of MCDM for appropriate sanitation technology selection

The research leveraged Multi-Criteria Decision Making (MCDM) techniques to select the most suitable sanitation technology for Kombolcha town, following the comprehensive understanding gained from the literature review, focus group discussions, and field observations. This MCDM approach involved defining a set of key criteria based on Kombolcha's specific context. These criteria encompassed factors like technical feasibility, environmental impact, social acceptability, economic viability, and community health requirements. Each criterion was further operationalized into measurable indicators to facilitate an objective evaluation process. Building upon this foundation, a shortlist of potential sanitation technologies was created, considering both established options and innovative solutions identified through the research. An appropriate MCDM technique, such as the Analytic Hierarchy Process (AHP), was then employed.

3. Results and Discussion

3.2. The Existing Town Context

I. Soil, Geology and Ground water characteristic of the area

The soil map of the study area is covered by sandy silt and clay soils as Food and Agricultural Organization (Food and Agricultural Organization, 2011). Sandy silt and clay soils are dominantly covered the area at 67.7 and 32.3% respectively and sandy silt with gravel content is more permeable than clay soils. The alluvial–colluvial sediments deposited at the Kombolcha town which dominantly covers the study area are characterized by clay, sand, gravel, pebbles, and boulders derived mainly from the escarpments and rivers. The alluvial deposits in the study area show alternating layers of sands, gravel, and clay implying that there are multiple layer aquifers from the well log data. The alluvial sediment is heterogeneous and their porosity and permeability make them are moderate to high (1.55 to 3.64 m/day) in the study area with hydraulic conductivity falling under ranges of 10^0 to 10^1m/day (Sn and Davis, 2003). Basaltic rocks are found in the northern, and southern part of the study area. These basalts are moderate to highly fractured in several places, and has hydraulic conductivity of (0.0247 to 0.704 m/day). Therefore, it has low to moderate permeability and productivity with hydraulic conductivity fall under ranges of 10^{-1} to 10^0m/day (Sn and Davis, 2003).

II. Socio-demographic characteristics of the study participants

In this study, 243 households were approached which was a 238 (97.94%) response rate. The majority of the respondents were head of household which were 191 (80.25%) of the respondent. In addition to this most of the respondents (76.05%) were owner of the housing units, however 23.95% of the respondents was rental (including Kuteba and Condominium houses) in the selected housing units. Housing condition of households 206 (86.55%) privet type with privet residents and about 32 (13.45%) were Apartment building (in multi-store building like Condominium houses) have at least one form of toilet facility

Table 11: - Population density of clustered area

Cluster No	Kebele Grouping	No. Population	Area coverage (km^2)	Population Density
1.	Yegof, Mitkolo, Kedida & Tuluadame	6959	32.12	216.5
2.	Berberie wenz, Meja Rasagez, Hurba, Shiwaber & Hudadu	51354	24.343	2109.6
3.	Borchele Kebele	6948	1.472	4720.1
4.	Quteba Kebele, Shishaber & Old Airport	29285	19.804	1478.74

NB: The estimated number of populations for each cluster in **Table *11*** is based on the housing units of land lords or house owners. The floating population and tenants are not considered. If they are considered the floating and tenants the population will be 2 or more times the above result; so, this figure does not consider the Kombolcha town population.

III. Existing Sanitation technology Arrangements and its satisfactions of the participants

The household survey results and observations show that 92.02% of the respondents have toilet facilities (private household toilets and shared toilets between two or more rental households in one housing unit), while the remaining 7.98% have access to communal toilet facilities or toilets shared by more than two housing units. Additionally, based on our survey, there were mostly five types of household toilet technologies in Kombolcha city. Additionally based on our survey there were mostly five types of household toilets technologies in Kombolcha city. These technologies included cistern flush toilets, pour/manual flush toilets, Ventilated Improved Pit latrine (VIP), pit latrine with and without slab. Based on observation the highest recorded percentage of respondents was who used simple pit latrine with a slab which is 38.6%. The other remaining technologies were cistern flush toilet (1.5%), pour/manual flush toilet (6.5%), VIP latrine (33.2%), and pit latrine without slab (20.2%) **(**

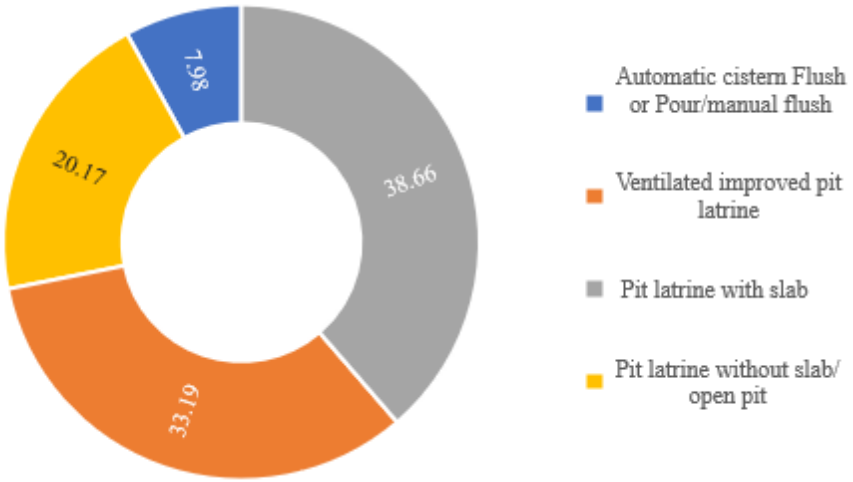

Figure). Most of latrine were found inside the housing compound however the communal toilet was found from 6-15m in the back yard of home. The Anal cleansing materials are Water, paper and tissue paper.

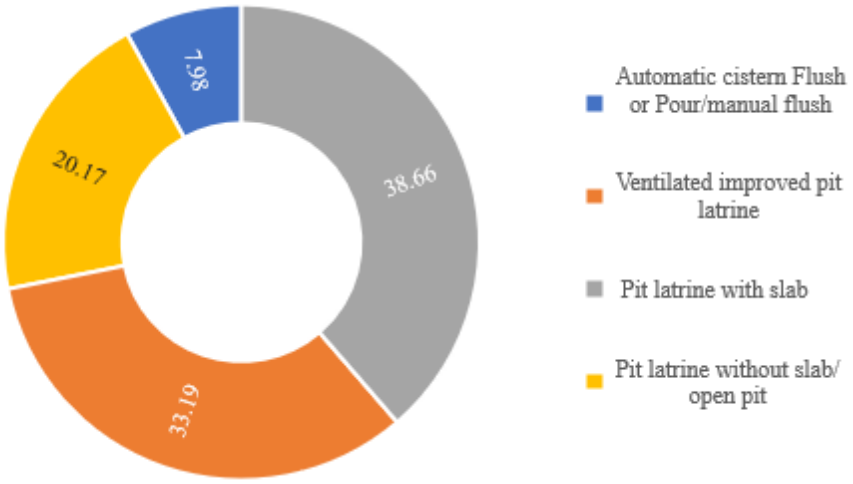

Figure 1: - Toilet facility household currently use

Based on our survey the level of satisfaction of selected technology were 64.7 % satisfied however 35.3% were not satisfied so it needs to upgrade the technology. The users were unsatisfied mostly by Privacy and Cleanliness which is 38.1% and 40.5% respectively. Whereas 14.3 % and 7.1% of unsatisfied users were unsatisfied due to Distance to toilet and Quality of construction respectively. The listed reason of difficulties accessing or using current toilet facility from the survey were dirty, the latrine was full, water shortage for flush, problem of slab and its smell. In the survey, we also assessed the awareness of available sanitation options among households. Results showed that 58.5% of respondents were aware of various toilet technologies, while 41.5% were unaware of alternatives. Factors influencing their choice of toilet facilities included cost, availability of space, and convenience. When asked about their interest in alternatives, 35.3 % of respondents expressed interest in upgrading to more advanced sanitation technologies.

IV. Identification of homogeneous areas or clusters and Key characteristics

The administrative divisions of Kombolcha town have 4 Sub cities and 14 Kebeles, each with population, household, and housing unit data. This study aims to identify or classify similar areas for household survey and selecting the appropriate sanitation system technologies. Similar ketenas or Kebeles in terms of population density, land use composition, soil type, topography, groundwater depth, land availability, land ownership patterns, water usage patterns, economic status, and built form were merged into groups. Consequently, 4 clusters of Kebeles were identified for the study with similar characteristics for technology option adaptation or intervention (**Figure**). Those clusters were identified after reaching an agreement with the land administrative bodies and consultation with experts along with repeated field observation and by collecting and referring the data related to urban, physical, and socio-economic contexts.

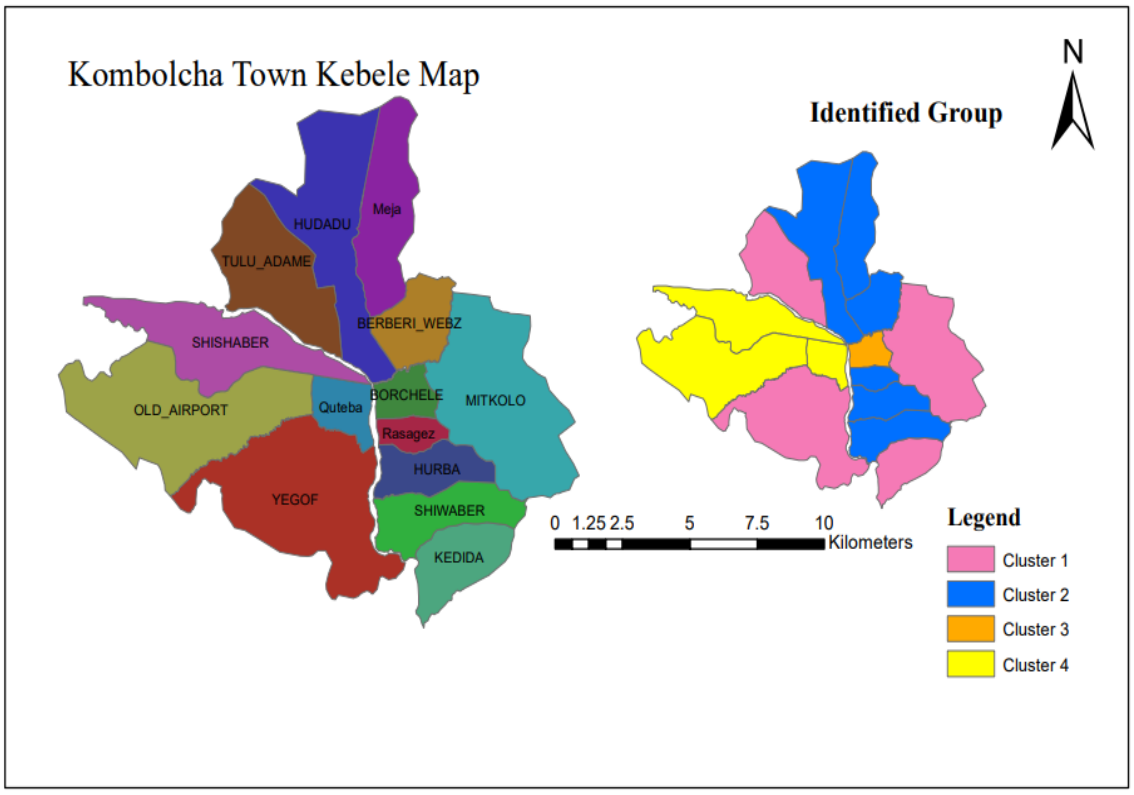

Figure 3: - Identification of areas with similar characteristics

Cluster-1 encompassed the outskirts of Kombolcha town, specifically the kebeles of Yegof, Mitikolo, Kedida, and Tuluadame. These peripheral areas are characterized by scattered settlements with lower population density. Additionally, they have a shallow groundwater table (the depth which is less than 3m), abundant land (reserve area for sanitation system installation > 20 m²), and varied topography with permeable soil. Water access in these settlements is irregular, and sanitation practices often rely on traditional latrines or open defecation and the community has low perceptions of sanitation technology options. Berberie Wenz, Meja, Hudadu, Rasagez, Shiwaber, and Hurba kebeles were similar in physical, urban, and socioeconomic context and categorized as **cluster-2**. This cluster is characterized by a high groundwater table (> 6m average depth), relatively abundant land (200-450 m^2 per landlord or average reserve area for sanitation system installation > 2 m² and < 20 m²), high population density, and mostly flat topography with permeable soil. The water supply usage pattern is in good condition (about 50 l/c/d).

Cluster-3 referred to Borchele kebele only which is characterized by high population density, scarce land availability (reserve area for sanitation system installation < 5 m²), high groundwater table (> 10 m average depth), and varied topography with permeable soil. The water supply usage pattern is in good condition (about 50 l/c/d). **Cluster-4** comprehended the kebeles of Kuteba, Shishaber & Old Airport. This cluster is characterized by high population density, scarce land availability (reserve area for sanitation system installation < 5 m²), relatively low groundwater table (< 15 m average depth), and flat topography with permeable soil. The water supply usage pattern is in good condition (about 50 l/c/d). The existing sanitation technologies in this cluster are mostly septic tanks without outlets having saturated soil for liquid absorption due to frequent infiltration and a high greywater release.

3.3. Appropriate Sanitation systems and technology options for selected Area

The sanitation systems in this study were selected based on a multi-faceted approach, considering population demand, environmental constraints, local context, population density, and existing sanitation practices. Based on the experts sought, CMS Water & sanitation for all Methodological Guides 2015, and case studies from similar contexts, an improved onsite sanitation system has been selected for cluster-1 and cluster-4. Whereas, solid free, and simplified sewer systems have been selected for cluster-2, cluster-3, and cluster-4 (**Table 12**). Solid free sewer systems are more cost-effective due to shallower installation and smaller-diameter pipes. Its key distinction lies in collecting only greywater and a portion of blackwater, which is pretreated at the household level using a septic tank. Whereas simplified sewerage systems collect wastewater like conventional systems but are more cost-effective due to shallower installation and smaller pipes. They collect greywater and blackwater directly, without pretreatment, and transport it to a treatment facility.

Table 12: - Possible sanitation systems for identified clusters

Sanitation systems	Cluster-1	Cluster-2	Cluster-3	Cluster-4
Improved onsite sanitation system	Extremely Feasible	Slightly feasible	Slightly feasible	Moderately Feasible
Solid Free Sewer System	Slightly feasible	Strongly Feasible	Strongly Feasible	Strongly Feasible
Simplified Sewer System	Slightly feasible	Moderately Feasible	Moderately Feasible	Moderately Feasible
Conventional sewerage system	Not feasible	Not feasible	Not feasible	Not feasible

3.4. Sanitation technology options along the sanitation value chain

In this study, the sanitation system technology options along with the sanitation services chain were pre-screened based on the fact sheet from CMS Water & sanitation for all Methodological Guides 2015and Reuter, S., et al. (2022) along with referring different literature concerning sanitation options. This study classifies various technologies for comparison from different categories: user interface and storage, evacuation/transport, and (safe disposal/treatment). Based on the proposed sanitation system described so far, the following sanitation technology alternatives for each cluster has presented as follows:

Possible Technology Options for Cluster 1: **As** cluster 1 is characterized by low groundwater table, permeable soil, and low population density with abundant surface area having varied topography, the possible alternative sanitation technology options are:

1. Ventilated Improved Pit latrine (VIP) + soak away
2. Ventilated Improved Double Pit (VIDP) toilet
3. Urine Diverting Dry Toilet (UDDT)
4. Pour Flush toilet connected to Twin Pits
5. Flush toilet + septic tank + soak away or infiltration trenches

Possible Technology Options for Cluster 2: High groundwater table (> 6m average depth), saturated soil, and densely populated areas with a relatively abundant land or average reserve area for sanitation system installation > 2 m² and < 20 m²) are the characteristcs of cluster 2 where the following technology options can be feasible.

1. Pour flush toilet + sink and shower + watertight septic tank

2. Watertight VIP toilet + sink and shower + solid free sewer system
3. Flush toilet + sink and shower + septic tank + solid free sewer system
4. Flush toilet + sink and shower + simplified sewerage system

Possible Technology Options for Cluster 3: cluster 3 has similar characteristics with cluster 2 except the availability of space is scarce. Hence the possible alternatives are:

1. Pour flush toilet + sink and shower + watertight septic tank
2. Watertight VIP toilet + sink and shower + solid free sewer system
3. Flush toilet + sink and shower + septic tank + solid free sewer system
4. Flush toilet + sink and shower + simplified sewerage system

Possible Technology Options for Cluster 4: This cluster is characterized by low groundwater table, permeable soil, and average population density with a limited surface area having mostly condominiums and Kuteba houses along with flat topography where the following alternative technologies are feasible.

1. Flush toilet + sink and shower + septic tank + soak away or infiltration trenches
2. Flush toilet + sink and shower + ABR + Anaerobic filter + soak away
3. Flush toilet + sink and shower + septic tank + solid free sewer system
4. Flush toilet + sink and shower + simplified sewerage system

In selecting the appropriate sanitation technology for each cluster, we first identified possible technology alternatives based on the characteristics of each cluster. We then organized a kickoff meeting with key stakeholders, including community representatives, health office officials, staff from the Water Supply and Sanitation Office, urban planning officers, environmentalists, and skilled professionals from higher education institutions. During this meeting, we provided a detailed description of each technology option. The experts, through a collaborative ground discussion, used Multi-Criteria Decision Analysis (MCDA) to evaluate and rank the options based on key criteria such as environmental impact, health benefits, technical feasibility, and cost.

3.5. Relative weight of main criteria Using the AHP Method

In this study, both pairwise comparison and surveying methods were used. Seven experts in sanitary engineering, public health, environmental engineering, and social sciences/anthropology were engaged to determine the relative weights of the main criteria and sanitation system alternatives. In addition, FGD was held and participants were selected from local government officials, toilet masons, and community representatives. The experts filled out the matrix independently. In the case of FGD, the researchers guided the discussion by presenting pairs of criteria and indicators, prompting participants to debate and reach a consensus on which one is more important.

Pairwise comparisons were conducted. Each criterion was compared to every other criterion, with judgments made on their relative importance using a scale of 1 to 9 (1 = Equally important and 9 = Extremely more important). Then the importance and the relative weight of each main criterion was determined for all four clusters. Criteria of environmental, Economic, Socio-cultural, Technical, and Health

were compared each other using the pairwise comparison technique of AHP. The individual weightings of the experts, and aggregated group weightings on the main criterion are presented in **Table 4**.

Table 13: - Comparison matrix for criteria in AHP analysis

Criteria	Environmental	Technical	Socio-cultural	Health	Economic
Environmental	1	4	7	1	5
Technical	0.25	1	3	0.25	2
Socio-cultural	0.14	0.33	1	0.143	0.33
Health	1	4	7	1	6
Economic	0.2	0.5	3	0.17	1
Sum	**2.59**	**9.83**	**21.00**	**2.56**	**14.33**

The comparison matrix showing relative importance have been presented in table 4 above which further used to determine normalized Principal Eigen vector with the help of approximation technique. The value of Principal Eigen value (λmax) and consistency index (*CI*) have been estimated as 5.12 and 0.03 respectively. As Five criteria have been considered in the decision, the random consistency index (RI) comes out to be 1.12. The consistency ratio for the present decisions has been computed as **0.027 or 2.7 %,** which is less than 10 %, hence the inconsistency in the decision is acceptable and the weights obtained can be used for selecting technology options.

After normalized the above relative importance of the selected criteria we were get the final weights for those criteria **Table 14.**

Table 14: - Computation of final weights for main criteria

Criteria	Environmental	Technical	Socio-cultural	Health	Economic	**Weight**
Environmental	0.39	0.41	0.33	0.39	0.35	**37.3%**
Technical	0.10	0.10	0.14	0.10	0.14	**11.6%**
Socio-cultural	0.06	0.03	0.05	0.06	0.02	**4.3%**
Health	0.39	0.41	0.33	0.39	0.42	**38.7%**
Economic	0.08	0.05	0.14	0.07	0.07	**8.1%**

3.6. Ranking Sanitation System Technology Alternatives

The final step is where AHP reveals the top contender. To evaluate and rank different options, the weighted score for each option was determined by multiplying its score on a particular criterion by the weight of that criterion. Once the weighted scores for all criteria were obtained, they were summed up for each alternative. The alternative with the highest total weighted score has been identified as the top-ranked choice. This final weight and rank were done after normalized of the data based on average recorded value. From

Table 15 rank data the possible technology option for cluster 1 was option-4 which is **Pour Flush toilet connected to Twin Pits** and second possible option was option-2 which is **Ventilated Improved Double Pit (VIDP) toilet**.

Table 15: - Final weight of technology options and ranking for cluster 1

Technology Options	Criteria					Weighted score	Rank
	Environmental (31.3%)	Technical (11.6%)	Socio-cultural (4.3%)	Health (38.7%)	Economic (8.1%)		
Option-1	0.23	0.12	0.05	0.40	0.08	**0.88**	**5**
Option-2	0.33	0.11	0.04	0.40	0.08	**0.96**	**2**
Option-3	0.44	0.11	0.02	0.26	0.08	**0.91**	**4**
Option-4	0.31	0.12	0.05	0.42	0.08	**0.98**	**1**
Option-5	0.26	0.12	0.05	0.46	0.08	**0.96**	**3**

Option-1* Ventilated Improved Pit latrine (VIP) + soak away

Option-2** Ventilated Improved Double Pit (VIDP) toilet

Option-3*** Urine Diverting Dry Toilet (UDDT)

Option-4*** Pour Flush toilet connected to Twin Pits

Option-5***** Flush toilet + septic tank + soak away or infiltration trenches

The first choice, the Pour Flush toilet connected to Twin Pits is a water-based system utilizing the Pour Flush Toilet (pedestal or squat pan) and Twin Pits to produce a partially digested, humus-like product, that can be used as a soil amendment. This system is suited to peri-urban areas with suitable soil that can continually & adequately absorb the leachate where the groundwater is low.

Based on the result shown on **Table 7** for cluster 2 ranking data, the possible technology option was option-1 which is **Pour flush toilet + sink and shower + watertight septic tank** and second possible also **Flush toilet + sink and shower + septic tank + solid free sewer system**.

Table 16: - Final weight of technology options and ranking for cluster 2

	Criteria					Weighted score	Rank
Technology Options	Environmental (31.3%)	Technical (11.6%)	Socio-cultural (4.3%)	Health (38.7%)	Economic (8.1%)		
Option-1	0.35	0.12	0.04	0.36	0.09	**0.96**	**1**
Option-2	0.33	0.10	0.05	0.37	0.08	**0.94**	**3**
Option-3	0.31	0.12	0.04	0.39	0.08	**0.94**	**2**
Option-4	0.27	0.12	0.04	0.43	0.07	**0.92**	**4**

Option-1* Pour flush toilet + sink and shower + watertight septic tank

Option-2** Watertight VIP toilet + sink and shower + solid free sewer system

Option-3*** Flush toilet + sink and shower + septic tank + solid free sewer system

Option-4**** Flush toilet + sink and shower + simplified sewerage system

From the compared four possible technology option described so far, pour flush toilet + sink and shower + watertight septic tank ranked first and followed by Flush toilet + sink and shower + septic tank + solid free

sewer system. This technology is most commonly applied at the household level. Larger, multi-chamber septic tanks can be designed for groups of houses and/ or public buildings (e.g., condominiums or schools). A septic tank is mostly appropriate where there is a way of dispersing or transporting the effluent. However, in this cluster, there is a high groundwater table and a moderately dense population which means no onsite infiltration is possible. Instead, the septic tanks should be connected to some type of conveyance technology, through which the effluent is transported to a subsequent Treatment or Disposal site.

Like the above description in cluster 3 the viable and possible technology option was option-4 which is **Flush toilet + sink and shower + simplified sewerage system** and also option-3 which is **Flush toilet + sink and shower + septic tank + solid free sewer system** was second possible technology option (**Table 17**).

Table 17: - Final weight of technology options and ranking for cluster 3

	Criteria					**Weighted score**	**Rank**
Technology Options	**Environmental (31.3%)**	**Technical (11.6%)**	**Socio-cultural (4.3%)**	**Health (38.7%)**	**Economic (8.1%)**		
Option-1	0.35	0.11	0.03	0.36	0.09	**0.94**	**3**
Option-2	0.33	0.10	0.04	0.37	0.08	**0.92**	**4**
Option-3	0.31	0.12	0.05	0.39	0.08	**0.95**	**2**
Option-4	0.27	0.13	0.05	0.42	0.07	**0.95**	**1**

Option-1* Pour flush toilet + sink and shower + watertight septic tank

Option-2** Watertight VIP toilet + sink and shower + solid free sewer system

Option-3*** Flush toilet + sink and shower + septic tank + solid free sewer system

Option-4**** Flush toilet + sink and shower + simplified sewerage system

Since this is a cluster characterized by high population density and high groundwater table, the first choice is suitable and appropriate. Simplified sewers can be installed in almost all types of settlements and are especially appropriate for dense urban areas where space for onsite technologies is limited.

The option of Flush toilet + sink and shower + septic tank + solid free sewer system was the first suitable and first ranked technology option for cluster-4 and option-2 which is Flush toilet + sink and shower + ABR + Anaerobic filter + soak away were second alternative technology **(**

Table 18).

Table 18: - Final weight of technology options and ranking for cluster 4

	Criteria					**Weighted score**	**Rank**
Technology Options	**Environmental (31.3%)**	**Technical (11.6%)**	**Socio-cultural (4.3%)**	**Health (38.7%)**	**Economic (8.1%)**		
Option-1	0.34	0.11	0.04	0.33	0.09	**0.91**	**4**
Option-2	0.33	0.12	0.04	0.37	0.08	**0.93**	**2**
Option-3	0.33	0.12	0.04	0.41	0.08	**0.99**	**1**

Option-4	0.26	0.12	0.05	0.44	0.07	**0.93**	**3**

Option-1* Flush toilet + sink and shower + septic tank + soak away or infiltration trenches

Option-2** Flush toilet + sink and shower + ABR + Anaerobic filter + soak away (reuse)

Option-3*** Flush toilet + sink and shower + septic tank + solid free sewer system

Option-4**** Flush toilet + sink and shower + simplified sewerage system

The first technology choice is in its right place because cluster 4 is characterized by its low groundwater table and mostly condominium residents. Mostly on condominium sites, more wastewater is connected to septic tanks and results in frequent filling, even for onsite infiltration the ground becomes oversaturated and contaminated, and wastewater may rise up to the surface, posing a serious health risk.

3.7. Evacuation, treatment, and disposal segment of the sanitation value chain

In this study, great care does have been taken to select the suitable sanitation technology option along the service chain. Moreover, the study more focused on user interface, Collection and Storage segments of the sanitation service chain. For clusters with onsite sanitation system technologies (cluster 1 and 2) need to have pit emptying options. Fortunately, the selected technology option for cluster-1 needs no emptying service since the households use double pit latrine system which enables them to reuse the dried sludge for agriculture. Whereas, for cluster-2 the best technology option is septic tank with regular emptying due to the existence of high ground water table. Consequently, Cluster-2 requires mechanical pit emptying solutions, such as motorized pumps or vacuum trucks. These trucks are equipped with a pump connected to a hose, which is inserted into a tank (like a VIP or septic tank) or pit, allowing sludge to be pumped into the truck's holding tank. This setup is commonly known as a vacuum truck. For densely populated areas with restricted access, various alternative motorized vehicles and machines have been designed. Options like the Vacutug, Dung Beetle, Molsta, and Kedoteng are equipped with smaller sludge tanks and pumps, enabling them to navigate narrow pathways effectively. According to Endris et al. (2024), the municipality of Kombolcha has an 8 m^3 vacuum truck, while Wollo University operates another exclusively for its own use. Due to insufficient municipal services, residents rely on private vacuum trucks, which are not locally available but can be hired from Dessie, a nearby town 23 km away, with capacities ranging from 6–10 m^3.

For clusters 3 and 4 with simplified and solid free sanitation systems, the emptying and transport segment differs. For cluster-3 simplified sewer system, no evacuation or emptying equipment is needed as the faces and gray water transport pipelines. Whereas, cluster-4 with solid free sewer system having (flush toilet + sink and shower + septic tank + solid free sewer system) a combination of on-site sanitation for excreta (septic tank) and a settled (solid free) sewerage system for greywater, it needs a hygienic motorized emptying option as mentioned earlier. As this sludge contains a significant amount of blackwater, there are often high levels of solid matter present. As a result, the first level of treatment aims to extract this solid waste by reducing its pollution load (it then becomes known as treated sludge). However, Kombolcha town currently have an extensive faecal sludge treatment plant. The FSTP consists of solar (unplanted) drying beds with extensive effluent treatment system (waste stabilization ponds). Nevertheless, as reports or studies showed that the FSTP is currently close to malfunctioning due to operational and maintenance related issues. Thus, rehabilitation works and optimization of the treatment components along with monitoring system is recommended.

4. Conclusions

In conclusion, this study developed a framework for assessing and selecting suitable sanitation technologies for the urban context of Kombolcha. Through a comprehensive analysis of technical, environmental, social, economic, and institutional criteria, we aimed to identify appropriate sanitation options for different clusters within the city. The study employed a combination of surveys, interviews, focus groups, observations, and document analysis to gather insights from various stakeholders. Based on these findings, we grouped Kebeles with similar characteristics, such as population density, land use, and socio-economic conditions, into four clusters. Using Multi-Criteria Decision Analysis (MCDA), we ranked sanitation technologies based on the weighted criteria of environmental impact, health benefits, technical feasibility, socio-cultural factors, and economic viability. The selected technologies for each cluster varied: Cluster 1 was assigned "Pour Flush Toilet connected to Twin Pits," Cluster 2 "Pour Flush Toilet + Sink and Shower + Watertight Septic Tank," Cluster 3 "Flush Toilet + Sink and Shower + Simplified Sewerage System," and Cluster 4 "Flush Toilet + Sink and Shower + Septic Tank + Solid-Free Sewer System."

This approach provides a structured method for selecting appropriate sanitation solutions tailored to the unique characteristics of each cluster, offering a potential pathway for improving urban sanitation in Kombolcha. while this study utilized multiple data collection methods, including surveys, FGDs, and KIIs, the findings are based on qualitative assessments that may be influenced by participant biases. To further validate the results and assess the practicality of the selected sanitation technologies, we recommend implementing pilot projects in the identified clusters. These projects will allow for the evaluation of the feasibility and impact of the proposed technologies on improving urban sanitation in Kombolcha.

Author Contributions: S.E. and T.D. conceived and developed the research framework. M.A., T.Y., and A.Y. undertook the data processing and analysis. T.D. and A.A. wrote and revised the manuscript. N.M. supervised and revised the manuscript. All authors have read and agreed to the published version of the manuscript.

Acknowledgments: The research was implemented under a collaborative partnership with Wollo University so the authors would like to thank to these organizations for the financial and other support during this work. We also acknowledge the anonymous reviewers, whose comments greatly improved the paper.

Funding statement: -There is no funding Agency.

Data Availability Statement: Data sets generated during the current study are available from the author on reasonable request..

Ethics statement: This research protocol received approval from Wollo University, specifically from the Kombolcha Institute of Technology's Research and Community Service Directorate Office, in accordance with the relevant guidelines and regulations of Wollo University.

Declarations

Competing Interests: The author declares no competing interests.

Consent to participant: Informed consent was obtained from all individual participants included in the study.

References

Abegaz, W. B., & Abera, E. A. (2020). Climatology & Weather Forecasting Temperature and Rainfall Trends in North Eastern Ethiopia. 1–6. https://doi.org/10.35248/2332-2594.2020.8.262

CSA. (2007). The 2007 Population and Housing Census of Ethiopia. In Mortality, 385.

CSAE, WHO, UNICEF, & World Bank. (2017). Drinking Water Quality in Ethiopia. December, 9–56.

Endris, S., Kebede, A., Assefa, E., Ali, A., & Desale, T. (2024). Excreta flow mapping along the sanitation service chain, a case of Kombolcha town, Ethiopia. Scientific Reports, 14(1). https://doi.org/10.1038/s41598-024-53724-7

Fid, M., Castro, C. P., Matos, R. V., Alves, L., & Matos, S. (2023). Dry Sanitation Technologies : Developing a Simplified Multi-Criteria Decision Analysis Tool.

Food and Agricultural Organization. (2011). Ethiopia Country Programming Framework 2012-2015. Office of the FAO Representative in Ethiopia to AU and ECA, 60.

Hastuti, E., Riyana, R., Joy, B., Supratman, U., & Pamekas, R. (2021). Integrated Community Onsite Sanitation System for Close Loop Faecal Management. 01005, 1–9.

Kombolcha Town administration. (2018). Annual magazine:Summerized reports of Health, education, demography and Housing.

Naznin, F. (2017). Performance Evaluation of Fecal Sludge Treatment Plant at Khulna City and Proposal for Sustainable Development by.

Neilson, T. (2011). King of charcoal: Japanese create new life for dying industry. Inwood Magazine, II(96), 32–33.

Singh, A. S., Masuku, M. B., & Department. (2011). Sampling techniques & determination of sample size in applied statistics research. Inwood Magazine, II(96), 32–33.

Sn & Davis, R. (2003). Groundwater in Fractured Rocks. Wiley and Sons, Inc., New York-London-Sydney.

Strande, L., Ronteltap, M., & Brdjanovic, D. (2014). Faecal Sludge Management. In Faecal Sludge Management. https://doi.org/10.2166/9781780404738

UNICEF/WHO. (2015). WHO / UNICEF JOINT MONITORING REPORT 2012 : PROGRESS ON SANITATION AND DRINKING WATER Draft PR — 29 February 2012 — WHO / WASH / OED approved. February 2012.

Velkushanova, K., Strande, L., Ronteltap, M., Koottatep, T., Brdjanovic, D., & Buckley, C. (2021). Methods for faecal sludge analysis. In Methods for Faecal Sludge Analysis. https://doi.org/10.2166/9781780409122

WHO & UNICEF. (2017). Progress on Drinking Water, Sanitation and Hygiene: 2017 Update and SDG Baseline. In World Health Organization. https://doi.org/10.1016/j.pnpbp.2017.06.016

Reuter, S., Demant, D., Heredia, G., Lüthi, C., Reymond, P., Schertenleib, R., Ulrich, L., & Zurbrügg, C. (2022). Compendium of sanitation systems and technologies for the wider Caribbean region. Bremen Overseas Research and Development Association (BORDA), Bremen, Germany.

Theme 5

Climate Change, Variability and Impacts

Effect of Climate Change on Surface Water availability at Hare Watershed, Rift Valley Basin, Southern Ethiopia

Chekole Tamalew Asnik[1], Behailu Hussien Ibrahim[2] and Aschalew Cherie Workneh*[1]

[1]Faculty of Water Resources and Irrigation Engineering, Arba Minch University, Arba Minch, Ethiopia
[2]Water Resources Research Center, Arba Minch University, Arba Minch, Ethiopia

*Corresponding author: aschalewc@gmail.com

Abstract

Climate change and variability are threatening the availability of water resources worldwide since they can initiate extreme weather events, making water scarcer, and unpredictable. The study was conducted with the primary aim of investigating the impact of climate change on the water availability due to stress of water resource and increasing irrigation water demand of the Hare watershed. Daily data of stream flow, precipitation, air temperature, relative humidity, and sunshine hour were collected from near stations. Two climate change scenarios (SSP 4.5 and SSP 8.5) and climate model (HadGEM2-ES) were used. The performance of the climate model was evaluated for the base period (1971-2000), and future period (2021-2050), and (2051-2080) under SSP 4.5 and SSP 8.5 climate scenarios. The HEC-HMS hydrological model was used to predict water availability in the watershed for present and future time horizons. The model was calibrated and validated for future predictions of streamflow. According to the findings, average monthly precipitation is expected to slightly increase by 0.06mm (2021-2050) and 0.08mm (20512080) for SSP 4.5 and 0.01 (2021-2050) and -0.04mm (2051-2080) for SSP 8.5 respectively. On the other hand, average monthly minimum and maximum temperatures changed over the watershed by 0.407oc (2021–2050) and 0.412oc (2051–2080) for SSP 4.5 and 0.105oc and 0.158oc for SSP 8.5, respectively. The HEC-HMS model was calibrated where sensitive model parameters were identified and the model performance resulted in NSE = 0.62 and R2 = 0.68 during calibration, and for validation, NSE = 0.68 and R2 = 0.72 were obtained. The projected average annual runoff at the outlet of the watershed is expected to increase by 8% as compared to the observed runoff. Therefore, the study highlights the impact of climate change on water resources availability for future water resources development and irrigation water requirement in Hare watershed.

Keywords: *Climate change impact; SSP; HEC-HMS; Water availability; Hare watershed*

1. Introduction

Climate change is a state change that is discernible from variations in its mean and/or variance over an extended period, usually a decade or more (Gebresellase et al., 2022). External forces or human-made processes may be to blame for climate change (Liu et al., 2020); Tramblay et al., 2020). This will have an impact on some hydrological cycle elements, including precipitation (Heo et al., 2015), runoff (Gebre, 2015), and their constituents. Moreover, the spatial and temporal distribution of water resources(Coulibaly et al., 2018) can also shift as a result of climate change (Tabar et al., 2015). Consequently, a rise in variability would raise the likelihood of floods (Dibaba et al., 2020; Kaushal et al., 2017; and droughts Meresa et al., 2022).

Although climate change impacts are wide and vast, many studies have tried to show its extended impact on agriculture (Edamo et al., 2022; (Sun et al., 2019), health, water resources (Kusangaya et al., 2014)) and fisheries (Eide & Heen, 2002) are just a few to mention. Furthermore, water supply issues in several basins

are predicted to get worse due to recent climate change and variance. The management of irrigation and drinking water supply were impacted by the hydrological consequences of changes in climate factors like temperature and precipitation (Belihu et al., 2020), (Obaideen et al., 2022), flood risks (Hagos et al., 2022), and hydropower production (Wasti et al., 2022). Developing countries in general and African nations in particular are undoubtedly among the most vulnerable to the effects of climate change due to their lack of economic, development, and institutional capabilities (Konapala et al., 2020; Fayiah et al., 2020).

Ethiopia is particularly vulnerable to climate change and variability because of its heavy reliance on rain-fed agriculture (Villamizar et al., 2019) and rainfall distribution for food production (Demmissie et al., 2018). Hare watershed is the central role of water resources in the socio-economic fabric of the region, understanding the impacts of climate change on the Hare Watershed is essential for developing sustainable management and adaptation strategies. This research aims to analyze the extent of climate change effects on water availability in the watershed to propose actionable solutions to enhance resilience and ensure water security for present and future generations using the HEC-HMS hydrological model.

2. Methodology

2.1. Description of the study area

The watershed is located near Arba Minch town within the Southern Ethiopian Rift Valley Basin. It covers an area of 182 km², with elevations ranging from 1,200 to 3,482 meters above mean sea level, positioned between latitudes 6°03′ to 6°18′ and longitudes 37°27′ to 37°37′ (Yirgu et al., 2020). The mean annual maximum and minimum temperatures for the lowland and highland regions are 23°C and 14°C, respectively, with an average annual rainfall of 1,050 mm. The land is divided into various agroecological zones, comprising approximately 55.56% Dega, 22.84% Woyna Dega, 11.73% Wurch, and 9.25% Kola whereas the watershed is characterized by two major soil types: cambisols and ferralsols (Yisehak, 2021).

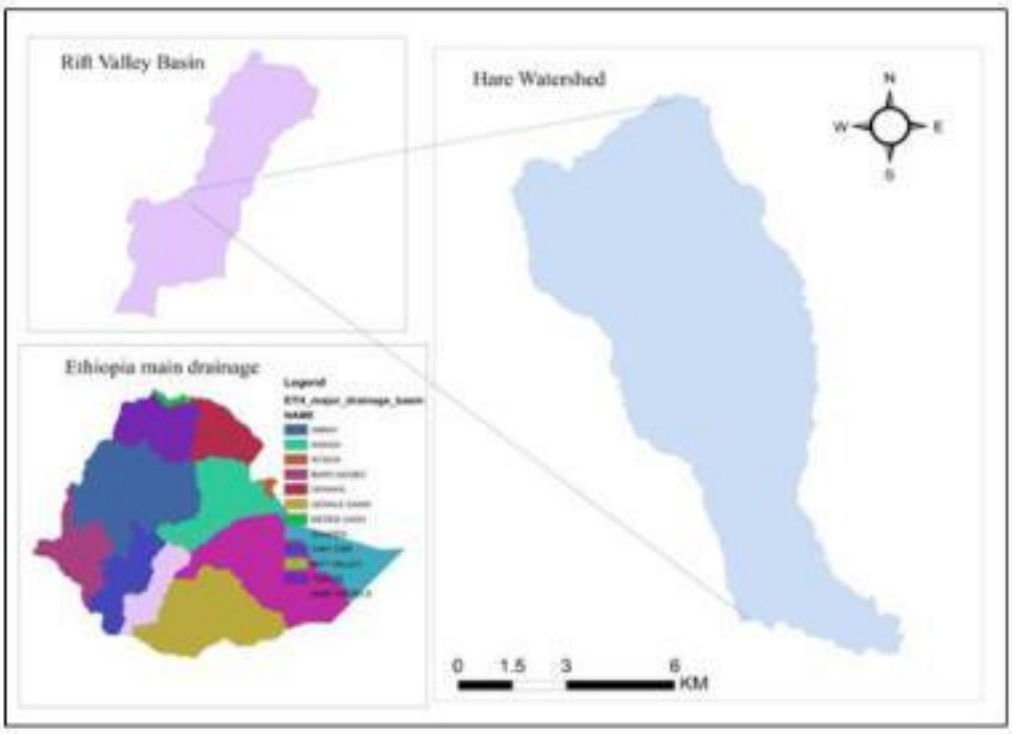

Figure 1: Location map of Hare watershed

2.2. Data collection

The accuracy of the model's input data and its outcomes depended on the reliability of the raw meteorological and hydrological data used. Meteorological data were obtained from the National Meteorological Agency at Mirab Abaya, Chencha, and Arba Minch stations, while hydrological data were provided by the Ministry of Water and Energy, covering the period from 1987 to 2007.

The downscaling process was conducted using the latest version of the Regional Climate Model RCA4, developed by the Centre and adapted from IWMI's climate change experiment. This model considered four RCP scenarios such as SSP2.6, SSP4.5, SSP6.0, and SSP8.5 (San José et al., 2016). However, SSP4.5 and SSP8.5 were specifically used to assess the effects of climate change on the watershed.

2.3. Climate change modeling

To demonstrate statistical linkages between recorded broad-level circulating and local-level climatic variables like precipitation and temperature, downscaling approaches were developed. However, bias correction in a climate model (Tong et al., 2021) is very important before using it for any hydrological model and water resources analysis. For both the SSP4.5 and SSP8.5 emission scenarios, downscaled rainfall and air temperature data for the period 1976-2100 were retrieved in the form of NetCDF (Network Common Data Form) from the spatial grid resolutions of all CORDEX Africa programs.

Various bias correction techniques are employed to reduce errors between observed and simulated historical climate data using statistical quintile factor, distribution quintile mapping, and simple scaling were the common methods to refine the raw climate model outputs. Among those methods, a simple scaling factor was used to downscale GCM outputs of precipitation and temperature for the periods 2031-2060 and 2061-2090 years.

2.4. Evaluating the accuracy of rainfall climate model simulations

Evaluating the accuracy of rainfall climate model simulations is crucial for understanding the reliability of these models in representing real-world precipitation patterns. Here are some methods typically used for evaluating the accuracy of rainfall climate model simulations in the watershed; percent of bias, root mean square error (RMSE), and coefficient of variation (CV) as follows;

$$\text{Bias P}=100*\frac{R_{rcp}-R_{obs}}{\bar{R}_{obs}} \quad (1)$$

$$\text{RMSE}=\sqrt{\frac{\sum_{K=1}^{N}(R_{rcp}-R_{obs})2}{N}} \quad (2)$$

$$\text{CV}=100*\frac{\delta R_{rcp}}{\delta R_{obs}} \quad (3)$$

$$\text{Bias P} = \ 100 * \frac{Rrcp - Robs}{Robs} \quad (1)$$

$$\text{RMSE} = \frac{\sqrt{\sum_{K=1}^{N} (Rrcp - Robs)^2}}{N} \quad (2)$$

$$\text{CV} = \ 100 * \frac{\delta Rrcp}{\delta Robs} \quad (3)$$

Where:
N indicates the analysis period; R denotes the average rainfall value in a certain year subscripts *rcp* and *obs* show the rainfall and temperature amount found from RCP simulation and observation, respectively; δ shows the standard deviation of either the RCP or observed rainfall and temperature data.

2.5. Trend analysis

To ensure an accurate evaluation of the watershed, trends were assessed using Mann Kendall test at a 5% significance level, providing insight into general increasing or decreasing patterns over time. This method facilitates the detection of long-term climatic changes by numerically comparing observed trends with projected future values. 2.7 Climate Change Impact Analysis.

Climate change effects on annual, seasonal, and monthly precipitation, minimum, and maximum temperature were examined by determining the relative changes from the baseline period. The climate impact was assessed using the formula as shown in Equation 4.

$$\% \text{ Change} = \left(\frac{Future(monthly, seasonal, annual) - baseline}{baseline}\right) * 100 \quad (4)$$

2.6. Hydrological model selection

The selection of an appropriate HEC-HMS model depends on the study's objectives (Tassew et al., 2019) such as flood forecasting, water resource management, or long-term hydrologic analysis ensuring the model's capabilities align with the intended application (Gebre, 2015). It also considers watershed characteristics, including size, topography, soil type, land use, and vegetation cover, as well as the availability of data (Sanjay Shekar & Vinay, 2021). By thoroughly evaluating these factors, the HEC-HMS model was chosen as the most suitable option to deliver reliable and meaningful results.

2.6.1. HEC-HMS models

HEC-HMS is a versatile hydrologic modeling tool used to simulate rainfall-runoff processes across diverse geographical regions. The model incorporates components for base flow, channel flow, direct runoff (including overland and interflow), and various other hydrologic structures and inputs. In this study, the watershed was divided into three sub-watersheds, represented by basin models W40, W50, and W60, with areas of 75.7 km², 69.7 km², and 33.8 km², respectively. To evaluate the simulated flow against historical total flow records for these sub-basins, the basin model utilized the outflow element. The choice of sub-basin depends on the specific time frame and the availability of relevant data.

2.6.2. Model sensitivity, calibration, and validation analysis

Model sensitivity, calibration, and validation analysis are critical components in assessing the performance and reliability of a model. A sensitivity analysis was carried out to understand the behavior of the model parameters about the model result (the model hydrograph). Choosing the most sensitive model parameter for model calibration and validation is the major goal of sensitivity analysis. NSE and RVE objective

functions were used to identify sensitive parameters manually by increasing and decreasing the value of one model parameter at a time up to 60% at a 20% interval.

The model's initial run is likely to produce unsatisfactory results because the input data do not accurately reflect the real world (Sanjay Shekar & Vinay, 2021). Some hydrological model parameter needs adjustment to fine-tune the model and increase its reliability. The data from 1990 and 1991 were used for warming, while the period from 1992 to 2001 was used for calibration. The calibration was performed manually through a trial-and-error process, adjusting one model parameter at a time until the simulated streamflow aligned with the observed streamflow.

Testing is required to determine whether parameter values represent the underlying hydrological processes and are not just the outcome of curve fitting. Model validation was conducted during the 2002 to 2007 period to verify calibrated model outputs using independent data sets without further adjustment at various spatial and temporal scales.

2.6.3. Model Performance Evaluation

A variety of researchers have put out various standards for hydrological model performance evaluation criteria. Model efficiency criteria have to be applied to examine the level at which the required performance of the model is achieved. Coefficient of determination (R^2) and Nash-Sutcliffe efficiency (NSE) are the most commonly utilized statistics for reporting for calibration and validation (Khoi, 2015)) and these performance evaluation indices were used.

3. Result and Discussions

3.1. Evaluating the accuracy of climate model simulations

Raw RCP performance shows significant deviations from observed data, especially in certain months with extreme overestimations for May and June, and bias-corrected shows marked improvement, with biases (-0.08), RMSE (0.05), and MAE (0.00) reduced across all months. Corrected values were far more accurate and reliable for projections and used for any hydrological model analysis.

3.1.1. Climatic trends of the base period

The trend for annual rainfall in the base period shows no significant change. This implies that, in the past (base period), rainfall levels were relatively stable, and there wasn't a noticeable shift in rainfall patterns (See Figure 2a). This could suggest a lack of long-term trends in rainfall, such as an increase or decrease, in the observed period. In contrast to rainfall, the minimum and maximum temperatures show a significant increasing trend (See Figure 2b&c). This means that, over the base period, temperatures have been rising consistently, both during the day (maximum) and at night (minimum). This is typically linked to global warming or climate change, where increased greenhouse gases trap more heat in the atmosphere, causing temperatures to rise over time (See Figure 2).

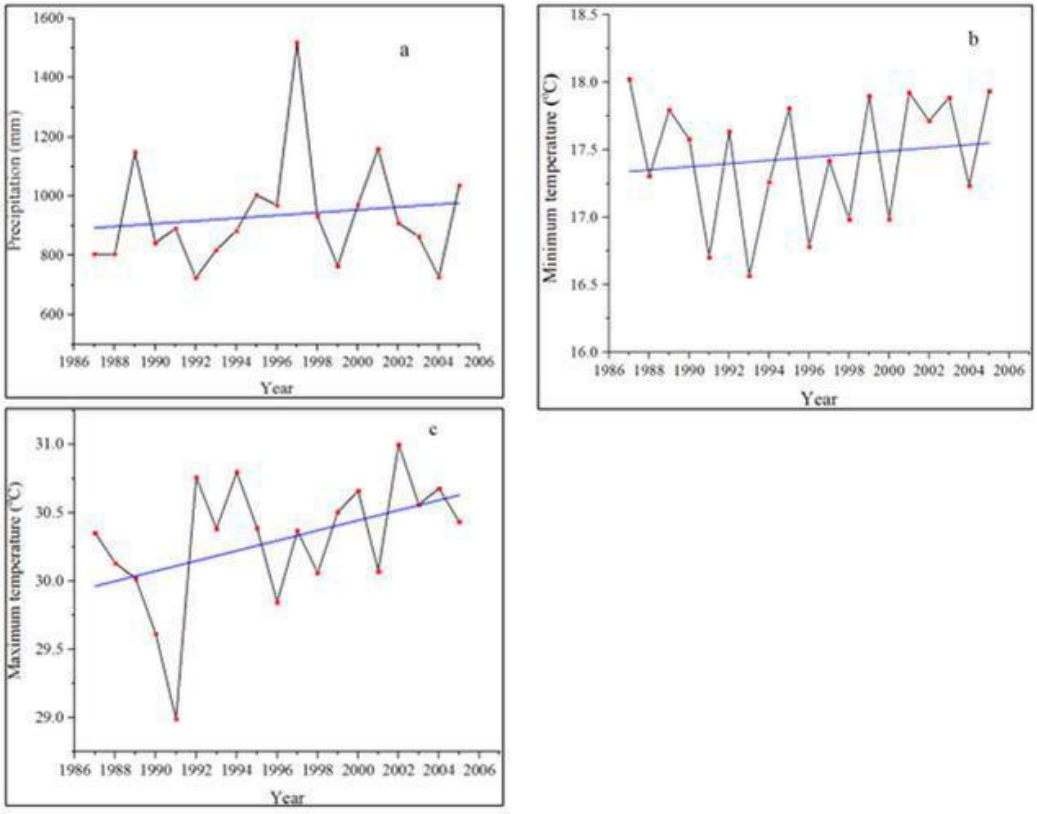

Figure 2: Trends of observed precipitation (a), minimum temperature (b), maximum temperature (c)

3.2. Bias correction results for the base period

Figure 3 shows the downscaled RCP mean months are slightly underestimated for January, February, March, April, November, and December while May, June, July, August, September, and October are overestimated. All annual and seasonal mean precipitation shows overestimated when compared with observed data. Air temperature for both maximum and minimum temperature compared to the recorded temperature for the base period of scenarios is underestimated. The minimum and maximum temperature range for bias-corrected in this watershed increased from 15.83ºC to 19.97ºC and 25.59ºC to 34.21ºC respectively (1987-2005) (See figure 3). This finding suggests that there is a significant amount of uncertainty in hydrological analysis when utilizing the RCP output data without bias correction.

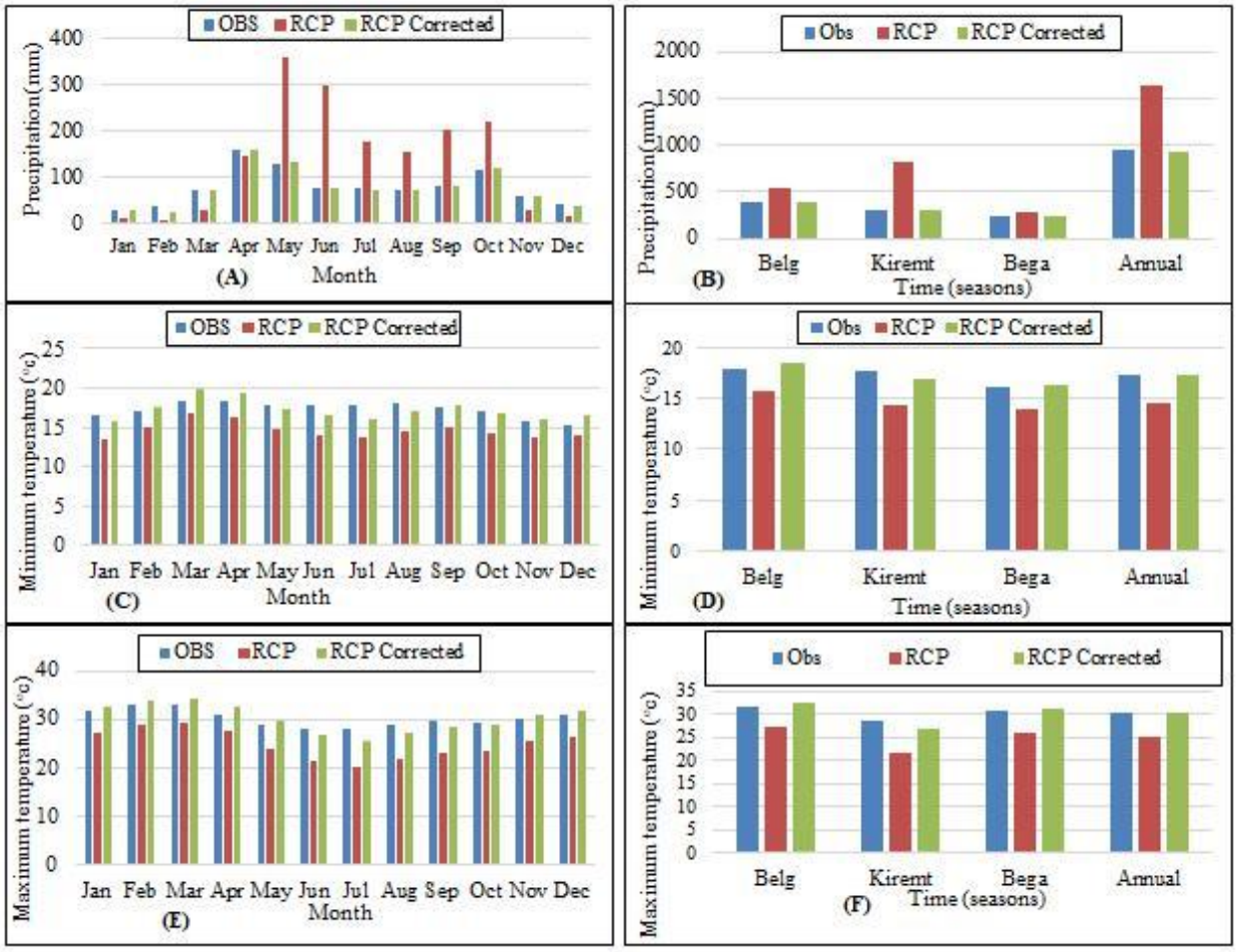

Figure 3: Bias correction results for precipitation, maximum and minimum temperature

3.3. Future climate scenarios developed

After bias correction, three categories of future SSP scenarios baseline period (1971-2000), short term (2021-2050), and long term were formed (2051-2080).

The future climate scenario result shows slight increasing trend for average monthly precipitation as compared to the base period. Average monthly watershed precipitation is expected to slightly increase as compared to the base period by 0.06 mm (2021-2050) and 0.08mm (2051-2080) for SSP 4.5 and 0.01 (2021-2050) and -0.04 (2051-2080) for SSP 8.5 respectively (See figure 4).

As shown in figure 4, monthly average minimum temperature expected to decrease by -5.83ºc and -5.91ºc for SSP 4.5 and -1.5ºc and -2.25ºc for SSP 8.5 scenarios of (2021-2050) and (2051-2080), respectively whereas maximum temperature indicated an increasing trend by 0.44ºc and 0.34ºc for Short term (2021-2050) and long term (2051-2080) for SSP 4.5 and decreasing by -1.31ºc and - 2.07ºc for SSP 8.5 scenario of (2021-2050) and (2051-2080) correspondingly as compared to the baseline period (See figure 4). The SSP 8.5 consistently results in more drastic temperature increases, especially later in the century whereas SSP 4.5 shows smaller but still significant increases, emphasizing the importance of mitigation efforts.

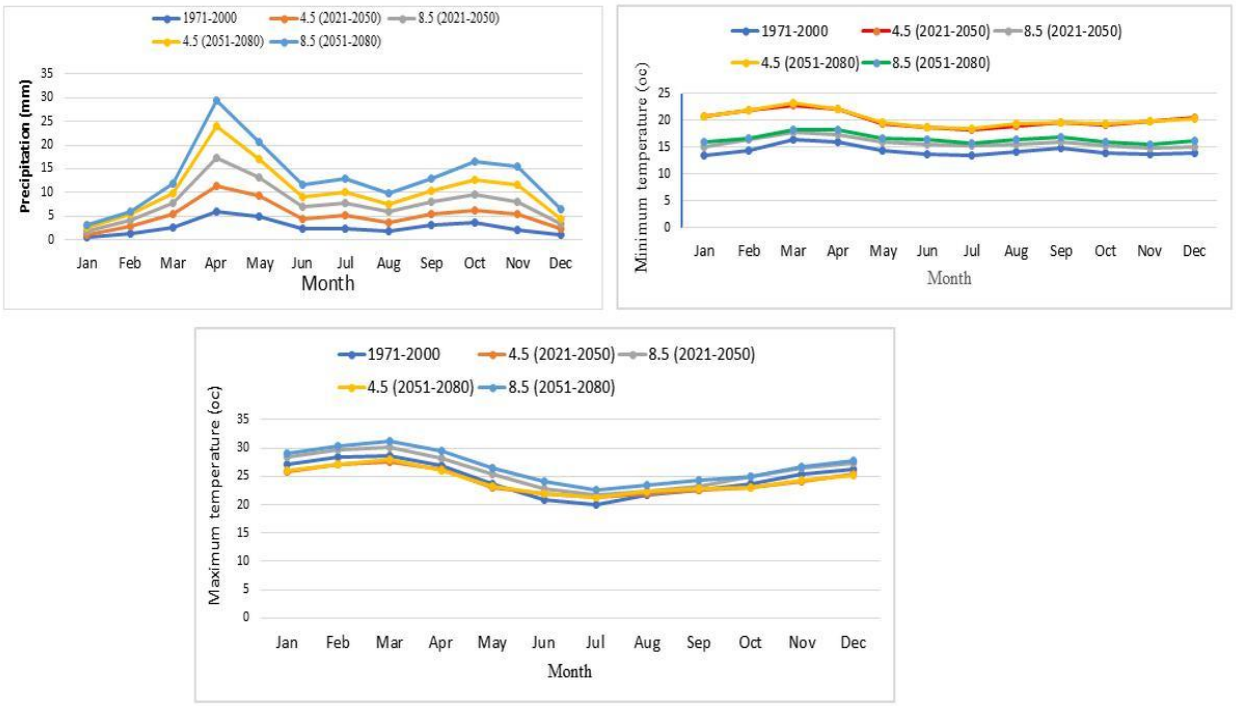

Figure 4: Average monthly precipitation, maximum and minimum temperature for future scenarios

3.4. Climate change impact in the future scenarios

Figure 5 shows the SSP 4.5 scenarios of average monthly precipitation changes for each of the months and the average precipitations will likely change by 2.35% (2021-2050) and -0.65% (2051-2080) for SSP 4.5 over the watershed. For the SSP 8.5 scenario, average monthly precipitation will be changed by 5.7% (2021-2050) and 9.51% (2051-2080).

According to SSP 4.5 scenarios, the average monthly minimum temperature changes over the watershed will be expected to rise by 0.41^{o}c (2021-2050) and 0.412^{o}c (2051-2080) while SSP 8.5 scenarios will increase of 0.11^{o}c (2021-2050) and 0.16^{o}c on average (2051-2080) (see figure 5). This result shows there is no significant change in SSP 8.5 scenarios as compared to other scenarios.

Figure 5 indicates the average monthly maximum temperature over the watershed for the future period is expected to decrease by -1.46^{o}c (2021-2050) and -1.01^{o}c (2051-2080) for the SSP 4.5 scenario. In the SSP 8.5 scenarios, average monthly temperature changes are expected to increase by 5.40^{o}c (2021-2050) and 8.57^{o}c (2051-2080).

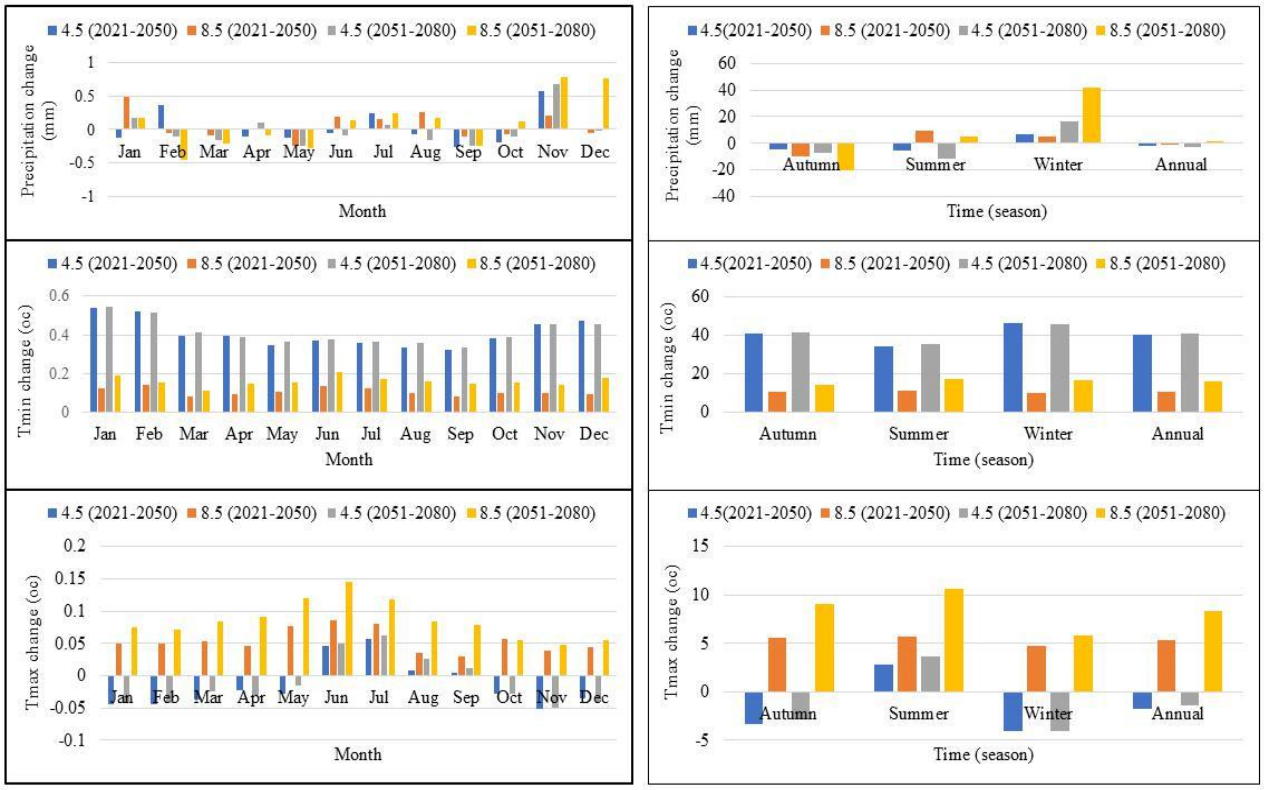

Figure 5: Percentage change of climate impact on monthly, seasonal and annual precipitation, maximum and minimum temperature

3.5. Model calibration and validation

Sensitivity analysis of HEC-HMS model parameters was evaluated manually by trial and error. According to the sensitivity analysis, constant rate (CR) and storage coefficient (SC) were more sensitive model parameters while other parameters were relatively less sensitive. After identifying sensitive model parameters, calibration and validation were done. The result shows the model has a very strong relation with observed and simulated hydrograph pattern of flow since NSE gives 0.62 and R^2 0.68 for calibration and NSE gives 0.71 and R^2 0.73 for validation. Generally, the model has a good agreement and is applicable at the watershed (See Figure 6).

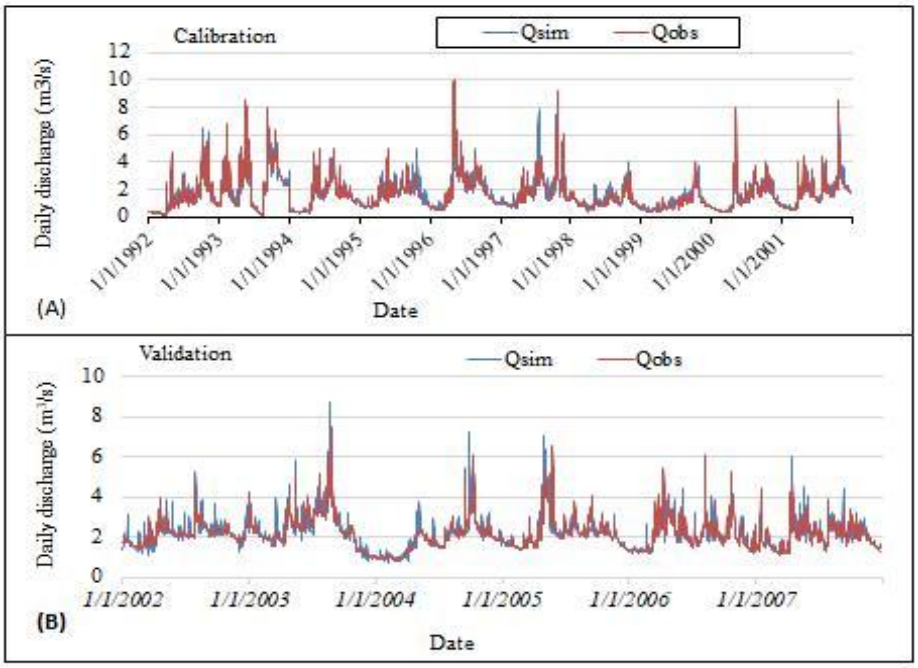

Figure 6: Daily simulated and observed flow hydrograph

3.6. Climate change impact on future water availability

3.6.1. Impact on future average monthly, seasonally, and annual flow simulation

In both SSP 4.5 and SSP 8.5 scenarios, there will be a slight increase in average projected flow in the autumn and winter seasons except for SSP 4.5 (2051-2080) scenario as figure 7 shows when compared with observed stream flow. On the other hand, the water availability in summer (rainy season) in the stream was expected to decrease. The availability of water in the stream will be expected to increase by 8% in the future as compared to the observed stream flow data in the river (See Figure 7).

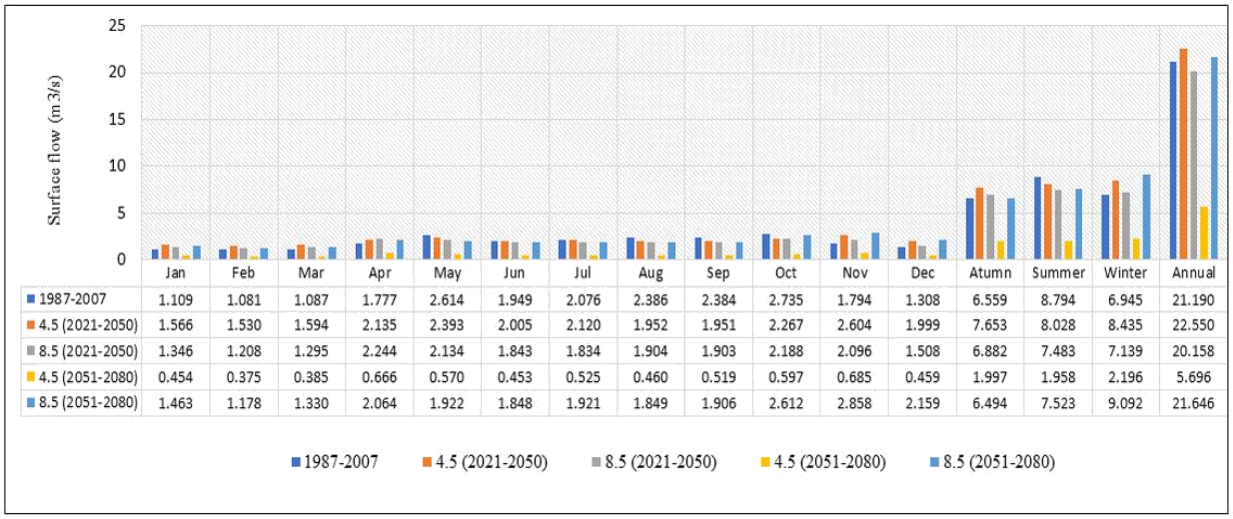

Figure 7: Projected monthly, seasonal and annual runoff at the outlet of Hare watershed

3.6.2. Climate change impacts on projected simulated surface runoff

The average seasonal surface runoff is expected to decrease by 71.8% under SSP 4.5 from 2051 to 2080 and increase by 14.51% under SSP 8.5. For the earlier period (2021-2050), the runoff is expected to increase by 8.1% under SSP 4.5 and decrease by 3.6% under SSP 8.5 (See figure 8). The sharp decline in seasonal surface runoff under SSP 4.5 in the later period is likely due to rising annual air temperatures, which increase evapotranspiration. The outcomes vary significantly depending on the emissions scenario and the time period considered, with SSP 4.5 leading to a dramatic reduction in runoff in the later period due to higher temperatures, while SSP 8.5 shows an increase in runoff, possibly due to more extreme precipitation events despite higher temperature.

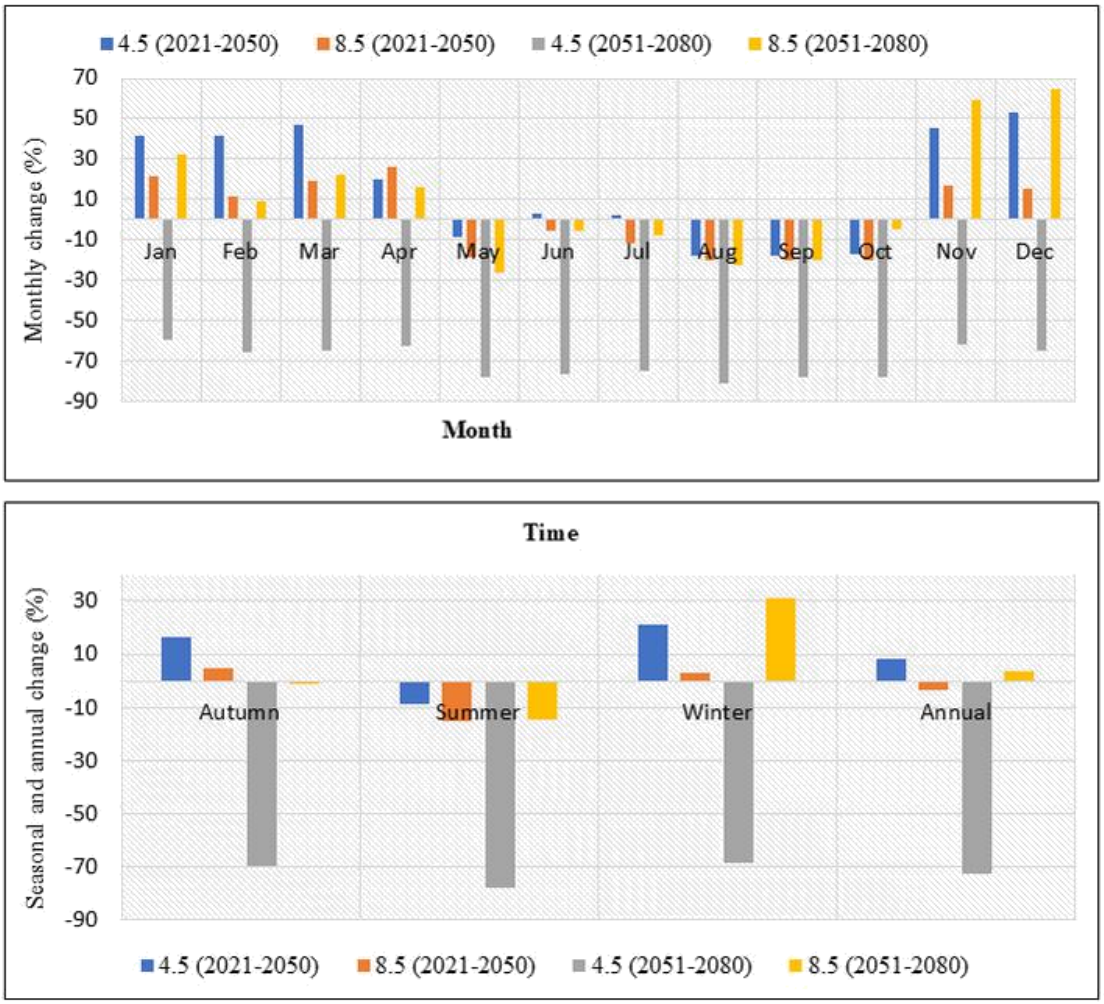

Figure 8: Percentage changes in monthly, seasonal and annual flows at the outlet with the reference baseline.

4. Conclusions

Climate change is likely to have severe effects on the water resource planning of the Hare watershed on Hare irrigation water management. The result of climate projection reveals that the SSP data can be seen considering different scenarios that include SSP 4.5 and SSP 8.5 for short and long terms based on their relative importance.

Sensitivity analysis of HEC-HMS model parameters was evaluated manually by trial and error. According to the sensitivity analysis, constant rate (CR) and storage coefficient (SC) were more sensitive model parameters while other parameters were relatively less sensitive. We used three rainfall stations and one continuous river flow data and the model performance was very good agreement for both calibration and validation.

Accuracy of models representing the rainfall of the study area with SSP 4.5 and SSP 8.5 was done. Therefore, the performance shows (Bias = 74.24 %) overestimated and RMSE (24.62 mm per month) for 19 years of rainfall data obtained and it show bias correction was important before using for any hydrological analysis. An investigation was carried out to identify trends in climate parameter time series of stations over the whole Hare watershed using the Mann-Kendall test. Thus, the annual rainfall amount shows a little bit of increasing trends and maximum and minimum temperatures also show increasing and decreasing trends respectively.

After bias correction was done the future SSP scenarios were developed and divided into three periods of time series which are the base period (1971-2000), Short term (2021-2050), and long term (2051-2080). Thus, the result shows that projected precipitation, maximum, and minimum temperature were increased monthly, seasonally, and annually with the reference to baseline period.

Annual, seasonal, and monthly impact of climate change on minimum and maximum temperature were analyzed and it shows an average increase over the watershed by 0.407^{o}c (2021-2050) and 0.412^{o}c (2051-2080) for SSP 4.5 and 0.105^{o}c and 0.158^{o}c for SSP 8.5 respectively. Surface water availability in the watershed shows slight increased by 8% as compared to observed flow.

Despite these changes, water resource availability in the Hare watershed is not expected to be severely stressed during the wet season, even with rising temperatures. This suggests that the surrounding communities and agricultural activities may not face significant adverse impacts, allowing for continued water resource development and sustainable food security.

Overall, the findings underscore the importance of adaptive water resource management strategies to harness future water availability effectively. By leveraging these projections, the Hare watershed can contribute to enhancing the region's resilience to climate change and supporting long-term economic and food security goals.

References

Belihu, M., Tekleab, S., Abate, B., & Bewket, W. (2020). Hydrologic response to land use land cover change in the Upper Gidabo Watershed, Rift Valley Lakes Basin, Ethiopia. *HydroResearch*, *3*, 85–94. https://doi.org/10.1016/j.hydres.2020.07.001

Coulibaly, N., Coulibaly, T., Mpakama, Z., & Savané, I. (2018). The Impact of Climate Change on Water Resource Availability in a Trans-Boundary Basin in West Africa: The Case of Sassandra. *Hydrology*, *5*(1), Article 1. https://doi.org/10.3390/hydrology5010012

Demmissie, N. G., Demissie, T. A., & Tufa, F. G. (2018). Predicting the Impact of Climate Change on Kulfo River Flow. *Hydrology*, *6*, 78.

Dibaba, W. T., Demissie, T. A., & Miegel, K. (2020). *Watershed hydrological response to combined land use/land cover and climate change in highland Ethiopia: Finchaa catchment*. *12*(6), 1801.

Edamo, M. L., Bushira, K. M., Ukumo, T. Y., Ayele, M. A., Alaro, M. A., & Borko, H. B. (2022). Effect of climate change on water availability in Bilate catchment, Southern Ethiopia. *Water Cycle*, *3*, 86–99. https://doi.org/10.1016/j.watcyc.2022.06.001

Eide, A., & Heen, K. (2002). Economic impacts of global warming: A study of the fishing industry in North Norway. *Fisheries Research*, 261–274.

Fayiah, M., Dong, S., Singh, S., & Kwaku, E. A. (2020). A review of water–energy nexus trend, methods, challenges and future prospects. *International Journal of Energy and Water Resources*, *4*(1), 91–107. https://doi.org/10.1007/s42108-020-00057-6

Gebre, S. L. (2015). Application of the HEC-HMS Model for Runoff Simulation of Upper Blue Nile River Basin. *Journal of Waste Water Treatment & Analysis*, *06*(02). https://doi.org/10.4172/2157-7587.1000199

Gebresellase, S. H., Wu, Z., Xu, H., & Wada, I. M. (2022). *Evaluation of CMIP6 climate models for climate change impact assessments in upper Awash basin, Ethiopia*.

Hagos, Y. G., Andualem, T. G., Yibeltal, M., & Mengie, M. A. (2022). Flood hazard assessment and mapping using GIS integrated with multi-criteria decision analysis in upper Awash River basin, Ethiopia. *Applied Water Science*, *12*(7), 148. https://doi.org/10.1007/s13201-022-01674-85

Heo, J., Yu, J., Giardino, J. R., & Cho, H. (2015). Impacts of climate and land-cover changes on water resources in a humid subtropical watershed: A case study from East Texas, USA. *Water and Environment Journal : WEJ*, *29*(1), 51–60. https://doi.org/10.1111/wej.12096

Kaushal, S., Gold, A., & Mayer, P. (2017). Land Use, Climate, and Water Resources—Global Stages of Interaction. *Water*, *9*(10), 815. https://doi.org/10.3390/w9100815

Khoi, D. N. (2015). *Comparision of the hec-hms and swat hydrological models in simulating the streamflow*. 8.

Konapala, G., Mishra, A. K., Wada, Y., & Mann, M. E. (2020). Climate change will affect global water availability through compounding changes in seasonal precipitation and evaporation. *Nature Communications*, *11*(1), 3044. https://doi.org/10.1038/s41467-020-16757-w

Kuma, H. G., Feyessa, F. F., & Demissie, T. A. (2021). Hydrologic responses to climate and land-use/land-cover changes in the Bilate catchment, Southern Ethiopia. *Journal of Water and Climate Change*, *12*(8), 3750–3769. https://doi.org/10.2166/wcc.2021.281

Kusangaya, S., Warburton, M. L., Archer Van Garderen, E., & Jewitt, G. P. W. (2014). Impacts of climate change on water resources in southern Africa: A review. *Physics and Chemistry of the Earth, Parts A/B/C*, *67–69*, 47–54. https://doi.org/10.1016/j.pce.2013.09.014

Liu, Z., Cuo, L., Li, Q., Liu, X., Ma, X., Liang, L., & Ding, J. (2020). Impacts of Climate Change and Land Use/Cover Change on Streamflow in Beichuan River Basin in Qinghai Province, China. *Water (Basel)*, *12*(4), 1198. https://doi.org/10.3390/w12041198

Meresa, H., Tischbein, B., & Mekonnen, T. (2022). Climate change impact on extreme precipitation and peak flood magnitude and frequency: Observations from CMIP6 and hydrological models. *Natural Hazards*, *111*(3), 2649–2679.

Obaideen, K., Shehata, N., Sayed, E. T., Abdelkareem, M. A., Mahmoud, M. S., & Olabi, A. G. (2022). The role of wastewater treatment in achieving sustainable development goals (SDGs) and sustainability guideline. *Energy Nexus*, *7*, 100112. https://doi.org/10.1016/j.nexus.2022.100112

San José, R., Pérez, J. L., González, R. M., Pecci, J., Garzón, A., & Palacios, M. (2016). Impacts of the 4.5 and 8.5 RCP global climate scenarios on urban meteorology and air quality:Application to Madrid, Antwerp, Milan, Helsinki and London. *Journal of Computational and Applied Mathematics*, *293*, 192–207. https://doi.org/10.1016/j.cam.2015.04.024

Sanjay Shekar, N. C., & Vinay, D. C. (2021). Performance of HEC-HMS and SWAT to simulate streamflow in the sub-humid tropical Hemavathi catchment. *Journal of Water and Climate Change*, *12*(7), 3005–3017. https://doi.org/10.2166/wcc.2021.072

Sun, S., Zhou, T., Wu, P., Wang, Y., & Yin, Y. (2019). Impacts of future climate and agricultural land-use changes on regional agricultural water use in a large irrigation district of northwest China. *Land Degradation & Development*, *30*(10), 1158–1171. https://doi.org/10.1002/ldr.3287

Tabar, M. H., Akbari, A., & Shahraki, J. (2015). The Economic Impact of Climate Change on Optimal Allocation of Water Resources in Agricultural Sector (Case Study: Sarbaz River Basin of Sistan and Baluchestan Province). *International Journal of Economics and Finance*, *7*(6), p105. https://doi.org/10.5539/ijef.v7n6p105

Tassew, B. G., Belete, M. A., & Miegel, K. (2019). Application of HEC-HMS Model for Flow Simulation in the Lake Tana Basin: The Case of Gilgel Abay Catchment, Upper Blue Nile Basin, Ethiopia. *Hydrology*, *6*(1), 21. https://doi.org/10.3390/hydrology6010021

Tong, Y., Gao, X., Han, Z., Xu, Y., Xu, Y., & Giorgi, F. (2021). Bias correction of temperature and precipitation over China for RCM simulations using the QM and QDM methods. *Climate Dynamics*, *57*(5–6), 1425–1443. https://doi.org/10.1007/s00382-020-05447-4

Tramblay, Y., Llasat, M. C., Randin, C., & Coppola, E. (2020). Climate change impacts on water resources in the Mediterranean. *Regional Environmental Change*, *20*(3), 83, s10113-020-01665-y. https://doi.org/10.1007/s10113-020-01665-y

Villamizar, S. R., Pineda, S. M., & Carrillo, G. A. (2019). The Effects of Land Use and Climate Change on the Water Yield of a Watershed in Colombia. *Water (Basel)*, *11*(2), 285. https://doi.org/10.3390/w11020285

Wasti, A., Ray, P., Wi, S., Folch, C., Ubierna, M., & Karki, P. (2022). Climate change and the hydropower sector: A global review. *WIREs Climate Change*, *13*(2), e757. https://doi.org/10.1002/wcc.757

Yirgu, T., Yihunie, Y., Assele, A., & Wogayehu, T. (2020). Land Use/Land Cover Dynamics and its Environmental Impacts in Kulfo Watershed, Gamo Highlands, South Western Ethiopia. *Journal of Geography, Environment and Earth Science International*, 1–11. https://doi.org/10.9734/jgeesi/2020/v24i230197

Yisehak, B. (2021). Prediction of flood frequency under a changing climate, the case of Hare watershed, Rift Valley Basin of Ethiopia. *Sustainable Water Resources Management*, *7*(1), 9. https://doi.org/10.1007/s40899-021-00492-1

Impacts of climate change on blue and green waters in Tekeze-Atbara watershed, Nile Basin

Michale G.Gebreselassie*[1,4], Semu A.Moges[2], Zeleke Agide Dejen[3]

[1,4]Department of Water Resources Engineering and Management, Ethiopian Institute of Water Resources, Addis Ababa University, Addis Ababa,81134, Ethiopia, e-mail:mgk169@gmail.com

[2]School of Civil and Environmental Engineering, Addis Ababa Institute of Technology, Addis Ababa University, Addis Ababa, Ethiopia, e-mail: semu.moges.2000@gmail.com

[3]Water Resources and Irrigation Engineering and Management ,Ethiopian Institute of Water Resources, Addis Ababa University, Addis Ababa, Ethiopia, e-mail: zadejen15@gmail.com

[4]Water Resources and Irrigation Engineering Department, Shire Campus, Aksum University, Shire town, Ethiopia

*Corresponding author: mgk169@gmail.com

Abstract

This study examines the impacts of climate change on blue water flow (BWF), green water storage (GWS), and green water flow (GWF) components of water resources in the Tekeze Atbara watershed of the Nile basin. It employed five CMIP5 climate models under RCP4.5 and RCP8.5 scenarios along with a satisfactory SWAT model with acceptable predictive uncertainty. The results indicate that while mean annual changes in BWF (stream flow) and the green waters remain stable ($p>0.05$), considerable decline in all water components during the Belg season and spatially in the northeastern sub-basins of the watershed are projected. Moreover, statistically significant ($p<0.05$) changes in inter-annual variability, particularly for the green waters are projected with variability in BWF remaining high. One of the key findings of this study is the distinction between GWS (soil moisture) and GWF (actual evapotranspiration), revealing a decrease in both, in contrast to recent studies that suggest an increase in semi-arid regions when aggregated. This study highlights the critical need for localized and integrated water management strategies addressing both blue and green waters in the changing climate. Future research should integrate land use and water use scenarios to enhance the robustness of such assessments.

Key words: *Blue water; green water flow; green water storage; climate change; SWAT; Nile Basin*

1. Introduction

The Nile Basin, essential to the livelihoods of more 238 million people, faces unprecedented challenges of water scarcity due rapid population growth ,escalating water demands, and climate change (UNEP, 2013). Among the basin's tributaries, the Tekeze-Atbara basin plays a pivotal role, contributing approximately 13 % of the Nile's annual discharge and providing water for millions of rain fed farmers (UNEP, 2013). However, while the Blue Nile sub-basin has been the focus of most research, the Tekeze-Atbara watershed remains underexplored, and its hydrological dynamics poorly understood (Johnston & Smakhtin, 2014).

This gap in research is particularly concerning given the increasing pressures on water resources that include blue water flow (stream flow) and green waters, which encompass green water storage (GWS, soil moisture) and green water flow (GWF, actual evapotranspiration) (Faramarzi et al., 2013; Liu et al., 2022; Schuol et al., 2008). While blue water flow (BWF) is vital for water supply, irrigation and hydropower generation, green waters are essential for rain fed agricultural regions and ecosystem services (Schuol et al., 2008; UNEP, 2013).

However, many existing studies on future water resources of the Nile basins have primarily focused on BWF (e.g., Elshamy et al., 2009; Gizaw et al., 2017; Mekonnen & Disse, 2018; Mengistu & Sorteberg, 2012; Teklesadik et al., 2017; Woldesenbet et al., 2018). Majority of the studies are concentrated on Blue Nile sub-basin with a few studies (Gizaw et al., 2017; Mengistu & Sorteberg, 2012) examining the Tekeze-Atbara watershed . The impact focus of the previous studies on BWF showed consistence in the direction of increasing in temperature, serving as strong evidence of climate change in the Nile basins (Barnes, 2017). However, they disagree in future projections of BWF due to different climate models, hydrological models, and emission scenarios used in the studies (Barnes, 2017). This uncertainty have presented significant challenges for decision-making, as it complicates the planning and implementation of water resources management strategies (Barnes, 2017; UNEP, 2013).

Studies have shifted toward more integrated assessment, commonly using SWAT model, that also consider green water availabilities for holistic understanding of water resources availabilities (Faramarzi et al., 2013; Liu et al., 2022; Schuol et al., 2008).

However, previous integrated studies disagree in the future direction of green water availability due to the changing climate. The disagreement is primarily due to difference in how green water is conceptualized and quantified. For instance, some recent studies (e.g., Abate et al., 2024) by treating green water as combined metric of green water storage (GWS) and green water flow (GWF) projected increasing in green water availability mainly due to increasing in temperature , particularly on Denakil sub-basin in semi-arid region of northern Ethiopia. Other studies (e.g., Faramarzi et al., 2013) by separating green water availability into GWS (soil moisture storage) and GWF (actual evapotranspiration) reported a general decrease in green water availability across Africa due to decreasing in precipitation and increasing in temperature. This later view is critical. Combining GWS (soil moisture storage) and GWF in to single metric can obscure the potential impact of climate change on green water availabilities for rain-fed and semi-arid regions like Tekeze-Atbara watershed.

Therefore, the objective of this study to investigate the impact of climate changes on blue and green water resources (storage and flow) by addressing uncertainty analysis in future projections in the Tekeze-Atbara watershed. The findings will contribute to the development of more effective and integrated water management strategies that include blue and green waters, for sustainable water use in the Nile Basin and beyond in the changing climate.

2. Materials and methods

2.1. Study area

The Tekeze-Atbara (T-A) basin, a major sub-basin of the Nile, predominantly lies in Ethiopia, where it is called Tekeze (Figure. 1). It contributes approximately 13% of annual water flow to the Nile (Johnston & Smakhtin, 2014; Swain, 2011). This study focuses on the upper Tekeze watershed , encompassing 45,072 km² at the Embamadre gauging station (MoWE, 2015). The watershed features significant topographic diversity, with elevation variations having a standard deviation of 514 m above mean sea level. The Tekeze River, originating in northern Ethiopia's highlands, traverses sub-basins across Amhara (e.g., North Wollo Zone) and Tigray (e.g., Eastern Zone) regions, supporting domestic water needs and industrial activities. Tributaries such as Zarema, Werie, Ghiba, Suhul, Genfel, and Agulae are vital for local communities. The Embamadre gauging station, located in sub-basin 47, serves as a key monitoring point, recording an average annual flow of 9.1 BCM that continues westward to Sudan as the Atbara River.

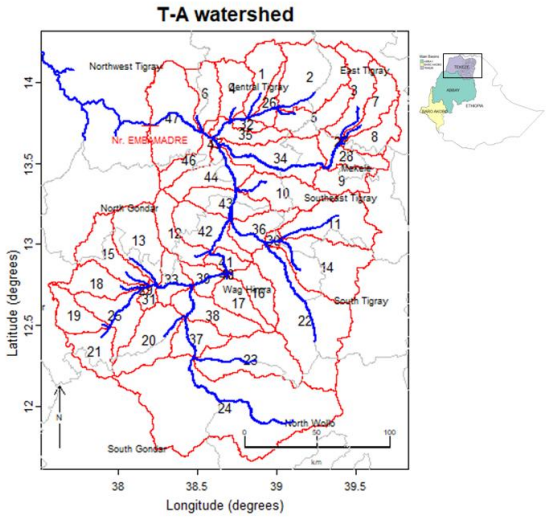

Figure. 1 Location of Tekeze-Atbara (T-A) watershed in northern Ethiopia, 47 sub-basins (red), overlaid by administration zones (gray), Tekeze-Atbara River and its tributaries (blue), outlet at Embamadare

Land use in the T-A watershed (see Figure. 2) is dominated by agriculture, with cropland covering over 50% of the area. Of the 13 soil types identified (GLC-SHARE; HWSD), Leptosols dominate, with Lithic Leptosols (LPq) and Eutric Leptosols (LPe) accounting for 52% and 18% of the area, respectively. The region experiences considerable climate variability, with annual precipitation (see **Error! Reference source not found.**) averaging 884 mm and ranging from 700 mm to 1,100 mm, w ith a coefficient of variability (CV) of 18.36%. Rainfall is concentrated in Kiremt (70%; June - September), followed by Belg (21%; February - May) and Bega (9%; October - January) .Mean annual temperature averages 20°C, varying between 18°C and 23°C .

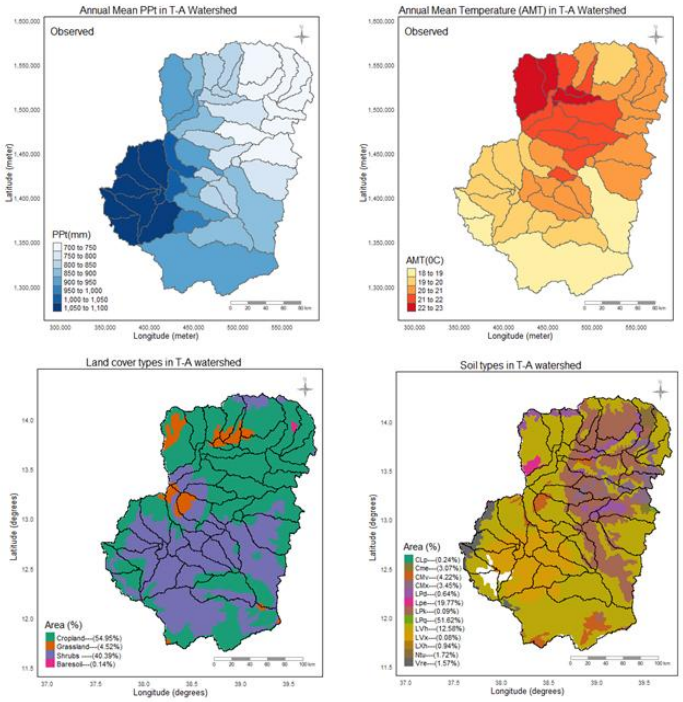

Figure. 2 Spatial distributions of annual precipitation (PPt), annual temperature (AMT) (top rows), land cover (in 2010) and soil types (in 2010) (bottom rows) in T-A watershed

2.2.SWAT model

In this study, the Soil and Water Assessment Tool (SWAT) was used to estimate blue water flow (BWF), green water storage (GWS), and green water flow (GWF) availabilities from simulated water balance components (Arnold et al., 2012; Faramarzi et al., 2013; Neitsch et al., 2011; Schuol et al., 2008). The SWAT model operates on the fundamental water balance equation. Following van Griensven et al., (2012) the equation as indicated in eq.1 can be written in terms of the blue and green waters with their detail derivations shown in Figure. 3

$$PPt = BWF + GWF + \Delta GWS + Losses \qquad (1)$$

Where, PPt is precipitation (mm); BWF is the water yield (mm) in SWAT; GWF is the (ET) actual evapotranspiration (mm) in SWAT; Δ GWS is the change in (SW) soil moisture (mm) in SWAT; Losses (mm) such as Revap which are lost from the system. As GWS (soil moisture storage) is a temporary storage in SWAT model, in this study the accumulated soil moisture is considered.

To apply the SWAT model, a QSWAT in the QGIS interface was used for data pre-processing, aggregation, and model setup (Dile et al., 2016). In order to capture local variations, the watershed was divided into 47 sub-basins using a Digital Elevation Model (DEM) at 90 m resolution, sourced from the Shuttle Radar Topographic Mission (SRTM) (http://srtm.csi.cgiar.org.). The DEM defined topographic features, including slope classes (0–5%, 5–10%, >10%) and the gauging station at

Embamadre served as an outlet. Land cover types were identified based on land use data at 1 km resolution from the GLC-SHARE (www.fao.org/geonetwork.). Soil types were identified based on soil data at 1km resolution obtained from the Harmonized World Soil Database (HWSD). Three hundred five (305) Hydrological Response Units (HRUs) were delineated using a 10% threshold for the soil, the land cover, and the slope categories. Observed historical climate data, critical for SWAT modeling, were sourced from the WATCH (Weedon et al., 2011) dataset . These datasets at 0.5 degree resolutions were obtained from the Inter Sectoral Impact Model Inter comparison Project (ISIMIP:www.isimip.org).Variables such as precipitation, temperature, wind speed, and humidity were downscaled to the sub-basin centres using bilinear interpolation using terra package (Hijmans, 2023) in R programming. Solar radiation was simulated using the SWAT weather generator with data from meteorological stations in Mekelle, Gonder, and Lalibela (Dile et al., 2016). Then Potential evapotranspiration (PET) was calculated using the Penman-Monteith method, surface runoff using the Soil Conservation Service (SCS) curve number method, and flow routing employed a variable storage routing method.

For model accuracy and reliability, initial SWAT model simulation at monthly time scale was done. The initial SWAT model simulations was transferred to SWAT-CUP, for sensitivity, calibration, validation and uncertainty analyses using sequential uncertainty fitting (SUFI-2) (Abbaspour, 2015) coupled with observed flow data from the Embamadre gauging station that were divided into calibration (1998–2005) and validation (2006–2010) periods. Ten sensitive SWAT parameters were indentified during calibration and uncertainty analysis in SWAT-CUP (see Table). The initial and final ranges of the parameters with their best-fitted values indicated in the table. These parameters control stream flow (Arnold et al., 2012) . The initial values of the SWAT parameters were adjusted during calibration to align with observed flow in T-A watershed, and the results fell within acceptable ranges recommended by Abbaspour et al., (2015) and van Griensven et al., (2012). Figure. 4 presents hydrographs of observed and simulated monthly flow during calibration and validation periods, with Nash-Sutcliffe efficiency (NS) > 0.5, RMSE-to-standard deviation ratio (RSR) < 0.7, and percent bias (PBIAS%) < 25% limits for both periods for satisfactory model evaluation criteria (Moriasi et al., 2007). For uncertainty analysis, the resulted P-factor (>0.6) and R-factor (<1.5) are within acceptable limits (Abbaspour et al., 2015) for both calibration and validation periods.

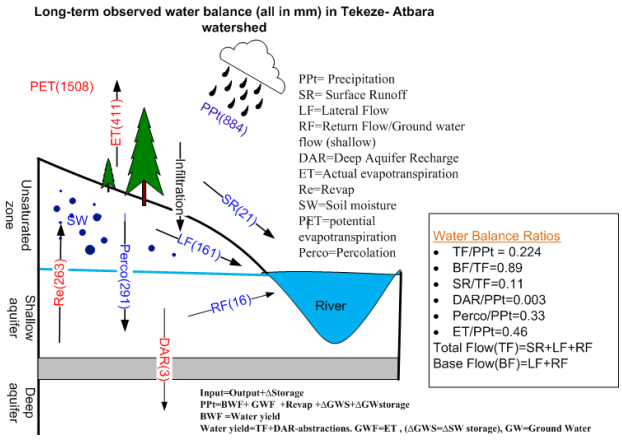

Figure. 3 Conceptual water balance model in SWAT, observed (1979-2015) water balance components, water balance ratios, hydrological equation, derivations of blue and green waters

Table 1: The ten selected SWAT parameters during calibration and uncertainty analysis in T-A watershed

Name	Definition	Initial range		Final range		Fitted
r__CN2.mgt	SCS runoff curve number for moisture condition II	-0.2	0.2	-0.225	-0.051	-0.182
r__SOL_AWC.sol	Soil available water storage capacity (mm /mm)	-0.2	0.2	-0.181	0.179	0.089
v__ESCO.hru	Soil evaporation compensation factor	0	1	0.019	0.89	0.118
v__SURLAG.bsn	Surface runoff lag coefficient (days)	0	10	0.019	4.98	0.101
v__ALPHA_BF.gw	Base flow alpha factor (days)	0	1	0.384	0.737	0.567
v__GW_REVAP.gw	Groundwater revap coefficient	0.02	0.2	0.163	0.2	0.2
v__GW_DELAY.gw	Groundwater delay time (days)	0	100	83.6	161.5	129.12
a__GWQMN.gw	Threshold depth of water in the shallow aquifer required for return flow (mm)	0	1000	888.6	1741.9	1642.3
v__REVAPMN.gw	Threshold depth of water in the shallow aquifer for revap to occur (mm)	0	500	85.64	452.9	250.9

v__RCHRG_DP.gw	Deep aquifer percolation fraction	0	1	0	0.35	0.011

Note: r_ parameter means the parameter value is to be multiplied by (1+ a fitted value) :v _ parameter means the parameter values is to be replaced by the fitted value: a_parameter means the parameter is to be added to the fitted value

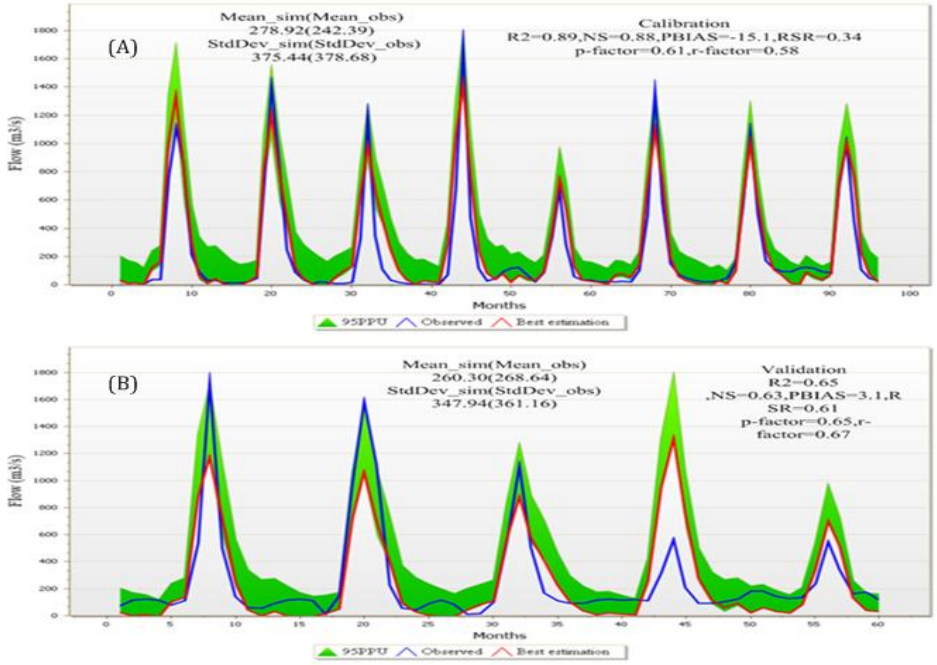

Figure. 4 Hydrographs of observed flow and simulations with predictive uncertainties during calibration (1998-2005) period (A) and during validation (2006-2010) period (B) in Tekeze-Atbara (T-A) watershed

Over all, this satisfactory SWAT model with best-fitted parameters and with acceptable predictive uncertainty was used describe the BWF, GWS, and GWF under observed and future climate conditions in the T-A watershed

2.3.Climate change scenarios

For future climatic conditions , this study used precipitation and temperature datasets (2020–2097) from five bias-corrected (Hempel et al., 2013) global climate models (GCMs) under the Coupled Model Intercomparison Project Phase 5 (CMIP5): HadGEM2-ES, IPSL-5 CM5A-LR, MIROC-ESM-CHEM, GFDL-ESM2M, and NorESM1-M. These datasets were obtained from the ISIMIP (www.isimip.org). Multi model averages outputs of the climate models were calculated. Two Representative Concentration Pathways (RCP4.5 and RCP8.5) were considered, following previous studies (Gizaw et al., 2017) in the Tekeze-Atbara watershed.

2.4.Calculation of impacts

Climate change impacts were assessed by evaluating long-term changes in annual average; in inter annual variability, in seasonality, and in spatial variations of the BWF and green waters (GWS and GWF) under the two RCPs for two future periods in 2020–2056 and 2061–2097 with the reference to observed or current period (1979-2015). By employing R-programming software (R Core Team, 2021), while a t-test was applied to determine if there were significant changes in the mean annual values between the observed and future periods, a var-test was applied whether there was significant changes in inter-annual variability. A significant level of ($p< 0.05$) was chosen for all statistical tests.

3. Results and Discussions

3.1.Blue and green water availabilities

Under observed (1979-2015) climatic conditions, estimated blue and green water resources show considerable spatial and temporal variability in T-A watershed (see Figure. 5). Annual basin averages are 201 mm for BWF, 172 mm for GWS, and 411 mm for GWF. GWF exceeds BWF, consistent with other African sub-basins (Schuol et al., 2008). Inter-annual variability is highest for BWF (CV = 38%) compared to GWS (CV = 14%) and GWF (CV = 11%). Kiremt (Jun to Sep) dominates seasonal contributions: 66.8% (BWF), 71.3% (GWS), and 55.4% (GWF). Belg (Feb to May) and Bega (Oct to Jan) contribute 15.6% and 17.5% to BWF, 12.2% and 16.3% to GWS, and 28.4% and 16.1% to GWF, respectively.

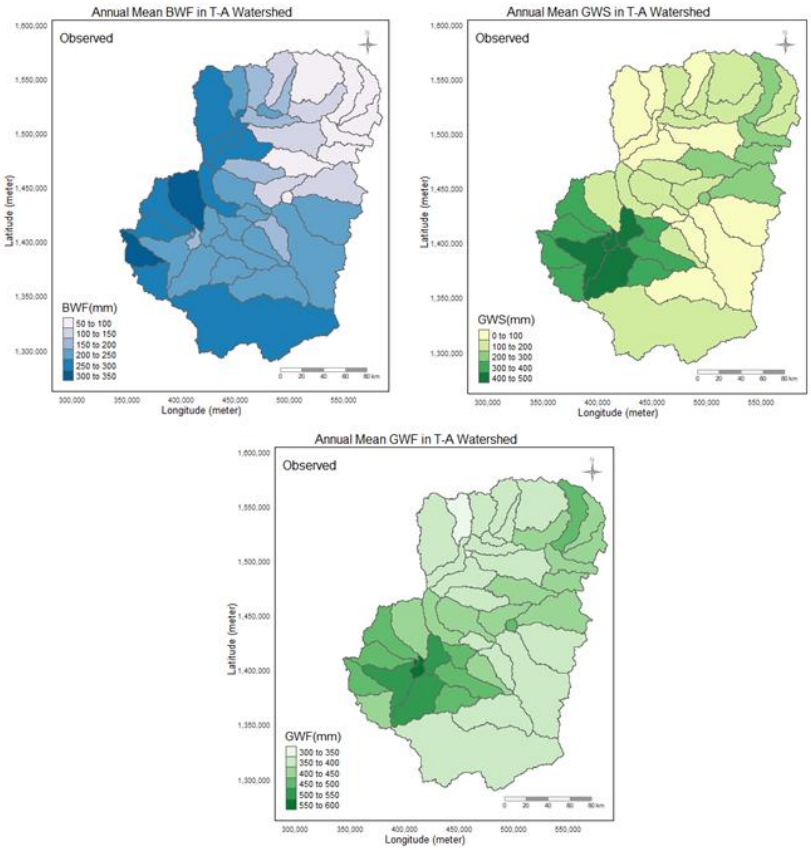

Figure. 5 Spatial distributions of observed (1979-2015) BWF (top left), GWS (top right), and GWF (bottom) in T-A watershed

3.2. Impact of climate change in blue and green waters

The impact of climate change in the blue and green waters in T-A watershed is due to changes in PPt and PET under both the RCPs for the two future periods (see Table**)**. While mean annual changes in PET are statistically significant ($p<0.05$), changes in PPt, BWF, and green waters (GWS and GWF) are not statistically significant in all scenarios across the entire watershed. However, considerable changes in spatial variability in the blue and green waters are projected (see Figure 6). For instance, a reduction in BWF by up to 40–50% is projected along with declines in green water resources in the northeastern parts of the watershed at the end of the 21st century . In addition, changes in inter-annual variability are found to be significant ($p<0.05$) under both RCPs, particularly for the green waters. Furthermore, Significant intra-annual variability are noted, for instance in general with a considerable decrease in all water components (BWF, GWS, and GWF) expected during the small rainy (Belg) season across all scenarios (see Table).

Table 2: Statistical summaries: changes in precipitation (PPt), PET, BWF, GWS, and GWF in T-A watershed, t-test used for testing the significance of changes in mean values and var-test used for the ratio of variances (expressed also as coefficient of variation (CV)). P values less than 0.05 are significant.

	PPt	PET	BWF	GWS	GWF
Observed (1979-2015)					
Mean(mm)	884.07	1507.53	200.94	171.81	410.96
CV (%)	18.36	5.33	37.91	14.46	11.37
RCP4.5_FP(2020-2056)					
Mean(mm)	926.23	1576.83	213.79	172.54	419.24
Mean change (%)	4.77	4.60	6.39	0.43	2.01
t-test(p value)	0.32	0.00	0.29	0.91	0.59
ratio of variances	1.44	0.93	0.78	1.66	2.94
var-test(p value)	0.28	0.84	0.47	0.13	0.00
CV (%)	21.01	4.93	30.00	18.56	19.12
RCP4.5_SP(2061-2097)					
Mean(mm)	869.69	1614.68	188.83	169.24	417.54
Mean change (%)	-1.63	7.11	-6.03	-1.50	1.60
t-test(p value)	0.76	0.00	0.37	0.76	0.71
ratio of variances	2.16	1.29	1.23	3.14	4.15
var-test(p value)	0.02	0.45	0.54	0.00	0.00
CV (%)	27.41	5.66	37.86	26.01	22.81
RCP8.5_FP(2020-2056)					
mean(mm)	945.74	1605.92	222.36	173.41	420.43
Mean change (%)	6.98	6.53	10.66	0.93	2.30
t-test(p value)	0.27	0.00	0.42	0.85	0.57

ratio of variances	3.38	1.52	1.63	3.17	3.57
var-test(p value)	0.00	0.21	0.15	0.00	0.00
CV (%)	31.57	6.17	46.43	25.51	21.00
RCP8.5_SP(2061-2097)					
Mean(mm)	852.68	1680.27	174.09	165.35	432.01
Mean change (%)	-3.55	11.46	-13.36	-3.76	5.12
t-test(p value)	0.52	0.00	0.06	0.43	0.23
ratio of variances	2.37	0.96	1.11	2.92	4.02
var-test(p value)	0.01	0.91	0.77	0.00	0.00
CV (%)	29.31	4.69	37.58	25.69	21.68

Table 3: Seasonal changes with reference to the observed period (1979-2015) period in T-A watershed. The variables are precipitation (PPt), potential evapotranspiration (PET), blue water flow (BWF), green water storage (GWS), and green water flow (GWF)

	PPt	PET	BWF	GWS	GWF
RCP4.5_FP(2020-2056)					
Kiremt change (%)	11.6	3.3	11.8	3.91	12.6
Belg change (%)	-20.9	8.8	-28.3	-10.4	-33.8
Bega change (%)	10.8	0.8	16.7	-6.4	28.5
RCP4.5_SP(2061-2097)					
Kiremt change (%)	2.5	5.9	-3.0	3.7	14.4
Belg change (%)	-20.4	11.2	-29.6	-16.1	-35.6
Bega change (%)	9.4	3.4	3.4	-12.5	23.2
RCP8.5_FP(2020-2056)					

Kiremt change (%)	11.6	5.2	11.8	6.3	14.7
Belg change (%)	-21.3	10.8	-20.7	-19.0	-34.7
Bega change (%)	35.6	2.7	34.3	-7.8	25.3
RCP8.5_SP(2061-2097)					
Kiremt change (%)	-5.3	10.9	-14.1	-2.5	18.0
Belg change (%)	-20.9	15.6	-34.1	-15.2	-39.9
Bega change (%)	48.3	7.2	7.9	-0.7	40.4

RCP8.5_FP indicate first half of the century (2020-2056) and RCP4.5_SP and RCP8.5_SP indicate at the end of 21st century

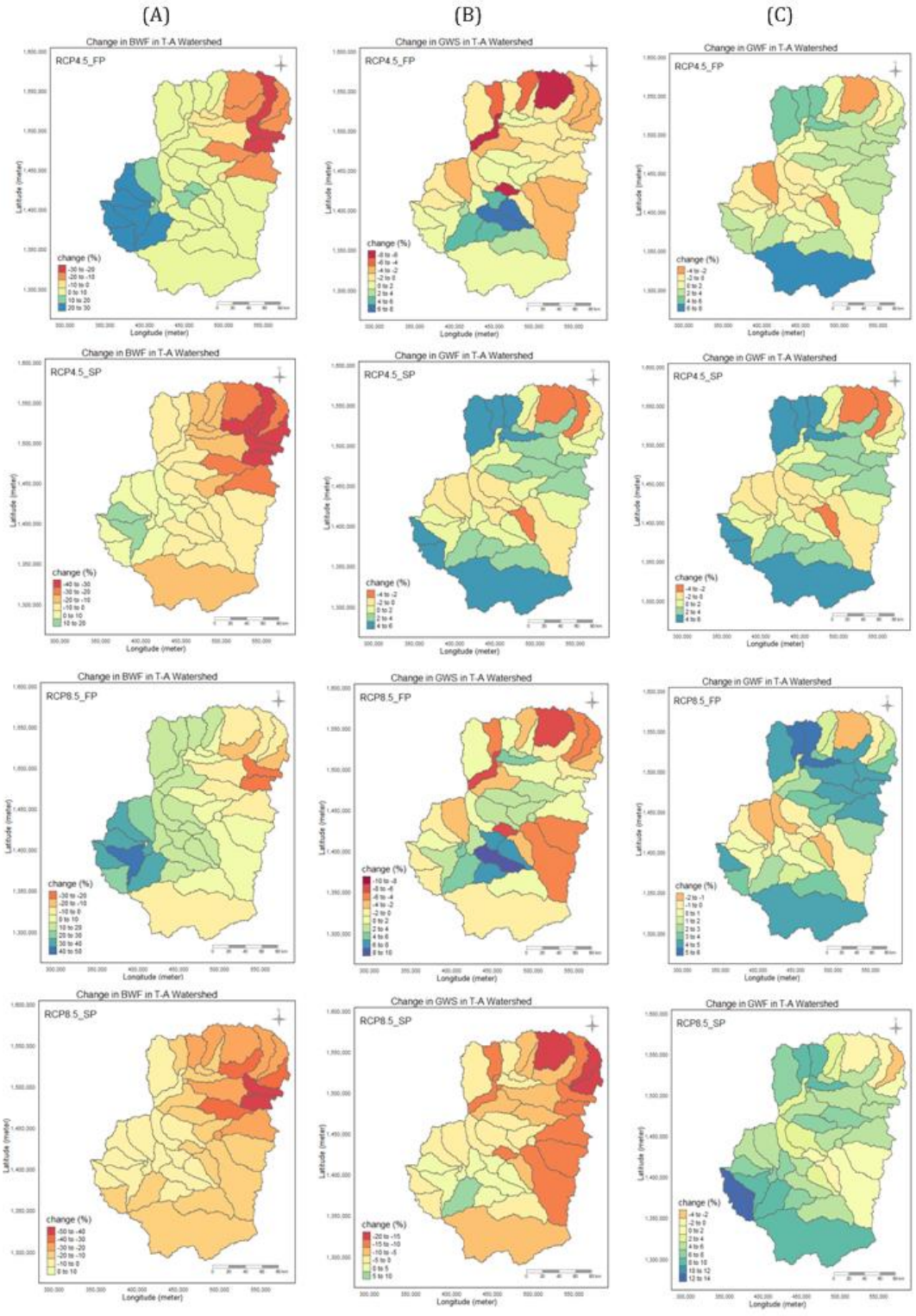

Figure 6. Spatial changes in mean annual BWF (A), GWS (B), and GWF (C) under RCP4.5 and RCP8.5 for two future periods (First period (FP) in 2020-2056 and Second period (SP) in 2061-2097) with reference to observed period (1979-2015)

This study provides an integrated assessment of the impacts of climate change on both blue water flow (BWF, stream flow), green water storage (GWS, soil moisture), and green water flow (GWF, actual evapotranspiration) in the T-A watershed of the Nile Basin. Using multi-model mean outputs from five CMIP5 climate models under RCP4.5 and RCP8.5 scenarios, our findings reveal important insights in to the future changes of the freshwater components. While we observe no significant changes in mean annual blue and green water resources across the entire watershed (Table), we identified considerable decline in all water components (BWF, GWS, and GWF) during the Belg (small rainy) season, coupled with spatial reductions in the northeastern part of the watershed (Figure 6.) These results are due to increasing in temperature associated with increasing in PET coupled with decreasing in precipitation in the season and in the areas. Moreover, statistically significant ($p<0.05$) changes in inter-annual variability, particularly for the green waters are projected. This result is mainly due to increasing in inter-annual variability of precipitation in all scenarios across the entire T-A watershed.

3.3.Comparison with previous studies

There are many studies on the impact of climate change on future water availability on the Nile Basin with a few studies (Gizaw et al., 2017; Mengistu & Sorteberg, 2012) in our study area (T-A watershed). Theses previous studies mainly focused on the impact of BWF (stream flow). However, they showed uncertainties in the future direction of the BWF availability. For instance ,while Mengistu & Sorteberg,(2012) indicated that future changes in mean annual BWF from CMIP3 GCMs would show no clear trend under the A2, A1B, and B1 emission scenarios. Conversely Gizaw et al., (2017) projected a decrease (increase) in mean annual BWF under RCP4.5 (RCP8.5) scenarios from CMIP5 GCMs , with an increase in mean annual precipitation for both RCPs.

These studies, however, focused on BWF (stream flow) and did not consider the role of green water resources, which is important for rain fed agricultural productivity.

Our study builds on existing research by incorporating both blue and green water resources, which has become an increasingly important approach in hydrological assessments. While previous studies have largely ignored green water resources, which is critical for rain-fed agriculture, studies in other regions of Africa have begun to recognize its importance. For instance, Faramarzi et al.,(2013) conducted a continent-wide assessment using SWAT and CMIP3 climate models under the old SRES emission scenarios, and reported a general decrease in both the blue and green water resources across Africa due to temperature rise and precipitation reduction. This continental study provides an essential overview of future blue and green waters (storage and flow) but lacks the spatial granularity to assess local vulnerabilities. Our results align with the broader trend of decreasing in blue and green water resources particularly in the northeastern sub-basins of T-A watershed. However, our findings emphasize the spatial variability of climate change impacts within the sub-basins in T-A watershed.

A more recent study by Abate et al.,(2024) focused on blue and green water resources at watershed scale on Denakil sub-basin in semi-arid region of northern Ethiopia, using SWAT model along with CIMP6 climate models under RCP4.5 and RCP8.5 scenarios. Our results stand in contrast with this recent study in terms future green water resources. A key difference between our study and the recent study is the treatment of green water. While the study by Abate et al., (2024) predicted increasing in green water availability mainly due increasing in temperature , we found that green waters both GWS (soil moisture) and GWF (actual evapotranspiration) would decrease, particularly during the Belg season and in the northeastern sub-basins of T-A watershed despite increasing in PET (Figure 6, B and C) . This difference could be attributed to methodological flaws in the study by Abate et al., (2024), where GWS (soil moisture) was combined with GWF , leading to overestimation of green water availability in semi-arid regions. In SWAT model's water balance equation, while GWS is temporary soil moisture storage, GWF represents the actual evapotranspiration (see Sec.2). In our study, we ensured that these two components were treated separately, offering a more accurate picture of future dynamics of green waters under the changing climate change.

Implication for Water Resources Management

Our study highlights the need for a more integrated approach to water resources management that considers both the blue and green water resources. The separation of green water in green water storage (GWS, temporary soil moisture) and green water flow (GWF, actual evapotranspiration) is particularly important in rain-fed and semi-arid regions like the T-A watershed. Furthermore, our findings emphasize the significance of temporal and spatial heterogeneity in the blue and green water resources for localized adaptation strategies under the changing climate. The declines in both blue and green water resources in the northeastern sub-basins need strategies that address green water conservation (e.g., soil moisture conservation, reforestation) and blue water infrastructures (e.g., construction of dams) to ensure future water scarcity in the region.

Limitations of the study

While our study presents a robust analysis by incorporating both blue and green water resources, we recognize limitations that may affect the broader applicability of our findings. One of the key assumptions in our study is that land use remains constant in the future. Land use change can have a significant impact on BWF and green waters (GWS and GWF) (Liu et al., 2022). While our study focused on future changes on climate variables, future research could incorporate land use change scenarios to understand the full impact on the water resources. In addition, our analysis does not account for water withdrawals due to industrial and irrigation usages. Integrating scenarios of water demands can enhance the assessment. Despite these limitations, our study incorporated uncertainty analysis using SWAT-CUP to assess the predictive uncertainty in our model results. Uncertainty in climate change and hydrological models has long been a challenge, particularly for in the Nile Basin, where variable models outputs hindered decision-making and policy development (Barnes, 2017; Johnston & Smakhtin, 2014; UNEP, 2013; van Griensven et al., 2012). Our study directly addressed this challenge by incorporating SWAT-CUP uncertainty analysis, ensuring that our results in P-factor and R-factor are within the acceptable limits (P-factor >0.6 and R-factor <1.5) (Abbaspour et al., 2015). This enhances the reliability of our findings.

4. Conclusion

This study provides a comprehensive analysis of the impacts of climate change on blue water flow (BWF), green water storage (GWS), and green water flow (GWF) components of water resources in the Tekeze-Atbara (T-A) watershed of the Nile Basin, filling critical gaps in the existing literature. It employed a satisfactory SWAT model with acceptable predictive uncertainty coupled with CMIP5 climate models under RCP4.5 and RCP8.4 scenarios.

Our key results indicate that while mean annual changes in BWF (stream flow), GWS (soil moisture), and GWF (actual evapotranspiration) are not significant across the entire watershed, considerable decline in all water components (BWF, GWS, and GWF) during the Belg (small rainy) season, coupled with spatial reductions in the northeastern part of the watershed are projected. This is due to increasing in temperature associated with increasing in PET coupled with decreasing in precipitation in the season and in the areas. Moreover, statistically significant ($p<0.05$) changes in inter-annual variability, particularly for the green waters (soil moisture and flow) are projected in all scenarios with the variability in BWF remaining high. These results underscore the need for more integrated approach to water resources management that consider both blue and green waters as well as their spatial and temporal availabilities in semi-arid and rain fed agricultural regions in the Nile Basin and beyond, where similar climate-induced shifts are likely to occur. The findings of this study are in contrast to recent integrated studies that predicted increasing in green water availability in similar semi-arid region. By distinguishing green water to its components (GWS and GWF), we avoided the over estimation observed in the previous studies. The separation is particularly important in the regions like the T-A watershed, where GWS and GWF resources play a vital role in rain fed agriculture and ecosystem services. While this integrated study is robust, it has limitations. Future studies should incorporate land use changes and water withdrawals to enhance the assessment.

Over all, while this study focuses on a critical yet understudied T-A watershed in the Nile Basin, the insights gained are applicable to global efforts to understand and mitigate the impacts of climate change on water resources. The projected dual water crisis on blue water flow and green waters (storage and flow) identified in the T-A watershed serves as a warning for other sub-basins in the Nile and other regions where water resources are already under water stress.

Acknowledgments

We extend our gratitude to the data centers that supplied the DEM, soil, land cover, and weather datasets used in this study.

Reference

Abate, B. Z., Alaminie, A. A., Assefa, T. T., Tigabu, T. B., & He, L. (2024). Modeling climate change impacts on blue and green water of the Kobo-Golina River in data-scarce upper Danakil basin, Ethiopia. Journal of Hydrology: Regional Studies, 53. https://doi.org/10.1016/j.ejrh.2024.101756

Abbaspour, K. C. (2015). SWAT-CUP: SWAT Calibration and Uncertainty Programs - A User Manual. Eawag. Swiss Federal Institute of Aquatic Science and Technology.

Abbaspour, K. C., Rouholahnejad, E., Vaghefi, S., Srinivasan, R., Yang, H., & Kløve, B. (2015). A continental-scale hydrology and water quality model for Europe: Calibration and uncertainty of a high-resolution large-scale SWAT model. Journal of Hydrology, 524, 733–752.

Arnold, J. G., Moriasi, D. N., Gassman, P. W., Abbaspour, K. C., White, M. J., Srinivasan, R., Santhi, C., Harmel, R. D., van Griensven, A., Van Liew, M. W., Kannan, N., & Jha, M. K. (2012). SWAT: MODEL USE, CALIBRATION, AND VALIDATION. American Society of Agricultural and Biological Engineers, 55(4), 1491–1508.

Barnes, J. (2017). The future of the Nile: Climate change, land use, infrastructure management, and treaty negotiations in a transboundary river basin. WIREs Clim Change, E449. https://doi.org/10.1002/wcc.449

Beyene, T., Lettenmaier, D. P., & Kabat, P. (2010). Hydrologic impacts of climate change on the Nile River Basin: Implications of the 2007 IPCC scenarios. Climatic Change, 100, 433–461. https://doi.org/10.1007/s10584-009-9693-0

Dile, Y. T., Daggupati, P., George, C., Srinivasan, R., & Arnold, J. (2016). Introducing a new open source GIS user interface for the SWAT model. Environmental Modelling & Software, 85, 129–138.

Elshamy, M. E., Seierstad, I. A., & Sorteberg, A. (2009). Impacts of climate change on Blue Nile flows using bias-corrected GCM scenarios. Hydrology and Earth System Sciences, 13, 551–565.

Faramarzi, M., Abbaspour, K. C., Vaghefi, S. A., Farzaneh, M. R., Zehnder, A. J. B., Srinivasan, R., & Yang, H. (2013). Modeling impacts of climate change on freshwater availability in Africa. Journal of Hydrology. http://dx.doi.org/10.1016/j.jhydrol.2012.12.016

Gizaw, M. S., Biftu, G. F., Gan, T. Y., Moges, S. A., & Koivusalo, H. (2017). Potential impact of climate change on streamflow of major Ethiopian rivers. Climatic Change. https://doi.org/10.1007/s10584-017-2021-1

Hempel, S., Frieler, K., Warszawski, L., Schewe, J., & Piontek, F. (2013). A trend-preserving bias correction – the ISI-MIP approach. Earth Syst. Dynam., 4, 219–236. https://doi.org/0.5194/esd-4-219-2013

Hijmans, R. J. (2023). terra: Spatial Data Analysis. R Package Version 1.7-18. Https://CRAN.R-Project.Org/Package=terra.

Johnston, R., & Smakhtin, V. (2014). Hydrological Modeling of Large river Basins: How Much is Enough? Water Resour Manage. https://doi.org/10.1007/s11269-014-0637-8

Liu, M., Wang, D., Chen, X., Chen, Y., Gao, L., & Deng, H. (2022). Impacts of climate variability and land use on the blue and green water resources in a subtropical basin of China. Scientific Report, 20993(12). https://doi.org/10.1038/s41598-022-21880-3

Mekonnen, D. F., & Disse, M. (2018). Analyzing the future climate change of Upper Blue Nile River basin using statistical downscaling techniques. Hydrology and Earth System Sciences, 22, 2391–2408. https://doi.org/10.5194/hess-22-2391-2018

Mengistu, D. T., & Sorteberg, A. (2012). Sensitivity of SWAT simulated streamflow to climatic changes within the Eastern Nile River basin. Hydrology and Earth System Sciences, 16, 391–407. https://doi.org/10.5194/hess-16-391-2012

Moriasi, D. N., Arnold, J. G., Van Liew, M. W., Bingner, R. L., Harmel, R. D., & Veith, T. L. (2007). MODEL EVALUATION GUIDELINES FOR SYSTEMATIC QUANTIFICATION OF ACCURACY IN WATERSHED SIMULATIONS. American Society of Agricultural and Biological Engineers, 50(3), 885−900.

MoWE. (2015). Hydrological Data. Ethiopian Ministry of Water and Engergy (MoWE).

Neitsch, S. L., Arnold, J. G., Kiniry, J. R., & Williams, J. R. (2011). Soil and Water Assessment Tool—Theoretical Documentation—Version 2009. Grassland, Soil and Water Research Laboratory, Agricultural Research Service and Blackland Research Center, Texas AgriLife Research.

R Core Team. (2021). R: A Language and Environment for Statistical Computing. R Foundation for Statistical Computing, Vienna, Austria. https://www.R-project.org/

Schuol, J., Abbaspour, K. C., Yang, H., Srinivasan, R., & Zehnder, A. J. B. (2008). Modeling blue and green water availability in Africa. WATER RESOURCES RESEARCH, 44, 1–18. https://doi.org/10.1029/2007WR006609

Swain, A. (2011). Challenges for water sharing in the Nile basin: Changing geo-politics and changing climate. Hydrological Sciences Journal, 56(4), 687–702. https://doi.org/10.1080/02626667.2011.577037

Taye, M. T., Ntegeka, V., Ogiramoi, N. P., & Willems, P. (2011). Assessment of climate change impact on hydrological extremes in two source regions of the Nile River Basin. Hydrology and Earth System Sciences, 15, 209–222. https://doi.org/10.5194/hess-15-209-2011

Teklesadik, A. D., Alemayehu, T., van Griensven, A., Kumar, R., Liersch, S., Eisner, S., Tecklenburg, J., Ewunte, S., & Wang, X. (2017). Inter-model comparison of hydrological impacts of climate change on the Upper Blue Nile basin using ensemble of hydrological models and global climate models. Climatic Change. https://doi.org/10.1007/s10584-017-1913-4

UNEP. (2013). Adaptation to Climate-change Induced Water Stress in the Nile Basin: A Vulnerability Assessment Report.Division of Early Warning and Assessment (DEWA). United Nations Environment Programme (UNEP).Nairobi, Kenya. http://www.earthprint.com.

van Griensven, A., Ndomba, P., Yalew, S., & Kilonzo, F. (2012). Critical review of SWAT applications in the upper Nile basin countries. Hydrology and Earth System Sciences, 16, 3371–3381. https://doi.org/10.5194/hess-16-3371-2012

Weedon, G. P., Gomes, S., Viterbo, P., Shuttleworth, W. J., Blyth, E., & Österle, H. (2011). Creation of the WATCH Forcing Data and Its Use to Assess Global and Regional Reference Crop Evaporation over Land during the Twentieth Century. J Hydrometeorol, 5(12), 823–848. https://doi.org/10.1175/2011JHM1369.1

Woldesenbet, T. A., Elagib, N. A., Ribbe, L., & Heinrich, J. (2018). Catchment response to climate and land use changes in the Upper Blue Nile sub-basins, Ethiopia. Science of the Total Environment, 644, 193–206. https://doi.org/10.1016/j.scitotenv.2018.06.198

The Role of Tropical Easterly Jet on improving the Predictability of Summer Rainfall variability over the Upper Blue Nile Basin in Ethiopia

Abebe Kebede*[1], Samuel Takele[2], Lev D. Labzovskii[3], Venkatraman Prasanna[4], B. Preethi[5]

[1]Arba Minch University Water Institute of Technology, Faculty of Meteorology and Hydrology, Arba Minch, Ethiopia

[2]Innovative Meteorological Research Department, National Institute of Meteorological Sciences (NIMS), 33, Seohobuk-ro, Seogwipo-si 63568, Jeju-do, Korea

[3]R&D Satellite and Observations Group, Royal Netherlands Meteorological Institute (KNMI), 3731GA De Bilt, the Netherlands

[4]Center for Climate Research Singapore (CCRS), Singapore, Singapore

[5]Indian Institute of Tropical Meteorology, Pune, 411008, India

*Corresponding author: abeasella@gmail.com

Abstract

Effective management of rain-fed agriculture in countries like Ethiopia, vulnerable to climate-driven droughts, necessitates a comprehensive understanding of rainfall variability and improved prediction capabilities. Several studies have explored the understanding of rainfall variability and prediction skills in Ethiopia, nevertheless, there remains a gap in the examination of this variability across different regions of Ethiopia, particularly over the Nile basin region. This study aims to fill a critical gap in understanding the role of the Tropical Easterly Jet (TEJ) in predicting summer rainfall variability over the Upper Blue Nile Basin. We utilized summer rainfall data from the Climate Hazards Group InfraRed Precipitation with Stations (CHIRPS) spanning the period 1981-2022. Additionally, specific humidity and wind data for the years 1979-2020 were obtained from ERA5. Wind data from both ERA5 and National Centers for Environmental Prediction (NCEP) reanalysis covering the period 1979-2020 were also incorporated. Seas surface temperature (sst) data for the period 1981-2020 complemented our dataset. Employing artificial neural network (ANN) models, utilizing CHIRPS, total column water vapor (tcwv), and temperature data for spatial rainfall prediction, and sst, 200hPa zonal wind, and ECMWF precipitation data for temporal station rainfall prediction. The feedforward connection and multiple network layers, employing the Levenberg Marquart algorithm to downscale the data. Across the stations the results of NARX shows strong association and pattern of prediction rainfall in comparison to the observed rainfall including low errors. The spatial prediction of summer rainfall distribution shows strong characteristics over the complex terrain of the basin. In overall, our findings advance the quality and the precision of summer rainfall forecasting and moisture transportation will help improving efficient resource planning for management of water.

Keywords: JJAS rainfall, prediction, humidity, sst, wind and VIL

1. Introduction

Sea surface temperature (SST) plays a crucial role in connecting with both the upper-level atmosphere, through the Tropical Easterly Jet (TEJ), and the lower level, via the East African Low-Level Jet (EALLJ) (Diro et al. 2011b). This linkage influences upper-level divergence and facilitates convection, crucial factors in the formation of rainfall over Ethiopia. Anomalies in sea surface temperatures have a direct impact on these jets, subsequently affecting rainfall patterns. The TEJ, situated northeast of Ethiopia, induces upper-level divergence and convection, while the EALLJ, part of the Indian monsoon pattern, positively influences summer rainfall in northern Ethiopia (Gleixner et al. 2017; Diro et al. 2011a). Warming of eastern equatorial Pacific SST weakens the EALLJ during dry summers, resulting in reduced moisture induction (Diro et al. 2011b).

There are very less number of studies have been done on rainfall prediction using machine learning techniques over Ethiopia including UBN_b. Less number of local meteorological parameters were used as input for to design model without consider global climatic indices rainfall was predicted at Bahir Dar, Ethiopia (Liyew and Melese 2021). According to the investigation of Endalie et al. 2022 over Jimma, Ethiopia developed neural network model with less number of local meteorological variables and stressed the importance of global climatic examining the rainfall dynamics and fit to appropriate model for forecasting Ethiopian rainfall was done by applying Box-Jenkins approach; Seasonal Autoregressive Integrated Moving Average (SARIMA) model in order to forecast monthly rainfall of Ethiopia for the period of twelve months ahead also examined (Berhane et al. 2018).

Previous findings showed that the prediction of rainfall over the UBN_b of Ethiopia were made based on SST variability, however, there was no emphasis given to the lower and upper level of wind circulation, atmospheric water components and temperature for prediction of monthly, seasonal, and long-term rainfall. As mentioned, this gap is undesired and our article aims to alleviate it by (a) analyzing the relationship of the zonal wind speed, atmospheric water components and temperature with summer rainfall based on non-linear approach, (b) determining the prediction summer rainfall using statistical downscaling methods over the domain of interest, (c) identifying single and multiple variables spatio-temporal rainfall prediction and d) investigating water vapor transport.

2. Data and Methodology

2.1. Description of study area

The UBN_b is situated north-western region of Ethiopia and the topography is a complex that varied from 499 m near Ethio-Sudan border and 4167 m (above sea level) near the central region of UBN_b (Fig.1). The climate of the region is a tropical highland monsoonal (Conway 2000). Because of its location, it is influenced by Inter-Tropical Convergence Zone (ITCZ), resulting dry winter and wet in summer (Awulachew et al. 2009). In general, the region receives annual rainfall amounting from 1400 to 1800 mm per year. It is frequently affected by drought and flood (Teferi et al. 2010 and Zaroug et al. 2014).

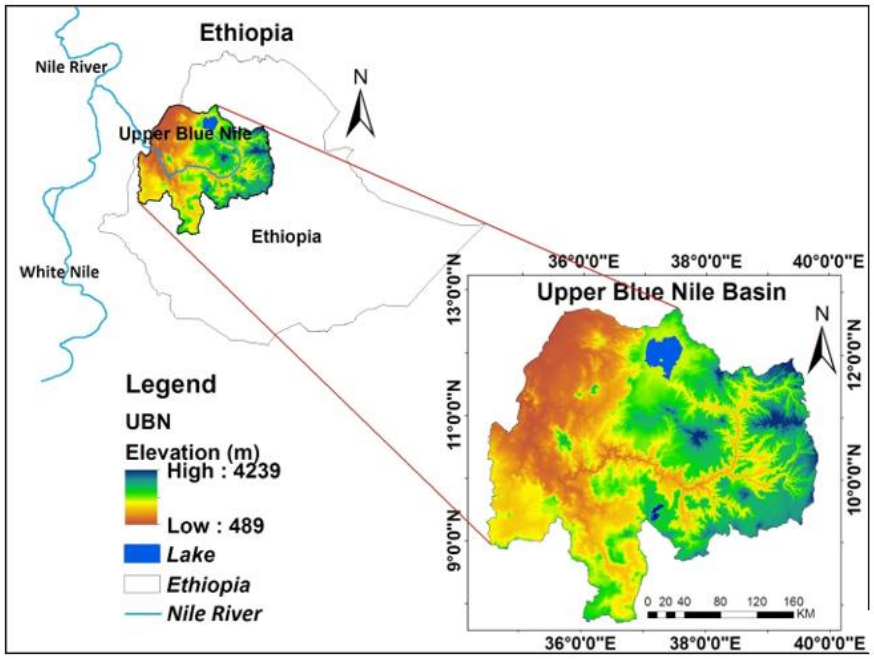

Fig. 1 The Elevation of Upper Blue Nile basin location of Ethiopia and Nile river.

2.2. Data

The specific humidity (q) data (in kg kg^{-1}), along with horizontal wind components (u and v, m s^{-1}) at various pressure levels, was derived from the monthly gridded output of the ECMWF model spanning the period from 1979 to 2020. Additionally, surface temperature and total column water vapor data covering the years 1981 to 2022 were also extracted from the ECMWF model output. For rainfall data, we utilized information from the Climate Hazards Group InfraRed Precipitation with Stations (CHIRPS) dataset, which provides a spatial resolution of 0.05 by 0.05 degrees. This dataset spans the years 1981 to 2022 and serves as a valuable resource for understanding precipitation patterns (available at chg.geog.ucsb.edu/data).

Furthermore, the multivariate ENSO index (MEI) was obtained from NCEP (http://www.esrl.noaa.gov/psd/data). These datasets contribute critical information for our comprehensive analysis of rainfall variability, allowing us to explore the intricate interplay between atmospheric parameters and precipitation patterns over the period from 1979 to 2017.

2.3. Methods

The short (Belg) and long (Summer) terms of rainy seasons of moisture content and wind patterns to the vertical are examined. The investigation into the variability of June to September (JJAS) rainfall distribution involved a detailed analysis of its correlation with the magnitude of wind components at various pressure levels (1000-100 hPa) and specific humidity.

In this study we also applied the nonlinear autoregressive network with exogenous inputs (NARX) is a dynamic recurrent neural network with feedforward connections that enclose several layers of the network; i.e., the input to output network (Carbonera et al. 2021). The structure of the NARX model has useful memory ability for the prediction of nonlinear time series (Tealab et al. 2017) and gains degrees of freedom by incorporating valuable information from exogenous inputs (Cadenas et al. 2016). The two different architectures of NARX are series-parallel architecture (open-loop) and the parallel architecture (close-loop) used in this research.

The Levenberg-Marquart algorithm implemented in this study requires more memory but less time is applied for the temporal rainfall prediction at each stations. In fitting problems, you want a neural network to map between a data set of numeric inputs and a set of numeric targets. The inputs (tcwv and temp) layers, hidden layers, and targets (CHIRPS) are key components in this research. The Neural Network Fitting Tool will help to select data, create and train a network, and evaluate its performance using mean square error and regression analysis. The network is adjusted to 70%, 15% and 15% for training, testing and validation respectively for spatio-temporal prediction. The correlation coefficient and Root Mean Squared Error (RMSE) are used to evaluate the predicted data.

3. Results and Discussion

Advection/convection of wind plays a crucial role in the transportation of moisture across different regions of the troposphere, influencing rainfall patterns in Ethiopia. Specifically, the upper level of the troposphere features the tropical easterly Jet (TEJ), characterized by strong easterlies extending from South East Asia across the Indian Ocean and Africa.

The complexity of relationships between temperature and water vapor in the atmosphere affects the radiation balance and hydrological cycle. The vertical profile of water vapor in the atmosphere, its variability over time, and spatial variation play a key role in the analysis of climate change and weather prediction (Wypych et al. 2018). Such complex association captured by non-linear relationships through applying neural network.

3.1. Specific humidity to the vertical level

The monthly decadal average precipitation and vertically integrated water (VIW) are depicted in Fig. 4. From November- March an amount of mean precipitation is recorded below 50mm. However, gradually there is increasing of the precipitation and reaches the peak in July over UBN_b. Therefore, June-September the agricultural activities are accomplished in the region due to long term rainfall. On the other hand, the average monthly value of VIW follows similar patterns to precipitation over UBN_b. According to this investigation in July and August maximum rainfall and VIW are found. Therefore, the summer season (JJAS) shows maximum rainfall and VIW and the moisture shows that a strong integrity with rainfall of over the region.

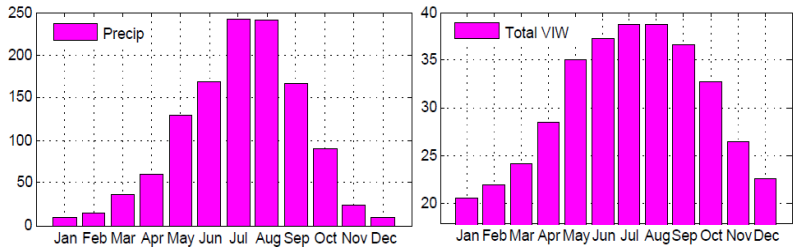

Figure.4 Monthly decadal average rainfall (left panel) and VIW (right panel) from 2009-2019

3.2. Stations rainfall prediction using artificial neural network

For the analysis of station rainfall prediction, data from sst, 200hPa wind speed, and total precipitation were utilized for Bahir Dar, Debremarkos, Nekemte, and Gore stations. These stations were selected based on their climatic conditions, considering the interaction of sea surface temperature with upper-level wind, as highlighted by Segele et al. (2009).

Understanding the teleconnections between these variables supports further investigations into rainfall estimation using the non-linear NARX approach over selected stations in the Upper Blue Nile basin (UBNb).As depicted in Figure 5, the performance of NARXsst200hp tends to overestimate rainfall predictions compared to NARXsst for Bahir Dar and Debremarkos stations. Conversely, NARXsst shows a higher frequency of overestimation compared to the predicted values for Nekemte and Gore stations across the given period. Despite these variations, both models (NARXsst and NARXsst200hpECMWF) exhibit a strong capacity to predict observed rainfall across the selected stations, showcasing minimal over- and underestimation.

The low rainfall observed in 2015, attributed to a strong El Niño phenomenon affecting the region's rainfall patterns, is appropriately identified by both models (Bayissa et al. 2017; Kebede et al. 2020). The results lead to the conclusion that NARXsst200hpECMWF and NARXsst, with slight variations, align closely with observed values at each station. This underscores the importance of sea surface temperature (SST) or its combination with other predictors in accurately predicting rainfall in the UBNb. Given that the UBNb is part of East Africa, SST is statistically related through teleconnections for June to September (JJAS) rainfall forecasts (Degefu et al. 2017; Diro et al. 2008).

The variations in summer rainfall (JJAS) are strongly correlated with regional and local atmospheric variables, such as the Tropical Eastern Jet (TEJ) and other zonal wind pressures, more than with SST anomalies (Segele et al. 2009). These findings suggest that incorporating SST anomalies alongside regional and local atmospheric factors enhances prediction accuracy.

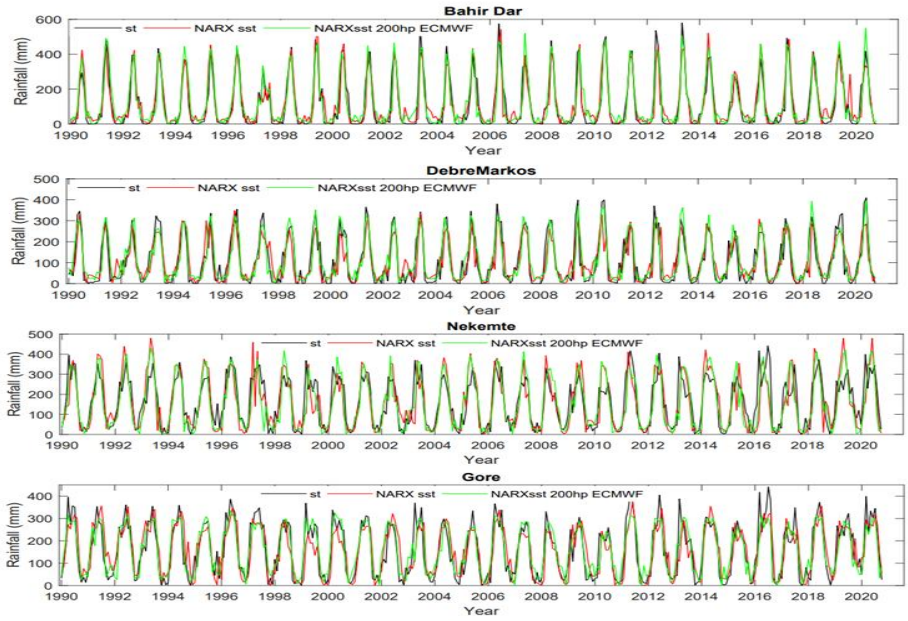

Figure. 5 Rainfall prediction at Bahir Dar, Debremarkos, Nekemte and Gore stations.

3.3. Spatial Summer (Kiremt) season rainfall prediction Using ANN

The CHIRPS precipitation product is a combined products of station rainfall and satellite rainfall estimation products used for monitoring rainfall, drought and early warning especially for east Africa region. In this research for evaluation the spatial summer average rainfall (June - September) of 2015 and 2022 total column water vapor (precip_tcwv); and both combined total column water vapor and surface temperature (precip_tcwv_temp) through application artificial neural network the rainfall are estimated and compared with CHIRPS data over Upper Blue Nile basin of Ethiopia. For the summer these two seasons of years the capturing abilities through applying these two models the promising results of rainfall prediction is identified including pocket areas frequently affected by drought.

The spatial distribution of rainfall in the range of 150-400mm is captured by CHIRPS and applied two models. The eastern and western parts of UBN_b show the lowest rainfall distribution for each summer seasons. The maximum amount of rainfall is identified in parts of central and southern regions of the basin. In comparison to the two seasons the 2022 magnitude and rainfall distribution is higher than the 2015. In the 2015 there was an El-Niño years parts of Upper Blue Nile affected by drought (Kebede et al. 2020). The pocket areas mainly affected by this natural hazard (Yared et al. 2017).

Such higher magnitude of rainfall is observed in 2022 in the parts of central and southern regions of the basin. This year is a La Niña phase during this ENSO phase the region of the basin receive much amount of precipitation compared to El-Niño (Zaroug et al. 2014).

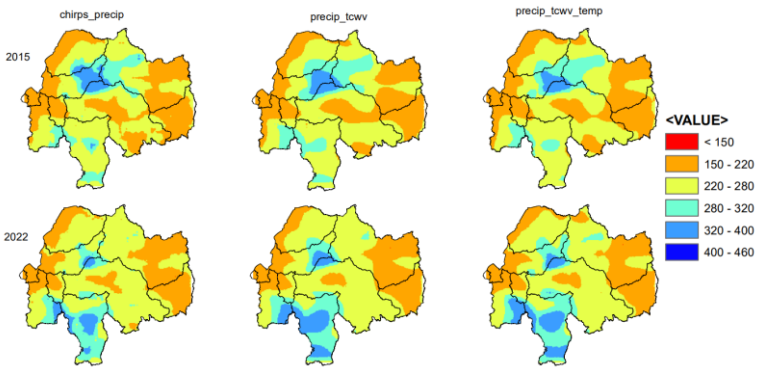

Figure. 6 Spatial precipitation prediction of summer season 2015 and 2022 prec-tcwv and prec-tcwv-temp.

3.4. Errors estimation of the Spatial Summer season rainfall prediction

The assessment of errors in the spatial prediction of summer season rainfall reveals minimal discrepancies between the predicted values (prec_tcwv and prec_tcwv_temp) and the target values (CHIRPS), as illustrated in Figure 7. Across most regions of the UBNb, the errors fall within the range of -10 to 10 mm, indicating a high level of accuracy in each model's estimations. For both the 2015 and 2022 summer seasons, the models exhibit low magnitudes of variation from the target CHIRPS data. Notably, when employing the combined precip_tcwv_temp and precip_tcwv models, there are instances of overestimation and underestimation in spatial errors. Despite these variations, both models demonstrate a significant capability to capture the spatial distribution of summer rainfall over the UBNb. The errors exhibited by each model are consistent across individual seasons.

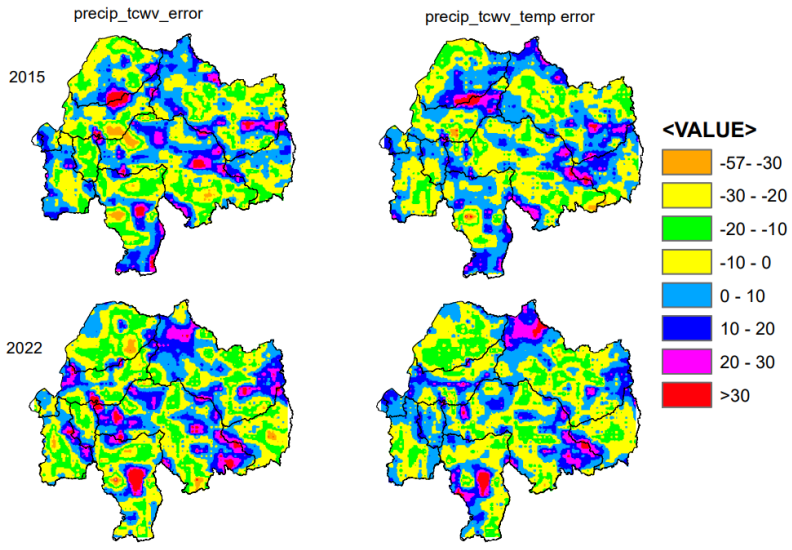

Figure. 7 The summer season CHIRPS rainfall compared with applied neural network of total column water vapor (tcwv) and combined (tcwv and temp2m).

4. Conclusions

Previous findings in prediction of summer rainfall over the UBN of Ethiopia mainly rely up on sea surface temperature without considering the lower and upper level of wind circulation pattern. Analyzing the relationship of the magnitude of the wind, evaluating the prediction, forecasting of summer rainfall and wind related predictors of summer rainfall at various pressure levels are identified. The spatio-temporal prediction of rainfall using single and multiple climate variables through applying neural network show a promising results of prediction over the basin. Prec-tcwv and prec-tcwv-temp show strong spatial rainfall estimation results over the basins. The variation of the results are low which is an indication of a strong capturing ability of precipitation over the basin. Their association among CHIRPS is 0.99 and low square root errors 0.016 and 0.049 for prec-tcwv and prec-tcwv-temp are identified respectively. The small change over estimation and under estimation of models values are investigated compared to observed value. The amount of rainfall based on the amount water vapor transport. In JJAS as the investigation shows the highest water vapor transportation in region of UBN_b.

Acknowledgments:

The authors would like to thank ERA5, NCEP and CHIRPS data sources for providing the data sets.

Author contributions Concept, Data analysis, Original draft the authors are participated. The authors discussed the results of the manuscript and supervision of the progress of the manuscript.

Funding We did not receive any funding from any organization/ institution to carry out this study.

Data and code availability will be provided on request.

Declarations

Conflict of interest We do not have any conflict of interest to disclose.

References

Awulachew SB, McCartney M, Steenhuis TS, Ahmed AA (2009) A review of hydrology, sediment and water resource use in the Blue Nile Basin, vol 131. IWMI

Bayissa, Y., Tadesse, T., Demisse, G. and Shiferaw, A., 2017. Evaluation of satellite-based rainfall estimates and application to monitor meteorological drought for the Upper Blue Nile Basin, Ethiopia. *Remote Sensing*, *9*(7), p.669.

Bekuretsion B and Beshah T (2013) Prediction of Rainfall for Ethiopian Upper Blue Nile Basin Using Soft Computing Models. HiLCoE Journal of Computer Science and Technology, p.26.

Berhane F, Zaitchik B, Dezfuli A (2013) Subseasonal analysis of precipitation variability in the Blue Nile River Basin. J Clim 27:325-344. doi:10.1175/JCLI- D-13-000941.

Berhane, T.M., Lane, C.R., Wu, Q., Autrey, B.C., Anenkhonov, O.A., Chepinoga, V.V. and Liu, H., 2018. Decision-tree, rule-based, and random forest classification of high-resolution multispectral imagery for wetland mapping and inventory. *Remote sensing*, *10*(4), p.580.

Cadenas, E., Rivera, W., Campos-Amezcua, R. and Heard, C., 2016. Wind speed prediction using a univariate ARIMA model and a multivariate NARX model. *Energies*, *9*(2), p.109.

Carbonera, L.F.B., Pinheiro Bernardon, D., de Castro Karnikowski, D. and Alberto Farret, F., 2021. The nonlinear autoregressive network with exogenous inputs (NARX) neural network to damp power system oscillations. *International Transactions on Electrical Energy Systems*, *31*(1), p.e12538.

Conway D (2000) The climate and hydrology of the Upper Blue Nile River. Geographical Journal, 166(1), pp.49-62.

Degefu, M.A., Rowell, D.P. and Bewket, W., 2017. Teleconnections between Ethiopian rainfall variability and global SSTs: observations and methods for model evaluation. *Meteorology and Atmospheric Physics*, *129*, pp.173-186.

Diro, G.T., Black, E. and Grimes, D.I.F., 2008. Seasonal forecasting of Ethiopian spring rains. *Meteorological Applications: A journal of forecasting, practical applications, training techniques and modelling*, *15*(1), pp.73-83.

Diro GT, Grimes DIF, Black E (2011a) Large scale features affecting Ethiopian rainfall. In: Williams CJR, Kniveton DR (eds) African climate and climate change, vol 43., Advances in global change research Springer, Netherlands, pp 13-50.

Diro GT, Grimes DIF, Black E (2011b) Teleconnections between Ethiopian summer rainfall and sea surface temperature: part I-observation and modelling. Clim Dyn 37:103-119. doi:10.1007/ s00382-010-0837-8.

Endalie, D., Haile, G. and Taye, W., 2022. Deep learning model for daily rainfall prediction: case study of Jimma, Ethiopia. *Water Supply*, *22*(3), pp.3448-3461.

Gleixner S, Keenlyside N, Viste E and Korecha D (2017) The El-Niño effect on Ethiopia summer rainfall. Climate dynamics, 49(5-6), pp.1865-1883.

Hastenrath S (1990) Prediction of Northeast Brazil rainfall anomalies. Journal of Climate, 3(8), pp.893-904.

Liyew, C.M. and Melese, H.A., 2021. Machine learning techniques to predict daily rainfall amount. J Big Data 8, 153 (2021).

Kebede, A., Raju, U.J.P., Korecha, D. and Nigussie, M., 2020. Developing new drought indices with and without climate signal information over the Upper Blue Nile. *Modeling Earth Systems and Environment*, *6*, pp.151-161.

Molla F, Kebede A and Raju UJP (2018) The Impact of the El-Niño Southern Oscillation Precipitation and the Surface Temperature over the Upper Blue Nile Region. Journal of Scientific Research and Reports, pp.1-15.

Segele ZT, Lamb PJ, Leslie LM (2009a) Large-scale atmospheric circulation and global sea surface temperature associations with Horn of Africa June-September rainfall. Int J Climatol 29:1075-110.

Tealab, A., Hefny, H. and Badr, A., 2017. Forecasting of nonlinear time series using ANN. *Future Computing and Informatics Journal*, *2*(1), pp.39-47.

Teferi Ermias S Uhlenbrook,Woldeamlak Bewket, JWenninger and Belay Simane (2010) The use of remote sensing to quantify wetland loss in the Choke Mountain range, Upper Blue Nile basin, Ethiopia. Hydrology and Earth System Sciences 14, no. 12, 2415-2428.

Viste, E.M., 2012. Moisture transport and precipitation in Ethiopia. Wolter Klaus and Michael S Timlin (2011) El-Niño /Southern Oscillation Behavior since 1871 as Diagnosed in an Extended Multivariate ENSO Index (MEI.ext) International Journal of Climatology 31.7, 1074-87.

Wypych, A., Bochenek, B. and Różycki, M., 2018. Atmospheric moisture content over Europe and the Northern Atlantic. *Atmosphere*, *9*(1), p.18.

Zaroug MA, Eltahir EA and Giorgi F (2014) Droughts and floods over the upper catchment of the Blue Nile and their connections to the timing of El-Niño and La-Niña events. Hydrology and Earth System Sciences.18(3):1239-1249.

Modeling the current land suitability and future dynamics for coffee (Coffea arabica L.) production under climate change scenarios in Western Ethiopia with MaxEnt model

Tesfaye Akafu*[1], Diriba Korecha[2]; Weyessa Garedew[1]; Abayineh Amare[1]

[1]Jimma University, College of Agriculture and Veterinary Medicine, Jimma, Oromia, Ethiopia
[2]University of California Santa Barbara, Santa Barbara, California, USA

Corresponding author*: tesfayeakafu65@gmail.com

Abstract

Coffee is the world's most popular beverage crop and the second-most traded commodity next to petroleum products. However, the production of coffee is heavily dependent on specific environmental conditions, making it vulnerable to the effects of climate change. Therefore, studying coffee crop responses to climatic conditions is crucial to developing strategies to support coffee crop resilience. This study aimed to model the current land suitability and future dynamics for Coffea arabica cultivation under climate change scenarios in the West Wolega Zone, Western Ethiopia. The study used bioclimatic variables and the current occurrence data of Coffea arabica. Modeling was done for current and anticipated shared socioeconomic pathways (SSP) at intermediate (SSP245), and very high (SSP585) emissions scenarios for 2050 and 2070. ArcGIS was used for data processing, whereas MaxEnt (Maximum Entropy) model for predicting suitability. The result showed 5294.30 km2 (50.8%) of the total land in the area is presently suitable for Coffea arabica cultivation. The predicted model shows 19-24% of the current suitable coffee cultivation areas may become unsuitable, while 20-22% more areas may become suitable for coffee cultivation. Based on Maxent model, the total suitable land for Coffea arabica cultivation could be reduced by 40.3 km², and 136.11 km² in 2050 under the SSP245, and SSP585 scenarios, respectively. The model simulation for 2070 indicates declines of 164.6 km2, and 177.8 km2 in SSP245, and SSP585, respectively. Therefore, designing a plan for species conservation and implementing climate change adaptation strategies are essential for sustaining the suitability of existing coffee growing areas.

Keywords: Climate change; Coffea arabica L.; MaxEnt; Modeling; Suitability

1. Introduction

Coffee is the world's most popular beverage crop and the second most traded commodity next to petroleum products (DaMatta et al., 2019). Nearly 25 million farmers globally, the majority of whom are smallholders, are engaged in the cultivation of coffee across an estimated 80 tropical countries (Bermudez et al., 2022). While there are more than 125 coffee varieties exist (Davis and Rakotonasolo, 2021), Arabica (*Coffea Arabica* Linnaeus) and Robusta (*Coffea Canophera*) coffees account for 99% of worldwide bean production (DaMatta, 2018). These are also responsible for 57% and 43% of the world coffee market, respectively (ICO, 2022).

Coffee production requires specific climatic conditions (DaMatta et al., 2019). Temperature and precipitation patterns are crucial factors that have a significant impact on coffee production. This sensitivity to climatic conditions makes coffee, particularly *C. arabica*, highly vulnerable to the negative

impacts of climate change (Bunn *et al.*, 2015). The optimal average mean annual temperature ranges for *C. arabica* lie between 18–23 ºC (Davis et al., 2012). The rainfall requirements are between 1600–2000 mm (Chemura et al., 2015), with a dry period ranging from 3–4 months near to harvest period (DaMatta et al., 2018).

In Ethiopia, the average yearly temperature has risen by 1 ºC over the last forty years, with significant fluctuations in precipitations trends showing increases in some regions and decreases in others. Projection of the high emission scenario revealed that mean annual temperature will rise by 1.8 ºC and 3.7 ºC by 2050 and 2080, respectively, accompanied by an overall increase of total annual precipitations from 3 mm to 6 mm (USAID, 2024). Nevertheless, there is high uncertainty in predicted precipitation distributions in space and time (MFA, 2018). Species (IPCC, 2022), especially coffee varieties, may experience heightened climatic pressures in their natural habitats, as they are particularly vulnerable to the effects of climate change (DaMatta et al., 2019). Therefore, examining the response of coffee crops to climatic conditions is crucial in developing strategies to support the crop's resilience toward the adverse impacts of climate change.

One way to investigate how climate change affects coffee production in coffee-producing regions is to employ contemporary analytical instruments like species distribution modeling (SDM). The SDM identifies the species occurrence and predicts the suitability of the habitat across space and time (Elith & Leathwick, 2009). Recent national models show Arabica coffee cultivation areas in Ethiopia may decrease (Moat et al., 2017), while regional studies suggest varied outcomes (Ovalle-Rivera et al., 2015). This indicates that the findings are not easily generalizable regionally, with some contradicting each other and mask national context studies. As a result, greater identification of the impact of climate change on particular locations or local coffee areas will be required.

West Wolega coffee is a wet-processed varietal grown in Western Ethiopia at elevations between 1493 m and 1798 m above sea level. In this zone, farmers and stakeholders in the coffee industry have been noticing a gradual decline in overall coffee yield. Good harvests, which were previously a yearly occurrence, have now become sporadic, manifesting only once every second or even third year. Furthermore, in their study, Moat et al. (2017) made a significant prediction that the coffee-producing area of Wolega is likely to face a high level of vulnerability to climate change. However, a more recent investigation by Chemura et al. (2021) provided contrasting insights. The contrasting conclusions of the two studies underscore the complexity and uncertainty often associated with climate change projections, emphasizing the critical need for sustained research to fully understand and prepare for the potential consequences facing the study area. Thus, this study aimed at modeling potential land suitability dynamics for *Coffea Arabica* Linnaeus cultivation under climate change in the West Wolega Zone, Western Ethiopia

2. Methods and Materials

2.1. Study site descriptions

The research was conducted in the West Wolega Zone, located in western Ethiopia (Figure 1). This zone consists of 23 districts, with 20 being rural and 3 urban administrations. Gimbi Town is the capital of the zone. The West Wolega Zone situated between 9º 00’ N latitude and 35º14’E longitude, bordered by Kelam Wolega Zone to the west, Benishangul Gumuz Region to the north, and East Wolega Zone to the

east. It also adjoins Illu Abbaa Boora, Buno Bedele Zones, and Benishangul Gumuz to the southeast. The surface area of the zone is 10,430.28 km^2. According to Hurni (1998), the agroecology of the West Wolega Zone has been classified into three zones: lowland 19.1% (1100–1700 m), midland 78.4% (1701–2200 m), and highland 2.5% (2201–2850 m). The zone exhibits monomodal rainfall patterns, with the wet season occurring from June to September (Korecha & Barnston, 2007).

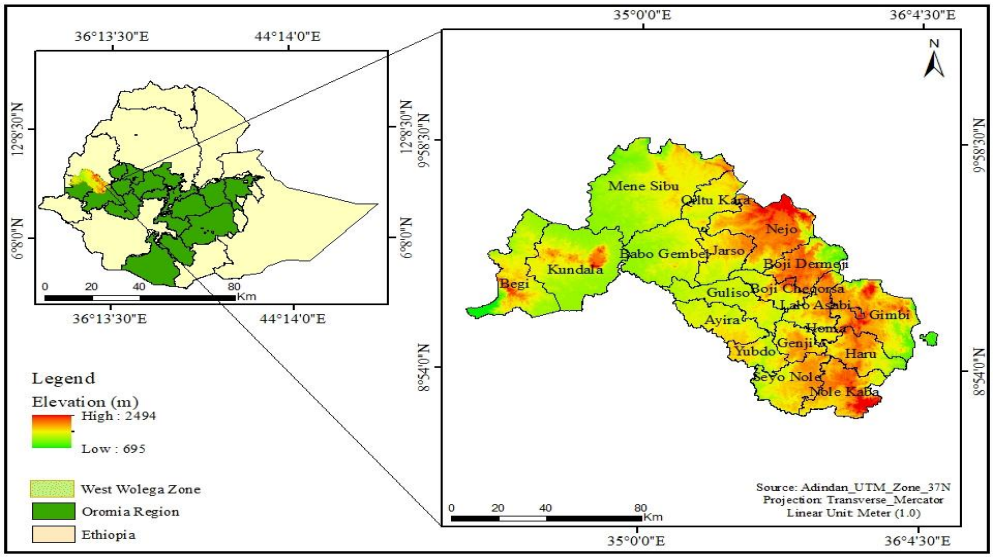

Figure 1. Study area map

2.2. Sampling methods

Purposive and simple random sampling methods were used for this study. Primarily, the West Wolega Zone was purposively selected because of its high coffee production potential, and no previous research had been conducted. Secondly, simple random sampling was used to collect the GPS point of *Coffea arabica* from the entire districts where coffee naturally grows.

2.3. Data Collection

Five hundred geographic coordinate points were collected from where *C. arabica* naturally occurs in the west Wolega zone. To map the current land suitability, climate data averaged over 30 years (1970–2000) was downloaded from WorldClim at 30 arc-second (~1 km2) spatial resolution. The database contains 19 bioclimatic variables. To predict in 2050 and 2070, variables from four GCMs in the Coupled Model Intercomparison Project Phase (CMIP6) were used. These includes HadGEM3-GC31-LL, ACCESS-CM2, INM-CM5-0, and the MRI-ESM2.

2.4. Modeling Approach and Model evaluation

The study used MaxEnt 3.4.4 to model *C. arabica* cultivation areas. In the Maxent model, we used bioclimatic variables as environmental predictors, and coffee occurrence point as sample data. Out of the 477-coffee presence, 75% were assigned for model training, while the remaining 25% for model

validation. The model was run using 11 bioclimatic variables in 15 replicates for current and projected climates in 2050 and 2070, considering moderate (SSP245), and very high (SSP585) emissions scenarios.

3. Result and Discussions

3.1. Model evaluation

The model performance for the current, 2050, and 2070 suitability models is displayed in Figures 2 (a-e). The MaxEnt model consistently demonstrated accuracy and reliability, as reflected by the impressive range of AUC values between 0.77 and 0.78. These values underscore the model's exceptional performance in predicting the presence/absence of *C. arabica* distribution in various scenarios (Elith et al., 2006). These results corroborate the findings by (Jayakody et al., 2024).

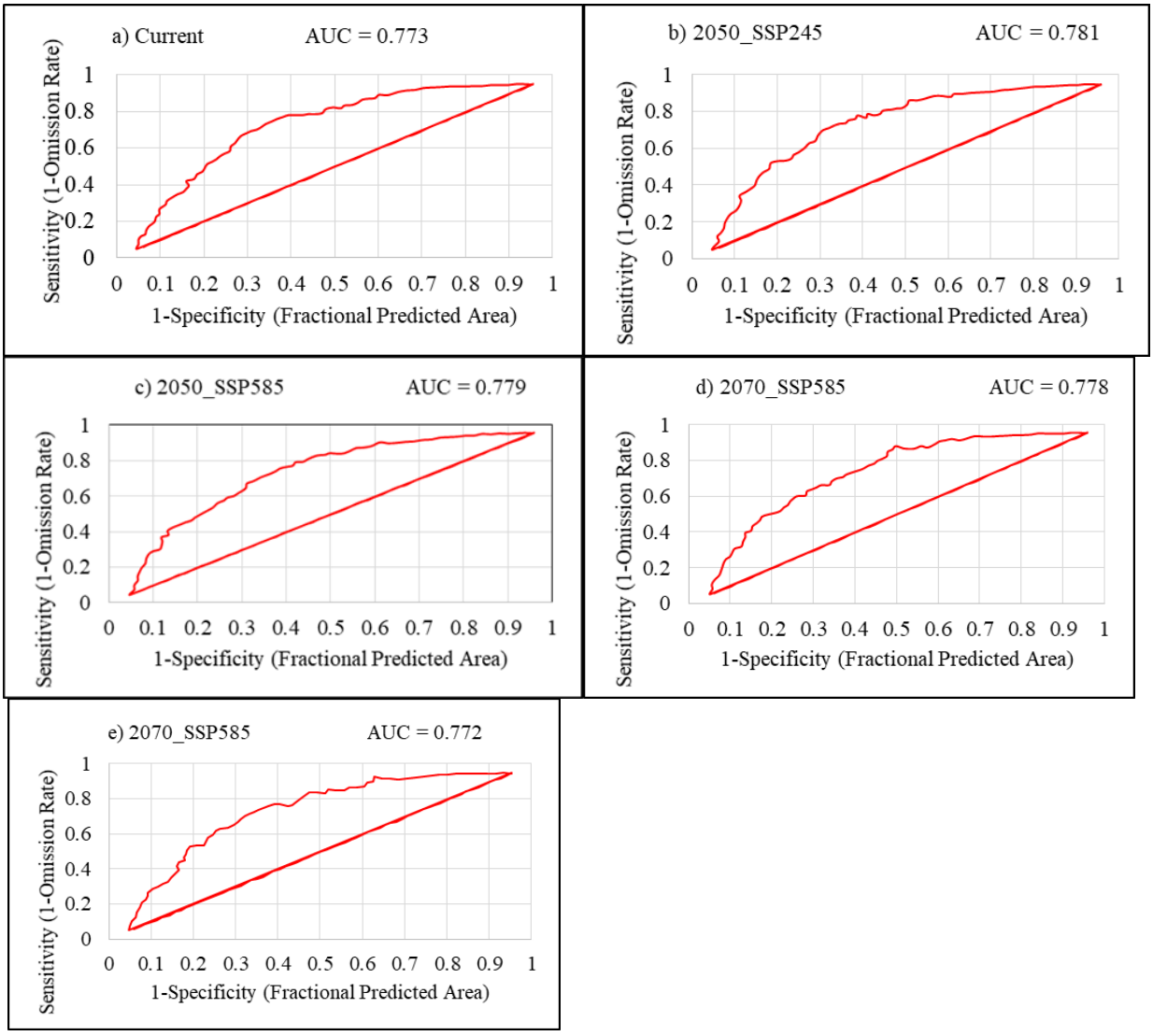

Figure 2. The ROC curve for the current and predicted suitability of *C. arabica* in the study area

3.2. Environmental variables contribution

Table 1 displays environmental variables entered in the Maxent for model simulation and their predicted contributions under the climate change scenario. The maximum temperature of the warmest month and the mean diurnal range temperature are among the temperature variables that had the higher predictive contribution for the present and future coffee suitability models. Of the precipitation variable, precipitation in the coldest quarter was the most significant factor for land suitability prediction. Overall, temperature variables were a key factor in determining *C. arabica* cultivation suitability under all climate change scenarios. This aligns with previous studies by Bunn et al. (2015) and Gomes et al. (2020) documenting the importance of temperature in coffee distribution modeling.

Table 1: Estimates of bioclimatic variables' contributions to the Maxent model

Code	Bioclimatic variables	Percentage contribution				
		Current	2050		2070	
			SSP245	SSP585	SSP245	SSP585
BIO1	Annual Mean Temperature	0.7	4.1	7.8	2.9	4.1
BIO2	Mean Diurnal Range temperature	16.4	18.6	16.7	16.5	18.2
BIO3	Isothermality (BIO2/BIO7) (×100)	2.9	4.1	1.5	8.4	3.2
BIO4	Temperature Seasonality	4.3	9.1	10.2	9	9.6
BIO5	Max Temperature of Warmest Month	34.3	13.3	14.9	18.4	15.9
BIO7	Temperature Annual Range	5.5	0.9	2	2.1	1.5
BIO9	Mean Temperature of Driest Quarter	0.3	0.3	0.9	0.2	0.8
BIO12	Annual Precipitation	6.9	6.9	8.6	7.5	7
BIO14	Precipitation of Driest Month	13.7	14.9	15.3	13.2	14.3
BIO15	Precipitation Seasonality	6.2	2.9	1.8	6.6	0.8
BIO19	Precipitation of Coldest Quarter	8.8	24.9	20.3	15.2	24.6

3.3. Current and future suitability

Following prior research on the modeling of species distribution (Abebe et al., 2024; Zafirah et al., 2021), we reclassified the suitability map into four suitability classes: <0.2 (unsuitable), 0.2–0.4 (low suitable), 0.4–0.6 (moderately suitable), and >0.6 (high suitable). The distributions of coffee are shown in Fig. 4a-e. In the current suitability map (fig.4a), only 989.64 km^2 (9.5%) of the area is classified as high coffee suitability, followed by 2743.90km^2 (26.3%) moderately suitable, 3069.62 km^2 (29.4%) low suitable, and a high proportion 3627.98 km^2 (34.9%) of the study area falls under unsuitable. The model predictions presented in Figure 4b-e for 2050 and 2070 revealed varying distributions in climatic suitability for coffee cultivation. The results for all climate change scenarios indicated significant potential for land transformation (Table 2). This result corroborate the findings of Davis et al. (2012).

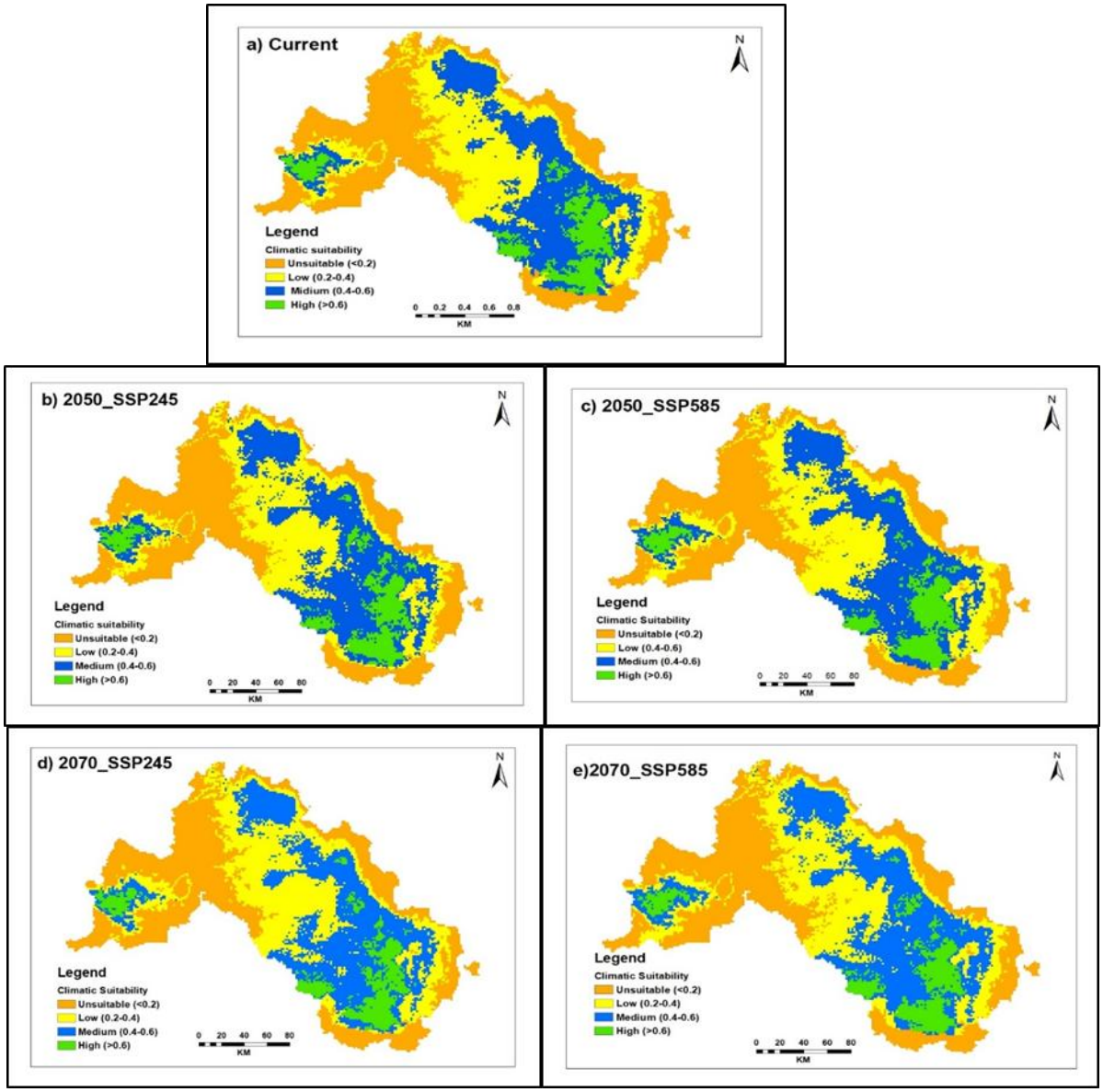

Figure. 3. Current and future climatic suitability for *C. arabica* cultivation in the West Wolega zone, Western Ethiopia

Table 2 *Coffee arabica* suitability distribution under future climate change scenarios in the West Wolega zone, Western Ethiopia

Period	Scenarios	Land suitability area in square kilometers and percentage							
		Unsuitable		Low suitable		Moderate suitable		High suitable	
		km^2	%	km^2	%	km^2	%	km^2	%
2050	SSP245	3532.14	33.86	3143.23	30.13	2808.49	26.92	947.27	9.08
	SSP585	3659.93	35.09	2958.50	28.36	2862.66	27.44	950.05	9.11
2070	SSP245	3491.86	33.48	3181.43	30.50	2883.49	27.64	874.35	8.38

	SSP585	3614.79	34.65	2946.69	28.25	2932.11	28.11	937.55	8.99

3.4. Predicted suitability losses and gains

The predicted change in climate is likely to negatively impact the areas currently suitable for coffee cultivation. In the 2050s, it was predicted the present suitability would be lost by 17.52%, 19.15%, and 21.78%, while it would be gained by 17.71%, and 20.58% under SSP245, and SSP585, respectively. Conversely, it is suggested that 63.14%, and 57.64% of the area will remain stable under SSP245, and SSP585, respectively (Fig. 5 a & b). The model projects that suitable areas could decline by 21.62%, and 24.26%, while it expects an increase of 20.76%, and 21.68% in suitable areas in 2070, under the SSP245, and SSP585 scenarios, respectively. Furthermore, the projections suggest about 57.62%, and 54.06%, is expected to remain unchanged by2070 under the SSP245, and SSP585 scenarios, respectively (Fig.5 c & d).

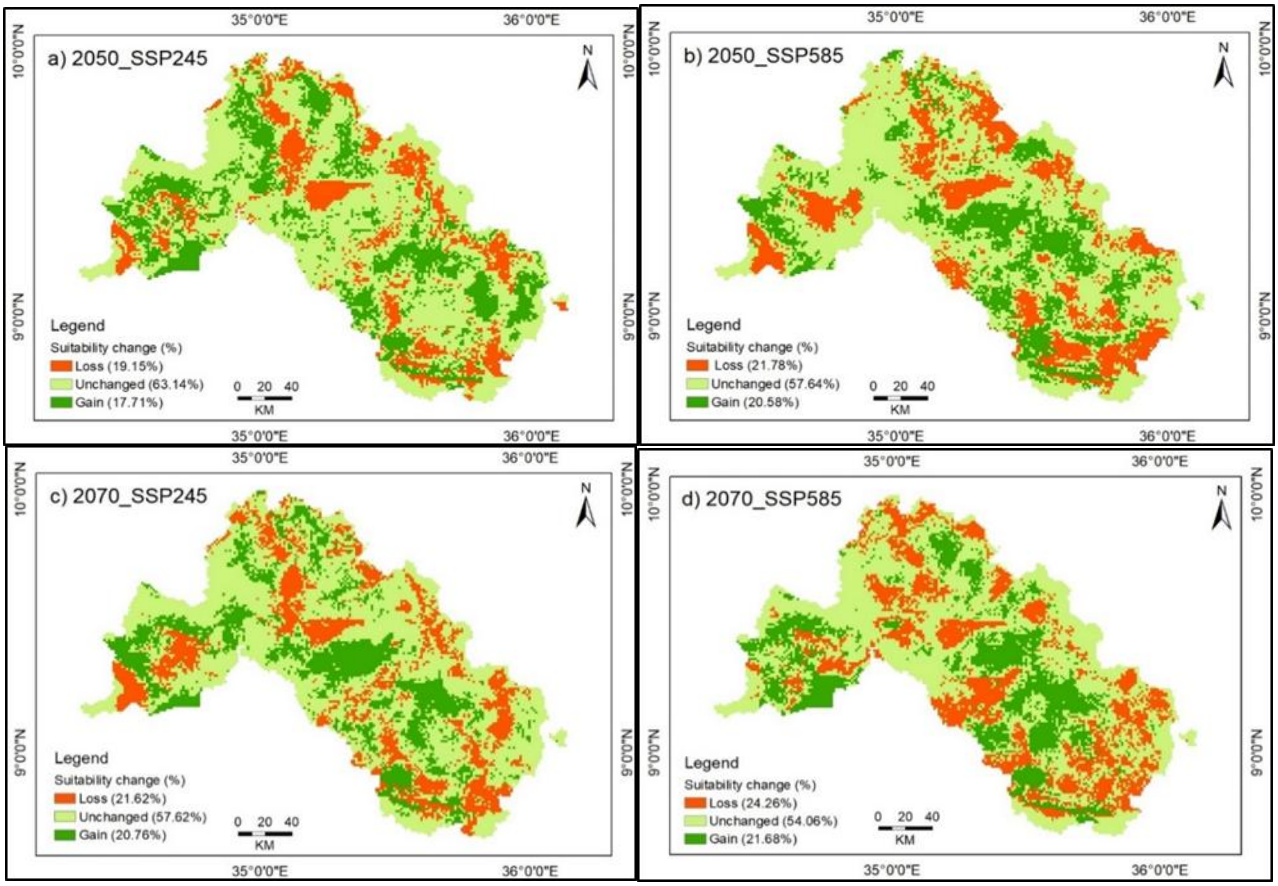

Figure. 4. The predicted suitability changes for *Coffea arabica* cultivation under future climate change scenarios in he West Wolega Zone, Western Ethiopia

3.5. Predicted change in total suitability areas

The land suitability area for coffee cultivation under current and future climate change scenarios are shown in Figure 4. The logistic threshold values were used to reclassify the map into suitable and unsuitable areas. The classification system denotes that values falling below the designated threshold are

believed unsuitable, whereas values above the specified threshold signify potential suitability for *C. arabica* cultivation (Merow et al., 2013). The land areas suitable for *C. arabica* cultivation could be reduced in all projected climate change scenarios as compared to the currently suitability areas (Table 3). The reduction in areas suitable for *C. arabica* cultivation has also been documented at both regional and global levels (Bunn et al., 2015; Gruter et al., 2022).

Table: 3. Predicted total suitability changes in *Coffea arabica* cultivation compared to current areas in the West Wolega zone, Western Ethiopia

Period	Scenarios	Total suitability area (km^2) and % of land				Total suitability change	
		Unsuitable		Suitable			
		Km^2	%	Km^2	%	Δ (Km^2)	Δ (%)
Current	Baseline	5135.98	49.25	5294.30	50.75	-	-
2050	SSP245	5176.25	49.63	5254.03	50.37	-40.28	0.38
	SSP585	5272.08	50.55	5158.20	49.45	-136.11	1.3
2070	SSP245	5300.55	50.82	5129.73	49.18	-164.58	1.57
	SSP585	5313.75	50.95	5116.53	49.05	-177.77	1.7

4. Conclusions

The research employed a MaxEnt model to map the current land suitability and future dynamics for *Coffea arabica* cultivation under climate change scenarios. The study used bioclimatic variables and coffee presence data for the suitability model. Based on the MaxEnt output, approximately half of the lands in the West Wolega Zone were identified as currently suitable for *Coffea arabica* cultivation. The projected result revealed that while current coffee cultivation areas may see a significant decline in their suitability, certain areas that were presently unsuitable for coffee cultivation will become suitable. In addition, a decrease in the total land area appropriate for coffee cultivation has been detected across all climate change scenarios in comparison to the current total land deemed suitable for coffee production. This decline may affect both the quality and quantity of coffee production. Overall, the sustainability of *Coffea arabica* cultivation is facing significant challenges in a substantial portion of the coffee-growing areas within the west Wolega Zone. This highlights the need to prioritize the development and implementation of effective adaptation and mitigation measures to ensure the long-term sustainability of coffee cultivation in the face of evolving climatic conditions.

References

Abebe, H., Desta, A. B., & Dejene, S. W. (2024). Modeling the distribution of Aloeankoberensis and A.debrana under different climate change scenarios in North Shewa Zone, Amhara National Regional State, Ethiopia. Ecological Processes, 13(1), 1–19. https://doi.org/10.1186/s13717-024-00511-x

Bermudez, S., Voora, V., & Larrea, C. (2022). Global market report: Coffee prices and sustainability.

Bunn, C., Läderach, P., Rivera, O. O., & Kirschke, D. (2015). A bitter cup : climate change profile of global production of Arabica and Robusta coffee. Climatic Change, 129, 89–101. https://doi.org/10.1007/s10584-014-1306-x

Chemura, A., Kutywayo, D., Chidoko, P., & Mahoya, C. (2015). Bioclimatic modeling of current and projected climatic suitability of coffee (Coffea arabica) production in Zimbabwe. Regional Environmental Change, 16(2), 473–485. https://doi.org/10.1007/s10113-015-0762-9

Chemura, A., Mudereri, B. T., Yalew, A. W., & Gornott, C. (2021). Climate change and specialty coffee potential in Ethiopia. Scientific Reports, 11(8097), 1–13. https://doi.org/10.1038/s41598-021-87647-4

DaMatta, F. M. (2018). Coffee tree growth and environmental acclimation. In Burleigh Dodds Science Publishing (pp. 1–28).

DaMatta, F. M., Avila, R. T., Cardoso, A. A., Martins, S. C. V., & Ramalho, J. C. (2018). Physiological and Agronomic Performance of the Co ff ee Crop in the Context of Climate Change and Global Warming: A Review. Agriculture and Food Chemistry, 66, 5264−5274. https://doi.org/10.1021/acs.jafc.7b04537

DaMatta, F. M., Rahn, E., Läderach, P., Ghini, R., & Ramalho, J. C. (2019). Why could the coffee crop endure climate change and global warming to a greater extent than previously estimated ? Climatic Change, 152, 167–178. https://doi.org/10.1007/s10584-018-2346-4

Davis, A. P., Gole, T. W., Baena, S., & Moat, J. (2012). The Impact of Climate Change on Indigenous Arabica Coffee (Coffea arabica): Predicting Future Trends and Identifying Priorities. 7(11), 10–14. https://doi.org/10.1371/journal.pone.0047981

Davis, A. P., & Rakotonasolo, F. (2021). Six new species of coffee (Coffea) from northern Madagascar. Kew Bulletin, 76(3), 497–511. https://doi.org/10.1007/s12225-021-09952-5

Elith, J., Graham, C. H., Anderson, R. P., Dudík, M., Guisan, A., Hijmans, R. J., Huettmann, F., Leathwick, J. R., Lehmann, A., Li, J., Lohmann, L. G., Loiselle, B. A., Manion, G., Nakamura, M., Nakazawa, Y., Overton, J. M., Townsend, A., Phillips, S. J., Richardson, K., … Zimmermann, N. E. (2006). Novel Methods Improve Prediction of Species' Distributions from Occurrence Data. Wiley on Behalf of Nordic Society Oikos, 29(2), 129–151.

Elith, J., & Leathwick, J. R. (2009). Species distribution models: Ecological explanation and prediction across space and time. Annual Review of Ecology, Evolution, and Systematics, 40, 677–697. https://doi.org/10.1146/annurev.ecolsys.110308.120159

Gomes, L. C., Bianchi, F. J. J. A., Cardoso, I. M., Fernandes, R. B. A., Filho, E. I. F., & Schulte, R. P. O. (2020). Agroforestry systems can mitigate the impacts of climate change on coffee production : A spatially explicit assessment in Brazil. Agriculture, Ecosystems and Environment, 294(106858), 1–11. https://doi.org/10.1016/j.agee.2020.106858

Gruter, R., Trachsel, T., Laube, P., & Jaisli, I. (2022). Expected global suitability of coffee , cashew and avocado due to climate change. PLOS ONE, 1–24. https://doi.org/10.1371/journal.pone.0261976

Hurni, H. (1998). Agro-ecologial belts of Ethiopia: Explanatory notes on three maps at a scale of 1:1,000,000. In Research Report, Soil conservation research program, Addis Ababa.

ICO. (2022). Coffee prices close 2022 on a stable note, coalescing at around 160 US cents / lb. In International coffee organization.

IPCC. (2022). Climate Change 2022_ Impacts, Adaptation and Vulnerability_Working Group II contribution to the Sixth Assessment Report of the Intergovernamental Panel on Climate Change. https://doi.org/10.1017/9781009325844.Front

Jayakody, S., Estacio, I., Sianipar, C. P. M., Onitsuka, K., & Basu, M. (2024). Maxent modeling for predicting the potential distribution of human-elephant conflict risk in Sri Lanka Human. Applied Geography, 103447, 1–11. https://doi.org/10.1016/j.apgeog.2024.103447

Korecha, D., & Barnston, A. G. (2007). Predictability of June – September Rainfall in Ethiopia. American Meteorological Society, 135, 628–650. https://doi.org/10.1175/MWR3304.1

Merow, C., Smith, M. J., & Silander, J. A. (2013). A practical guide to MaxEnt for modeling species' distributions: What it does, and why inputs and settings matter. Ecography, 36(10), 1058–1069. https://doi.org/10.1111/j.1600-0587.2013.07872.x

MFA. (2018). Climate Change Profile: Ethiopia. 1–26.

Moat, J., Williams, E., Baena, S., Wilkinson, T., Gole, T. W., Challa, Z. K., Davis, A. P., Demissew, S., & Williams, J. (2017). Resilience potential of the Ethiopian coffee sector under climate change. Nature Plants, 3(17081), 1–14. https://doi.org/10.1038/nplants.2017.81

Ovalle-rivera, O., Läderach, P., Bunn, C., & Obersteiner, M. (2015). Projected Shifts in Coffea arabica Suitability among Major Global Producing Regions Due to Climate Change. PLOS ONE, 1–13. https://doi.org/10.1371/journal.pone.0124155

USAID. (2024). Climate change risk profile: Ethiopia. 1–8.

Zafirah, N., Lah, A., Yusop, Z., Hashim, M., Salim, J. M., & Numata, S. (2021). Predicting the Habitat Suitability of Melaleuca cajuputi Based on the MaxEnt Species Distribution Model. Forest, 12(1449), 1–18.

Theme 6

Emerging Challenges

Analytical Framework to Elucidate the Intricate Relationship between Ethiopia and Egypt: The Issue of River Nile

Keneni Elias Shoro*[1]

[1]Assistant Professor, Jimma University, Institute of Technology

*Corresponding author: keneni.elias@ju.edu.et,

Abstract

This paper establishes an analytical framework to explicate the delicate relationship between Ethiopia and Egypt, centered on the influence of the Nile River. Historically, while pivotal for both nations, the issue of the Nile River has been creating a complex interplay, rooted in their geographical connection. The construction of Ethiopia's Grand Ethiopian Renaissance Dam (GERD) is a matter of "do or die" for Ethiopia, while Egypt considers it as a threat. The disputes over water rights and management, still underscore the need for innovative and more comprehensive analysis of this relationship, even though this subject matter is not new. The framework examines several interrelated dimensions: the historical context of Nile dependency, geopolitical dynamics influenced by national interests, socio-economic impacts of water management on food security and development, environmental concerns exacerbated by climate change, and the complexities of international legal frameworks governing transboundary watercourses. By adopting this holistic approach, the article aims to foster a deeper understanding of the Nile's role in shaping the interactions between Ethiopia and Egypt, while stimulating dialogue on sustainable solutions that respect the rights and needs of both nations, without ignoring the rights of other riparian countries. This initiative serves as a vital resource for the scientific community, in fostering collaboration and cooperation among Nile Basin countries.

Keywords: analytical framework; historical context; geopolitical dynamics; Ethiopia; Egypt; Nile

1. Introduction

The Nile River, an aquatic lifeline extending over 6,650 kilometers, not only holds the distinction of being the world's longest river but also serves as a historical and contemporary nexus of existence, affluence, and, regrettably, contention (Tikuye et al., 2023). For millennia, its perennial flow has intrinsically intertwined the fates of the nations it traverses, with Ethiopia and Egypt standing as prime examples. This link is described by a manifold and often strained interaction of historical precedence, intricate geopolitical maneuvering, pressing socio-economic constraints, environmental vulnerabilities amplified by climate change, and the relentlessly evolving framework of international water law (Kang, 2023). A detailed comprehension of this complex relationship is not merely academic; it is vital for nurturing sustainable development, promoting regional stability, and averting potential conflicts over diminishing resources (Li, 2020; Korwa & Wambrauw, 2023).

This paper proposes a solid and multi-dimensional analytical framework specifically designed to disentangle the diverse and often intermingled outfits that constitute the Ethiopian-Egyptian dynamics concerning the Nile. The Nile River serves as the central organizing principle, guiding the exploration of critical junctures where national aspirations intersect with the shared, yet often contested, responsibility

for managing a vital and finite resource (Keon-Sang, 2016). This framework enables a deeper understanding of the crucial considerations needed to map a sensible path toward collaborative stewardship of the Nile's resources. It will examine the historical roots of the relationship, the competing national interests at play, and the socio-economic inferences of water management decisions, the escalating environmental challenges (Zhang et al, 2023), and the legal and institutional landscape governing the river's use (Hung, 2023). Ultimately, this analysis aims to contribute to a more informed dialogue and a more cooperative approach to managing this essential resource for the benefit of all riparian nations and their future generations.

2. Material and Method

2.1. Historical context of Nile dependency

For millennia, the Nile has served as the very lifeblood of both Ethiopia and Egypt. It has been dictating not only settlement patterns and agricultural practices but also significantly influencing the rise and fall of civilizations across the region. Egyptian civilization, renowned for its monumental architectural achievements, sophisticated social organization, and enduring cultural legacy, flourished along the fertile banks of the Nile. The year-round floods provided rich silt deposits, enabling remarkable agricultural productivity that sustained a large population and facilitated the development of a complex hierarchical society, sophisticated irrigation systems, and loyal employment opportunities. The Nile was not just a water source; it was the foundation of their entire world. These and other similar facts, but not mentioned here, are undeniable.

Concurrently, the Ethiopian highlands, often referred to as the "water tower" of Northeast Africa, constitute the primary source of approximately 85% of the Nile's water volume. The Blue Nile (Abay) River, originating from Lake Tana in the Ethiopian highlands, contributes the majority of the Nile's flow, particularly during the rainy season. This intrinsic geographical asymmetry, where one nation is the home (source) for large proportion (85%) of the headwaters, and another depends on the downstream flow, has placed the foundation for a complex relationship that continued to this day. Understanding this historical fact of Nile, particularly the ingrained beliefs, cultural narratives, and economic practices associated with it, is crucial for comprehending the current dynamics between the two nations.

The historical narrative is further complicated by colonial-era agreements, negotiated primarily by and for European powers, which largely favored downstream states, particularly Egypt and Sudan, ignoring totally the upstream home country of the river. These agreements, often made without the meaningful participation or consent of upstream nations, granted downstream states disproportionate rights to the Nile's waters, leaving upstream nations with limited say in the river's management and hindering their ability to develop their own water resources for economic development. This legacy of colonial inequity continues to shape the perceptions and positions of the riparian states, fueling resentment and mistrust, and making it difficult to reach mutually agreeable solutions for the equitable and sustainable use of the Nile. For example, the 1929 Nile Waters Agreement, though later revised, remains a contentious point, as it granted Egypt a virtual veto power over upstream projects.

The Nile River basin is shared by eleven riparian countries: Burundi, DR Congo, Egypt, Eritrea, Ethiopia, Kenya, Rwanda, South Sudan, Sudan, Tanzania, and Uganda. Egypt and Sudan, as the two downstream nations, have historically enjoyed preferential access to the Nile's water resources, often invoking historical rights and treaties to justify their claims. They present the unfair agreements for all arguments. This historical control, enshrined in agreements such as the 1929 and 1959 Nile Waters Agreements, has become a major source of tension and resentment, particularly for upstream countries like Ethiopia, which have long sought a more equitable and participatory distribution of the Nile's waters, pertinent to their sovereign rights and developmental needs (Swain, 2018). The upstream nations maintain that those outdated agreements have evolved significantly since the colonial era, which cannot work anymore in the current situation, where only and only fairness and equity works in the modernized world. They add that the principles of equitable and reasonable utilization, as well as the obligation not to cause significant harm, should guide the management of transboundary water resources. The aspiration to overturn perceived historical injustices and establish a more equitable framework for water sharing fuels much of the present-day contestation and the drive for renegotiating existing agreements.

2.2. Geopolitical dynamics influenced by national interests

The Nile's geopolitical significance is utterly evident in the frequently conflicting national interests of Egypt and Ethiopia. Egypt, with its vast and growing population concentrated along the narrow Nile corridor, profoundly and undeniably needs the river for its agriculture, industry, domestic water supply, hydroelectric power generation, and overall economic stability. As a result, Egypt has historically prioritized its water security above nearly all other considerations, viewing unhindered access to the Nile's (Sprinkler, 1997). This deeply ingrained view has extremely influenced its foreign policy, shaped its interactions with upstream nations, and driven its efforts to maintain its historical dominance over the Nile's resources. Egypt has historically been suspicious of any upstream developments that could potentially reduce the flow of water reaching its territory, viewing such projects as existential threats to its national security. That is the main reason why Egypt considers GERD as a threat.

In contrast, Ethiopia, possessing abundant, but historically underutilized water resources, a rapidly growing population, and with ambitious development goals aimed at achieving middle-income status, views the Nile (specifically the Blue Nile) as a critical resource for alleviating widespread poverty, stimulating sustainable economic growth, and improving the living standards of its citizens (Tadesse, 2014). Ethiopia's developmental objectives hinge, in part, on harnessing the Nile's substantial hydropower potential to generate electricity, power its industries, and provide energy access to its rural population, a significant portion of which currently lives without electricity. Diversifying its energy mix and reducing its dependence on imported fossil fuels is also a key priority for Ethiopia.

The construction of the Grand Ethiopian Renaissance Dam (GERD) on the Blue Nile, thus, represents a watershed moment in the geopolitical landscape of the Nile Basin, dramatically intensifying the existing tensions and long-standing mistrust between Egypt and Ethiopia. Egypt perceives the GERD as a potential existential threat to its water security, fearing a significant reduction in water flow during the filling and operation phases, particularly during prolonged periods of drought. Cairo worries that the dam

could significantly impact its agricultural production, potentially leading to crop failures, reduced food security, and economic losses.

On the other hand, Ethiopia perceives the GERD as a vital development project, essential for generating clean and renewable electricity, promoting industrial growth, and fostering regional energy integration by exporting electricity to neighboring countries (Getahun, 2020). Ethiopia maintains that the dam is designed to operate without causing significant harm to downstream nations, emphasizing that it will regulate the flow of the Blue Nile and potentially even benefit downstream countries by mitigating the effects of floods and droughts. Ethiopia also reasons that the GERD is a symbol of its national pride and its determination to overcome poverty and achieve self-sufficiency. This fundamental divergence in national interests, rooted in differing perspectives on water security and developmental priorities, underscores the urgent need for a more refined, evidence-based, and collaborative understanding of the Nile's complex geopolitical implications. The GERD has become a focal point, embodying the broader struggle for control and influence over the Nile's resources and highlighting the competing visions for the future of the Nile Basin. Ethiopia further believes that all the riparian countries, including Egypt and Sudan, can wisely utilize the water resource of the Nile if reasonable dialogues are at place.

2.3. Socio-economic impacts of water management on food security and development

Water management practices along the Nile River have deep socio-economic ramifications for Ethiopia and Egypt, directly impacting food security, economic development, social well-being, and regional stability. The availability and efficient management of the Nile's waters are indispensable for food production. Egypt employs hundreds of thousands of people in the agriculture sector, which almost entirely utilizes Nile River water. In Ethiopia, the GERD is projected to have a transformative impact on the country's energy sector, significantly increasing electricity generation capacity, powering industrial growth, attracting foreign investment, and improving access to electricity for millions of households, particularly in rural areas where energy access is currently limited (Tadesse, 2014). Increased energy production also has cascading effects, potentially boosting agricultural productivity through mechanized irrigation, enabling the development of other sectors such as manufacturing and services, and improving access to education and healthcare. The GERD is thus seen as a catalyst for broader socio-economic development in Ethiopia.

A comprehensive understanding of the complex socio-economic impacts of water management is therefore critical for safeguarding a sustainable balance between the often-competing needs of both nations and ensuring equitable and sustainable development throughout the Nile Basin. This includes carefully bearing in mind the potential impacts on vulnerable populations, promoting equitable access to water resources, investing in water-efficient technologies and sustainable agricultural practices, and reinforcing social safety nets to mitigate the adverse effects of potential water scarcity. Moreover, fostering regional cooperation and trade could mitigate the impact of water scarcity by allowing countries to specialize in agricultural production based on their comparative advantages, thereby reducing overall water demand and promoting regional food security.

2.4. Environmental concerns exacerbated by climate change

Climate change is posing increasingly severe environmental challenges to the entire Nile Basin, exacerbating existing vulnerabilities related to water scarcity and creating new risks that threaten the long-term sustainability of the region. These challenges include altered precipitation patterns, leading to more frequent and intense droughts in some areas and more devastating floods in others; increased overall water scarcity, threatening agricultural production, human livelihoods, and ecosystem health; reduced water quality due to increased evaporation, higher salinity levels, and increased pollution from agricultural runoff and industrial discharge (Conway, 2005). The impacts of climate change are likely to disproportionately affect vulnerable populations.

Addressing these rising environmental concerns demands a collaborative, adaptive, and scientifically informed approach to water management, one that explicitly incorporates climate change projections and prioritizes the long-term ecological sustainability of the Nile's resources. This includes investing in climate-resilient infrastructure, such as improved irrigation systems and flood control measures; promoting water conservation practices in agriculture, industry, and domestic use; implementing integrated water resources management (IWRM) strategies that consider the interconnectedness of water, land, and ecosystems; strengthening regional cooperation on climate change adaptation and mitigation; and investing in research and monitoring to better understand the impacts of climate change on the Nile Basin. Failure to address these pressing environmental challenges effectively could lead to increased competition for dwindling water resources, further exacerbating tensions between Ethiopia and Egypt and potentially undermining regional stability. The long-term health of the Nile ecosystem, and the well-being of the millions of people who depend on it, hinges on a commitment to sustainable water management in the face of a changing climate. This requires meaningful collaboration of the two nations in particular.

2.5. International legal frameworks governing transboundary watercourses

The intricate relationship between Ethiopia and Egypt, which is centered on the transboundary Nile River, is further complicated by the complications of international legal frameworks governing shared water resources. These frameworks present both opportunities for collaboration and potential avenues for disagreement. The Nile Basin Initiative (NBI), established in 1999, serves as a vital platform for regional cooperation, facilitating dialogue, data sharing, and joint decision-making on water management. However, the NBI's effectiveness has been fragile by disagreements among member states, particularly concerning the Cooperative Framework Agreement (CFA). Egypt and Sudan have declined to sign the CFA due to concerns over water security and prior notification for projects.

The Convention on the Law of the Non-Navigational Uses of International Watercourses (CLNNUIW), adopted by the UN General Assembly in 1997, offers a broader legal framework for transboundary water management. It underlines principles such as equitable and reasonable utilization, the obligation not to cause significant harm, and the duty to cooperate. However, the CLNNUIW has not achieved universal ratification, and its interpretation and application remain subjects of debate. The absence of a universally accepted legal framework, combined with inconsistencies in the interpretation and application of existing

agreements, contributes to ongoing disputes and mistrust between Ethiopia and Egypt. This badly calls for very close attention from Ethiopia's side in particular. The diplomacy must be strong enough to shape the complex nature of the international conventions, to the fair share of the country.

2.6. The Part that can be played by the Nile Basin Initiatives (NBI) (NBI, 2021)

The Nile Basin Initiative is an important organization involved in facilitating cross-border water management and cooperation. It is a transitional partnership led by 10 Nile Basin countries, namely Burundi, DR Congo, Egypt, Ethiopia, Kenya, Rwanda, South Sudan, Sudan, Tanzania, and Uganda, while Eritrea participates as an observer. The institution was established quarter a century ago (1999) and is guided by a shared vision objective.

The shared objective of NBI is to attain sustainable socio-economic development through equitable utilization of, and benefit from, the common Nile Basin Water resources. Among the six goals, namely, Water security, Energy security, Food security, Environmental, Climate change adaptation, and Transboundary water governance, the Goal 6, Transboundary water governance, deals with the issue of Transboundary water management.

With this institution as the driver, since 2007, fifteen Nile Days have been hosted, basing their goal on sustainable use of water of Nile. The following table shows, the host countries till 2021.

Table 1 Nile day celebrations since 2007 in riparian member countries (Source: (NBI, 2021))

Year	Host country	City	Theme
2007	Rwanda	Kigali	Enhanced Cooperation on the Nile for Peace and Prosperity
2008	Ethiopia	Addis Ababa	Land Degradation and Climate Change: Address Shared Threats, Sustain Nile Basin Cooperation
2009	Burundi	Bujumbura	United in Diversity by the River Nile – Our Heritage, Source for Regional Cooperation
2010	Uganda	Kabale	Nurturing 10 Years of Cooperation and Progress
2011	DR Congo	Goma	All Together for Better Cooperation
2012	Uganda	Jinga	Water, Energy, Food – Importance of Nile Cooperation
2013	Ethiopia	Bahir Dar	Land Degradation and Climate Change: Address Shared Threats, Sustain Nile Cooperation
2014	Uganda	Kampala	Water and Energy: National Challenges, Transboundary Solutions
2015	Sudan	Khartoum	Water and Improved Livelihoods – Opportunities in Nile Cooperation
2016	Kenya	Vihiga	Nile Cooperation: Gateway to Regional Integration
2017	Tanzania	Dar es Salam	Our Shared Nile - Source of Energy, Food and Water for All
2018	Ethiopia	Addis Ababa	The Nile: Shared River Collective Action

2019	Rwanda	Kigali	NBI@20: Stronger Together
2020	Sudan	Khartoum	Joint Investments on the Nile for Regional Transformation
2021	Uganda	Kampala	Rethinking Regional Investments in the Nile Basin (virtual)

The Nile Day offers an opportunity for Basin populaces to come together to celebrate the benefits of Nile cooperation and interchange experiences, opinions and ideas on topical issues related to the cooperative management and development of the common Nile Basin water and related resources. The event is also used by Member States to re-affirm their commitment to Nile Cooperation. This is in addition to enhancing stakeholders' appreciation of the importance of and commitment to Nile Cooperation while at the same time increasing cognizance of the results and prominence of NBI. The Nile Day also provides an opportunity to celebrate the rich and varied cultures which exist within the Nile Basin, with admiration to cultural entertainment and traditional cuisine.

In addition, NBI convenes the Strategic Dialogue that brings together agents of NBI Partner States and of Development Partners to deliberate the Nile cooperation. The discourse seeks to strengthen the Nile cooperation through exploring options of institutional sustainability. The discussions reflect on the evolving context of emerging issues, challenges, opportunities to map prospects for institutional growth and sustainability. The strategic dialogue has been established as an instrumental forum in generating ideas on institutional, technical as well as financial sustainability for the Nile cooperation. The meeting is not a decision making body but a platform for scrutinizing issues and informing decisions of NBI governance as well as the development partners of NBI. The first Strategic Dialogue was held in 2006 and has been held annually. Beginning 2019, the event has been fixed on the NBI calendar to always take place on 23rd February of every year, just a day after the Nile Day celebrations.
Unfortunately, in all these years, we can't see Egypt hosting the Nile day, as can be observed from the table. It shows that NBI has many assignments to do. Furthermore, we believe that Egypt should realize the realistic mutual existence of the entire world. From Ethiopia's side also, the current stand and philosophy of the fair utilization of the Nile River should continue indefinitely for the years to come.

The elites of Ethiopia also assume more assignments regarding the dignity, the right to use the water resources of the country as well as the equitable use of the water for downstream countries in general; not just only Egypt and Sudan but also other countries. They can do a lot by extending the dialogue till finally the real agreement is reached! The country, Ethiopia, is doing her best in all cases for negotiation and equitable use of the water resources. The way GERD is completed is based on this philosophy of Ethiopia.

3. Conclusions

A wide-ranging and multi-dimensional analytical framework is essential to understanding the complex and deeply intertwined relationship between Ethiopia and Egypt, which revolves around the shared Nile River. This setting should take into account the geopolitical dynamics driven by diverging national interests and developmental aspirations, socio-economic impacts on food security, livelihoods, and economic growth, ever-increasing environmental concerns exacerbated by the global climate crisis, and the complex international legal frameworks governing transboundary watercourses. By embracing this

holistic approach, the scientific community, policymakers, and stakeholders can foster a deeper understanding of the Nile's pivotal role in shaping the interactions between Ethiopia and Egypt. This understanding can encourage positive dialogue on sustainable solutions that equitably respect the rights and developmental needs of both nations, as well as the interests of other riparian countries within the Nile Basin. Ultimately, collaborative stewardship of the Nile is crucial for fostering regional stability, economic prosperity, and environmental sustainability.

To settle the challenges surrounding the Nile River and the connection between Ethiopia and Egypt, several recommendations can be made:

a) Reinforce Regional Cooperation through the Nile Basin Initiative: Invest in enhancing the NBI as a platform for dialogue, data sharing, capacity building, and collaborative decision-making on integrated water resources management. This is to mean encouraging greater participation from all member states and promote a spirit of trust and cooperation.
b) Promote Legal Harmonization and Adherence to Fair International Principles: Encourage the ratification and implementation of the CLNNUIW by all Nile Basin countries. This is facilitating discussions aimed at aligning national policies with worldwide principles of equitable and reasonable utilization and the obligation not to cause significant harm.
c) Invest in Research and Analysis: Supporting rigorous, independent research and analysis on the socio-economic and environmental impacts of water management practices along the Nile Basin, including the impacts of climate change. This deals with ensuring that research findings are widely disseminated to inform policy decisions and promote evidence-based sustainable development. Also conducting joint studies involving researchers from all riparian countries is vital to foster mutual understanding and build trust.
d) Enhance Diplomatic Engagement and Conflict Resolution Mechanisms: Strengthen diplomatic efforts, involving both regional and international actors, to address the underlying geopolitical tensions between Ethiopia and Egypt. Foster open and transparent communication, build trust, and develop effective conflict resolution mechanisms to address emerging disputes. Explore opportunities for joint projects and investments that benefit both nations.
e) Promote Water-Efficient Technologies and Practices: Encourage the adoption of water-efficient technologies and agricultural practices throughout the Nile Basin to reduce water demand and enhance agricultural productivity. Invest in research and development of drought-resistant crops and irrigation systems.
f) Foster Public Awareness and Education: Raise public awareness about the importance of sustainable water management and the need for regional cooperation. Develop educational programs to promote understanding of the Nile's complex ecosystem and the challenges facing the basin.

References

Hung, P. H. (2023). The Influence of Cultural, Legal and Institutional Factors on Auditors' Roles, Responsibilities and Perceptions of Audit Quality. European Journal of Theoretical and Applied Sciences.

Kang, K. (2023). On contingency, confidence, and trust: how international water law stabilizes expectations under conditions of uncertainty. Water International, 48.

Keon-Sang, A. (2016). Ethiopian Contextualization: The Tradition of the Ethiopian Orthodox Tewahido Church. Mission Studies, 33, 147-162.

Korwa, J., & Wambrauw, M. S. F. (2023). A Constructivist Analysis of the Establishment of the AUKUS Security Pact and its Implications for Regional Stability in the Indo-Pacific. Journal Hubungan International.

Li, X. (2020). Transforming Our World: The 2030 Agenda for Sustainable Development: An Appeal of Global Cooperation for Building Green Civilization.

Nile Basin Initiative (NBI, 2021). The State of the River Nile Basin

Tikuye, B. G., Rusnák, M., Manjunatha, B., & Jose, J. (2023). Land Use and Land Cover Change Detection Using the Random Forest Approach: The Case of the Upper Blue Nile River Basin, Ethiopia. Global Challenges, 7.

Zhang, H., Yu, Z., Zhu, C., Yang, R., Yan, B., & Jiang, G. (2023). Green or not? Environmental challenges from photovoltaic technology. Environmental Pollution, 121066.

Concluding Remark

Excellencies, Distringsidhed Guests, Invited Keynote Speaker Professor Paulin Coulibaly, McMaster University, Canada; Paper Presenters and, Ladies and Gentlemen,

It's an honor to conclude the 23rd International Symposium on Sustainable Water Resources Development, organized by Arba Minch University's Water Technology Institute and Water Resources Research Center. With esteemed participants, including alumni and former staff, we've discussed various topics through scholarly papers, panel discussions, and poster presentations. Collaboration is key to our journey towards sustainable water management. We need qualified professionals, particularly engineers and innovators, to achieve our goals. Our partnership must extend beyond borders to other academic institutions. We seek your support in advancing our mission for the greater good.

Your excellences,
Ladies and gentlemen,
Certainly, the dimension of water politics cannot be overlooked, particularly in regions like the Horn of Africa where water scarcity and competition over resources can lead to tensions. It's imperative that we approach water management with knowledge, wisdom, and a commitment to peaceful solutions. As pioneers in water technology, the responsibility falls on the Water Technology Institute and its alumni to lead in this arena, ensuring the efficient and integrated use of water resources for sustainable development and peace. This symposium has been a testament to our collective efforts, and I extend my gratitude to all who have contributed, including the organizing committee, sponsors, and presenters. Your contributions have been invaluable, and I look forward to continued collaboration in the future. With that, I officially declare the 20th International Symposium on Sustainable Water Resources Development closed. Safe travels to all.

Thank you,
Dr. Teklu Wegayehu Zara (Associate Professor), Delegate for Vice President for Research and Community Services

Organizing Committee and Committee Members

Main Organizing Committee

Dr. Tamru Tesseme (Chairperson)
Dr. Elias Gebeyehu
Dr. Tekelu Wegayehu
Dr. Tesfaye Hailemariam
Mr. Abebe Temesgen
Mrs. Gizeshewerke Eshete

Transportation & Accommodation Sub Committee

Mrs. Gizeshewerke Eshete (Chairperson)
Mr. Aweke Genene
Mr. Andarge Alaro
Mr. Endale Seyoum
Mr. Yared Godene
Mr. Abaynehe (Warkawe)

Editorial and Publication Sub-Committee

Dr. Elias Gebeyehu (Chairperson)
Dr. Samuel Dagalo
Dr. Tamiru Paulos
Dr. Demelash Wendemeneh
Dr. Alemayehu Kassaye
Dr. Aschalew Chere
Dr. Sintayehu Yadete
Dr. Zelalem Abera
Dr. Tadesse Tujuba
Dr. Dagnachew Daniel
Dr. Yoseph Arba

Decoration & Stage Management Sub-Committee

Ms. Nazerawi Samuel (Chairperson)
Mr. Yohanes Mehari
Mr. Aklilu Alemayehu
Mr. Yohannes Tadesse
Ms. Fikerte Seyoum
Mr. Melkamu Ateka
Mr. Endale Seyoum
Mr. Tigistu Yisihak

Program Arrangement, Communication, Registration & Logistic

Mr. Behailu Hussen (Chairperson)
Mr. Muluneh Legesse
Mr. Esrael G/Silase
Mr. Assres Getenet
Mr. Daniel Getachew
Mr. Andarge Alaro
Mr. Ayalkie Belete
Mr. Tafesse Fintesa
Ms. Kidist Tadesse

Fund Raising & Finance Sub-Committee

Dr. Elias Gebeyehu (Chairperson)
Mr. Sufiyan Abdulmenan
Mr. Behailu Hussen
Mrs. Endalech Dea

Water Resources Research Center

The **Water Resources Research Center (WRRC)** at Arba Minch Water Technology Institute, **Arba Minch University (AMU)** is a specialized research institution dedicated to addressing critical water resource challenges through scientific research, innovation, and community engagement. The center plays a vital role in advancing sustainable water management, conservation, and utilization practices.

Key Focus Areas:

1. **Research & Innovation:**
   - Conducts multidisciplinary studies on water resources, hydrology, renewable energy, irrigation and drainage, Water Supply and Sanitation, Climate Change, Variability and Impacts, and Emerging Issues.
   - Investigates solutions for water scarcity, pollution, and sustainable water use for agricultural, hydropower and water supply.
2. **Community & Stakeholder Engagement:**
   - Works closely with local communities, government agencies, and NGOs to identify water-related challenges and implement practical solutions.
   - Promotes participatory research to ensure relevance and applicability of findings.
3. **Capacity Building & Training:**
   - Provides training programs for students, researchers, and professionals in water resource management.
   - Enhances technical expertise through workshops, seminars, and collaborative projects.
4. **Policy Support & Advocacy:**
   - Generates evidence-based research to inform water resource policies at regional and national levels.
   - Advocates for sustainable water use and integrated water resource management (IWRM).
5. **Technology & Infrastructure Development:**
   - Explores modern technologies for water conservation, rainwater harvesting, and efficient irrigation systems.
   - Supports infrastructure projects that improve water accessibility and quality.

Vision:

To be a leading hub of excellence in water resources research, fostering sustainable development and resilience in water-stressed areas.

Mission:

To advance knowledge, innovation, and practical solutions in water resource management through cutting-edge research, community partnerships, and policy influence. By bridging the gap between academia and real-world water challenges, the **WRRC at Arba Minch University** contributes ignificantly to Ethiopia's water security and environmental sustainability efforts


MFM
Menschen für Menschen
IWMI
International Water Management Institute
Anwarseid
General Contractor
Haverim
CONSTRUCTIONG.C
EEC
EWTI
ETHIOPIAN WATER TECHNOLOGY INSTITUTE